ER Folding Assistants Regulate ER-Mitochondria Contacts and Ca^{2+} Flux

by

Tomás Gutiérrez

A thesis submitted in partial fulfillment of the requirements for the degree of

Doctor of Philosophy

Department of Cell Biology

University of Alberta

Abstract

Eukaryotic cells are characterized by the presence of membrane-bound organelles. Close proximity between organelles has been observed for decades, but only recently we have really started to understand the importance of these contacts for cellular function. These contacts consist of areas of close apposition between the membranes of two organelles, and are the platform for the exchange of metabolites and signals which are essential for the normal function of the organelles. One of the most prominent inter-organelle contact is the one established between the endoplasmic reticulum (ER) and mitochondria. ER-mitochondria contacts are formed in a specialized region in the ER membranes known as Mitochondria-Associated Membranes (MAM), which mediates the exchange of lipids and Ca^{2+} between the two organelles. Mitochondrial Ca^{2+} activates several metabolic enzymes in the mitochondrial matrix, therefore the flux of Ca^{2+} from ER to mitochondria is essential to maintain a normal mitochondrial metabolism and oxidative phosphorylation. Reducing Ca^{2+} flux to mitochondria by increasing ER-mitochondria distance or blocking Ca^{2+} channels at the MAM compromises cellular metabolism due to reduced mitochondrial energy production. However, if mitochondria are overloaded with Ca^{2+}, cell death pathways are activated. To regulate this exchange, the MAM is populated by proteins that control its structure and function. Some of them are tethers that form physical proteinaceous bridges between ER and mitochondria membranes; others participate in the transfer of lipids or Ca^{2+}, like Ca^{2+} channels. One notable group of MAM regulatory proteins are ER chaperones and oxidoreductases, the proteins responsible for one of the main functions of the ER: the folding and maturation of newly synthesized proteins. Chaperones like BiP and Calnexin bind to recently synthesized peptides imported to the ER to assist on the folding and assembly of mature proteins,

and prevent the aggregation of misfolded proteins. Oxidoreductases like ERp57 and TMX1 assist chaperones by catalyzing the formation, reduction and isomerization of disulfide bonds by oxidizing and reducing cysteines in the target protein. These chaperones and oxidoreductases regulate MAM function by binding and/or chemically modifying tethers and Ca^{2+} channels, regulating the extent and distance of ER-mitochondria contacts, and the intensity of the release of Ca^{2+} from the ER.

In this work, we describe the role of the chaperone Calnexin and the oxidoreductase TMX1 in the regulation of MAM function. We found that Calnexin and TMX1 regulate the ER Ca^{2+} pump SERCA, responsible for the loading of Ca^{2+} in the ER, therefore controlling the amount of Ca^{2+} available for Ca^{2+} flux at the MAM. In addition, they regulate MAM formation, controlling the extent and distance of ER-mitochondria contacts. The effect of Calnexin and TMX1 in ER Ca^{2+} loading and ER-mitochondria distance results in the regulation of Ca^{2+} flux to mitochondria, mitochondrial Ca^{2+} content, and mitochondrial metabolism.

We also explored the role of the ER-mitochondria tether Mitofusin-2 in the regulation of MAM function. Mitofusin-2 connects ER and mitochondria together, but the loss of Mitofusin-2 activates an adaptive rescue mechanism that results in increased ER-mitochondria contacts and enhanced mitochondrial metabolism. These adaptations are characterized by the activation of ER stress signalling pathways and rearrangement of MAM protein composition.

Taken together, this doctoral thesis provides new knowledge about the role of Calnexin, TMX1 and Mitofusin-2 in the regulation of MAM tethers and Ca^{2+} channels, their impact on ER-mitochondria contact formation and Ca^{2+} flux to mitochondria, and ultimately their role in the regulation of mitochondrial function. These results provide new links between ER protein folding and energy production in the cell.

Preface

Chapter 3 of this thesis has been published in Raturi, A.; Gutiérrez, T.; Ortiz-Sandoval, C.; Ruangkittisakul, A.; Herrera-Cruz, M. S.; Rockley, J. P.; Gesson, K.; Ourdev, D.; Lou, PH.; Lucchinetti, E.; Tahbaz, N.; Zaugg, M.; Baksh, S.; Ballanyi, K. & Simmen, T. "TMX1 determines cancer cell metabolism as a thiol-based modulator of ER-mitochondria Ca^{2+} flux". *The Journal of Cell Biology*, 2016; 214:433-444. A. Raturi and I were responsible for the experimental design, data collection, data analysis, and manuscript writing, and contributed equally to the work. C. Ortiz-Sandoval assisted with the co-immunoprecipitation experiments and electron microscopy data analysis. N. Tahbaz assisted with the electron microscopy experiments and data collection. E. Lucchinetti, PH. Lou and M. Zaugg assisted with the oxygen consumption rate experiments, data collection and analysis. K. Ballanyi assisted with the fluorescent microscopy experiments, data collection and analysis. T. Simmen was the supervisory author and was involved with concept formation and manuscript composition. The specific contributions are indicated in the figure legends, all other components of this chapter are my original work conducted under the guidance and supervision of Dr. Thomas Simmen.

Chapter 4 of this thesis has been published in Gutiérrez, T.; Qi, H.; Yap, M. C.; Tahbaz, N.; Milburn, L. A.; Lucchinetti, E.; Lou, PH.; Zaugg, M.; LaPointe, P. G.; Mercier, P.; Overduin, M.; Bischof, H.; Burgstaller, S.; Malli, R.; Ballanyi, K.; Shuai, J. & Simmen, T. "The ER chaperone calnexin controls mitochondrial positioning and respiration". *Science Signaling*. 2020; 13 eaax6660. I was responsible for the experimental design, data collection, data analysis, and manuscript writing. M. Yap assisted with the SERCA redox state and subcellular fractionation experiments and data collection. N. Tahbaz

assisted with the electron microscopy experiments and data collection. LA. Milburn assisted with the cellular ATP experiments and data collection. E. Lucchinetti, PH. Lou and M. Zaugg assisted with the oxygen consumption rate experiments, data collection and analysis. P. LaPointe assisted with the SERCA ATPase experiments and data analysis. P. Mercier and M. Overduin assisted with the metabolomics experiments and data collection. K. Ballanyi assisted with the fluorescent microscopy experiments, data collection and analysis. T. Simmen was the supervisory author and was involved with concept formation and manuscript composition. The specific contributions are indicated in the figure legends, all other components of this chapter are my original work conducted under the guidance and supervision of Dr. Thomas Simmen.

Chapter 5 is part of a collaborative work. M. Yap assisted with the subcellular fractionation experiments and data collection. N. Tahbaz assisted with the electron microscopy experiments and data collection. PH. Lou and M. Zaugg assisted with the oxygen consumption rate experiments, data collection and analysis. S. Lingrell and JE. Vance assisted with the phospholipid transfer to mitochondria experiments, data collection and analysis. K. Ballanyi assisted with the fluorescent microscopy experiments, data collection and analysis. P. Mercier and M. Overduin assisted with the metabolomics experiments and data collection. The specific contributions are indicated in the figure legends, all other components of this chapter are my original work conducted under the guidance and supervision of Dr. Thomas Simmen.

Acknowledgements

Thanks to Dr. Simmen for receiving me in his lab. I still remember my first day in Canada (January 2014) and my first contact with the freezing Edmontonian cold. Dr. Simmen kindly was waiting for me at the airport and showed me the city. I'm honored to have been able to work with Dr. Simmen and learned so much in our scientific discussions.

A special thanks to my lab mates. Especially Sol and Carolina. It was really easy for me to adapt to a new country when I could talk sometimes in my mother language. I enormously appreciate the opportunity to share our homesickness about latin food.

Thanks to Arun for allowing me to continue your research.

Thanks to Megan for helping me with some experiments during the last two years of my PhD.

I'll be always grateful to our collaborators, nationals and internationals. They helped us to increase the quality of my work.

The administrative staff of the Cell Biology department deserves all the thanks I can possibly bestow for their invaluable help.

Thanks to my committee members for all your helpful advice through the years.

Last, but not least, my direct family and Fran's family. Even though they lived in Chile, I always felt their support. Thanks to my wife Fran, for being always with me. Thanks for allowing me to work hard and encourage me to do so.

Contents

List of Tables

List of Figures

Chapter 1

Introduction

One of the characteristics of eukaryotic cells is that they contain membrane-bound organelles, like the nucleus, mitochondria and Endoplasmic Reticulum (ER). Even though these are independent structures, they do not perform their function in isolation. They are constantly interacting with each other to perform their functions. These interactions can occur on membrane contact sites: close contacts between the organelles membranes, where they physically interact and exchange molecules and metabolites [1]. One of the most prominent inter-organellar contact site is the one between ER and mitochondria.

1.1 ER-mitochondria contacts and Mitochondria-Associated Membranes

Mitochondria-Associated Membranes (MAM) are a subdomain of the ER membranes that is in close association with mitochondria. This close association is required for the exchange of Ca^{2+}, lipids, and other signalling molecules between the two organelles [2,3]. The first observations of interaction between ER and mitochondria were made in early electron microscopy studies in the 1950s [4,5]. Nevertheless, these reports only showed morphological data, and the role of these contacts was un-

known since no physiological function was associated with them. This changed during the 1990s, when two breakthrough discoveries took place: the exchange of phospholipids and the transfer of Ca^{2+} at the MAM. The structure and function of the MAM will be discussed in the following sections.

1.1.1 Lipid exchange at the Mitochondria-Associated Membranes

Phospholipid synthesis and exchange was the first physiological function attributed to ER-mitochondria contacts [2]. Phospholipids are one of the major components of cellular membranes, and are comprised of a glycerol molecule that joins two hydrophobic fatty acid chains with a hydrophilic phosphate group. The phosphate in the hydrophilic head can be modified by the attachment of an additional group, giving origin to the different forms of phospholipids. For example, the addition of ethanolamine, choline and serine to the phosphate group makes phosphatidylethanolamine (PE), phosphatidylcholine (PC) and phosphatidylserine (PS) respectively [6]. In particular, MAM works as a platform for the synthesis of PE and PC from PS, where mitochondria also play an important role. PS is first synthesized in the ER by Phosphatidylserine Synthase 1 (PSS1) or 2 (PSS2). Newly made PS is preferentially transferred to the mitochondria [7,8], where it is decarboxylated into PE by PS Decarboxylase (PSD) in the inner mitochondrial membrane [9]. Since PS is synthesized in the ER and PSD is exclusively found in the mitochondria, the transfer of PS is essential for PE synthesis. The loss of PSD disrupts mitochondrial morphology resulting in round and fragmented mitochondria and is embryonically lethal [10]. Then, PC is synthesized from mitochondria-derived PE back in the ER by PE-*N*-methyltransferase. Since neither ER nor mitochondria contain the entire biosynthetic pathway required for the synthesis of these phospholipids, an exchange of phospholipids between the two organelles is required for the complete process. The critical understanding of this lipid transfer mechanism was achieved with the preparation of highly purified mitochondria, which showed that there was a fraction of the ER membranes that was tightly associated with mitochondria [2]. These membranes, named Mitochondria-Associated Membranes (MAM), were biochemically different from the rest of the ER; in particular, they were enriched in lipid synthesis enzymes like

PSS1 and PSS2, Diacylglycerol Acyltransferase (DGAT) and Acyl-CoA:cholesterol acyltransferase (ACAT) [11–13]. This close association was the platform for the transfer of PS to mitochondria and PE back to the ER for PC synthesis [7]. Experiments in permeabilized cells where the cytosol was diluted, suggest that this transfer does not require soluble elements like vesicles or transport proteins, only a close attachment between the two organelles is needed, in addition to ATP [14–16]. These findings not only demonstrated that MAM was a biochemically distinct domain of the ER membrane, they also showed that it had a specific function: the synthesis and transfer of lipids between ER and mitochondria.

The transfer of phospholipids between ER and mitochondria is mediated by proteins present in the ER and mitochondria membranes, even though their identity and mechanism of action has not been completely elucidated. In a reconstituted system of isolated organelles *in vitro*, protease treatment of mitochondria surface decreases PS transfer, suggesting the participation of some ER or mitochondrial membrane protein in the process [17]. But the identity of these PS-transferring proteins is not completely clear. In yeast, such function is attributed to the ER-Mitochondria Encounter Structure (ERMES) complex, a tether localized in the ER-mitochondria interface [18,19]. Three proteins in ERMES, Mmm1, Mdm12, and Mdm34, contain Synaptotagmin-like Mitochondrial-lipid binding Protein (SMP) domains, a lipid-binding domain proposed to participate in lipid transfer [20–22]. Mammalian cells do not have an ERMES complex homolog, but the protein PDZD8 is a paralog of Mmm1 and also contains a SMP domain [23]. PDZD8 also localizes in the MAM and tethers ER and mitochondria, increasing their contacts. The loss of PDZD8 results in reduced ER-mitochondria contacts and disruption of Ca^{2+} transfer to mitochondria, but its role in phospholipid transport has not been tested [23]. Another candidate are the Oxysterol-Binding Protein (OSBP)-Related Proteins (ORP), a family of lipid binding proteins that participate in the transport of lipids between membranes, mostly sterols and PI4P [24]. ORP5 and ORP8 are two ER anchored ORPs that mediate the exchange of PS and PI4P between ER and the plasma membrane [25]. ORP5 and ORP8 also localize at the MAM, were they interact with the mitochondrial protein Protein Tyrosine Phosphatase-Interacting Protein 51 (PTPIP51), suggesting that they could also participate in PS transfer to mito-

chondria. Knockdown of ORP5 or ORP8 does not affect the formation of ER-mitochondria contacts, but it disrupts mitochondrial morphology and function [26]. Nevertheless, the effect of ORP5 or ORP8 in PS transport to mitochondria was not tested. Thus, the identity of the ER and mitochondrial membrane proteins responsible for the transfer of phospholipids is still unknown.

1.1.2 Ca^{2+} transfer at the Mitochondria-Associated Membranes

Ca^{2+} is a versatile and ubiquitous second messenger used by all mammalian cells for a wide range of cellular processes. The basic components of the Ca^{2+} signalling machinery are shown in **Figure 1.1**. This machinery is composed of a series of Ca^{2+} pumps, channels and exchangers responsible for the transport and release of Ca^{2+} to and from different cellular compartments. Ca^{2+} signals consist of a transient increase of Ca^{2+} levels in the cytosol generated by the opening of Ca^{2+} channels. These Ca^{2+} channels are located either in the plasma membrane, generating an influx of Ca^{2+} from the extracellular medium; or in the ER membrane, generating a release of Ca^{2+} from the intracellular ER Ca^{2+} stores [27]. ER Ca^{2+} stores maintain a Ca^{2+} concentration that ranges between 500 and 1000 μM, around three orders of magnitude bigger than in the cytosol [28]. The steep gradient of Ca^{2+} concentration is maintained by Sarco/Endoplasmic Reticulum Ca^{2+} ATPase (SERCA), a Ca^{2+} pump located in the ER membranes that transport Ca^{2+} from the cytosol to the ER lumen at the expense of ATP hydrolysis [29]. Vertebrates have three SERCA gene paralogs, each with multiple splice variants. The major SERCA isoforms are the ubiquitous SERCA2b, and the more specialized SERCA2a, present in muscle tissue [30]. ER Ca^{2+} stores can also be refilled by Store Operated Ca^{2+} Entry (SOCE), a Ca^{2+} influx mechanism activated upon ER Ca^{2+} depletion. SOCE is composed by the Ca^{2+} sensing protein Stromal Interaction Molecule 1 (STIM1), located in the ER membrane [31–33]; and the ORAI Ca^{2+} channels located in the plasma membrane [34–36]. Upon ER store depletion, STIM1 moves to ER regions closely associated with the plasma membrane [37], where it binds and opens the ORAI channel triggering the influx of Ca^{2+} [38]. Ca^{2+} can be released from the ER Ca^{2+} through the ubiquitous Inositol Trisphosphate Receptor (IP_3R), a Ca^{2+} channel located in the ER membrane. IP_3R is activated by binding IP_3, which is generated from extracellular ligands that bind

to G-protein coupled receptors, like histamine [39] and ATP [40]. Excitable cells like muscle and neurons also have Ryanodine Receptor (RyR), an ER Ca^{2+} channel that release Ca^{2+} from intracellular stores in response to an influx of Ca^{2+} from the extracellular medium during muscle contraction and synaptic transmission [41]. An additional form of Ca^{2+} release is the passive Ca^{2+} leak, a slow but constitutive form of release mediated by different channels including the translocon, the channel that transport nascent proteins from the cytosol to the ER lumen during proteins synthesis [42].

Mitochondria also play an important role in the regulation of Ca^{2+} signals in the cell. They have been recognized as a Ca^{2+} storing organelle for a long time [43]. Yet, it was not clear how Ca^{2+} crossed the two mitochondrial membranes to reach the mitochondrial matrix, and what was the function of mitochondrial Ca^{2+}. Breakthrough discoveries in the 90s demonstrated that the close proximity between ER and mitochondria is essential for the efficient transfer of Ca^{2+} to the mitochondria [44]. When Ca^{2+} is released from ER Ca^{2+} stores through IP_3R, a transient microdomain of high Ca^{2+} concentration is generated in the proximity of the channel. For this reason, mitochondria that are forming contacts with the ER at the MAM are exposed to Ca^{2+} at a concentration much higher than the concentration reached in the bulk of the cytoplasm [3,45]. After IP_3R opening, Ca^{2+} concentration measurements at the ER-mitochondria interface show that these Ca^{2+} microdomains can reach tenfold higher concentrations than the bulk of the cytoplasm, at least 10 to 20 μM [46,47]. In turn, mitochondria are also equipped with a series of Ca^{2+} channels that allow the transport of Ca^{2+} from the ER-mitochondria interface to the mitochondrial matrix **(Figure 1.1)**. The mitochondrial surface is populated by the pore-forming Voltage-Dependent Anion Channel (VDAC), which makes the outer mitochondrial membrane highly permeable to Ca^{2+} ions and other metabolites [48]. VDAC can be in open or closed states, but in both cases is highly permeable to Ca^{2+} [49]. When Ca^{2+} reaches the inner mitochondrial membrane it can cross into the mitochondrial matrix through the Mitochondrial Ca^{2+} Uniporter (MCU) complex, whose uptake capacity is driven by the inner mitochondrial membrane potential generated by the electron transport chain [50–52]. MCU complex is composed of the pore forming protein MCU [53,54], and other regulatory proteins that modulate its activity. Two of these regulatory proteins are MICU1 and MICU2, which form a heterodimer located in the intermembrane

space that acts as a gatekeeper of mitochondrial Ca^{2+} uptake. They set a threshold that inhibits Ca^{2+} uptake at low cytoplasmic Ca^{2+} concentration, but opens the channel at high Ca^{2+} concentrations [55]. This gating mechanism prevents mitochondrial overload by small changes in Ca^{2+} concentration in the cytoplasm, and allows for efficient Ca^{2+} entry exclusively in the high concentration microdomains at the MAM [56]. Ca^{2+} is extruded from mitochondria via two main mechanisms, the mitochondrial Na^+/Ca^{2+} exchanger (NCLX) and the mitochondrial H^+/Ca^{2+} exchanger (mHCX), that release Ca^{2+} from the matrix in exchange of Na^+ and H^+ respectively [57,58].

The accumulation of Ca^{2+} in the mitochondrial matrix has two functions: the induction of apoptotic cell death, and the activation of the mitochondrial metabolism. They will be described in the following sections.

1.1.2.1 Mitochondrial Ca^{2+} and cell death

Excessive accumulation of Ca^{2+} in the mitochondria is an important inducer of cell death [59]. Indeed, many apoptotic stimuli, like ceramide [60], adriamycin [61], photodynamic therapy [62] and H_2O_2 [63] trigger a release of Ca^{2+} through the IP_3R resulting in mitochondrial Ca^{2+} accumulation and cell death. Mitochondrial Ca^{2+} uptake during this signal depends on VDAC isoform 1, which forms a complex with IP_3R that is strengthened during apoptosis [64]. In the inner mitochondrial membrane, overexpression of MCU also correlates with mitochondrial Ca^{2+} accumulation and increased susceptibility to apoptosis induction by ceramide and H_2O_2 [53]. Similarly, the loss of the MCU gatekeeper MICU1 results in mitochondria constitutively loaded with Ca^{2+}, and enhanced susceptibility to cell death [56]. This excessive accumulation of Ca^{2+} initiates a process known as Mitochondrial Permeability Transition (MPT), which consists on the permeabilization of the inner mitochondrial membrane, loss of mitochondrial potential, disruption of mitochondrial morphology, and loss ATP production [65]. Mechanistically, MPT requires the formation of the mitochondrial Permeability Transition Pore (mPTP), the pore responsible for the permeabilization of the inner mitochondrial membrane. The mPTP is composed of the prolyl isomerase Cyclophilin D, located in the mitochondrial matrix [66], and possibly the ATP synthase [67], even though its precise composition

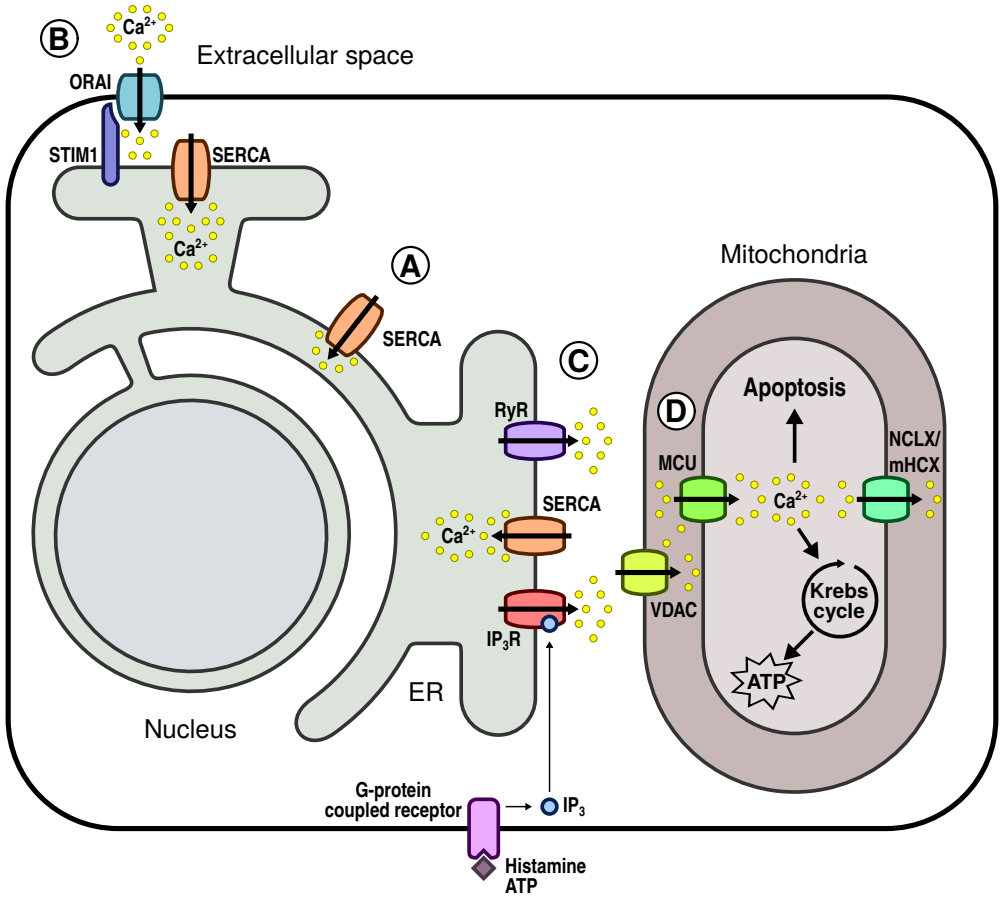

Figure 1.1 – Schematic of the localization and function of the main Ca^{2+} pumps and channels in the cell. ER is the main Ca^{2+} store in the cell, and maintains a Ca^{2+} concentration that ranges 500 to 1000 µM, around three orders of magnitude higher than the cytosol. **(A)** This steep Ca^{2+} concentration difference is maintained by the Ca^{2+} pump Sarco/Endoplasmic Reticulum Ca^{2+} ATPase (SERCA), which takes Ca^{2+} from the cytosol into the ER lumen and maintains ER Ca^{2+} stores. **(B)** To prevent ER Ca^{2+} depletion, ER Ca^{2+} stores can also be filled from the extracellular medium by Store Operated Ca^{2+} Entry (SOCE), composed of the ER Ca^{2+} sensor Stromal Interaction Molecule 1 (STIM1) and the plasma membrane Ca^{2+} channel ORAI. **(C)** Ca^{2+} signals are generated by the release of Ca^{2+} from the ER to the cytosol through the Ca^{2+} channels Inositol Trisphosphate Receptor (IP_3R, ubiquitously expressed) and Ryanodine Receptor (RyR, specific for muscle and neurons). IP_3R are opened by Inositol Trisphosphate (IP_3), which is generated in response to extracellular stimuli like histamine and ATP. When these Ca^{2+} channels are opened, a high Ca^{2+} concentration microdomain forms in their immediate vicinity. **(D)** These Ca^{2+} microdomains are detected by neighboring mitochondria in ER-mitochondria contact sites. The released Ca^{2+} can cross the outer and inner mitochondrial membranes through Voltage-Dependent Anion Channel (VDAC) and the Mitochondrial Ca^{2+} Uniporter (MCU) complex respectively. Inside mitochondria, Ca^{2+} activates mitochondrial respiration and ATP production, but if mitochondria are overloaded with Ca^{2+}, a cell death signalling cascade is activated. Ca^{2+} is extruded from mitochondria through the mitochondrial Na^+ /Ca^{2+} exchanger (NCLX) and the H^+/Ca^{2+} exchanger (mHCX). Once in the cytosol, Ca^{2+} is quickly cleared by SERCA, which takes Ca^{2+} back into the ER lumen.

and mechanism of action is still mater of debate. High levels of Ca^{2+} in the mitochondrial matrix triggers the switch of the mPTP to an open conformation that allows the diffusion of ions, dissipates mitochondrial potential, and releases pro-apoptotic factors to the cytosol [68], making mitochondrial Ca^{2+} a critical component of mPTP mediated cell death. Accordingly, blocking mitochondrial Ca^{2+} entry prevents mPTP opening, even in the presence of an apoptotic stimuli [69]. The permeabilization of the mitochondrial membranes by mPTP also elicits the release of pro-apoptotic factors like Cytochrome C, which binds and activates IP_3R in a feed forward loop that amplifies the apoptotic signal [70]. ER Ca^{2+} stores play an important role in the apoptotic Ca^{2+} signal, and many pro- and anti-apoptotic proteins modulate the Ca^{2+} availability at the ER to regulate cell death. For example, the pro-apoptotic protein p53 promotes the accumulation of Ca^{2+} in the ER, increasing Ca^{2+} availability and Ca^{2+} flux to mitochondria, which results in an enhanced apoptosis induction by adriamycin [61]. Similarly, the anti-apoptotic protein Bcl-2 increases passive ER Ca^{2+} leak and prevents ER Ca^{2+} uptake, resulting in a depletion of ER Ca^{2+} stores, and a reduction of apoptotic Ca^{2+} flux to mitochondria and apoptosis induction by ceramide [60]. Thus, the excessive accumulation of mitochondrial Ca^{2+}, induced either by increased mitochondrial Ca^{2+} uptake or ER Ca^{2+} release, can result in mPTP opening and cell death.

MAM, as the platform for ER-mitochondria Ca^{2+} flux, is also connected to apoptosis signalling. During stress conditions, like nutrient deprivation and ER stress, ER-mitochondria contacts become tighter and more abundant, a condition that favors apoptotic Ca^{2+} flux to mitochondria [71]. In later stages of ER stress, the oxidoreductase Endoplasmic Reticulum Oxidoreductase 1 α (Ero1α) mediates the induction of apoptosis by activating IP_3R and increasing Ca^{2+} flux to mitochondria [72]. Cardiac ischemia/reperfusion is another example of a stressful condition that increases ER-mitochondria contacts. The aforementioned MAM tether PTPIP51 is increased during ischemia/reperfusion, promoting ER-mitochondria contacts, Ca^{2+} flux to mitochondria and apoptosis [73]. Indeed, many proteins localized in the MAM regulate cell death by interacting with IP_3R and modulating its activity and Ca^{2+} flux to mitochondria, such as Promyelocytic Leukemia (PML) [74], Breast and Ovarian Cancer Susceptibility Gene 1 (BRCA1) [75], BRCA1-Associated Protein 1 (BAP1) [76], Phosphatase and

Tensin Homolog Deleted on Chromosome 10 (PTEN) [77], Bcl-XL [78] and mammalian Target of Rapamycin Complex 2 (mTORC2) [79].

1.1.2.2 Mitochondrial Ca^{2+} and metabolism

A basal level of Ca^{2+} transfer to the mitochondria is required for the maintenance of mitochondrial oxidative phosphorylation [80]. More specifically, Ca^{2+} regulates mitochondrial enzymes involved in the Krebs cycle and ATP production. One of these enzymes is the mitochondrial ATP synthase, which is activated by Ca^{2+}, increasing ATP production [81]. In addition, Ca^{2+} activates some mitochondrial dehydrogenases that participate in the supply of NADH and $FADH_2$ to the electron transport chain, increasing the substrates required for mitochondrial ATP production. The first one discovered was glycerol-3-phosphate dehydrogenase, located in the inner mitochondrial membrane, that transfers electrons from cytoplasmic NADH produced in glycolysis to the electron transport chain in the mitochondria in the form of $FADH_2$ [82]. Pyruvate Dehydrogenase (PDH) is part of the pyruvate dehydrogenase complex, the group of enzymes that converts pyruvate in acetyl-CoA, the "point of no return" that links glycolysis with the Krebs cycle and glucose oxidation. PDH is indirectly activated by Ca^{2+} through PDH phosphatase, which is activated by Ca^{2+} and removes an inhibitory phosphorylation in PDH [83]. The last two Ca^{2+} regulated mitochondrial proteins are isocitrate dehydrogenase and oxoglutarate dehydrogenase, two enzymes that catalyze the third and fourth steps of the Krebs cycle respectively [84,85]. Thus, Ca^{2+} can regulate mitochondrial ATP production at two stages; it activates the Krebs cycle and production of reducing agents in the mitochondrial matrix for electron transport chain, and it activates ATP synthase to increase ATP output.

The metabolic control of Ca^{2+} is, in turn, tightly linked to Ca^{2+} signals in the cytosol; the release of Ca^{2+} from the ER is closely followed by an increase in mitochondrial Ca^{2+} and mitochondrial energization [86]. For example, fertilization of mammalian oocytes initiates Ca^{2+} oscillations in the cytoplasm that are required for the activation of development signalling pathways. The cytoplasmic signal is closely mimicked by mitochondrial Ca^{2+} oscillations that stimulate mitochondrial ATP production [87]. This coupling is particularly important for tissues with large energy demands like the

cardiac muscle. In the heart, each contraction is triggered by a release of Ca^{2+} from the ER, a process that can consume a large amount of ATP per contraction, which is mostly provided by mitochondrial respiration [88]. Yet, despite the high ATP turnover, ATP levels remain stable during increased workload, suggesting a coupled signalling between consumption and production of ATP [89]. Ca^{2+} measurements show that mitochondrial Ca^{2+} increases beat by beat following cytoplasmic Ca^{2+}, suggesting that Ca^{2+} used for contraction signalling is also linked to increased mitochondrial respiration [90,91]. Accordingly, preventing the flux of Ca^{2+} to mitochondria after the release of Ca^{2+} through IP_3R results in a reduction in mitochondrial respiration and ATP production. The reduction in mitochondrial energy output reduces cellular energy levels, and activates signalling pathways that aim to restore the energetic balance in the cell [80]. The metabolic sensor AMP-protein Kinase (AMPK) detects low levels of ATP and activates glucose and fatty acid catabolism to restore energy levels [92]; and autophagy is induced to recycle cellular components to synthesise new macromolecules and as fuel for energy production [93]. Similarly, disruption of Ca^{2+} entry to the mitochondria by reducing the expression of the MCU complex gatekeeper MICU1 also results in reduced Ca^{2+} uptake after IP_3R release and impaired mitochondrial respiration, as well as activation of AMPK and autophagy [94]. In skeletal muscle tissue, the deletion of the pore forming unit MCU reduces mitochondrial Ca^{2+} uptake and PDH activity, and shifts the metabolism from glucose oxidation to glycolysis. As a result, the muscle fibres have reduced force generation and impaired exercise performance [95]. In summary, mitochondrial Ca^{2+} activates mitochondrial metabolism and energy production, and this regulation is tightly linked to the flow of Ca^{2+} from ER to mitochondria at the MAM.

1.1.3 Structural features and protein composition of ER-mitochondria contact sites

When observed under the electron microscope, the ER-mitochondria contact sites look like a juxtaposition of the ER membrane with the mitochondrial outer membrane, with the two running in parallel for lengths that can reach several hundreds of nanometers [96]. The distance between organelles is relatively constant along the extension of the contact, but it depends on the type of ER membrane

associated with mitochondria. For smooth ER, the cleft width varies between 10 to 25 nanometers; while in the rough ER, because of the presence of ribosomes, the distance reaches 50 to 80 nanometers [96]. The functional differences between these two forms of ER contacts is unknown, but they are regulated by distinct mechanisms, suggesting specific functions for each one [97]. In general, closer contacts correlates with increased MAM functions like Ca^{2+} and lipids transfer. Nevertheless, there is a limit to the optimal ER-mitochondria distance determined by the size of the Ca^{2+} channels themselves. Using ER-mitochondria spacers with fixed sizes, it was shown that distances of 10 nm were more efficient than 5 nm in terms of Ca^{2+} transfer, probably because there is not enough room to fit IP_3R [46]. Because of the spatial limitations, and the diffusion properties of Ca^{2+}, it has been suggested that the ideal distance for ER-mitochondria Ca^{2+} transfer is between 12 and 24 nm, while shorter distances would be more appropriate for lipid transfer [98].

ER-mitochondria contact sites are not formed simply by the chance of the two organelles lying close. Electron microscopy images show the presence of structures that physically connect the membranes of the two organelles [71]. These structures are protein complexes that tether ER and mitochondria together at the contact sites. Interestingly, there is no master tethering complex that can turn the contacts on or off. Nevertheless, there is a diverse set of tethers that can regulate the extent of ER-mitochondria contact sites in the cell. Perhaps the most studied ER-mitochondria tether is Mitofusin-2 (Mfn2), a GTPase that, together with Mitofusin-1 (Mfn1), mediate mitochondrial fusion [99]. Mitofusins are tail-anchored proteins that are targeted to the mitochondrial surface, where they tether and fuse mitochondria outer membranes by forming homo and heterodimers [99]. But Mfn2, unlike Mfn1, can also be found in the surface of the ER, and can form homodimers tethering ER and mitochondria [100]. The loss of Mfn2 results in alterations in ER and mitochondrial morphology, and also in a reduction of ER-mitochondria juxtaposition and Ca^{2+} transfer from the ER [100]. More details about the Mfn2 function in the MAM will be discussed in chapter 5.

Another example of a MAM tether is the ER protein Vesicle-Associated Membrane Protein-Associated Protein B (VAPB), which binds to the outer mitochondrial membrane Protein Tyrosine

Phosphatase-Interacting Protein 51 (PTPIP51). This interaction is required for normal Ca^{2+} transfer to mitochondria; if any of the two proteins is knocked down, Ca^{2+} flux triggered by a release of Ca^{2+} from the ER is disrupted [101]. Notably, a mutation in the gene encoding VAPB (VAPBP56S) causes Amyotrophic Lateral Sclerosis (ALS). This mutated form of VAPB shows enhanced PTPIP51 binding and induces the clustering of mitochondria in the perinuclear area. As a result, VAPBP56S improves Ca^{2+} transfer to mitochondria, suggesting that an excessive mitochondrial Ca^{2+} accumulation, and increased apoptosis susceptibility, could be responsible for the neurodegenerative effects of this mutant [101].

Some tethers have specific functions in addition to forming physical links. The complex formed by the Ca^{2+} channel IP_3R in the ER surface, VDAC1 on the mitochondrial surface, and the cytosolic chaperone Grp75 is perhaps the tethering complex that better represents the functional and mechanistic link between MAM tethering and Ca^{2+} flux [102]. Both IP_3R and VDAC1 are part of the Ca^{2+} machinery responsible for the transfer of Ca^{2+} to the mitochondria, while GRP75 is a cytosolic member of the HSP70 family of chaperones with a close association with the mitochondrial outer membrane [103]. Mechanistically, IP_3R interacts with VDAC1 increasing mitochondrial Ca^{2+} uptake and Ca^{2+} flux, and GRP75 is required for this interaction [102]. Later studies show that other proteins can regulate the IP_3R-GRP75-VDAC1 complex, modulating its function. The obesity-induced PDK4 also localizes in the MAM and interacts with IP_3R, GRP75 and VDAC1 [104]. Obesity induces an increase in PDK4 levels, stabilizing the IP_3R-GRP75-VDAC1 complex and increasing ER-mitochondria contacts in muscle cells. As a result, these cells show mitochondrial Ca^{2+} overload, reduced mitochondrial ATP production, and are more resistant to insulin signalling. But the inhibition of PDK4 prevented the increased IP_3R-GRP75-VDAC1 complex formation induced by obesity, normalizing mitochondrial Ca^{2+} levels and insulin signalling [104]. Similarly, the Parkinson's Disease (PD)-related protein DJ-1 is also localized in the MAM and interacts with the IP_3R-GRP75-VDAC1 complex. Loss of DJ-1 results in destabilization of IP_3R-GRP75-VDAC1, reduction of mitochondrial Ca^{2+} flux, and disruption of ER-mitochondria contacts [105]. Interestingly, PD-associated DJ-1 mutations are unable to restore normal ER-mitochondria contacts, suggesting that loss of IP_3R-GRP75-VDAC1 could

be associated with PD pathogenesis [105].

Many proteins localized in the MAM regulate the tethering between ER and mitochondria. Because of the close relation between ER-mitochondria distance and MAM function, most tethers also correlate with increased Ca^{2+} and/or lipid transfer. Other examples of tethers and MAM regulators are Apolipoprotein E (ApoE) [106], Mitochondrial antiviral-signalling protein (MAVS) [107,108], Nogo-B [109], Phosphofurin acidic cluster sorting protein 2 (PACS-2) [110] and Thymocyte expressed, positive selection associated 1 (Tespa1) [111].

1.1.4 ER-mitochondria contacts are dynamic structures that change depending on cellular conditions

The dynamic nature of energy requirement suggests that MAM formation could be regulated in order to mediate specific functions. This idea has been explored in previous works that show that ER-mitochondria contacts are dynamic structures. The first observation was that ER and mitochondria contacts became closer and more abundant with apoptosis triggers like removal of growth factors and ER stress. This suggests that increasing ER-mitochondria contacts might be an important step to generate an apoptotic mitochondrial Ca^{2+} signal and ensure the progress of the cell death program [71]. But ER-mitochondria contact dynamics can also be used to boost mitochondrial metabolism. For example, early stages of ER stress promote the movement of mitochondria to the perinuclear area, increasing ER-mitochondria contacts and Ca^{2+} transfer. These adaptations increase mitochondrial respiration and ATP production. This suggests that ER stress induces an early metabolic adaptation that provides the energy required to adapt to the stress [112]. The dynamic nature of MAM has also been observed *in vivo*. In postprandial liver (6 hours after feeding), the hepatocytes show an increased length of ER-mitochondria contacts. The extended contacts are controlled by the inhibition of mTORC1, a master regulator of cell metabolism, suggesting that these changes are part of the hepatocyte metabolic adaptation during the fasting period [96]. Indeed, many metabolic and stress signalling pathways converge at the MAM to regulate MAM protein functions and ER-mitochondria

contact formation, as will be explained below.

We are just beginning to understand how the metabolic and stress sensing systems in the cell communicate with MAM regulatory proteins. Perhaps the most studied condition is ER stress, when there is a change in contact formation and MAM protein composition. ER stress is a cellular stress response triggered by the accumulation of unfolded proteins in the ER or the disruption of the protein folding capacity. During ER stress, the cell aims to recover the ER function by increasing folding capacity and inhibiting protein synthesis, but ER stress results in cell death if homeostasis is not recovered [113]. One of the adaptive mechanisms during ER stress is the change in MAM protein composition. Cellular fractionation experiments show that the ER chaperone CNX usually resides at the MAM, but during ER stress it moves from the MAM to the bulk ER [114]. This change in CNX localization is an adaptive mechanism that increases CNX folding capacity, in order to cope with the accumulation of unfolded proteins, and also increases the transfer of Ca^{2+} to mitochondria, providing the increased energy production required to alleviate the stress [114]. The increase in ER-mitochondria contacts during early ER stress [112] requires the activation of Protein Kinase A (PKA), which also contributes to the improved Ca^{2+} transfer and mitochondrial respiration [115]. PKA acts through the phosphorylation and inhibition of Dynamin-Related Protein 1 (DRP1), a protein involved in mitochondria and ER structure remodelling [115]. Interestingly, PKA activation is shared by early ER stress and the aforementioned mTORC1 inhibition. Nevertheless, these two conditions generate distinctive patterns of ER-mitochondria contacts. mTORC1 inhibition increases ER-mitochondria contacts in the entire cell, with more colocalization of the MAM regulator PACS-2 with mitochondria [116]. On the other hand, during early ER stress, ER-mitochondria contacts increase specifically in the perinuclear region, driven by Mfn2 tethering and a loss of CNX colocalization with mitochondria specifically in the peripheral areas [116]. PACS-2 also regulates the changes to MAM induced by growth factors, like insulin and serum. mTORC2 and Akt are activated and targeted to the MAM in the presence of growth factors. Active Akt at the MAM phosphorylates PACS2. This results in increased ER-mitochondria contacts, Ca^{2+} flux, and mitochondrial function [79]. These works highlight the diverse signalling networks that are integrated in MAM function.

There is an additional layer of control for mitochondria proximity to the ER, and this is Ca^{2+} itself. Mitochondria are connected to the microtubule network, which drives mitochondrial movement around the cell. Mitochondria connect to microtubules through the Ca^{2+} sensitive proteins Miro1 and Miro2, that bind to motor proteins at low Ca^{2+} levels but detach from them at high Ca^{2+} concentration [117]. When Ca^{2+} levels are elevated in the cytoplasm, for example around open ER Ca^{2+}channels, mitochondria stop moving, parking themselves close to the ER [118]. During ER stress there is also an increased leak of Ca^{2+} from the ER to the cytosol. This increased leak is a consequence of the expression of a truncated form of SERCA1, S1T. SERCA1 normally pumps Ca^{2+} from the cytosol to the ER lumen, but S1T cannot pump Ca^{2+} like normal SERCA1. On the contrary, it is a leak channel that releases Ca^{2+} into the cytosol. This leak results in increased ER-mitochondria juxtaposition and improved Ca^{2+} flux [119]. The movement through the microtubular network driven by the increased Ca^{2+} leak is required for the rearrangement of mitochondria in early stages of ER stress [112]. Thus, ER-mitochondria contacts are increased during ER stress by triggering the movement of mitochondria towards the ER through the microtubule network driven by ER Ca^{2+} leak.

In summary, ER-mitochondria contacts are not a static set of tethers and Ca^{2+} channels, they are dynamic structures that change depending on cellular conditions. Contact formation can increase energy production as an adaptive mechanism to cope with stress or as a metabolic adaptation. Different tethers, MAM regulators and Ca^{2+} channels coordinate their function to adjust MAM to the cellular needs. It is important to gain a better understanding on how MAM tethers and regulators are targeted by cellular signals in order to dynamically mold MAM in response to the cell requirements.

1.2 MAM regulation by ER chaperones and oxidoreductases

Protein folding is one of the main functions of the ER. The ER contains a diverse set of chaperones, oxidoreductases and folding assistants that participate in the correct folding of newly synthesized proteins. Notably, many of these proteins are also localized in the MAM. The following section will describe the function of some MAM localized chaperones and oxidoreductases, and how they regulate

ER-mitochondria contacts and/or Ca^{2+} signalling at the MAM.

1.2.1 Protein folding and maturation in the ER

Protein folding is one of the most studied activities of the ER. The successful folding of newly synthesized proteins depends on three critical steps: import of proteins to the ER, folding by chaperones, and addition of secondary modifications. A series of chaperones, lectins and oxidoreductases working in close association take the bulk of the enzymatic work required for functionally folded proteins [120]. ER-targeted proteins are co-translationally imported into the ER lumen through the translocon, a pore-forming protein complex in the ER membrane that is associated to the ribosomes on the cytosol and to chaperones on the ER lumen. One of the main ER chaperones is BiP, which is associated with the translocon and binds to hydrophobic residues in the nascent peptide as soon as it enters the ER, preventing protein aggregation and assisting the protein to reach its mature conformation [121].

One of the secondary modifications during protein folding is *N*-glycosylation, the addition of a branched oligosaccharide to the peptide. The oligosaccharide consists on three glucoses, nine mannoses, and two *N*-acetylglucosamines, and is transferred to the target protein by Oligosaccharyltransferase in a specific sequence in the target protein, usually Asn-Xaa-Ser/Thr (Xaa can be any amino acid except for proline) [122]. The three glucoses in the tip of one of its branches function as a code that indicates the folding stage of the protein. ER glucosidases trim the top two glucoses forming the mono-glucosylated oligosaccharide that is recognized by the lectins Calreticulin (CRT) and Calnexin (CNX) [123]. These lectins are chaperones that assist in glycosylated protein folding and prevent aggregation and degradation of unfolded intermediates [124,125]. The destiny of CRT/CNX client glycoproteins depends on the interplay between α-glucosidase II and UDP-glucose:glycoprotein glucosyltransferase 1 (UGGT1). α-glucosidase II trims the last glucose in the mono-glucosylated oligosaccharide, preventing CRT/CNX binding [126]. Then, UGGT1 can detect if the glycoprotein is misfolded and re-mono-glucosylate the glycan, returning the protein back for another CRT/CNX folding cycle [127]. If the protein is properly folded, it proceeds to the Golgi apparatus. Glycoproteins that are retained in the CNX cycle for prolonged periods of time have a mannose from another

branch trimmed by ER mannosidase I. This reduces UGGT1 affinity and glucosylation, preventing further reentry to the cycle and targeting the glycoprotein for degradation [128].

The second form of secondary modification during protein folding is the formation of disulfide bonds, a covalent bond between the free thiol groups of two cysteines. This modification is catalyzed by the Protein Disulfide Isomerase (PDI) family proteins, a diverse group of oxidoreductases characterized by the presence of a thioredoxin-like domain, the catalytic domain that contains two critical cysteines in a CXXC motif [129]. A schematic of the reaction of PDI family oxidoreductases with their target protein is shown in **Figure 1.2**. When the thioredoxin domain is in its oxidized state, the two cysteines in the catalytic site form a disulfide bond. In this oxidized state, PDI oxidoreductases can catalyze the formation of disulfide bonds by taking the electrons from the reduced cysteines in the target protein, transferring its disulfide bond to the cysteines in the target protein, and leaving the thioredoxin domain in a reduced state. Some members of the PDI family reduce or isomerize the disulfide bonds in the target protein, breaking or reorganizing the bonds; these oxidoreductases maintain their thioredoxin domain in its reduced state and transfer electrons to the oxidized cysteines in the target protein in order to reduce the disulfide bond. This isomerization of disulfide bonds is a process required for the correct folding of some proteins [130]. Thus, some PDIs oxidize and others reduce target proteins, depending on their oxidation state and the redox environment. An equilibrium between oxidized and reduced forms must be maintained to balance oxidation and isomerization reactions during the folding process. The maintenance of an oxidative environment inside the ER is required for disulfide bond formation by PDIs, and the addition of reducing agents like dithiothreitol (DTT) stops this process [131]. ERp57 is an ER oxidoreductase of the PDI family that links disulfide bond formation with glycosylation; it interacts with the chaperones CNX and CRT, which allows it to target preferentially glycoproteins for disulfide bond formation [132]. Other oxidoreductases of the PDI family have a preferential reductase function, and act mostly by reducing disulfide bonds. One example is Thioredoxin-related Transmembrane Protein 1 (TMX1), one of the four members of the TMX subgroup of PDI oxidoreductases, a group characterized by the presence of a transmembrane domain [133]. As other ER oxidoreductases, TMX1 assists in protein folding but with a preference

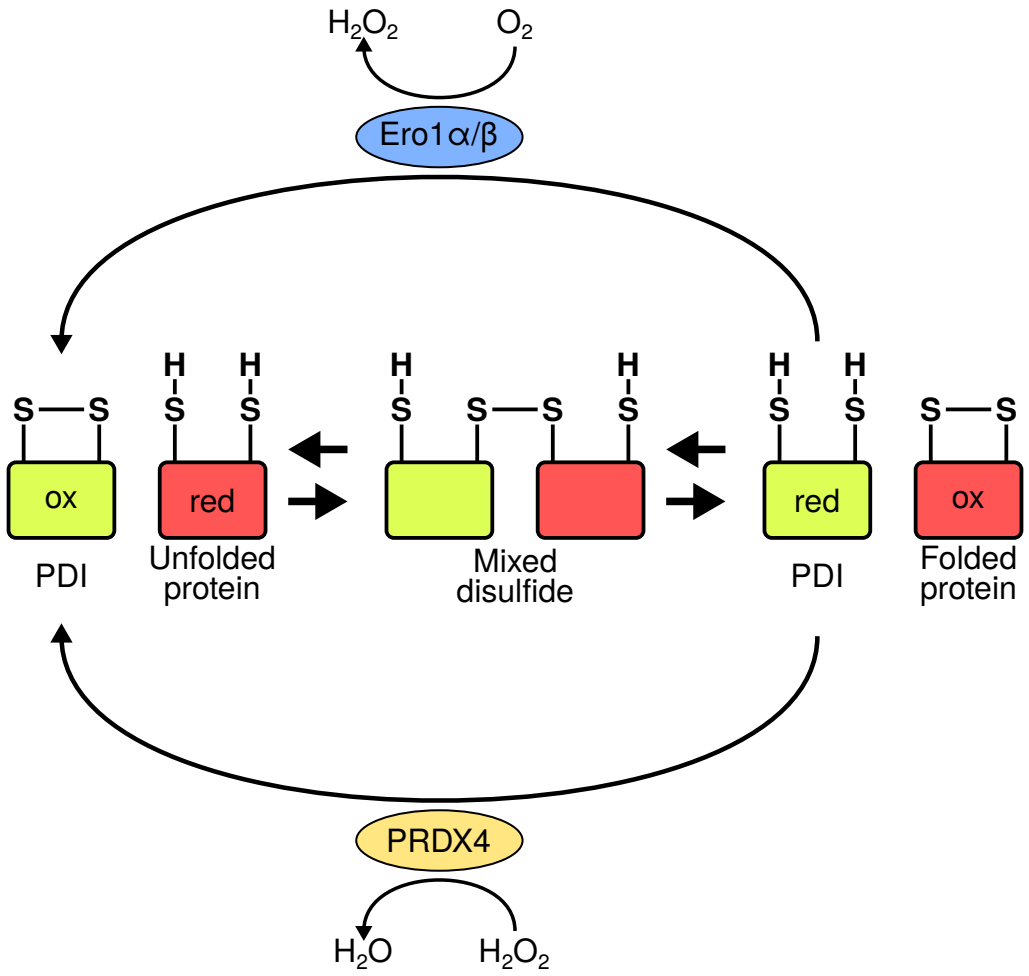

Figure 1.2 – Schematic of the disulfide bond exchange reaction by PDI proteins during protein folding. ER oxidoreductases of the PDI family catalyze the formation of disulfide bonds in newly synthesized proteins when the two cysteines in their active site are oxidized (left). The PDI oxidoreductase forms a transient mixed disulfide with the target protein (center) before completing the transfer of the disulfide bond (right). This results with the PDI oxidoreductase in its reduced state, and the target protein in its oxidized state and mature conformation. To start a new oxidation cycle, the cysteines in the catalytic site of the PDI oxidoreductase must be re-oxidized. There are two proteins that catalyze this re-oxidation: the Endoplasmic Reticulum Oxidoreductase 1 (Ero1) proteins Ero1α and Ero1β, which transfer the electrons from the reduced PDI to O_2, producing H_2O_2 as a result (top); and Peroxiredoxin IV (PRDX4), which transfer the electrons from reduced PDI to H_2O_2, producing H_2O as a result (bottom). Some oxidoreductases of the PDI family, like TMX1, catalyze the reduction of disulfide bonds. The reaction of these reductases proceed from right to left in the schematic; they start in a reduced state, and transfer electrons to the target protein to remove the disulfide bond.

for transmembrane proteins, and is also closely associated with CNX [134,135]. TMX1 participates more in later stages of protein folding, like retention and isomerization of disulfide bonds of misfolded proteins rather than early stages of disulfide bond formation, and its thioredoxin domain is mostly in its reduced form [134,136]. TMX1 also reduces disulfide bonds of terminally misfolded proteins for their export in ER-Associated Degradation (ERAD), the process of translocating misfolded proteins in the ER lumen to the cytosol for their proteasomal degradation [137,138].

Once the thioredoxin domain transfers the disulfide bond, it is left in its reduced state. In order to continue forming disulfide bonds, the thioredoxin domain has to be recycled to its oxidized state. The reoxidation is catalyzed by Endoplasmic Reticulum Oxidoreductase 1 (Ero1) proteins, which transfers electrons from reduced oxidoreductases to O_2, forming H_2O_2 as a product [139,140]. Mammals have two Ero1 paralogs: Ero1α and Ero1β. Both have similar function, but Ero1α is ubiquitously expressed while Ero1β is mostly expressed in secretory cells in gut, pancreas, testis, liver, appendix, thyroid, and pituitary gland [141,142]. An additional reoxidation mechanism parallel to the Ero1 system is catalyzed by antioxidant enzyme Peroxiredoxin IV (PRDX4) [143]. PRDX4 transfers electrons from reduced oxidoreductases to H_2O_2 generated by Ero1 or other ER H_2O_2 sources, and produces H_2O [144].

1.2.2 ER chaperones and oxidoreductases are targeted to the MAM and regulate Ca^{2+} flux

Many of these chaperones and oxidoreductases are targeted to the MAM, and have secondary functions in addition to protein folding. Some of them can move between the MAM and the bulk of the ER in response to cellular signals, with specific functions depending on the location [145].

CNX is one of the ER chaperones targeted to the MAM. The two lectin chaperones, CRT and CNX, share their activity as folding assistants of glycoproteins and have a similar structure; the main difference between them is that CRT is a soluble protein inside the ER lumen, while CNX is a transmembrane protein. The short cytosolic domain of CNX is a target for different post-translational

modifications that control CNX function, interaction with other proteins, and distribution in the ER. CNX cytosolic domain harbours two cysteines that form part of a palmitoylation site near the transmembrane domain; the palmitoylation of CNX in these cysteines is the switch that targets CNX to the MAM. If the palmitoylation sites are mutated, CNX does not localize to the MAM and is redistributed to the bulk of the ER membranes [146]. Interestingly, non-palmitoylated CNX participates more actively in protein folding and maturation, suggesting that palmitoylation also controls CNX chaperoning activity [114]. In addition, palmitoylation regulates CNX interaction with other proteins. In the MAM, palmitoylated CNX interacts with the ER Ca^{2+} pump SERCA2b, while non-palmitoylated CNX interacts with its folding partner the oxidoreductase ERp57, accordingly with its increased folding activity [114]. The palmitoylation of CNX also increases the interaction with and stabilization of the ribosome-translocon complex, and moves CNX to the ribosome-decorated rough ER [147]. Since MAM can be formed by either rough or smooth ER, this interaction suggests that palmitoylation leads CNX to a type of MAM enriched in ribosomes [97,98]. Similar to palmitoylation, the cytoplasmic domain of CNX can also be modified by phosphorylation in three serines [148]. The phosphorylation in CNX cytoplasmic region in serine 583 by ERK-1 promotes the interaction with ribosomes [149] and SERCA2b [150]. The two other phosphorylation sites in serines 554 and 564, controlled by CK2, also promote interaction with ribosomes, presumably increasing CNX glycoprotein folding activity [149]. Notably, the CK2 phosphorylation controls the interaction of CNX with the sorting protein PACS-2, a regulator of ER-mitochondria contact formation [110]. The non-phosphorilated CK2 sites interact with PACS-2 and promotes the retention of CNX in the MAM [151]. The palmitoylation of CNX is a reversible modification, and it can change depending on cellular conditions, with the corresponding change in CNX localization. For example, during ER stress CNX palmitoylation is lost and CNX moves from the MAM to the ER to support protein folding [114].

The dynamic regulation of CNX location and interacting partners points at the multiple roles of CNX in the ER. In addition to its glycoprotein folding duties, CNX also regulates Ca^{2+} signalling through its interaction with SERCA2b. This was first studied in *Xenopus* oocytes, where SERCA2b interaction

with CNX reduced intracellular Ca^{2+} oscillations, suggesting a lower SERCA2b activity [150]. A later report showed that CNX silencing reduced ER Ca^{2+} uptake in cardiomyocytes, suggesting that CNX increases SERCA activity [152]. Similarly, a previous work from our lab shows that CNX interacts with SERCA2b and increases ER Ca^{2+} content, suggesting that CNX activates SERCA2b. The loss of CNX not only results in a decrease in ER Ca^{2+} content, it also increases the transfer of Ca^{2+} from the ER to mitochondria, but not the release of Ca^{2+} from the ER to the cytoplasm [114]. This suggests that the loss of CNX increases ER mitochondria contacts making Ca^{2+} flux to mitochondria more efficient. The mechanism that CNX uses to regulate SERCA2b activity is still unclear, but it is associated with CNX palmitoylation and MAM targeting [114].

The ER oxidoreductase of the PDI family ERp57 can also modulate SERCA activity. This was demonstrated by measuring cytosolic Ca^{2+} oscillations in *Xenopus* oocytes, whose frequency depends on SERCA activity [153]. The co-expression of ERp57 and SERCA2b resulted in a reduction in the frequency of Ca^{2+} oscillations compared to the expression of SERCA2b alone, suggesting that ERp57 have an inhibitory effect on SERCA activity [154]. Two lumenal cysteines in one of the loops in SERCA2b were required for the inhibitory effect of ERp57; if these cysteines were mutated, the effect of ERp57 on SERCA was lost. Similarly, a mutant ERp57 without oxidoreductase activity was also unable to inhibit SERCA2b, suggesting that ERp57 inhibits SERCA2b by forming an inhibitory disulfide bond in one of SERCA2b lumenal loops [154]. This inhibitory mechanism is counteracted by another member of the PDI family proteins, the ER reductase ERdj5, which targets SERCA2b when ER Ca^{2+} content is low to reduce the lumenal disulfide bond resulting in SERCA2b activation [155]. TMX1 is another oxidoreductase that could potentially regulate SERCA2b, but its effects are currently unknown. TMX1 localizes in the MAM with a mechanism very similar to CNX, a palmitoylation on its cytosolic domain, close to the transmembrane domain. The loss of this palmitoylation site results in a relocation of TMX1 to the bulk of the ER [146]. Its MAM targeting and close interaction with CNX suggest that it might also regulate ER Ca^{2+} content through SERCA2b regulation, but this remains to be tested.

In addition to the disulfide bond on the lumenal side, other forms of oxidative modifications also regulate SERCA2b activity. For example, the apoptosis inducer adriamycin activates SERCA2b, resulting in increased ER Ca^{2+} content, and improved apoptotic Ca^{2+} transfer to the mitochondria that results in cell death [61]. During this process, the tumor suppressor p53 is targeted to the MAM and also interacts with SERCA2b, increasing its activity and promoting apoptosis. Cells that lack p53, like cancer cells, show reduced SERCA2b activity and apoptotic Ca^{2+} signalling during apoptosis induction by adriamycin. This apoptosis resistance is a consequence of an increased level of SERCA2b *S*-sulfenylation, an oxidative modification that inhibits SERCA2b activity and prevents apoptotic Ca^{2+} signalling. Thus, by acting as a reducing agent, p53 prevents the inhibitory SERCA2b oxidation and maintains SERCA2b activity during apoptosis [61]. In general, the addition of oxidizing agents result in the inactivation of SERCA, most likely due to oxidative modifications in some of its cysteines [156–158]. However, oxidative modifications can also increase SERCA activity under certain conditions. Nitric Oxide (NO) seems to play an important role in increasing SERCA activity. For example, in vascular smooth muscle cells, NO induces a reduction in cytosolic Ca^{2+} levels and muscle relaxation that depends on SERCA activity [159]. The key modification is a *S*-glutathionylation in Cys674 induced by NO, which has been associated with increased SERCA activity [160,161]. But the type of oxidative modification is critical for activity induction. If the same Cys674 is sulfonylated, SERCA is inhibited and the activating effect of *S*-glutathiolation is lost [162].

Another ER oxidoreductase that regulates Ca^{2+} signalling is Ero1α, which also localizes in the MAM under normal conditions, but loses its MAM localization upon the reduction of the ER environment [163]. In particular, Ero1α increases the passive leak of Ca^{2+} from the ER, and also the release through IP_3R and Ca^{2+} flux to mitochondria [164]. Ero1α plays an important role in apoptosis induction activated by the pro-apoptotic transcription factor CHOP during later stages of ER stress [165]. CHOP increases the expression of Ero1α, which activates IP_3R resulting in an increase of Ca^{2+} release from the ER and apoptotic Ca^{2+} flux [72]. Opposing the activatory effects of Ero1α is the oxidoreductase ERp44, which binds to IP_3R and inhibits Ca^{2+} release [166]. ERp44 inhibition depends on the binding of reduced cysteines in the third lumenal loop found in IP_3R isoform 1, but

not in isoforms 2 or 3. This inhibitory effect is not related to ERp44 oxidoreductase activity, but it does require a reducing redox environment in the ER [166]. The requirement of reduced cysteines inside the ER indicates that the lumenal redox environment regulates the inhibitory effect of ERp44. Accordingly, lumenal ROS production from Ero1α has an activatory effect on IP_3R, in part due to reduced IP_3R1-ERp44 interaction [164]. The activatory effect of Ero1α can also be observed in the heart, where Ero1α knockout mice have reduced Ca^{2+} signal amplitude in cardiomyocytes. As a result, mutant Ero1α mice hearts have impaired contractility, but are also protected against heart failure generated by sustained workload stress [167].

Other oxidative modifications on the cytosolic loops in IP_3R also have an activatory effect on Ca^{2+} release. Exposure of IP_3R to different forms of ROS species causes oxidation of cytosolic cysteines and sensitization of the receptor to IP_3, leading to an increase in the release of Ca^{2+} from the ER [156,168–170]. This is also observed in the regulatory effect of mitochondrial ROS on IP_3R. When Ca^{2+} is released from the ER through IP_3R and enters the mitochondrial matrix, there is a concomitant influx of K^+ and H_2O to the mitochondria. This causes a swelling of mitochondrial matrix and a decrease in mitochondrial cristae volume that provokes a release of H_2O_2 contained within the cristae. This creates a microdomain of high H_2O_2 concentration in the ER-mitochondria interface, similar to the Ca^{2+} microdomain in the proximity of Ca^{2+} channels. This results in an activation of IP_3Rs located close to mitochondria [171]. Thus, both Ca^{2+} and ROS microdomains are used at the ER-mitochondria contact sites to communicate signals.

In summary, some ER chaperones and oxidoreductases are localized in the MAM, where they regulate Ca^{2+} channels like IP_3R and SERCA by protein-protein interactions or oxidative modifications. As a result, these chaperones and oxidoreductases modulate the flux of Ca^{2+} from ER to mitochondria, regulating mitochondrial metabolism and cell death.

1.3 Thesis objective

Given the role of MAM in the regulation of cellular metabolism and apoptosis induction, it is important to have a better understanding of how it is regulated. Many proteins located at the ER-mitochondria interface are known regulators of MAM function. Some of them are tethers that connect ER and mitochondria, others regulate Ca^{2+} channels localized in the MAM. As a consequence, these MAM regulators can control the flux of Ca^{2+} from ER to mitochondria, the critical step that controls mitochondrial metabolism and apoptosis induction. Interestingly, many ER chaperones and oxidoreductases, usually associated with oxidative protein folding, are located at the MAM and regulate Ca^{2+} flux. The goal of my work is to gain a better understanding of these diverse MAM regulatory proteins, with a focus on TMX1, CNX and Mfn2.

TMX1 is an ER oxidoreductase that is localized in the MAM, but its MAM functions have not been characterized. In chapter 3, **TMX1 determines cancer cell metabolism as a modulator of ER-mitochondria Ca^{2+} flux**, I will study how TMX1 regulates SERCA2b activity, ER Ca^{2+} content, Ca^{2+} flux to mitochondria, and the formation of ER-mitochondria contacts. Then, I will evaluate the effects of these Ca^{2+} regulation in mitochondrial function, particularly in cancer cells.

CNX is an ER chaperone that is also localized in the MAM. It can bind to SERCA2b and regulate ER Ca^{2+} content and flux to mitochondria, suggesting a regulation of SERCA2b Ca^{2+} pumping activity. Nevertheless, the mechanism of SERCA2b regulation, and the consequences for ER-mitochondria contact formation and mitochondrial function by CNX are unknown. In chapter 4, **Calnexin regulates ER-mitochondria contact formation and Ca^{2+} flux**, I will study the mechanism of SERCA2b regulation by CNX, and the effect of CNX in ER-mitochondria contacts, Ca^{2+} flux to mitochondria, and mitochondrial function.

Mfn2 participates in mitochondrial fusion, but is also localized in the ER. It was originally described as a MAM tether, forming dimers that connect ER and mitochondria. Nevertheless, there are conflicting results regarding the effect of Mfn2 in the formation of ER-mitochondria contacts. In chapter 5, **ER stress compensates for the loss of Mitofusin-2 ER-mitochondria tethers**, I will study the role

of Mfn2 in ER-mitochondria contact formation. Even though Mfn2 was characterized as a tether between ER and mitochondria, cells that lack Mfn2 have more ER-mitochondria contacts. I will investigate the adaptive mechanisms activated by the loss of Mfn2, including the formation of a novel MAM protein complex that promotes ER-mitochondria contacts during ER stress.

Together, this work will provide new knowledge about the MAM regulatory functions of TMX1, CNX and Mfn2, and a better understanding of the complex interplay between tethers, chaperones and oxidoreductases in the regulation of MAM function. These results will provide new links between ER protein folding and the regulation of ER-mitochondria contacts and mitochondrial function.

Chapter 2

Material and Methods

2.1 Reagents

Table 2.1 – Chemicals and reagents

Reagent	Supplier
10x Phosphate Buffered Saline	Cellgro Mediatech, Inc.
25x Complete Protease Inhibitors	Roche
Acetone	BDH Chemicals
Acrylamide	BioRad
Ammonium Persulfate	BioRad
Ampicillin	Sigma
Bovine Serum Albumin	Sigma
Bromophenol Blue	BioRad
CellROX	Thermo Fisher Scientific
CHAPS	Sigma-Aldrich
Dulbecco's modified eagle medium	Gibco

Table 2.1 – Chemicals and reagents *(continued)*

Reagent	Supplier
EDTA	EMD
EGTA	Sigma-Aldrich
EMbed 812	Electron Microscopy Sciences
Fetal Bovine Serum	Gibco
Fluo-8	AAT Bioquest
Geneticin	Thermo Fisher Scientific
Hanks' Balanced Salt solution, no calcium, no magnesium, no phenol red	Gibco
Hanks' Balanced Salt solution, with calcium, with magnesium, no phenol red	Gibco
HEPES	Sigma
Hygromycin B	Invitrogen
Metafectene Pro	Biontex
MitoSOX	Thermo Fisher Scientific
MitoTracker Deep Red FM	Invitrogen
MitoTracker Green FM	Invitrogen
Oligofectamine	Invitrogen
OptiMEM	Gibco
Percoll	GE Healthcare
PhosSTOP	Roche
poly-L-lysine	Sigma
Precision Plus Protein Dual Colour Standards	BioRad
Propylene Oxide	Electron Microscopy Sciences

Table 2.1 – Chemicals and reagents *(continued)*

Reagent	Supplier
Protein A Sepharose Beads CL-4B	GE Healthcare
Puromycin	Thermo Fisher Scientific
Pyruvate Kinase / Lactate Dehydrogenase	Sigma
Sodium azide	ICN Biomedical Inc.
Sodium dodecyl sulphate (SDS)	J.T. Baker
Tetramethylethylenediamine (TEMED)	OmniPur/EMD
TMRM	Sigma
Trans-blot nitrocellulose	BioRad
Tris	Bio Basic Inc.
Triton X-100	Sigma
Trypsin 2.5%	Gibco
B-Mercaptoethanol	BioShop

Table 2.2 – Buffers and solutions

Buffer	Methodology	Composition
ATPase Reaction buffer	ATPase assay	50 mM HEPES pH 7.2, 125 mM NaCl, 1 mM MgCl2, 0.1 mM CaCl2, 1 mM DTT, 0.6 mM NADH, 2 mM ATP, 1 mM phosphoenol pyruvate, 2.5 μL of pyruvate kinase/lactate dehydrogenase, 0.02% DMSO
Membrane Resuspension Buffer (MRB)	ATPase assay	50 mM HEPES pH 7.2, 125 mM NaCl, 1 mM MgCl2

Table 2.2 – Buffers and solutions *(continued)*

Buffer	Methodology	Composition
CHAPS lysis buffer	Cell lysates preparation	1% CHAPS, 10 mM Tris pH 7.4, 150 mM NaCl, 1 mM EDTA
Sample buffer	Cell lysates preparation	60 mM Tris-HCL pH 6.8, 2% SDS, 10% glycerol, 10% β-mercaptoethanol, 0.004% bromophenol blue
PBS	Cell lysates preparation, Lipid transfer, Subcellular fractionation, SPLICS, SERCA redox	137 mM NaCl, 2.7 mM KCl, 10 mM Na2HPO4, 1.8 mM KH2PO4 pH 7.4
Hanks' Balanced Salt Solution with Calcium (HBSS/Ca)	Confocal fluorescence microscopy Calcium measurements, Mitochondrial membrane potential, Mitochondrial dynamics	0.34 mM Na2HPO4 pH 7.4, 137.93 mM NaCl, 4.17 mM NaHCO3, 0.44 mM KH2PO4, 5.33 mM KCl, 0.41 mM MgSO4, 0.49 mM MgCl2, 1.26 mM CaCl2, 5.55 mM Glucose
Hanks' Balanced Salt Solution without Calcium (HBSS/noCa)	Confocal microscopy Calcium measurements	0.34 mM Na2HPO4 pH 7.4, 137.93 mM NaCl, 4.17 mM NaHCO3, 0.44 mM KH2PO4, 5.33 mM KCl, 0.41 mM MgSO4, 1.75 mM MgCl2, 5.55 mM Glucose, 0.1 M EGTA
Electron Microscopy fixation buffer	Electron microscopy	2% paraformaldehyde, 2% glutharaldehyde and 100 mM Sodium Cocadylate pH 7.4
Sodium Cocadylate (Cacod) buffer	Electron microscopy	100 mM Sodium Cocadylate pH 7.4

Table 2.2 – Buffers and solutions *(continued)*

Buffer	Methodology	Composition
Hanks' Balanced Salt Solution with Calcium and BSA (HBSS/Ca/BSA)	Fluorometer Calcium measurements, Reactive oxygen species	0.1% BSA, 0.34 mM Na2HPO4 pH 7.4, 137.93 mM NaCl, 4.17 mM NaHCO3, 0.44 mM KH2PO4, 5.33 mM KCl, 0.41 mM MgSO4, 0.49 mM MgCl2, 1.26 mM CaCl2, 5.55 mM Glucose
Mitochondria Homogenization Buffer (MHB)	Subcellular fractionation, ATPase assay	10 mM HEPES-OH pH 7.4, 1 mM EDTA, 1 mM EGTA, 250 mM Sucrose
4x Separating Gel buffer	Western blot	1.5 M Tris pH 8.8, 0.4% SDS
4x Stacking Gel buffer	Western blot	0.5 M Tris pH 6.8, 0.4% SDS
Gel Running buffer (SDS-PAGE)	Western blot	25 mM Tris, 200 mM Glycine, 0.1% SDS
Membrane Blocking buffer	Western blot	10 mM Tris pH 8.0, 150 mM NaCl, 0.05% Triton X-100, 2% BSA
TBS-T	Western blot	10 mM Tris pH 8.0, 0.15 M NaCl, 0.05% Triton X-100

Table 2.3 – Inhibitors and drugs

Inhibitor or drug	Effect	Concentration	Supplier
2-Deoxy-D-glucose (2-DG)	Inhibits glycolysis	25 mM	Tocris
ATP	Activates IP3R	600 μM (MEF) and 50 μM (HeLa and A375p)	Sigma
BAPTA-AM	Chelates intracellular calcium	10 μM	Thermo Fisher Scientific
EN460	Inhibits Ero1α and Ero1β	25 μM	Sigma
FCCP	Dissipates mitochondrial potential	10 μM	Sigma
GKT-137831 (GKT)	Inhibits NOX4	5 μM	Focus Biomolecules
GSK-2606414 (GSK)	Inhibits PERK	10 μM	Tocris
Histamine	Activates IP3R	50 μM	Sigma
N-Acetyl-L-cysteine	Antioxidant	5 mM	Sigma
Oligomycin	Inhibits mitochondrial ATP synthase	1 μM	Sigma
Rotenone	Inhibits mitochondrial Complex I	1 μM	Sigma
tert-Butylhydroquinone (TBHQ)	Inhibits SERCA	60 μM	Sigma
Thapsigargin	Inhibits SERCA	10 μM	Alexis Biochemicals
Tunicamycin	Inhibits protein glycosylation, activates ER stress	1 μg/mL	Alexis Biochemicals

Table 2.4 – Commercial kits

Kit	Supplier
ATP Determination kit	Molecular Probes
EZ-Link Iodoacetyl-PEG2-Biotin (BIAM) kit	Thermo Fisher Scientific
Mouse Embryonic Fibroblast Nucleofector Kit 1	Lonza
Pierce BCA Protein Assay Kit	Thermo Fisher Scientific
QIAGEN plasmid midi kit	QIAGEN
TXNDC (TMX1) Human Gene Knockout Kit (CRISPR)	OriGene

2.2 Cell culture

2.2.1 Maintenance of cell lines

Cell lines were cultured at 37°C with 5% CO_2 and humidified air. They were passaged every two to three days to a maximum passage number of 50. The regular culture media consisted of DMEM with 10% FBS. The cell lines used in this work are listed in **Table 2.5**.

2.2.2 Plasmid-based transfection

Transfection of exogenous plasmids was used to express specific genes in the cells. Two different transfection methods were used depending on the cell line and experiment, as described in each experiment. The method used depended on the transfection efficiency for each cell line. In general, MEF cells had better efficiency with electroporation, and HeLa and A375p cells had better efficiency with lipid base transfection.

2.2.2.1 Electroporation-based transfection

Electroporation was applied on MEF cells using a Amaxa Nucleofector 2b Device (Lonza) and the MEF 1 Nucleofector kit. Following manufacturer's instructions, 2×10^6 MEF cells were transfected with 5 μg of plasmid using the A-023 program. For microscopy experiments, the transfected cells were seeded in poly-L-lysine coated 12 mm glass coverslips in 24-well plates at a concentration of 3×10^5 cells per well and kept them growing for 24 hours before the experiments. For other experi-

Table 2.5 – Cell lines

Cell line	Source
A375P	Wellcome Trust Functional Genomics Cell Bank
HeLa	European Collection of Authenticated Cell Cultures (ECACC)
HeLa TMX1 wild type	Made with CRISPR
HeLa TMX1 knockout	Made with CRISPR
MEF CNX wild type	Dr. Marek Michalak, Department of Biochemistry, University of Alberta
MEF CNX knockout	Dr. Marek Michalak, Department of Biochemistry, University of Alberta

ments, cells were seeded as described in each experiment.

2.2.2.2 Lipid based transfections

Cells were seeded in 6-well plates at a concentration of 5×10^5 cells per well. For each well, 3 μg of plasmid and 9 μL of Metafectene Pro (Biontex) were mixed in 200 μL of Opti-MEM (Thermo Fisher Scientific), and incubated for 20 minutes at room temperature. Then, this solution was added to the cells (on top of 2 mL of regular medium) and incubated for 4 hours. After the incubation, the medium was changed to fresh culture media. Cells were grown for another 24 to 48 hours, as described in each experiment.

2.2.3 siRNA mediated knockdown

Cells were seeded in 6-well plates at a concentration of 1×10^6 cells per well. A solution containing 10 μL of 20 μM siRNA (scrambled siRNA for controls) and 4 μL of Oligofectamine (Thermo Fisher Scientific) mixed in 200 μL of Opti-MEM (Thermo Fisher Scientific) was prepared for each well. The mix was incubated for 30 minutes at room temperature. Then, the cell culture media was replaced with 800 μL of Opti-MEM, and the 200 μL of siRNA mix were added. Finally, the cells were incubated for 4 hours. When the incubation was finished, the medium was replaced with fresh culture media.

2.2.4 Generation of stable transfection overexpressing and knockdown cell lines

Cells were transfected with the plasmids indicated in **Table 2.6** following the directions in section 2.2.2.2 about lipid-based transfections. After 24 hours of transfection, cells were trypsinized, transferred to a 15 cm dish, and mixed with 20 mL of culture media with Puromycin (Thermo Fisher Scientific) 1 μg/mL, Geneticin (Thermo Fisher Scientific) 500 μg/mL or Hygromycin B (Invitrogen) 50 μg/mL, depending on the plasmid. After 2 to 3 weeks, growing colonies were picked and transferred to a 24-well plate with 1 mL of culture media with the corresponding antibiotic. When the clones grew confluent, they were transferred to a 6-well plate. After the cells grew confluent, they

Table 2.6 – Stable transfections

Cell line	Expression	Backbone vector	Selection antibiotic
HeLa	Small hairpin control (shCtrl)	pSIH1	Puromycin
HeLa	Small hairpin TMX1 (shTMX1)	pSIH1	Puromycin
A375p	Empty vector	pIRES2-EGFP	Geneticin
A375p	FLAG-TMX1	pIRES2-EGFP	Geneticin
MEF CNX knock out	Empty vector	pcDNA5	Hygromycin
MEF CNX knock out	CNX-WT-FLAG	pcDNA5	Hygromycin

were tested for the protein levels of the protein of interest using western blot (see section 2.8). The clones that showed the phenotype of interest were selected for further experiments.

Stably transfected cell lines used in this work are listed in **Table 2.6**.

2.2.5 Generation of CRISPR knockout cell lines

Hela TMX1 KO cells lines were generated using the TXNDC (TMX1) Human Gene Knockout Kit (CRISPR) (OriGene). First, cells were co-transfected with two plasmids: a pCas-Guide plasmid containing the Cas-9 gene and the guiding RNA sequence targeted to the TMX1 gene; and a pUC plasmid containing a cassette with GFP and Puromycin resistance genes flanked by homologous arms to the cutting site. After transfection, cells were passaged nine times and transferred to a 15 cm dish with 20 mL of culture media and 1 μg/mL Puromycin (Thermo Fisher Scientific). After 2 to 3 weeks, growing colonies were picked and transferred to a 96-well plate. The insertion of the cassette was confirmed by the presence of GFP using flow cytometry, and the absence of TMX1 protein with western blot. Further validation was performed by sequencing of the target region in the TMX1 gene to identify the presence of the GFP insertion.

2.3 Ca^{2+} measurement

The measurement of Ca^{2+} signals is a central part of this thesis. Ca^{2+} measurements were used for three main objectives. First, to determine the activity of *specific Ca^{2+} channels and pumps* like IP_3R,

SERCA and SOCE. Second, to measure the *amount of Ca^{2+} in different subcellular compartments* like ER and mitochondria. Third, as an indirect estimation of *ER-mitochondria contact formation* by measuring the transfer of Ca^{2+} from ER to mitochondria. Ca^{2+} was measured in living cells using different fluorescent Ca^{2+} probes. These probes bind Ca^{2+} and have a fluorescence that is proportional to the amount of Ca^{2+} they bind. Some of these probes are targeted to specific subcellular compartments, specifically the ER and mitochondria. These are protein probes that have targeting sequences to the specific organelles. Chemical probes were used for cytoplasmic Ca^{2+} measurements.

All Ca^{2+} experiments were performed in living cells using fluorescence microscopy, and the changes in Ca^{2+} concentration was recorded over time effectively making "movies" of Ca^{2+} signals. A variety of drugs were used in order to determine the activity of specific Ca^{2+} channels. These drugs open or close these Ca^{2+} channels and induce changes in intracellular Ca^{2+} levels. By analyzing the characteristics of these Ca^{2+} signals, it is possible to determine if the activity of the channel is altered.

To evaluate the activity of IP_3R, cells were loaded with the cytoplasmic Ca^{2+} probe Fura-2, and treated with ATP, which triggers the opening of the IP_3R. Fura-2 fluorescence over time will show a flat baseline at the beginning of the measurement. Then, when ATP is added, the fluorescence increases indicating that Ca^{2+} was released into the cytoplasm. Finally, the Ca^{2+} is cleared from the cytosol and the fluorescence goes back down. The size of the peak will be proportional to the activity of IP_3R.

A similar approach was used for the quantification of Ca^{2+} content in ER and mitochondria. In this case, probes that are specifically targeted to the ER and mitochondrial (ER-LAR-GECO1 and mito-LAR-GECO1.2) were used as Ca^{2+} indicators. The GECO probes are single-wavelength indicators that cannot determine Ca^{2+} concentration precisely, because their fluorescence can change depending on differences in retention and loading of the probe between samples. But they are good at determining changes in Ca^{2+} levels over time within one sample, as described before. For this reason, Ca^{2+} content in ER and mitochondria was measured by recording Ca^{2+} levels under normal conditions for a few minutes, and then depleting the Ca^{2+} from the organelles. Then, the fluorescence value of the

starting baseline was compared to the fluorescence value at zero Ca^{2+}. The drop in fluorescence after depleting Ca^{2+} was used as an indirect measurement of Ca^{2+} content.

2.3.1 Confocal fluorescence microscopy

Ca^{2+} experiments were performed on an FV1000 laser-scanning confocal microscope (Olympus) using a 20× objective (XLUMPLANFL, NA 1.0; Olympus), equipped with a PL-A686 6.6 megapixel camera (Capture-se software; PixeLINK), and a perfusion system with a peristaltic pump (for the FV1000 system, Watson-Marlow Alitea-AB; Sin-Can). The perfusion medium was either Hanks' Balanced Salt Solution (HBSS) with Ca^{2+} (HBSS/Ca) or HBSS without Ca^{2+} and 0.1 M EGTA (HBSS/noCa), and the flow speed was set at 5 mL/minute. The laser and filters settings depended on the Ca^{2+} probe used during the measurement. A 559 nm excitation laser with a 575-675 nm band-pass emission filter was used for ER-LAR-GECO1 and mito-LAR-GECO1.2; and a 473 nm excitation laser with a 490-540 nm band-pass emission filter for Fluo-8. All measurements were made at room temperature. The images have a size of 512×512 pixels, and it takes approximately 1 second to take each picture. Acquisition was performed with the Olympus Fluoview software.

2.3.1.1 ER Ca^{2+} content

The probe used to measure ER Ca^{2+} was the low affinity ER-LAR-GECO1 [172]. This is a protein probe that was expressed in the cells by transfection with a plasmid containing the probe. For MEF cells, 2×10^6 cells were transfected with 5 μg of plasmid containing the ER-LAR-GECO1 probe following the instructions in section 2.2.2.1 about electroporation-based transfections. Transfected cells were then seeded in poly-L-lysine coated 12 mm glass coverslips in 24-well plates at a concentration of 3×10^5 cells per well and kept growing for 24 hours before the experiment. For Hela and A375P cells, cells were seeded in poly-L-lysine coated 12 mm glass coverslips in 24-well plates at a concentration of 5×10^4 cells per well. Next day, cells were transfected with 0.5 μg of plasmid and 2.5 μL of Metafectene per well. After 4 hours of incubation, the cell culture medium was replaced with fresh media, and the cells were incubated for an extra 24 to 48 hours before the experiment.

For the experiment, cells were incubated in regular culture medium with the drugs indicated in each experiment or the vehicle for the controls. Then, the coverslips containing the treated cells were transferred to the perfusion chamber in the microscope and perfused with HBSS/Ca. Cells were kept under the perfusion flow for 5 to 10 minutes, while searching and focusing the cells before the measurements started. Between 10 and 20 cells were captured in each coverslip per measurement.

After the cells were selected and the focus adjusted, a 1 minute recording was performed, taking images every 5 seconds. The objective of this short capture is to detect *drifting coverslips* or *cells with unstable signal*. *Drifting coverslips* happens when there is small debris under the coverslip (for example, small shards of a broken coverslips) or because the perfusion flow moves the coverslip. This results in a slow movement of the coverslip inside the perfusion chamber. This drift causes serious problems for the measurement, like cells moving out of focus or out of the recorded field. Even slight movements can render the cells impossible to quantify and analyze in later stages of the experiment. *Cells with unstable signal* are cells that, for unknown reasons, have a fluorescent signal that goes constantly up or down without any stimulus. Since a stable baseline is required to perform the analysis of this experiment, the unstable cells cannot be used. Even though these events are rare, they are, due to their slow nature, almost impossible to detect while focusing. Hence, this 1 minute recording is used to quickly assess whether any of these problems is present. If the measurement is fine, the experiment continues; if not, the coverslip is adjusted and new cells are selected.

At the beginning of each experiment, cells are recorded for 30 seconds to establish a baseline, taking images every 5 seconds. Then, the perfusion medium was changed to HBSS/noCa with the SERCA inhibitors TBHQ 60 μM or thapsigargin 3 μM for 10 minutes, followed by 5 minutes of HBSS/noCa. This combination removes the availability of extracellular Ca^{2+} and stops the SERCA pump, depleting the ER Ca^{2+} stores. The ER Ca^{2+} content was estimated by calculating the average fluorescence of the first 100 seconds (the media take approximately 90 second to reach the perfusion chamber, resulting in a real measured baseline of 120 seconds) and the last 100 seconds of measurement, after the signals reached a stable baseline. The difference between the starting and the ending baselines is the total

drop of the Ca^{2+} signal and is proportional to the Ca^{2+} content of the ER. In addition, the speed at which Ca^{2+} escapes the ER was also calculated. This represents the speed of passive ER Ca^{2+} leak. The leak was estimated by calculating the slope of the Ca^{2+} fluorescence signal for the first 30 seconds of ER Ca^{2+} depletion.

2.3.1.2 Mitochondrial Ca^{2+} content

The measurement of mitochondrial Ca^{2+} content shares many similarities with the measurement of ER Ca^{2+} content. The probe used to measure mitochondrial Ca^{2+} was mito-LAR-GECO1.2 [172]. This is a protein probe that was expressed in the cells by transfection with a plasmid containing the probe. For MEF cells, 2×10^6 cells were transfected with 5 μg of plasmid containing the mito-LAR-GECO1.2 probe following the instructions in section 2.2.2.1 about electroporation-based transfections. Transfected cells were then seeded in poly-L-lysine coated 12 mm glass coverslips in 24-well plates at a concentration of 3×10^5 cells per well and kept growing for 24 hours before the experiment. For Hela and A375P cells, cells were seeded in poly-L-lysine coated 12 mm glass coverslips in 24-well plates at a concentration of 5×10^4 cells per well. Next day, cells were transfected with 0.5 μg of plasmid and 2.5 μL of Metafectene per well. After 4 hours of incubation, the cell culture medium was replaced with fresh media, and the cells were incubated for an extra 24 to 48 hours before the experiment.

For the experiment, cells were incubated in regular culture medium with the drugs indicated in each experiment or the vehicle for the controls. Then, the coverslips containing the treated cells were transferred to the perfusion chamber in the microscope and perfused with HBSS/Ca. Cells were kept under the perfusion flow for 5 to 10 minutes, while searching and focusing the cells before the measurements started. Between 10 and 20 cells were captured in each coverslip per measurement.

After the cells were selected and the focus adjusted, a 1 minute recording was performed, taking images every 5 seconds. The objective of this short capture is to detect *drifting coverslips* or *cells with unstable signal* (see section 2.3.1.1 about ER Ca^{2+} for more details).

At the beginning of each experiment, cells are recorded for 30 seconds to establish a baseline, taking images every 5 seconds. Then, the perfusion medium was changed to HBSS/noCa with FCCP 10 μM for 10 minutes, followed by 5 minutes of HBSS/noCa. This combination removes the availability of extracellular Ca^{2+} and dissipates mitochondrial potential. Since mitochondrial potential is essential to retain Ca^{2+} in the mitochondrial matrix, the dissipation of this electrochemical gradient results in a quick depletion of mitochondrial Ca^{2+}. The mitochondrial Ca^{2+} content was estimated by calculating the average fluorescence of the first 100 seconds (the media take approximately 90 second to reach the perfusion chamber, resulting in a real measured baseline of 120 seconds) and the last 100 seconds of measurement, after the signals reached a stable baseline. The difference between the starting and the ending baselines is the total drop of the Ca^{2+} signal and is proportional to the Ca^{2+} content inside mitochondria.

2.3.1.3 Store Operated Ca^{2+} Entry

Store Operated Ca^{2+} Entry (SOCE) is a mechanism that allows Ca^{2+} to flow from the extracellular medium in order to reestablish Ca^{2+} balance after Ca^{2+} stores depletion. The procedure to measure SOCE has two steps. First, cellular ER Ca^{2+} stores are depleted using a combination of SERCA inhibition and removal of extracellular Ca^{2+}. Then, extracellular Ca^{2+} is added back, generating a flow of Ca^{2+} into the cell mediated by SOCE. The amount of Ca^{2+} going into the cells is proportional to SOCE activity.

SOCE was determined using the cytoplasmic Ca^{2+} probe Fluo-8. Unlike the GECO probes, Fluo-8 is a chemical Ca^{2+} indicator. Thus, cells are loaded with Fluo-8 by incubating them with the probe for some time. No transfections are necessary. The day before the experiment, cells were seeded in poly-L-lysine coated 12 mm coverslips in 24-well plates at a concentration of 5×10^4 cells per well.

For the experiment, cells were incubated in regular culture medium with the drugs indicated in each experiment or the vehicle for the controls. Then, the cells were incubated with Fluo-8 1 μM for 30 minutes in regular culture medium at 37°C. Then, the coverslips containing the Fluo-8 loaded cells

were transferred to the perfusion chamber in the microscope and perfused with HBSS/Ca. Cells were kept under the perfusion flow for 5 to 10 minutes, while searching and focusing the cells before the measurements started. Between 30 and 50 cells were captured in each coverslip per measurement.

After the cells were selected and the focus adjusted, a 1 minute recording was performed, taking images every 5 seconds. The objective of this short capture is to detect *drifting coverslips* or *cells with unstable signal* (see section 2.3.1.1 about ER Ca^{2+} for more details).

At the beginning of each experiment, cells are recorded for 30 seconds to establish a baseline, taking images every 5 seconds. Then, the perfusion medium was changed to HBSS/noCa with 10 μM thapsigargin for 10 minutes. This combination removes the availability of extracellular Ca^{2+} and stops the SERCA pump, depleting the ER Ca^{2+} stores. Finally, the medium is changed back to HBSS/Ca for 10 minutes, inducing an influx of Ca^{2+} from the extracellular medium through SOCE.

SOCE activity was estimated by calculating the average fluorescence of the last 100 seconds before the reintroduction of Ca^{2+}, and the fluorescence value of the peak after the reintroduction of Ca^{2+}. The difference between the baseline and the Ca^{2+} peak is proportional to SOCE activity.

2.3.1.4 Ca^{2+} transfer from ER to mitochondria

Ca^{2+} transfer from the ER to mitochondria was used as a functional measurement of ER-mitochondria contacts. The probe used to measure mitochondrial Ca^{2+} was mito-LAR-GECO1.2 [172]. This is a protein probe that was expressed in the cells by transfection with a plasmid containing the probe. For MEF cells, 2×10^6 cells were transfected with 5 μg of plasmid containing the mito-LAR-GECO1.2 probe following the instructions in section 2.2.2.1 about electroporation-based transfections. Transfected cells were then seeded in poly-L-lysine coated 12 mm glass coverslips in 24-well plates at a concentration of 3×10^5 cells per well and kept growing for 24 hours before the experiment. For Hela and A375P cells, cells were seeded in poly-L-lysine coated 12 mm glass coverslips in 24-well plates at a concentration of 5×10^4 cells per well. Next day, cells were transfected with 0.5 μg of plasmid and 2.5 μL of Metafectene per well. After 4 hours of incubation, the cell culture medium was replaced

with fresh media, and the cells were incubated for an extra 24 to 48 hours before the experiment.

For the experiment, cells were incubated in regular culture medium with the drugs indicated in each experiment or the vehicle for the controls. Then, the coverslips containing the treated cells were transferred to the perfusion chamber in the microscope and perfused with HBSS/Ca. Cells were kept under the perfusion flow for 5 to 10 minutes, while searching and focusing the cells before the measurements started. Between 10 and 20 cells were captured in each coverslip per measurement.

After the cells were selected and the focus adjusted, a 1 minute recording was performed, taking images every 5 seconds. The objective of this short capture is to detect *drifting coverslips* or *cells with unstable signal* (see section 2.3.1.1 about ER Ca^{2+} for more details).

At the beginning of each experiment, cells are recorded for 30 seconds to establish a baseline, taking images every 5 seconds. Then, the perfusion medium was changed to HBSS/Ca with ATP 600 μM for 5 minutes for MEF cells, and ATP 50 μM for 5 minutes for Hela and A375P cells. ATP triggers a release of Ca^{2+} from the ER by opening the IP_3Rs. Once Ca^{2+} is released, it is transferred to the mitochondria. Under normal conditions, this results in an increase in the mitochondrial Ca^{2+} fluorescent signal, which represents an increase in mitochondrial Ca^{2+} levels. If ER-mitochondria contacts are disrupted, the transfer is less efficient and the increase in mitochondrial Ca^{2+} is smaller. On the other hand, if ER-mitochondria contacts are augmented, the transfer is more efficient and the increase in mitochondrial Ca^{2+} is bigger.

2.3.1.5 Image processing, quantification and analysis

The result of the microscopy experiments is a stack of images for each condition. Each image in the stack is a time point during the measurement. It is similar to a movie where changes in fluorescence intensity represents changes in Ca^{2+} levels in the cell over time. The objective of the analysis is to quantify the fluorescent Ca^{2+} signal of each cell over time, and compare these signals between the different conditions. All Ca^{2+} experiments were analyzed in a similar way. The processing of image data obtained from the microscope can be broken down into the following steps:

All fluorescent microscopy measurements and analysis was performed in the Fiji[1] [173] distribution of ImageJ[2] [174]. The images are in `.oib` format, a proprietary format from Olympus, and were imported into Fiji using the Bio-Formats[3] plugin [175]. Each image contains between 10 and 50 cells depending on the size, confluency and efficiency of transfection of the experiment. Fluorescence intensity over time was measured in each individual cell using one Region Of Interest (ROI) per cell. This ROI is a circular selection of 310 μm^2, big enough to fit a considerable area of the cytosol without extending into the nucleus or the extracellular space. The fluorescent signal inside each ROI was quantified using the Fiji plug-in Time Series Analyzer v3.[4] Because of the high variability between individual cells, this step of the processing can be particularly subjective. For this reason, the following criteria was followed to select the cells that would be incorporated into the analysis:

- Always measure every cell in the captured field.
- If a cell does not have a positive signal for the probe (for example not transfected), the cell is discarded.
- The ROI is placed in an area of the cytoplasm where the signal is the strongest. This is particularly important in probes with a specific cellular localization like ER or mitochondria.
- The cell has to remain stationary and not move out of the ROI. It also cannot have dramatic changes of shape during the measurement. These movements will introduce drops, peaks or other artifacts in the fluorescence signal that should not be included in the data. The amount of movement varies with the cell type used. For example, MEF cells are particularly prone to movement. That is why experiments are always performed in coated coverslips, which prevents this movement. Sometimes cells move in response to the drug added, like thapsigargin or FCCP. If the change in the fluorescence signal is due to cell movement, and not in response to the drug added, the cell is discarded.
- The baseline (the fluorescence signal during the first 100 seconds), has to be stable. If the

[1] https://fiji.sc/
[2] https://imagej.net/
[3] https://www.openmicroscopy.org/bio-formats/
[4] https://imagej.nih.gov/ij/plugins/time-series.html

baseline fluorescence is going up or down, the cell is discarded. Stable baselines are essential for the next steps in the quantification procedure. Most of the time an unstable baseline is a consequence of the cell moving out of the ROI. Moving cells are impossible to measure, so they have to be discarded.

- The cell has to respond to the added drug. If the fluorescence signal remains stable and flat for the entire measurement, the cell is discarded. It is important to note that the question of the experiment is never whether thapsigargin/TBHQ/histamine/ATP/FCCP is able to move Ca^{2+} between compartments. They are used because they are strong stimuli that will trigger a specific movement of Ca^{2+}. Hence, unresponsive cells are dysfunctional and are not considered. They introduce an irrelevant variable to the experiment and make data harder to quantify and interpret.

When the cell selection is complete, the mean fluorescence intensity inside each of the ROIs is quantified for each time point. The resulting data is stored in a `.csv` or `.xlsx` file.

After the quantification is completed, the signal at each time point is normalized against the baseline value of each of the cells. The objective of this normalization is to make the measurements comparable between cells. The raw fluorescence values cannot be used because differences in probe transfection/loading and differences in cell size introduce a great variability between individual cellular fluorescence values. With the normalization is possible to focus on the behavior of the cells independent of the raw value of the signal. In order to do the normalization, the average fluorescence intensity of the first 100 seconds is calculated, this is the *starting baseline value*. Then, each time point is divided by the *starting baseline value*. This results in all cells having a starting baseline of 1 and then the signal goes up or down in relation to this starting point. This normalization is represented as F_1/F_0 in the figures.

Alternatively, in experiments to measure ER or mitochondria Ca^{2+} content, the baseline is not calculated from the first 100 seconds. Instead, it is calculated when the signal reached a stable minimum in the last 100 seconds of measurement, this is the *ending baseline value*. Then, each time point is

divided by the *ending baseline value*. As a result, all cells finish their measurement at a value of 1, but they start their measurement at a higher value. This normalization is represented as F_1/F_{final} in the figures.

After each individual cell is normalized, the values of all single cells are averaged. The resulting average of normalized fluorescence signals over time is the basic data element of the experiment. This is the data reported in graphs, and from were Ca^{2+} peaks and slopes are calculated.

The analysis of the Ca^{2+} signal curves depends on the experiment. Peaks are calculated Ca^{2+} transfer to mitochondria and SOCE by measuring the difference between the starting baseline (which corresponds to a value of 1) and the maximum fluorescence value of the signal. ER and mitochondrial Ca^{2+} content are calculated by measuring the difference between the end baseline (which corresponds to a value of 1) and the average of the first 100 seconds. Slopes are calculated by doing a linear regression of a segment of the fluorescence signal of approximately 30 seconds.

2.3.2 Fluorometer

The fluorometer was used to measure cytosolic Ca^{2+}, in particular, the activity of the IP_3R. Cells were seeded in 60 mm dishes at a concentration of 2×10^6 cells per dish. Next day, cells were incubated in regular culture medium with the drugs indicated in each experiment or the vehicle for the controls. For Fura-2 loading, cells were washed with HBSS/Ca buffer with 0.1% BSA (HBSS/Ca/BSA) and incubated in 1.5 mL of HBSS/Ca/BSA with 1 μM Fura-2 for 30 minutes at room temperature in the dark. Then, the buffer was replaced with fresh HBSS/Ca/BSA and incubated for a further 15 minutes at room temperature in the dark. After the cells were loaded with Fura-2, they were transferred to the cuvette used in the fluorometer. To transfer the cells, they were lifted from the dish by removing the HBSS/Ca/BSA and incubating them with 0.5 mL trypsin for 3 minutes. Then, the trypsin was quenched with 1 mL DMEM 10% FBS, and the cells were transferred to an epp tube. Next, cells were washed by spinning them at 0.1 rcp for 5 minutes and resuspending them in 1 mL of HBSS/Ca/BSA twice. Finally, the resuspended cells were transferred to the cuvette in a final volume of 1.5 mL of

HBSS/Ca/BSA.

For the measurement, the cuvette was loaded in the fluorometer while maintaining the cells in suspension using a magnetic stirring bar. Fura-2 fluorescent signal was detected at 505 nm emission from 340 and 380 nm excitation wavelength using a PTI 814 Photomultiplier Detection System. First, a 200 seconds baseline was established. Then, 50 μM histamine was added as 100 μL of a 200× stock solution prepared in HBSS/Ca/BSA. The measurement ended 400 seconds after histamine.

Cytoplasmic Ca^{2+} levels were estimated by calculating the ratio between the 505 nm emission at 340 and 380 nm excitations (340/380 ratio) at each time point. This ratiometric measurement corrects for different loading of Fura-2 or different amount of cells inside the cuvette.

Ca^{2+} release through the IP_3R was calculated by comparing the average 340/380 ratio of the starting baseline, and the 340/380 ratio of the peak after the addition of histamine. The difference between the baseline and the Ca^{2+} peak is proportional to IP_3R activity. In addition, the speed at which Ca^{2+} levels go down after the peak was also calculated. This cytoplasmic Ca^{2+} clearance speed was used as a measurement of SERCA activity, since SERCA mediates the removal of Ca^{2+} from the cytoplasm. The clearance speed was calculated by measuring the slope of the 340/380 ratio for the first 20 seconds after the histamine peak.

2.4 Protein quantification

Protein quantification was used to measure the amount of protein in the samples for the ATPase assay described in section 2.6. Proteins were quantified using the Pierce BCA Protein Assay Kit (Thermofisher).

Albumin protein standards of 0, 0.025, 0.125, 0.25, 0.5, 0.75, 1, 1.5 μg/μL were prepared for a standard concentration curve, 10 μL of each sample and protein standard were used for the measurements. Next, a solution of Reagents A and B from the kit were mixed in a 50:1 ratio, with a final volume of 200 μL × the number of samples (including the standard concentration curve). Then, each 10 μL of

sample was mixed with 200 μL of the reagents A and B solution in an epp tube, and incubated in a thermoregulated water bath at 37°C for 30 minutes. Finally, the BCA absorbance was measured at 562 nm using a NanoDrop 2000c spectrophotometer (Thermo Scientific).

2.5 Subcellular fractionation and Mitochondria-Associated Membranes isolation

Subcellular fractionation techniques were used to separate the different cellular components and analyze their protein composition. These techniques are used to identify the presence of proteins in the Mitochondria-Associated Membranes (MAM), and the distribution of proteins between MAM and the bulk of the ER. In addition, they were used to isolate ER membranes in order to measure SERCA ATPase activity (see section 2.6 for more details on SERCA ATPase assay).

2.5.1 Differential centrifugation fractionation

Cytosol, Heavy membranes, and Light membranes were separated by differential centrifugation. In this protocol, Light membranes are composed mainly by ER and other organelles membranes; while Heavy membranes are composed mainly by mitochondria, but they also contain the ER membranes that are closely associated to mitochondria, the MAM. So ER proteins found in the Heavy membranes are considered to be present in the MAM, since this is the only ER subdomain present in this fraction. Whereas ER proteins found in the Light membranes are proteins that are non-MAM proteins and are not closely associated with mitochondria.

Cells were seeded in 10 cm dishes and cultured until they reached 80% confluence. Then, they were incubated in regular culture medium with the drugs indicated in each experiment, or the vehicle for the controls. When the drug incubation was complete, the dishes were transferred to ice and the cells were washed with cold PBS. Then, 600 μL of Mitochondria Homogenization Buffer (250 mM Sucrose, 10 mM HEPES-OH pH 7.4, 1 mM EDTA, 1 mM EGTA) with protease inhibitors

(cOmplete, Roche) were added to each dish, and the cells were scraped and transferred to an epp tube. Cells were homogenized by passing them 7 times through a 26½ G needle. Then, the resulting lysates were centrifuged at 800 rcf for 10 minutes to remove nuclei and unbroken cells, and the pellet was discarded.

To obtain the *Heavy membranes*, the post-nuclear supernatant was centrifuged at 10,000 rcf for 10 minutes, and the pellet was resuspended in 60 μL of 2× Sample buffer (1× Sample buffer: 60 mM Tris-HCL pH 6.8, 2% SDS, 10% glycerol, 10% β-mercaptoethanol, and 0.004% bromophenol blue).

To obtain the *Light membranes*, the remaining supernatant of the Heavy membranes separation was centrifuged at 60,000 rpm (100,000 rcf) for 1 hour at 4°C in a Beckman tabletop ultracentrifuge using a TLA 120.2 rotor (Beckman Coulter), and the pellet was resuspended in 60 μL of 2× Sample buffer.

To obtain the *Cytosol* proteins, the remaining supernatant after the 100,000 rcf centrifugation was divided in two epp tubes, and the proteins were precipitated by adding 1 mL acetone to each tube and incubating overnight at -20°C. Next day, the precipitated proteins were centrifuged at 16,000 rcf for 20 minutes at 4°C. The acetone supernatant was discarded, and the proteins were resuspended in 30 μL of 2× Sample buffer (60 μL total per sample).

The protein composition of each fraction was analyzed using western blot (described in 2.8).

2.5.2 Mitochondria-Associated Membrane separation with Percoll

Percoll fractionation is a separation of cellular components by differential centrifugation with an additional step to separate the Heavy membranes into MAM and pure mitochondria.

Cells were seeded in 15 20-centimetre dishes and cultured until they reached 80% confluence. Then, they were incubated in regular culture medium with the drugs indicated in each experiment or the vehicle for the controls. When the drug incubation was completed, the dishes were transferred to ice and the cells were washed with cold PBS. Then, each set of 15 dishes was scraped with 5 mL

of Mitochondria Homogenization Buffer (250 mM Sucrose, 10 mM HEPES-OH pH 7.4, 1 mM EDTA, 1 mM EGTA) with protease inhibitors (cOmplete, Roche), and the resuspended cells were transferred to a 50 mL conical tube. The cells were centrifuged at 300 rcf for 5 minutes at 4°C, the supernatant was discarded, and the cells were resuspended in 5 mL of Mitochondria Homogenization Buffer with protease inhibitors. The cells were homogenized in a ball-bearing homogenizer (Isobiotec, Heidelberg, Germany) with a ball clearance of 18 μm; the cells were passed through the homogenizer 7 times. Then, the resulting homogenate was centrifuged at 600 rcf for 10 minutes at 4°C to remove unbroken cells and nuclei.

To obtain the *Crude Mitochondria* fraction (equivalent to the Heavy membranes), the post-nuclear lysates were centrifuged at 10,000 rcf for 10 minutes. Then, the pellet (Crude Mitochondria fraction) was resuspended in 1 mL of Mitochondria Homogenization Buffer with protease inhibitors. 40 μL of the Crude Mitochondria fraction were separated and mixed with 5× Sample buffer (1× Sample buffer: 60 mM Tris-HCL pH 6.8, 2% SDS, 10% glycerol, 10% β-mercaptoethanol, and 0.004% bromophenol blue) for analysis.

To obtain the *Microsomes* fraction (equivalent to the Light membranes), the Crude Mitochondria suspension was transferred to four 1.4 mL ultracentrifuge tubes and spun at 60.000 rpm for 1 hour at 4°C in a Beckman tabletop ultracentrifuge using a TLA 120.2 rotor (Beckman Coulter). The pellets, which correspond to the Microsomes fraction, were resuspended in a final volume of 1.2 mL with 1× Sample buffer.

To obtain the *Cytosol* proteins, the remaining supernatant was divided in twelve epp tubes, and the proteins were precipitated by adding 1 mL acetone to each tube and incubating overnight at -20°C. Next day, the precipitated proteins were centrifuged at 16,000 rcf for 20 minutes at 4°C. The acetone supernatant was discarded, and the proteins were resuspended in 1.2 mL of 1× Sample buffer.

To separate the Crude Mitochondria into *Pure Mitochondria* and *MAM*, the remainder 950 μL of resuspended Crude Mitochondria were carefully layered on top of 7.9 mL of 18% Percoll in a poly-carbonate ultracentrifuge tube (also prepared with Mitochondria Homogenization Buffer). Then, the

Crude Mitochondria suspension was centrifuged at 95,000 rcf for 30 minutes at 4°C in a Type 90 Ti rotor (Beckman Coulter). After the centrifugation, the sample separated into two bands, a heavy and cloudy band near the bottom of the tube corresponding to Pure Mitochondria, and a lighter and thinner band above it corresponding to MAM. 2 mL of the MAM band were extracted and transferred it to two 1.4 mL ultracentrifuge tubes. To clean the MAM fraction of the Percoll, the MAM suspension was centrifuged at 60.000 rpm for 1 hour at 4°C in a TLA 120.2 rotor (Beckman Coulter). Then, 200 μL of the MAM pellet were extracted and transferred to an epp tube, mixed it with 50 μL of 5× Sample buffer, and the final volume was adjusted to 300 μL with 1× Sample buffer. In parallel, 2 mL of the Pure Mitochondria band were extracted and transferred to 4 epp tubes, and 1 mL of Mitochondria Homogenization Buffer was added to each of the tubes. To clean the Pure Mitochondria fraction of the Percoll, the Pure Mitochondria suspension was centrifuged at 10,000 rcf for 10 minutes at 4°C. Then, the supernatant was discarded and the pellet was resuspended with 1 mL of fresh Mitochondria Homogenization Buffer, and the centrifugation was repeated. Finally, the supernatant was discarded and the Pure Mitochondria pellets were resuspended in a final volume of 300 μL of 1× Sample buffer.

The protein composition of each fraction was analyzed using western blot (described in 2.8).

2.6 SERCA ATPase activity assay

The enzymatic ATPase activity assay was used to measure the ATPase activity of the Ca^{2+} pump SERCA. Since the Ca^{2+} pumping activity of SERCA depends on the hydrolysis of ATP, the ATPase activity is a direct measurement of SERCA Ca^{2+} pumping activity. The ATPase assay consisted of an enzyme coupled reaction where the regeneration of ATP is coupled to the oxidation of NADH [176]. The ATPase activity was measured as a decrease in NADH absorbance at 340 nm over time. It is important to note that this assay will measure all ATPase activity present on the sample, not only from SERCA. Two adjustments were made to obtain specifically SERCA ATPase activity. The first one was to remove fractions of the cell where we know that SERCA is not present, like cytosol and

nuclei, by subcellular fractionation. The second is to use a specific SERCA inhibitor, to determine specifically the ATPase activity from SERCA.

The preparation and seeding of cells depended on the experimental conditions. Cells were seeded in 10 cm dishes at a concentration of 4×10^6 cells per dish. Next day, cells were incubated in regular culture medium with the drugs indicated in each experiment or the vehicle for the controls.

If cells were transfected with a plasmid (for example, for the CNX rescue experiment in CNX knock-out cells), they were seeded in 6-well plates at a concentration of 1×10^6 cells per well. Next day, cells were transfected using Metafectene, following the procedure described in section 2.2.2 about plasmid transfections. After 24 hours of transfection, cells were trypsinized and transferred to a 10 cm dish. Next day, cells were incubated in regular culture medium with the drugs indicated in each experiment or the vehicle for the controls.

If cells were treated with a siRNA for a knockdown experiment, they were seeded in 6-well plates at a concentration of 1×10^6 cells per well. Next day, cells were incubated with siRNA following the procedure described in section 2.2.3 about siRNA mediated knockdown. After 24 hours, cells were trypsinized and transferred to a 10 cm dish. Next day, cells were incubated in regular culture medium with the drugs indicated in each experiment or the vehicle for the controls.

2.6.1 Light membranes separation

The first step of the ATPase assay is the separation of the Light membranes by differential centrifugation (see section 2.5.1). Light membranes are composed mainly by ER and other organelles membranes, and most SERCA can be found in this fraction. The objective is to concentrate SERCA by separating it from other ATPases found in other fractions of the cell. This helps to obtain a cleaner measurement without the interference of ATPases present in the discarded fractions.

First, cells were put in ice and washed with cold PBS. Then, 600 µL of Mitochondria Homogenization Buffer (250 mM Sucrose, 10 mM HEPES-OH pH 7.4, 1 mM EDTA, 1 mM EGTA) with protease inhibitors (cOmplete, Roche) were added to each dish, and the cells were scraped and transferred to

an epp tube. Cells were homogenized by passing them 7 times through a 26½ G needle. Then, the resulting lysates were centrifuged at 800 rcf for 10 minutes to remove nuclei and unbroken cells, and the pellet was discarded. The post-nuclear lysate was centrifuged at 10,000 rcf for 10 minutes and the pellet was discarded. To obtain the Light membranes, the remaining supernatant was centrifuged at 60,000 rcf for 1 hour, and the pellet was resuspended in 300 μL of Membrane Resuspension Buffer (MRB) (50 mM HEPES pH 7.2, 125 mM NaCl, 1 mM $MgCl_2$). Then, the protein concentration in each sample was quantified using the Pierce BCA Protein Assay Kit described in section 2.4 about protein quantification.

2.6.2 ATPase assay

All samples were measured in triplicate, in a 96-well plate with a final volume of 100 μL. The final conditions for all the reactions were 50 mM HEPES pH 7.2, 125 mM NaCl, 1 mM $MgCl_2$, 0.1 mM $CaCl_2$, 1 mM DTT, 0.6 mM NADH, 2 mM ATP, 1 mM phosphoenol pyruvate, 2.5 μL of pyruvate kinase/lactate dehydrogenase (Sigma), and 0.02% DMSO. In order to obtain the specific SERCA ATPase activity, each sample had an identical parallel reaction treated with 10 μM thapsigargin, a specific SERCA inhibitor. The specific SERCA activity was obtained by subtracting the thapsigargin-treated reaction from the untreated reactions.

The concentration of each sample was set to 0.05 mg/mL by adjusting the volume with MRB. 20 μL (1 μg) of each sample was added to 6 wells in the 96-well plate, a set of triplicates with thapsigargin and a set of triplicates without thapsigargin. Then, the reaction was started by adding 80 μL of a solution containing $CaCl_2$, DTT, NADH, ATP, phosphoenol pyruvate and pyruvate kinase/lactate dehydrogenase either with or without thapsigargin, adjusted to reach the final concentration in 100 μL. NADH absorbance was measured at 340 nm every one minute for 120 minutes using a microplate reader (Synergy, BioTek) and the path-length correction function. Then, NADH absorbance was converted to micromoles of ATP using Beer's law, and expressed as a function of time with the equation $[ATP]_{\mu M} = ((Absorbance_0/6220)-(Absorbance_i/6220)) \times 1000000)$. The result was a curve showing the reduction of ATP concentration over time. From this data, a linear regression was fitted

and the slope was used as a measurement of ATPase activity. Finally, the difference in ATPase activity from the samples with and without thapsigargin is the specific SERCA ATPase activity per μg of protein.

2.7 Cell lysates preparation

Whole cell lysates were used to measure protein levels and also to detect protein phosphorylation. Cells were seeded in 60 mm dishes and cultured until they reached 80% confluence. Then, the dishes were transferred to ice and the cells were washed with cold PBS. Next, 300 μL of cold CHAPS buffer (10 mM Tris-HCl pH 7.4, 150 mM NaCl, 5 mM EDTA, 1% Triton X-100, and 1% CHAPS) with protease inhibitors (cOmplete, Roche) and phosphatase inhibitors (PhosSTOP, Roche) were added to each dish, and the cells were scraped and transferred to an epp tube. The resulting lysates were centrifuged at 800 rcf for 10 minutes to remove nuclei and unbroken cells. To denature the protein samples, the post nuclear lysate was mixed with 5× Sample buffer (1× Sample buffer: 60 mM Tris-HCL pH 6.8, 2% SDS, 10% glycerol, 10% β-mercaptoethanol, and 0.004% bromophenol blue) and boiled for 5 minutes. Finally, equal amounts of protein per sample were analyzed using Wester blot (see section 2.8).

2.8 Western blotting

Western blot was used to measure protein levels and phosphorylation in whole cell lysates preparation (see section 2.7) and for subcellular fractionation (see sections 2.5.1 for Simple Fractionation and section 2.5.2 for Percoll protocols).

Western blotting consists of the separation of the proteins by molecular weight using gel electrophoresis, followed by a transfer of the proteins to a membrane, and detection of these proteins using specific antibodies.

2.8.1 Sodium Dodecyl Sulphate Polyacrylamide Gel Electrophoresis (SDS-PAGE)

SDS-PAGE was used to separate the proteins by molecular weight. Samples were loaded into a polyacrylamide gel composed by a stacking section of 4% acrylamide, 125 mM Tris pH 6.8, 0.1% SDS 0.1% TEMED and 0.2% ammonium persulfate; and a separating section of 8, 10 or 12% acrylamide, 375 mM Tris pH 8.8, 0.1% SDS, 0.1% TEMED, and 0.1% ammonium persulfate. The acrylamide concentration of the separating section depended on the molecular weight of the proteins analyzed. Proteins of 100 or more kDa were separated with 8% acrylamide gels, and proteins of 40 or less kDa were separated using 12% acrylamide gels. Proteins between 100 and 40 kDa were separated with 10% gels. The samples were run at 150 V for 60-70 minutes using a Mighty Small II gel running system (Amersham).

2.8.2 Transfer

Proteins were transferred from the polyacrylamide gel to a nitrocellulose membrane in Carbonate transfer buffer (10 mM $NaHCO_3$, 3 mM Na_2CO_3 and 20% Methanol), at 400 mA for 120 minutes at 4°C using a Mini Transblot Cell apparatus (BioRad).

2.8.3 Antibody incubation

To prevent nonspecific binding of the antibodies to the nitrocellulose membrane and other proteins, the membranes were blocked with Blocking buffer (10 mM Tris pH 8, 150 mM NaCl, 0.05% Triton X-100, and 2% BSA) for 30 minutes at room temperature. Then, the membranes were incubated with the primary antibodies prepared in TBS-T 2% milk overnight at 4°C. The concentration used for each primary antibody can be found in table **Table 2.7**.

When the primary antibody incubation was finished, the membrane was washed with TBS-T for 5 minutes 3 times, and the corresponding secondary antibody prepared TBS-T 2% milk was added and incubated for 1 hour at room temperature, and washed again. The concentration used for each secondary antibody can be found in table **Table 2.8**. Then, the secondary antibodies were visualized

Table 2.7 – Primary antibodies

Protein	Host	Dilution (use)	Supplier
Actin	Rabbit	1:10000 (WB)	Thermo Fisher Scientific
AMPK	Rabbit	1:1000 (WB)	Millipore
BiP	Mouse	1:5000 (WB)	BD Biosciences
Calnexin	Rabbit	1:5000 (WB)	Serum
CHOP	Mouse	1:1000 (WB)	Thermo Fisher Scientific
Complex 2 (SDHB)	Mouse	1:5000 (WB)	Abcam
Ero1α	Mouse	1:1000 (WB)	Serum
ERp57	Mouse	1:2500 (WB)	StressMarq
FLAG tag	Mouse	1:1000 (WB)	Rockland
GAPDH	Rabbit	1:5000 (WB)	Cell Signaling
GLUT4	Rabbit	1:1000 (WB)	Abcam
Hexokinase 1	Rabbit	1:1000 (WB)	Cell Signaling
Hexokinase 2	Rabbit	1:1000 (WB)	Cell Signaling
IP3 Receptor type 1	Rabbit	1:1000 (WB)	MD
IP3 Receptor type 2	Rabbit	1:1000 (WB)	Alomone
IP3 Receptor type 3	Mouse	1:1000 (WB)	BD Biosciences
MCU	Rabbit	1:1000 (WB)	Sigma
Mfn2	Rabbit	1:1000 (WB)	Sigma
myc tag	Mouse	1:1000 (WB)	Millipore
NOX4	Rabbit	1:1000 (WB)	Abcam
p62	Mouse	1:2000 (WB)	BD Biosciences
PDH	Rabbit	1:1000 (WB)	Cell Signaling
PERK	Rabbit	1:1000 (WB)	Cell Signaling
phospho AMPK	Rabbit	1:1000 (WB)	Millipore
phospho PERK	Rabbit	1:1000 (WB)	Cell Signaling
PKM2	Rabbit	1:1000 (WB)	Cell Signaling
SERCA2b	Mouse	1:1000 (WB)	Millipore
TMX1	Rabbit	1:1000 (WB)	Serum
Tubulin	Mouse	1:10000 (WB)	Sigma
VDAC1	Mouse	1:5000 (WB)	Abcam
XBP1	Rabbit	1:1000 (WB)	Abcam

Table 2.8 – Secondary antibodies

Antibody	Dilution (use)	Supplier
Goat anti mouse AlexaFluor 680	1:10000 (WB)	Invitrogen
Goat anti rabbit Alexa Fluor 750	1:10000 (WB)	Invitrogen

using a LI-COR imaging system (Biosciences). The quantification of the bands was performed using the `Gel Analyzer` function in the Fiji[5] [173] distribution of ImageJ[6] [174].

2.9 Mitochondrial membrane potential

Mitochondrial membrane potential measurements were used to evaluate mitochondrial function. The mitochondrial potential is the electrochemical gradient formed in the inner mitochondrial membrane as a result of the proton pumping out of the mitochondrial matrix due to the electron transport chain. Mitochondrial potential was measured in living cells using the mitochondrial potential probe Tetramethylrhodamine (TMRM) and fluorescence microscopy.

TMRM experiments were performed on an FV1000 laser-scanning confocal microscope (Olympus) using a 20× objective (XLUMPLANFL, NA 1.0; Olympus), equipped with a PL-A686 6.6 megapixel camera (Capture-se software; PixeLINK), and a perfusion system with a peristaltic pump (for the FV1000 system, Watson-Marlow Alitea-AB; Sin-Can). The perfusion medium was Hanks' Balanced Salt Solution (HBSS) with Ca^{2+} (HBSS/Ca) and the flow speed was set at 5 mL/minute. Images of the live cells were taken every 5 seconds, with the 559 nm laser excitation and a 575–675 nm band-pass emission filter using a PL-A686 6.6 megapixel camera (Capture-se software; PixeLINK). All measurements were made at room temperature. The images have a size of 512×512 pixels, and it takes approximately 1 second to take each picture. Acquisition was performed with the Olympus Fluoview software.

Cells were seeded in poly-L-lysine coated 12 mm glass coverslips in 24-well plates at a concentration

[5] https://fiji.sc/
[6] https://imagej.net/

of 5×10^4 cells per well. For the experiment, cells were incubated in regular culture medium with the drugs indicated in each experiment or the vehicle for the controls. Then, the cells were incubated with TMRM 40 nM for 30 minutes in regular culture medium at 37°C. Then, the coverslips containing the TMRM loaded cells were transferred to the perfusion chamber in the microscope and perfused with HBSS/Ca. Cells were kept under the perfusion flow for 5 to 10 minutes, while searching and focusing the cells before the measurements started. Between 30 and 50 cells were captured in each coverslip per measurement.

After the cells were selected and the focus adjusted, a 1 minute recording was performed, taking images every 5 seconds. The objective of this short capture is to detect *drifting coverslips* or *cells with unstable signal* (see section 2.3.1.1 about ER Ca^{2+} for more details).

At the beginning of each experiment, cells are recorded for 30 seconds to establish a baseline, taking images every 5 seconds. Then, the perfusion medium was changed to HBSS/Ca with 10 μM FCCP for 10 minutes. FCCP is a protonophore that dissipates mitochondrial potential, generating a steep drop in TMRM fluorescence. The mitochondrial potential was estimated by calculating the average fluorescence of the first 100 seconds (the media take approximately 90 second to reach the perfusion chamber, resulting in a real measured baseline of 120 seconds) and the last 100 seconds of measurement, after the signals reached a stable baseline.The difference between the starting and the ending baselines is proportional to the mitochondrial potential.

TMRM measurements were analyzed with the same methodology used for ER and mitochondrial Ca^{2+} content described in section 2.3.1.5.

2.10 Quantification of ER-mitochondria contact formation

The distance between ER and mitochondria is the essential measurement of ER mitochondria contact formation. Two different approaches were used to measure the distance between ER and mitochondria: electron microscopy and the SPLICS fluorescent probes.

2.10.1 Electron microscopy

Cells were seeded in 10 cm dishes and cultured until they reached 80% confluence. For the experiment, cells were incubated in regular culture medium with the drugs indicated in each experiment or the vehicle for the controls. When the incubation with the indicated drugs was completed, cells were fixed with a fixation buffer (2% paraformaldehyde, 2% glutharaldehyde and 100 mM Sodium Cocadylate at pH 7.4) for 30 minutes at room temperature. After the fixation, cells were washed with 100 mM Sodium Cocadylate at pH 7.4 (Cacod buffer) three times, scraped, and transferred to an epp tube in 1 mL of Cacod buffer. Then, a hard and compact cell pellet was made by applying a series of centrifugations:

- 1,000 rcf for 5 minutes
- 3,000 rcf for 5 minutes
- 6,000 rcf for 5 minutes
- 12,000 rcf for 5 minutes

For the secondary fixation, the supernatant was discarded and the pellets were incubated with 1% osmium tetroxide in Cacod buffer for 1 hour in ice and protected from light. Then, the pellets were washed with water and stained with 1% uranyl acetate in water overnight at 4°C and protected from light.

Next day, the pellets were dehydrated through a series of incubations in graded ethanol solutions:

- 2× wash with water to remove uranyl acetate
- 3× 70% ethanol for 5 minutes in ice
- 3× 90% ethanol for 5 minutes in ice
- 4× 100% ethanol for 5 minutes in ice

For resin infiltration, the pellets were incubated two times with propylene oxide for 10 minutes, followed by a 2 hours incubation with a 50:50 mix of propylene oxide and EMbed 812 resin under vacuum, and then a 1 hour incubation in 100% EMbed 812 resin also under vacuum. Then, the

pellets were transferred to a beam filled with 100% EMbed 812 resin and incubated at 60°C for 48 hours for polymerization.

An Ultracut E (Reichert-Jung) was used for sample sectioning, and imaging was done with a CCD camera (iTEM, Olympus Soft Imaging Solutions) mounted on a Philips 410 TEM.

ER tubules and mitochondria were visually identified in each of the images. When these structures were closer than 50 nm, the length of the contact and the distance between the two organelles was measured. The Fiji[7] [173] distribution of ImageJ[8] [174] was used for image analysis and quantification.

2.10.2 SPLICS fluorescent probes

SPLICS are split-GFP-based contact site sensors designed to emit fluorescence when they are under a certain distance. It consists of two non-fluorescent portions of a GFP protein that can restore their fluorescence upon self assembly. One portion is targeted to the ER and the other to the mitochondria as membrane proteins facing the cytosol. Only when they are close enough, their fluorescence is restored. There are two versions of SPLICS: SPLICS-short measures ER-mitochondria contacts between 8 and 10 nm wide, and SPLICS-long, which measures distances between 40 and 50 nm [177].

2.10.2.1 Sample preparation

Cells were electroporated with SPLICS-short or SPLICS-long following the procedure described in section 2.2.2.1 about plasmid transfection. Once transfected, 3×10^5 cells were seeded in 12 mm coverslips coated with poly-L-lysine and cultured for 48 hours. Then, cells were incubated in regular culture medium with the drugs indicated in each experiment or the vehicle for the controls. When the incubation with the indicated drugs was completed, cells were stained with 1 μM MitoTracker Red for 30 minutes at 37°C also in regular culture medium. Then, cells were fixed with 4% paraformaldehyde

[7] https://fiji.sc
[8] https://imagej.net

for 20 minutes at room temperature and protected from light. Finally, cells were washed with cold PBS and kept in PBS at 4°C protected from light.

2.10.2.2 SPLICS imaging

SPLICS imaging was performed on an FV1000 laser-scanning confocal microscope (Olympus) using a 60× objective (XLUMPLANFL, NA 1.0; Olympus), equipped with a PL-A686 6.6 megapixel camera (Capture-se software; PixeLINK). A 559 nm excitation laser and a 575–675 nm band-pass emission filter was used to capture MitoTracker Red fluorescence, and a 473 nm laser excitation with a 490-540 nm band-pass emission filter was used for the SPLICS probes. Acquisition was performed with the Olympus Fluoview software.

2.10.2.3 Image processing and analysis

The images were processed following the procedure described by the designers of the probe [177]. All image processing and analysis was perfrmed in the Fiji[9] [173] distribution of ImageJ[10] [174].

Images were convoluted, filtered with a Gaussian blur (sigma = 3), the background was subtracted with the `Rolling Ball` plugin (radius = 60), and an `Auto Local Threshold` (MidGrey method, radius = 30) was applied.

The number of SPLICS puncta, which corresponds to the number of ER-mitochondria contacts in the cells, was counted by drawing a mask for each cell, and then using the Analyze Particles plugin with a lower size threshold of 20.

2.11 Total ATP determination

To measure cellular ATP levels, an ATP determination kit (Molecular Probes) based on a Luciferase enzymatic reaction was used.

[9] https://fiji.sc/
[10] https://imagej.net

Cells were seeded in 6-well plates at a concentration of 5×10^5 cells per well. Next day, cells were incubated in regular culture medium with the drugs indicated in each experiment or the vehicle for the controls. When the incubation was completed, cells were lifted by incubating them with 0.3 mL trypsin for 3 minutes, trypsin was quenched with 1 mL DMEM 10% FBS, and cells were transferred to an epp tube. Then, 6×10^5 viable cells were counted and separated. These cells were spun at 100 rcf for 5 minutes, and resuspended in 500 μL of CHAPS buffer (10 mM Tris pH 7.4, NaCl 150 mM, 1 mM EDTA, 1% CHAPS) with protease inhibitors (cOmplete, Roche).

For the luminescence measurement, 50 μL of the resuspended cells were mixed with 500 μL of Standard Reaction Solution (0.5 mM D-luciferin, 1.25 μg/mL firefly Luciferase, 25 mM Tricine buffer pH 7.8, 5 mM $MgSO_4$, 100 μM EDTA and 1 mM DTT) from the kit. Then, the luminescence was measured at 560 nm using a Lumat LB 9507 (Berthold Technologies) luminometer. All samples were measured in sextuplicate.

2.12 Oxygen consumption rate

Oxygen consumption rate was used as a direct measurement of mitochondrial respiration. Oxygen is consumed by mitochondria in the final step of the electron transport chain in the inner mitochondrial membrane, where it is reduced into H_2O. A high-resolution Oxygraph-2K (Oroboros) respirometer was used for all respiratory measurements.

Cells were seeded in 60 mm dishes at a concentration of 2×10^6 cells per dish. Next day, cells were incubated in regular culture medium with the drugs indicated in each experiment or the vehicle for the controls. When the incubation was completed, cells were lifted with 0.5 mL trypsin for 3 minutes, the trypsin was quenched with 4 mL DMEM 10% FBS, the cells were transferred to an 15 mL conical tube, and viable cells were counted. Then, cells were centrifuged at 100 rcf for 5 minutes, and resuspended in regular culture medium adjusting the final volume to reach a concentration of 1×10^6 cells/mL. For the measurements, 2 mL of resuspended cells were transferred to the oxygraph chamber maintained at 37°C. Basal respiration; ATP turnover and proton leak (after addition of the ATP

synthase inhibitor oligomycin); and maximal respiration capacity (after addition of the protonophoric uncoupler FCCP) were measured for each sample. To discard non-mitochondrial respiration, all measurements were corrected by blocking mitochondrial respiration with 2.5 μM antimycin A. Oxygen consumption rate is expressed as pmol O_2/s/Citrate Synthase activity.

2.13 Mitochondrial dynamics

Mitochondrial size and number per cell were quantified to evaluate if the mitochondrial network connectivity. The mitochondrial fluorescent probe MitoTracker Green was used to observe mitochondria with fluorescence microscopy. MitoTracker Green imaging was performed on an FV1000 laser-scanning confocal microscope (Olympus) using a 60× objective (XLUMPLANFL, NA 1.0; Olympus), equipped with a PL-A686 6.6 megapixel camera (Capture-se software; PixeLINK). A 473 nm laser excitation with a 490-540 nm band-pass emission filter was used to capture MitoTracker Green fluorescence. Acquisition was performed with the Olympus Fluoview software.

Cells were seeded in poly-L-lysine coated 12 mm coverslips in 24-well plates at a concentration of 5×10^4 cells per well. For the experiment, cells were incubated in regular culture medium with the drugs indicated in each experiment or the vehicle for the controls. Then, cells were incubated with 1 μM MitoTracker Green for 30 minutes in regular culture medium at 37°C. The coverslips containing the MitoTracker Green loaded cells were transferred to the perfusion chamber in the microscope and maintained in HBSS/Ca. Between 10 and 30 cells were captured in each coverslip per measurement.

For the image processing, the background was subtracted with the Rolling Ball plugin (radius = 20), and a Local Threshold (Huang dark method) was applied. The size and number of mitochondrial particles using was measured using the Analyze Particles plugin in the Fiji[11] [173] distribution of ImageJ[12] [174].

[11] https://fiji.sc/
[12] https://imagej.net/

2.14 Extracellular metabolomics

Extracellular metabolomics was used to measure the glucose consumption and lactate secretion of cells. These metabolites were measured using Nuclear Magnetic Resonance (NMR) on the extracellular medium.

Cells were seeded in 10 cm dishes at a concentration of 2×10^6 cells per dish. Next day, cell media was replaced with 7 mL of fresh culture media with the indicated inhibitors or vehicle for the controls. After 24 hours, the culture media was extracted, filtered with 0.2 μm filters, and mixed with the DSS reference solution. For the spectroscopy, a 2.2-K pumped 800-MHz Oxford magnet updated to a Bruker Neo-Advance IV console equipped with a 5-mm cryoprobe was used, at the NANUC National High Field NMR Facility.[13] The one-dimensional NMR spectra was collected at 25°C using the standard noesypr1d pulse sequence with a transmitter presaturation delay of 990 ms for water suppression, a 100 ms mixing time, 8 steady-state scans, and a spectral width of 12 ppm. The total acquisition time was 4 seconds per transient, with 128 transients acquired per sample. The data was processed with the Chenomx Processor module from the Chenomx NMR suite. The free induction decays (fids) were apodized with an exponential window function corresponding to a line broadening of 0.1 Hz, zero-filled to 128K complex points, Fourier-transformed, phased, and baseline-corrected for further analysis. The methyl peak of DSS was used as the reference peak for reference deconvolution to correct for line shapes. The metabolites were quantified using the Chenomx NMR Suite software version 8.4 (Chenomx, Inc.)[14] and normalized by the number of viable cells at the time of the experiment.

2.15 SERCA redox state

SERCA oxidation state was measured to find oxidative secondary modifications on SERCA. To detect SERCA redox state, the EZ-Link Iodoacetyl-PEG2-Biotin (BIAM) kit (Thermo Fisher Scientific)

[13] http://www.nanuc.ca/
[14] https://www.chenomx.com/

was used. The detection is based on the reaction of the iodoacetyl group of the BIAM molecule with reduced sulfhydryl groups (–SH) in the target protein. Sulfhydryl groups are the main site of oxidative modifications, If sulfhydryl groups are oxidized, the iodoacetyl group cannot react with it and the protein is not labelled. If the sulfhydryl group is reduced, BIAM will bind to the target protein. The iodoacetyl group forms a strong bond with the sulfhydryl group during the labelling. Then, BIAM is detected by its biotin group.

But the BIAM will label all reduced proteins. To specifically detect the oxidation state of SERCA, cells were transfected with myc tagged SERCA (myc-SERCA). Then, myc-SERCA was immuno-precipitated and the biotin group on the BIAM molecule was detected using western blot.

Cells were seeded in 10 cm dishes at a concentration of 1×10^6 cells per dish. Next day, cells were transfected with a plasmid containing myc-SERCA using Metafectene, following the procedure described in section 2.2.2 about plasmid transfections. After 24 hours of transfection, cells were treated with 10 mM DTT for 10 min, 5 mM Diamide for 5 min, or vehicle for the controls. Then, cells were rinsed with warm PBS twice, and lysed with the BIAM reaction buffer (50 mM Tris-HCl pH 8, 50 mM NaCl, 5 mM EDTA, 1% Triton X-100, 0.1% IGEPAL CA-630 and 200 μM BIAM) with protease inhibitors (cOmplete, Roche). The resulting lysates were centrifuged at 800 rcf for 10 minutes to remove nuclei and unbroken cells. Then, samples were incubated at 25°C for 90 minutes and protected from light to allow the iodoacetyl reaction with the sulfhydryl groups. The reaction was stopped and the free BIAM molecules were washed out with Bio-Spin P-6 columns (Bio-Rad), and the buffer was changed to CHAPS (10 mM Tris-HCl pH 7.4, 150 mM NaCl, 5 mM EDTA, 1% Triton X-100, and 1% CHAPS) with protease inhibitors (cOmplete, Roche).

myc-SERCA was immunoprecipitated by incubating the protein lysates with a mouse anti-c-Myc antibody (Thermo Fisher Scientific) at 4°C rocking overnight. Next day, Protein G Sepharose beads (GE Healthcare) were added to the lysates, and the samples were incubated at 4°C rocking for 1 hour. Then, the sepharose beads were separated from lysate by spinning the samples, the supernatant was discarded, and the beads were resuspended in 500 μL of CHAPS buffer. This washing was

repeated four times, and then the beads were resuspended in 2× Sample buffer containing 50 mM DTT and boiled for 10 minutes. The samples were analyzed using western blot (see section 2.8). Biotinylated SERCA was detected with a goat anti-biotin (Sigma), and the myc tag with rabbit anti-Myc (Millipore).

2.16 Reactive oxygen species

Cellular ROS levels were determined using two different probes: MitoSOX (excitation 510 nm, emission 580 nm, Thermo Fisher Scientific), which is targeted to the mitochondria; and CellROX Orange (excitation 545 nm, emission 565 nm, Thermo Fisher Scientific), which measures ROS in the whole cell. The fluorescence signal of MitoSOX and CellROX was measured with a flow cytometer (LSRFortessa, BD).

Cells were seeded in 6-well plates at a concentration of 5×10^5 cells per well. Next day, cells were incubated with 5 μM MitoSOX for 10 minutes or 5 μM CellROX for 30 minutes in regular culture medium at 37°C. When the incubation was completed, cells were lifted with 0.3 mL trypsin for 3 minutes. Then, trypsin was quenched with 1 mL DMEM 10% FBS, and cells were transferred to an epp tube. Next, cells were washed by spinning them at 100 rcf for 5 minutes and resuspending them in 1 mL of HBSS/Ca/BSA twice. Finally, the resuspended cells were transferred to a flow cytometry tube in a final volume of 1 mL of HBSS/Ca/BSA and measured in the flow cytometer.

2.17 Cell viability

Viable cells were counted using the Trypan Blue exclusion method. After cells were trypsinized and resuspended, 20 μL of cell solution were mixed with 20 μL of 0.4% Trypan Blue, and the stained cells were counted with an hemocytometer. Viable cells exclude Trypan Blue, while dead cells are stained blue.

2.18 Phospholipid transfer to mitochondria

Lipid transfer between ER and mitochondria was used as a functional measurement of ER-mitochondria contacts. Lipid transfer was measured by analyzing phosphatidylethanolamine (PE) synthesis from phosphatidylserine (PS). PS is synthesized in the ER and then transferred to mitochondria at the MAM, where it is decarboxylated into PE. To quantify PE and PS levels, cells are incubated with radio-labeled serine, which is incorporated into PS and, from there, into PE.

Cells were seeded in 15×60 mm dishes at a concentration of 1.7×10^6 cells per well. Next day, cells were labelled with 1 mL of serum-free DMEM with 2.5 μCu/mL of ^{3}H-labelled serine. The labelling was done in triplicate, and at 0, 2, 4, 6 and 8 hours time points. After the labelling was completed, cells were washed with 2 mL cold PBS, and stored at -20°C for 10 minutes. Then, 1 mL of cold PBS was added to each dish, and the cells were scraped and transferred to an epp tube. Finally, samples were sonicated and their protein content was quantified.

To extract the lipids, a mixture of $CHCl_3$ and MeOH (2:1 v/v ratio) was added to the samples. This generates two phases, aqueous on top and $CHCl_3$ at the bottom. Then, the bottom phase was extracted, where the lipids, including PS and PE, are located.

PS and PE were separated using thin-layer chromatography (TLC). The samples were run with a solvent mix composed of $CHCl_3$, MeOH, acetic acid, 98% formic acid and H_2O in a 70:30:12:4:1 v/v ratio. The samples were dried out, resuspended in 50 μL of $CHCl_3$, and spotted in silica TLC plates. Then, the plates were loaded into a running tank filled with the solvent mix and run for 30 minutes. When the run was completed, the silica plates were taken out of the tank, dried out, and stained with iodine to label the lipids.

To quantify radio-labelled phospholipids, the bands corresponding to PS and PE were scrapped from the silica plates, and the collected silica scrapes were transferred to a scintillation tube. 5 mL of scintillating solution was added to each tube, and the tubes were loaded in a scintillating counter programmed to measure ^{3}H.

Counts were normalized by the protein concentration in each sample, and the lipid transfer was expressed as *PE/(PE+PS) vs Time*.

2.19 Data analysis and statistics

Data was analyzed with LibreOffice Calc 6.2[15] and R 3.6[16] [178] (with RStudio 1.2[17]) using the tidyverse 1.3 package[18] [179]. Student's *t*-test was used to compare the differences between two samples. To compare the differences between more than two samples, Student's *t*-test was used with the Holm adjustment method for multiple comparisons.

2.20 Other software

Figures were made with a combination of the ggplot2 3.2 package (from tidyverse 1.3 [179]) and Inkscape 0.92.[19]

This thesis was written using Atom 1.43[20] and the R package Bookdown 0.17.[21] References were managed with JabRef 4.3.[22]

All the computer work was performed in MX Linux 18[23] and Manjaro[24] GNU/Linux operating system distributions.[25] All the software used was free (as in freedom) or open source, unless no alternatives existed. Free software was preferred to ensure reproducibility, long-term preservation and easy distribution of all data and analyses, and for educational purposes.

[15] https://www.libreoffice.org/
[16] https://www.r-project.org/
[17] https://rstudio.com/
[18] https://www.tidyverse.org/
[19] https://inkscape.org/
[20] https://atom.io/
[21] https://bookdown.org/
[22] https://www.jabref.org/
[23] https://mxlinux.org/
[24] https://manjaro.org/
[25] https://www.gnu.org/

Chapter 3

TMX1 determines cancer cell metabolism as a modulator of ER-mitochondria Ca^{2+} flux

3.1 Introduction

Ca^{2+} transfer from the ER to mitochondria activates mitochondrial metabolism and respiration [80]. Ca^{2+} can be released through Ca^{2+} channels located in the ER membrane, the most ubiquitous being the Inositol Trisphosphate Receptor (IP_3R). Once Ca^{2+} is released to the cytoplasm, it can reenter the ER through the SERCA pump, also located in the ER membrane [30]. Alternatively, it can be transferred to the mitochondria [3,44]. This transfer of Ca^{2+} occurs at a specialized ER region where ER and mitochondria are in close proximity, known as the Mitochondria-Associated Membranes (MAM) [2,46]. While this flow of Ca^{2+} to the mitochondria is required to maintain normal energy levels [80], sustained elevated mitochondrial Ca^{2+} results in cell death by opening of the mitochondrial Permeability Transition Pore [67,69]. The flow of Ca^{2+} to mitochondria and the control of mitochondrial function can be altered in different pathophysiological conditions, including cancer.

3.1.1 Mitochondrial Ca^{2+} and Mitochondria-Associated Membranes in cancer

Energy metabolism and cell death are intimately related to cancer and tumorigenesis. In fact, the reprogramming of energy metabolism and resistance to cell death are hallmarks of cancer cells [180]. Mitochondrial Ca^{2+} accumulation, and in particular the flow of Ca^{2+} from ER to mitochondria, is disrupted in some cancer cells, preventing the normal induction of apoptosis. The first indication of the relevance of Ca^{2+} signalling in cancer was the discovery that the oncoprotein Bcl-2 has Ca^{2+} regulatory functions at the ER that control the sensitivity to cell death. Bcl-2 lowers the amount of ER Ca^{2+}, resulting in a reduction of available Ca^{2+} for Ca^{2+} release [181,182]. It lowers the ER Ca^{2+} levels by two mechanisms: increasing the leak through IP_3R leading to a depletion of ER Ca^{2+} stores [183,184]; and inhibiting the refill of ER Ca^{2+} stores by destabilizing SERCA protein structure and inactivating its ATPase activity [185]. As a result, Bcl-2 increases the resistance to cell death in cancer cells [60]. This reduced Ca^{2+} transfer to mitochondria also correlated with the inhibition of mitochondrial metabolism in tumors. Early studies on cancer metabolism revealed that cancer cells limit their energy production mostly to glycolysis, even under normoxic conditions where normal cells would largely rely on mitochondrial respiration [186]. The maintenance of this accelerated glycolysis is sustained by the upregulation of glucose transporters and other glycolytic enzymes [187]. But the altered metabolism in cancer is not limited to aerobic glycolysis, as originally observed. Increased glutamine metabolism, and activation of nucleotide, amino acid, and lipid biosynthetic pathways are also commonly found in cancer [188–191]. The combination of these metabolic alterations provide the required building blocks for biosynthetic pathways, and results in a reprogrammed metabolism that supports the increased anabolic needs of proliferating cancer cells in early stages of tumorigenesis [192].

In spite of these metabolic adaptations and the close relation between mitochondrial Ca^{2+} and apoptosis, cancer cells still need a basal mitochondrial metabolic activity. The inhibition of Ca^{2+} flux to mitochondria results in cancer cell death due to compromised mitochondrial energy production, suggesting that cancer cells still require a basal mitochondrial function to survive and proliferate [193].

Other recent reports indicate that accumulation of mitochondrial Ca^{2+} can be beneficial for cancer cells, as long as cell death is avoided. For example, upon pharmacological inhibition of cell death, increased mitochondrial Ca^{2+} confers cancer cells improved proliferation, migration and invasion [194]. The beneficial effects of mitochondrial Ca^{2+} are associated with the increased ROS production by mitochondria. Similar to mitochondrial Ca^{2+}, high ROS levels can also trigger cell death. Nevertheless, ROS produced by mitochondria has been shown to contribute to tumor progression by increasing the metastatic potential of cancer cells, as long as cell death is avoided. [195]. Accordingly, some oncoproteins are associated with the flux of Ca^{2+} to mitochondria, like Mcl-1, which promotes Ca^{2+} transfer to mitochondria by binding to VDAC, resulting in increased ROS generation and migration [196]. Thus, mitochondrial Ca^{2+} flux can be detrimental for cancer cells by promoting cells death, or beneficial by promoting migration and metastasis.

3.1.2 TMX1 is an ER oxidoreductase involved in protein maturation and folding

Thioredoxin-related transmembrane protein 1 (TMX1) is a member of the Protein Disulfide Isomerase (PDI) family proteins. These proteins are the responsible for disulfide bond formation during protein synthesis, and are mostly expressed in the ER, where they perform their folding duties [133]. TMX1 forms part of the TMX subgroup of PDI proteins; as other members of the TMX subgroup, TMX1 contains a transmembrane domain, and one thioredoxin domain [197]. The thioredoxin domain is the catalytic domain that confers PDI proteins their oxidoreductase activity. This domain contains two cysteines in its active site that are critical for the oxidoreductase activity and disulfide bond formation, in a CXXC sequence [129].

Similar to other oxidoreductases, TMX1 is found in the ER, where it participates in the folding of newly synthesized proteins, and degradation of misfolded proteins. Its membrane localization gives TMX1 a high selectivity for other transmembrane proteins [134,135]. While other ER oxidoreductases like ERp57 catalyze the formation of disulfide bonds by oxidizing cysteines in the target protein, it is proposed that TMX1 has mostly a reductase activity in the ER. It catalyzes the disulfide bond reduction of terminally misfolded proteins, breaking their disulfide bonds for their translocation to

the cytosol and proteasomal degradation [137,138]. This is also supported by the observation that it is found mostly in its reduced form in cells [136], and that it has reductase activity *in vitro* [197]. In addition, TMX1 participates in the folding and maturation of glycosylated proteins through the cooperative interaction with the lectin chaperone Calnexin (CNX), and its preferential reductase activity suggest that it acts as an isomerase that assists in the reorganization of disulfide bonds in misfolded proteins, rather than catalyzing the formation of new disulfide bonds [135,136].

3.1.3 TMX1 is enriched in the Mitochondria-Associated Membranes

There is a strong link between ER protein folding, and Mitochondria-Associated Membranes (MAM). This functional link is mediated by the interaction between ER chaperones and oxidoreductases with ER Ca^{2+} channels. The latter are essential for an efficient Ca^{2+} transfer to mitochondria, which regulates mitochondrial metabolism and ATP production [80]. The prime example of the interplay between ER protein folding and ER-mitochondria communication is ER stress. During ER stress, the accumulation of misfolded proteins in the ER results in an enhanced Ca^{2+} flux to mitochondria, this increases mitochondrial ATP production and provides the required energy to cope with the misfolded proteins [112]. Some oxidoreductases and chaperones that exemplify this link are ERp44, an oxidoreductase that binds and inhibits IP_3R Ca^{2+} channels [198]; Ero1α, which oxidizes and activates IP_3R promoting Ca^{2+} flux to mitochondria [164]; and CNX, a chaperone that binds and activates the ER Ca^{2+} pump SERCA and inhibits Ca^{2+} transfer to mitochondria [114]. Thus, ER chaperones and oxidoreductases can regulate MAM and mitochondrial function.

Unsurprisingly, these MAM regulatory proteins also localize to this ER membrane domain. Ero1α, for example, is particularly enriched at the MAM, while ERp44 can be found at the MAM and also in the bulk ER and Golgi [163]. CNX is also enriched in the MAM fraction; this enrichment is controlled by a reversible palmitoylation. As mentioned previously, palmitoylated CNX is targeted to the MAM, where it interacts with SERCA and regulates its activity. But when this palmitoylation is lost, CNX moves from the MAM to the ER, stops interacting with SERCA, and is more active in its protein folding role [114]. Interestingly, TMX1 can also be found in the MAM, and shares the

palmitoylation MAM-targeting mechanism with CNX. Thus, only palmitoylated TMX1 can be found in the MAM; if the palmitoylation is lost, TMX1 loses its MAM targeting [146]. Nevertheless, the effect of TMX1 on MAM function has not been explored. Its MAM targeting suggests that TMX1 might be regulating Ca^{2+} channels and Ca^{2+} flux to mitochondria. Since CNX palmitoylation also mediates its SERCA interaction and regulation, it is possible that TMX1 shares the palmitoylation-dependent SERCA binding and regulation [114]. Nevertheless, whether TMX1 interacts with or regulates SERCA, or any other MAM function, is unknown.

3.1.4 Aims

In this chapter, the role of TMX1 in the regulation of SERCA and mitochondrial Ca^{2+} flux, and its impact on mitochondrial metabolism will be investigated. In order to do this, the following aims are proposed: (*i*) determine if TMX1 regulates SERCA activity and ER Ca^{2+} loading; (*ii*) evaluate if TMX1 regulates ER-mitochondria contacts and Ca^{2+} flux; (*iii*) measure the effects of TMX1 on mitochondrial function and metabolism; and (*iv*) evaluate if TMX1 regulates tumor growth. These aims were evaluated in TMX1 knockout HeLa cells, HeLa cells stably transfected with a plasmid containing a small hairpin RNA for TMX1 knockdown, and A375p melanoma cells (low TMX1 expressing cells [146]) stably transfected with a plasmid encoding a TMX1 gene for TMX1 overexpression, in addition to other molecular tools to overexpress different TMX1 mutants.

The results show that TMX1 binds to SERCA and inhibits its function, resulting in a reduction in Ca^{2+} import to the ER. This reduced ER Ca^{2+} retention is accompanied with increased ER-mitochondria contacts and Ca^{2+} flux to mitochondria, resulting in increased mitochondrial metabolism. Accordingly, TMX1 shows a tumor suppressing effect on cancer cells, shifting their metabolism towards mitochondrial respiration and away from their characteristic aerobic glycolysis. Together, this work expands the functions of TMX1, and demonstrates that it is a critical regulator of Ca^{2+} flux at the MAM and mitochondrial metabolism, with a regulatory effect on tumor growth.

3.2 Results

3.2.1 TMX1 binds to SERCA

TMX1 is a MAM targeted protein, suggesting that it may regulate ER-mitochondria communication. Its MAM targeting is regulated by palmitoylation; palmitoylated TMX1 is targeted to the MAM, and non-palmitoylated TMX1 is relocated to the bulk ER [146]. Since Ca^{2+} flux to the mitochondria takes place at the MAM, the effect of TMX1 on Ca^{2+} signalling was explored. CNX is an ER chaperone localized in the MAM and whose MAM targeting also depends on palmitoylation. Palmitoylated CNX also interacts with SERCA2b, and regulates Ca^{2+} loading in the ER [114]. Therefore, the interaction and regulation of SERCA2b by TMX1 was evaluated. To measure TMX1-SERCA2b interaction, A375p melanoma cells were transfected with a plasmid containing myc tagged SERCA2b; then, myc-SERCA2b was immunoprecipitated using an anti-myc antibody. The result shows that TMX1 co-immunoprecipitated with myc-SERCA2b **(Figure 3.1A)**. As expected, CNX also co-immunoprecipitated with myc-SERCA2b [146]. Since TMX1 and CNX interact with SERCA2b and are located at the MAM, the results suggest that they are interacting at the same time. To evaluate the cross-interaction between TMX1, CNX and SERCA, the interaction of TMX1 and SERCA was evaluated in the absence of CNX. In order to do this, CNX knockout MEF cells were co-transfected with FLAG tagged TMX1, and myc tagged SERCA2b. Just like endogenous TMX1, FLAG-TMX1 co-immunoprecipitated with myc-SERCA2b. In addition, the interaction between FLAG-TMX1 and myc-SERCA2b was significantly increased in CNX knockout cells **(Figure 3.1B)**. Then, the co-immunoprecipitation of CNX with myc-SERCA2b was tested in TMX1 knockout HeLa cells. As expected, CNX co-immunoprecipitated with myc-SERCA2b, and the interaction was increased in cells that lack TMX1 **(Figure 3.1C)**. Taken together, these results suggest that TMX1 interacts with SERCA. In addition, TMX1 and CNX interact with SERCA2b in a competitive way, so that the presence of one interferes with the other. But under normal conditions both proteins can be found interacting with SERCA, even though possibly only one can interact with SERCA at a time.

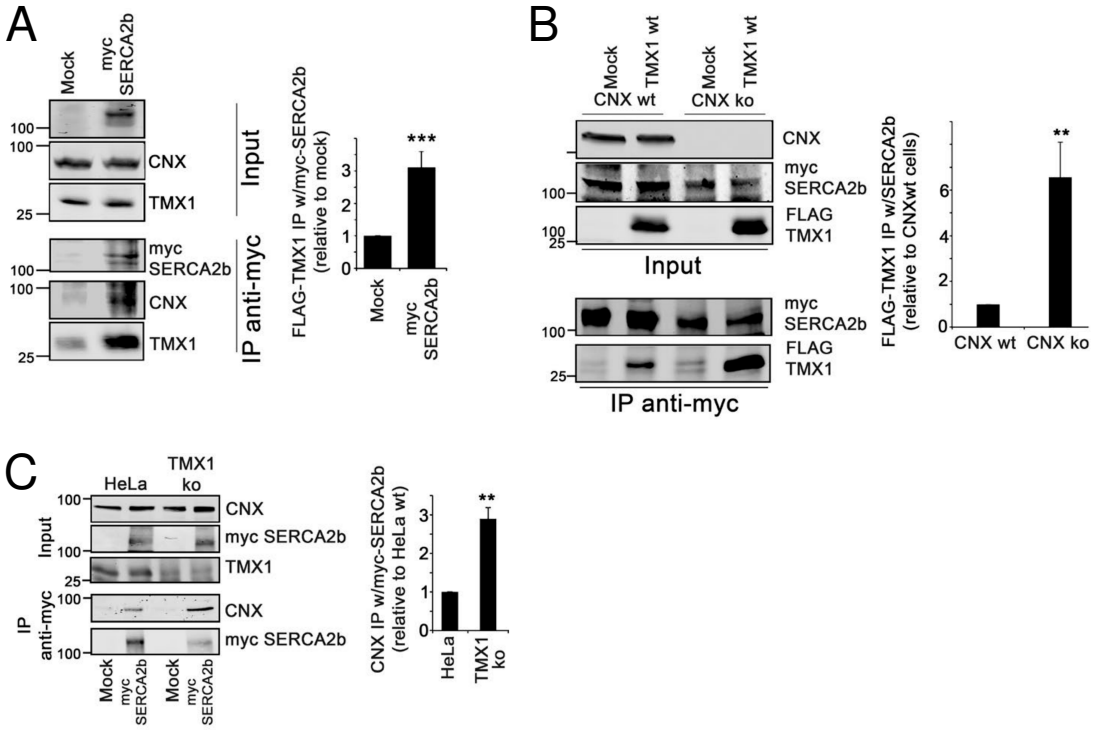

Figure 3.1 – TMX1 interacts with SERCA2b. A: Co-immunoprecipitation of endogenous TMX1 and CNX with myc tagged SERCA2b from protein extracts of A375p cells transfected with a myc-SERCA2b plasmid. n = 3; p = 0.001. **B:** Co-immunoprecipitation of FLAG tagged TMX1 with myc tagged SERCA2b from protein extracts of CNX wild type and knockout MEF cells transfected with both a myc-SERCA2b plasmid and a FLAG-TMX1 plasmid. n = 4; p = 0.0114. **C:** Co-immunoprecipitation of endogenous CNX with myc tagged SERCA2b from protein extracts of TMX1 wild type and knockout HeLa cells transfected with a myc-SERCA2b plasmid. n = 3; p = 0.005. *All experiments in this figure were performed by Carolina Ortiz-Sandoval.*

3.2.2 TMX1 inhibits SERCA and Ca^{2+} import to the ER

The interaction between TMX1 and SERCA2b suggests that TMX1 might influence SERCA function. SERCA activity was estimated by measuring the ER Ca^{2+} content, which depends on SERCA function. To measure ER Ca^{2+} content, ER Ca^{2+} stores were depleted with a combination of the SERCA inhibitor tert-Butylhydroquinone (TBHQ) and medium without Ca^{2+}; then, ER Ca^{2+} stores were refilled by the removal of TBHQ and the addition of extracellular Ca^{2+} back. To measure ER Ca^{2+}, cells were transfected with a plasmid containing the ER-targeted fluorescent Ca^{2+} probe ER-LAR-GECO1. Cells that lack TMX1 had a greater ER Ca^{2+} refill than TMX1 wild type cells, suggesting that the absence of TMX1 increases SERCA activity **(Figure 3.2A)**. At the same time, the drop in the ER Ca^{2+} signal after Ca^{2+} depletion was bigger in TMX1 knockout cells **(Figure 3.2B)**. These results suggest that TMX1 inhibits SERCA and reduces ER Ca^{2+} content.

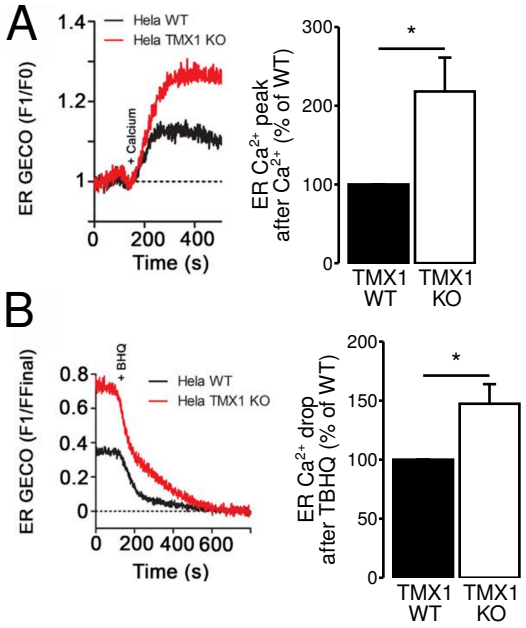

Figure 3.2 – TMX1 reduces ER Ca^{2+} content. A: ER Ca^{2+} content was measured in TMX1 wild type and knockout HeLa cells transfected with ER-LAR-GECO1. ER Ca^{2+} stores were depleted by removing extracellular Ca^{2+} and treating the cells with 60 μM of the the reversible SERCA inhibitor TBHQ, then TBHQ was removed and extracellular Ca^{2+} was added back. The size of the peak after adding Ca^{2+} was measured. n = 4; p = 0.029. **B:** ER Ca^{2+} content was measured in TMX1 wild type and knockout HeLa cells transfected with ER-LAR-GECO1. ER Ca^{2+} stores were depleted by removing extracellular Ca^{2+} and treating the cells with 60 μM TBHQ. The drop in ER Ca^{2+} was measured. n = 7; p = 0.018.

3.2.3 TMX1 promotes Ca^{2+} release from the ER and prevents cytoplasmic Ca^{2+} clearance

The interaction of TMX1 with SERCA2b, and its effects on ER Ca^{2+} loading, suggest that TMX1 regulates Ca^{2+} signalling. To evaluate if TMX1 regulates the release of Ca^{2+} from the ER, TMX1 wild type and knockout cells were loaded with the fluorescent indicator Fura-2, and Ca^{2+} release was triggered through the IP_3R using histamine. In the presence of extracellular Ca^{2+}, cells that lack TMX1 have significantly smaller peaks of cytosolic Ca^{2+} than TMX1 wild type cells after histamine treatment **(Figure 3.3A)**. A similar result was found for TMX1 knockdown HeLa cells **(Figure 3.3B)**. This indicates that TMX1 increases the release of Ca^{2+} from the ER through the IP_3R. Then, the experiment was repeated but keeping the cells in medium without Ca^{2+}. This eliminates the contribution of Ca^{2+} influx from the extracellular medium to the cytosolic Ca^{2+} signals by reducing the refilling of the ER Ca^{2+} stores. Under these conditions there was no statistically significant difference in the cytoplasmic Ca^{2+} peaks between TMX1 wild type and knockout cells after histamine, suggesting that the influx of Ca^{2+} from the extracellular medium could contribute to the Ca^{2+} release in TMX1 wild type cells, resulting in an equilibration in Ca^{2+} release. In addition, the equilibrated cytoplasmic Ca^{2+} signals allow for a better comparison of the Ca^{2+} peak shape between TMX1 wild type and knockout cells. The analysis of the clearance slope after the peak shows that TMX1 knockout cells cleared the Ca^{2+} from the cytoplasm faster than their wild type counterparts **(Figure 3.4)**. Since SERCA is responsible for cytoplasmic Ca^{2+} clearance, this result suggests that TMX1 is inhibiting SERCA Ca^{2+} pumping activity. Together, the results show that TMX1 inhibits SERCA and reduces ER Ca^{2+} content, but promotes Ca^{2+} release from the ER.

3.2.4 TMX1 promotes Ca^{2+} transfer from ER to mitochondria and mitochondrial respiration

To further understand the role of TMX1 in Ca^{2+} signalling, the effect of TMX1 in Ca^{2+} transfer from the ER to mitochondria was also explored. The reduced release of Ca^{2+} to the cytoplasm observed in

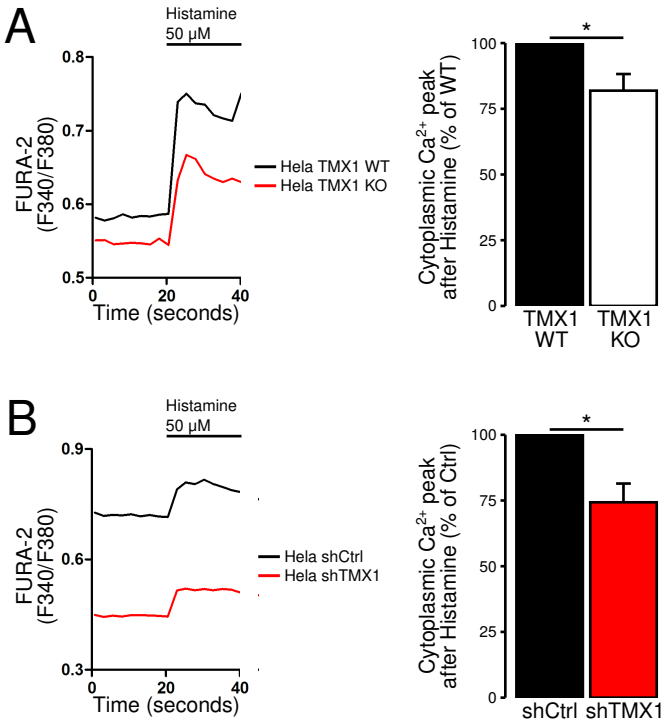

Figure 3.3 – TMX1 increases Ca^{2+} release from the ER. A: Cytoplasmic Ca^{2+} was quantified using the Fura-2 fluorescent Ca^{2+} probe in TMX1 wild type and knockout HeLa cells. 50 µM histamine was added to trigger a Ca^{2+} release through the IP_3Rs. Peak height was measured as release of Ca^{2+}. n = 8; p = 0.013. **B:** Cytoplasmic Ca^{2+} was quantified using the Fura-2 fluorescent Ca^{2+} probe in HeLa cells stably transfected with a shTMX1 expressing plasmid for TMX1 knockdown. 50 µM histamine was added to trigger a Ca^{2+} release through the IP_3Rs. Peak height was measured as release of Ca^{2+}. n = 3; p = 0.023.

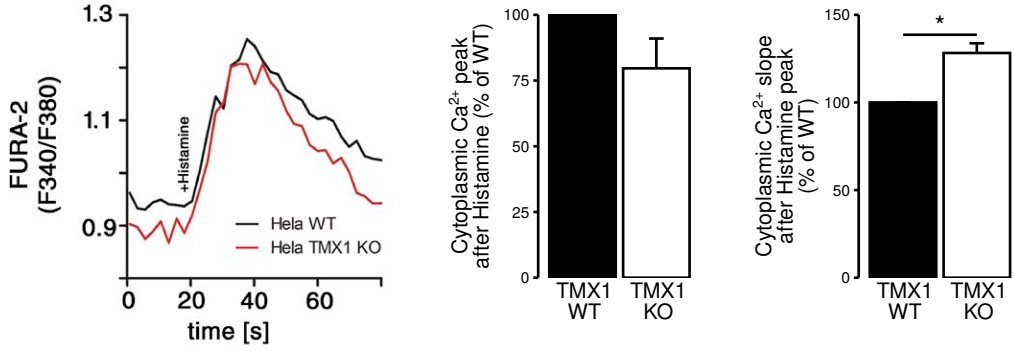

Figure 3.4 – TMX1 reduces cytoplasmic Ca^{2+} clearance. Cytoplasmic Ca^{2+} was quantified using the Fura-2 fluorescent Ca^{2+} probe in TMX1 wild type and knockout HeLa cells in medium without extracellular Ca^{2}. 50 µM histamine was added to trigger a Ca^{2+} release through the IP_3Rs. Peak height was measured as release of Ca^{2+} (n = 3; p = 0.15) and cytoplasmic Ca^{2+} clearance was determined by the decay slope after the peak (n = 4; p = 0.0022).

the previous result suggests that cells that lack TMX1 will also have reduced Ca^{2+} transfer from the ER to mitochondria. Mitochondrial Ca^{2+} flux was measured by transfecting the cells with a plasmid containing the mitochondrial targeted fluorescent Ca^{2+} probe mito-LAR-GECO1.2, and triggering a release of Ca^{2+} from the ER through the IP_3R using histamine. Consistent with previous results, TMX1 knockout cells have impaired Ca^{2+} flux to mitochondria upon histamine treatment compared to TMX1 wild type cells, regardless of the presence of Ca^{2+} in the extracellular medium **(Figure 3.5A and B)**. Similarly, TMX1 knockdown cells also showed a reduction in Ca^{2+} transfer to mitochondria compared to control cells **(Figure 3.5C and D)**. These results show that TMX1 promotes the transfer of Ca^{2+} from the ER to mitochondria, consistent with the reduced retention of Ca^{2+} in the ER and the increased release of Ca^{2+} to the cytosol.

To confirm the effect of TMX1 in the transfer of Ca^{2+} to mitochondria, the experiment was repeated in TMX1 overexpressing cells. The naturally low TMX1-expressing A375p cells [146] were used, stably transfected with a plasmid expressing TMX1 **(Figure 3.6A)**. Consistent with the previous results, TMX1 overexpressing cells have better transfer of Ca^{2+} to mitochondria after histamine treatment than cells transfected with an empty vector, even though the difference was not statistically significant **(Figure 3.6B)**. The same result was observed when Ca^{2+} transfer was measured in medium without extracellular Ca^{2+}, where the transfer Ca^{2+} was significantly increased in TMX1 overexpressing A375p cells **(Figure 3.6C)**. These results confirm that TMX1 promotes the transfer of Ca^{2+} from the ER to mitochondria. Since Ca^{2+} flux to mitochondria is an important regulator of mitochondrial metabolism [80], the effect of TMX1 on mitochondrial respiration was also evaluated. A375p cells transfected with a shTMX1 expressing plasmid for TMX1 knockdown show a reduced mitochondrial respiration, while TMX1 overexpression have an increased respiration compared to the mock transfection **(Figure 3.6D)**. Taken together, these results indicate that TMX1 promotes mitochondrial metabolism and respiration, suggesting that the improved Ca^{2+} flux induced by TMX1 results in an activation of mitochondrial function.

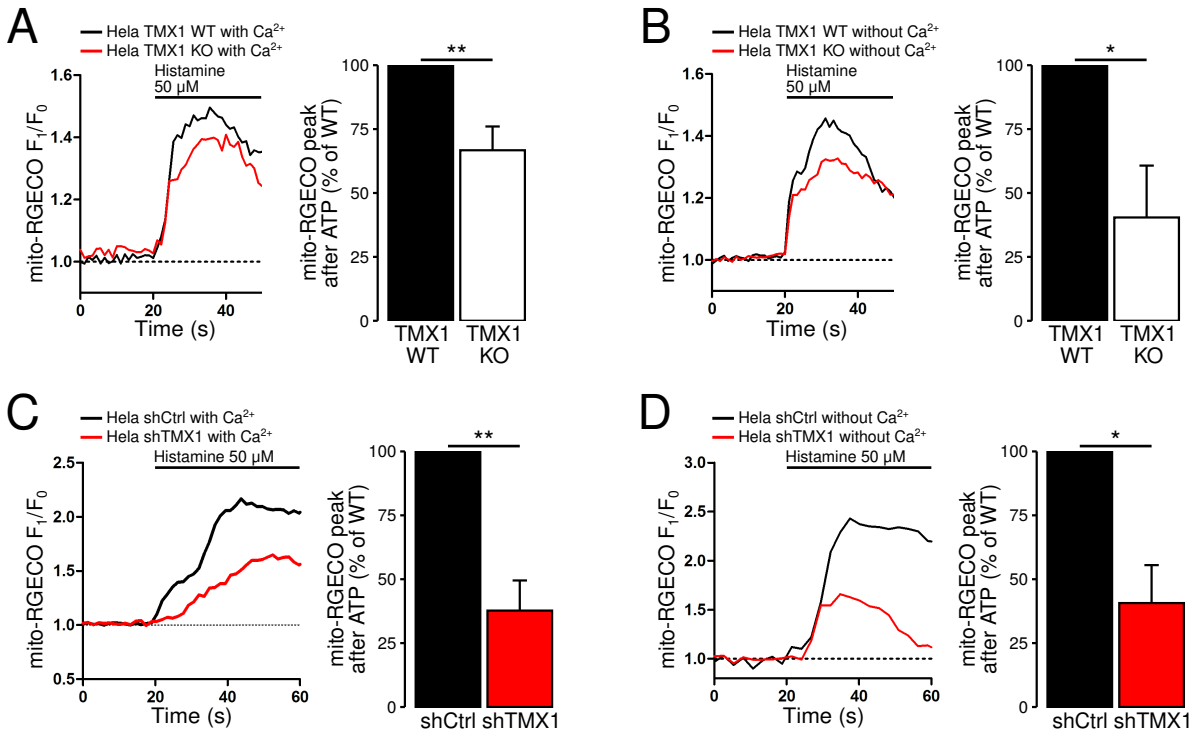

Figure 3.5 – TMX1 increases Ca^{2+} transfer from ER to mitochondria. A: Mitochondrial Ca^{2+} was measured in TMX1 wild type and knockout HeLa cells transfected with the mitochondrial Ca^{2+} indicator mito-LAR-GECO1.2. In the presence of extracellular Ca^{2+}, 50 µM histamine was added to trigger a Ca^{2+} release through the IP_3Rs. Peak height was measured as transfer of Ca^{2+} to the mitochondria. n = 6; p = 0.005. **B:** Mitochondrial Ca^{2+} was measured in TMX1 wild type and knockout HeLa cells transfected with the mitochondrial Ca^{2+} indicator mito-LAR-GECO1.2. In the absence of extracellular Ca^{2+}, 50 µM histamine was added to trigger a Ca^{2+} release through the IP_3Rs. Peak height was measured as transfer of Ca^{2+} to the mitochondria. n = 3; p = 0.043. **C:** Mitochondrial Ca^{2+} was measured in HeLa cells stably transfected with a shTMX1 expressing plasmid for TMX1 knockdown, and transfected with the mitochondrial Ca^{2+} indicator mito-LAR-GECO1.2. In the presence of extracellular Ca^{2+}, 50 µM histamine was added to trigger a Ca^{2+} release through the IP_3Rs. Peak height was measured as transfer of Ca^{2+} to the mitochondria. n = 4; p = 0.0019. **D:** Mitochondrial Ca^{2+} was measured in HeLa cells stably transfected with a shTMX1 expressing plasmid for TMX1 knockdown, and transfected with the mitochondrial Ca^{2+} indicator mito-LAR-GECO1.2. In the absence of extracellular Ca^{2+}, 50 µM histamine was added to trigger a Ca^{2+} release through the IP_3Rs. Peak height was measured as transfer of Ca^{2+} to the mitochondria. n = 3; p = 0.016.

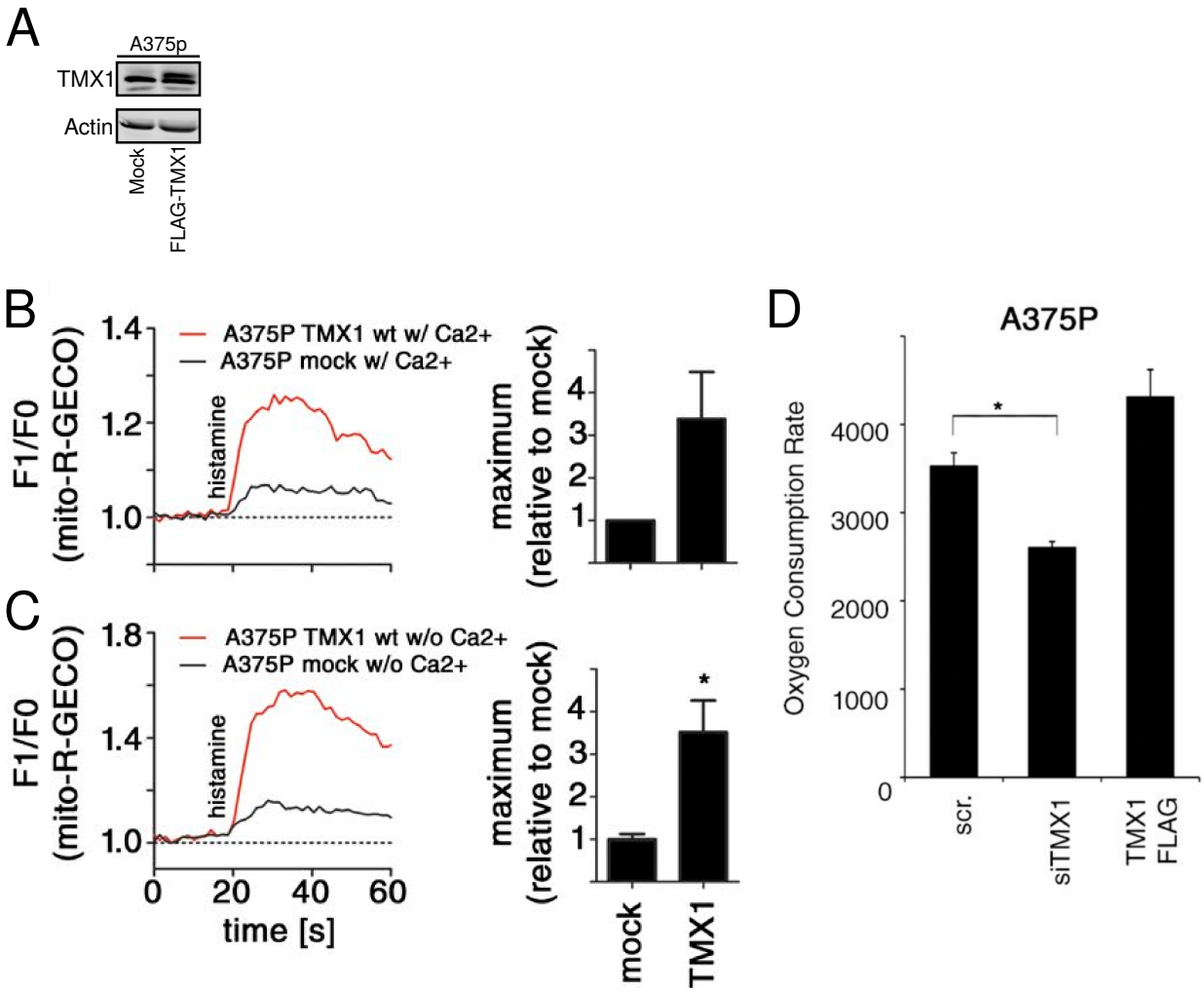

Figure 3.6 – TMX1 overexpression increases Ca^{2+} transfer from ER to mitochondria and mitochondrial respiration in A375p melanoma cells. A: A375p cells stably transfected with a FLAG-TMX1 expressing plasmid for TMX1 overexpression and immunoblotted for TMX1 and Actin as a loading control. **B:** Mitochondrial Ca^{2+} was measured in A375p cells stably transfected with a FLAG-TMX1 expressing plasmid for TMX1 overexpression, and transfected with the mitochondrial Ca^{2+} indicator mito-LAR-GECO1.2. In the presence of extracellular Ca^{2+}, 50 µM histamine was added to trigger a Ca^{2+} release through the IP_3Rs. Peak height was measured as transfer of Ca^{2+} to the mitochondria. n = 4. **C:** Mitochondrial Ca^{2+} was measured in A375p cells stably transfected with a FLAG-TMX1 expressing plasmid for TMX1 overexpression, and transfected with the mitochondrial Ca^{2+} indicator mito-LAR-GECO1.2. In the absence of extracellular Ca^{2+}, 50 µM histamine was added to trigger a Ca^{2+} release through the IP_3Rs. Peak height was measured as transfer of Ca^{2+} to the mitochondria. n = 4; p = 0.01. **D:** Mitochondrial respiration was measured in A375p cells stably transfected with a shTMX1 expressing plasmid for TMX1 knockdown or a FLAG-TMX1 expressing plasmid for TMX1 overexpression. n = 3; Control *vs* shTMX1: p = 0.018. *Experiments in panels A and D were performed by Carolina Ortiz-Sandoval and Arun Raturi respectively.*

3.2.5 TMX1 palmitoylation and oxidoreductase activity are required for its MAM localization and Ca^{2+} regulatory effect

Next, the effect of palmitoylation and oxidoreductase activity on TMX1 Ca^{2+} regulation was evaluated. In order to test this, A375p melanoma cells and TMX1 knockout HeLa cells were transfected with FLAG tagged TMX1. In addition, to evaluate the dependence on palmitoylation, cells were transfected with a TMX1 mutant with altered palmitoylation site (FLAG-TMX1-CCAA); this mutation prevents TMX1 MAM targeting [146]. Furthermore, to address the role of the oxidoreductase activity, cells were transfected with a TMX1 mutant with a modification in the two cysteines in the active site of its thioredoxin domain (FLAG-TMX1-SXXS). As expected, subcellular fractionation shows that wild type TMX1 is distributed between MAM and microsomes. In contrast, the palmitoylation mutant FLAG-TMX1-CCAA is not targeted to the MAM, and is restricted to the microsomes fraction, were the bulk ER is located. Surprisingly, the oxidoreductase mutant FLAG-TMX1-SXXS also loses its MAM targeting, suggesting that an active thioredoxin domain is required for normal TMX1 localization **(Figure 3.7A)**. A similar result was observed when the interaction of SERCA with the TMX1 mutants was evaluated. In this case, both FLAG-TMX1-CCAA and FLAG-TMX1-SXXS co-immunoprecipitated less with SERCA2b than wild type TMX1. This result suggest that both the palmitoylation and an active thioredoxin domain are required for TMX1-SERCA2b interaction **(Figure 3.7B)**. In terms of ER Ca^{2+} loading ability, consistent with previous results, the expression of wild type TMX1 reduced the amount of Ca^{2+} in the ER. On the other hand, FLAG-TMX1-SXXS had a small effect reducing ER Ca^{2+} content, while FLAG-TMX1-CCAA reached an intermediate effect between wild type and FLAG-TMX1-SXXS **(Figure 3.7C)**. Consistent with previous results, TMX1 knockout HeLa cells rescued with FLAG-TMX1 have a significantly better Ca^{2+} transfer to mitochondria after histamine treatment than mock transfected cells. In addition the thioredoxin mutant FLAG-TMX1-SXXS and the palmitoylation mutant FLAG-TMX1-CCAA were unable to rescue the Ca^{2+} transfer **(Figure 3.7D)**. These results indicate that both palmitoylation and thioredoxin domains are necessary for TMX1 effect on Ca^{2+} regulation and MAM localization; and that some oxidative modification of SERCA might be involved in TMX1 function.

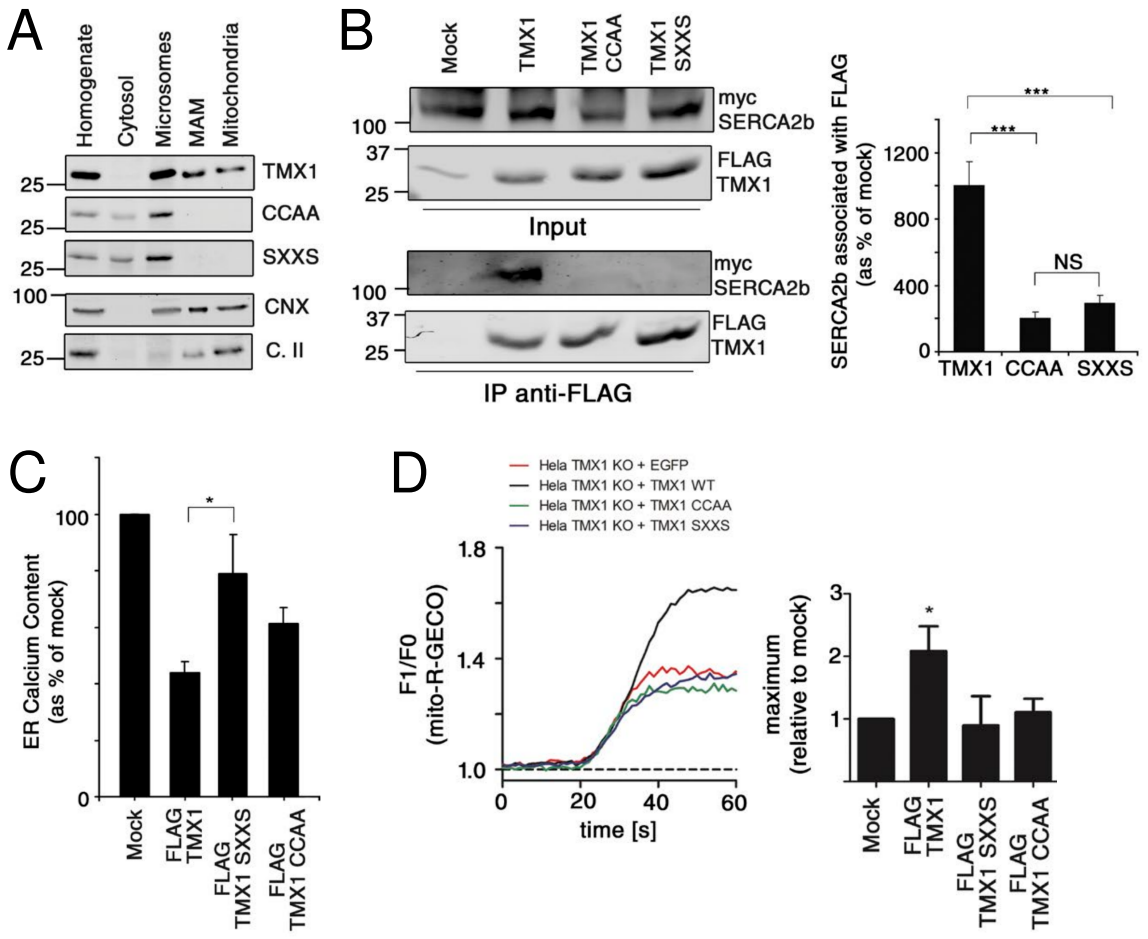

Figure 3.7 – Palmitoylation and thioredoxin domains are necessary for TMX1 effect on Ca^{2+} regulation and MAM localization. A: Western blot of a Percoll fractionation showing the Homogenate and Cytosol, Microsomes, MAM and Mitochondria subcellular fractions from A375p melanoma cells transfected with a FLAG-TMX1, FLAG-TMX1-SXXS (thioredoxin mutant) or FLAG-TMX1-CCAA (palmitoylation mutant) expressing plasmid. CNX was used as a MAM marker and Complex 2 was used as a mitochondrial marker. **B:** Co-immunoprecipitation of FLAG tagged TMX1 mutants with myc tagged SERCA2b from protein extracts of A375p melanoma cells transfected with a FLAG-TMX1, FLAG-TMX1-SXXS (thioredoxin mutant) or FLAG-TMX1-CCAA (palmitoylation mutant), and myc-SERCA2b expressing plasmids. n = 3. FLAG-TMX1 *vs* FLAG-TMX1-CCAA: p = 0.000013. FLAG-TMX1 *vs* FLAG-TMX1-SXXS: p = 0.000197. **C:** ER Ca^{2+} content measured in A375p melanoma cells transfected with a FLAG-TMX1, FLAG-TMX1-SXXS (thioredoxin mutant) or FLAG-TMX1-CCAA (palmitoylation mutant) expressing plasmid. n = 3. FLAG-TMX1 *vs* FLAG-TMX1-SXXS: p = 0.01. **D:** Mitochondrial Ca^{2+} was measured in TMX1 knockout HeLa cells transfected with a FLAG-TMX1, FLAG-TMX1-SXXS (thioredoxin mutant) or FLAG-TMX1-CCAA (palmitoylation mutant) expressing plasmid, and transfected with the mitochondrial Ca^{2+} indicator mito-LAR-GECO1.2. In the presence of extracellular Ca^{2+}, 50 µM histamine was added to trigger a Ca^{2+} release through the IP_3Rs. Peak height was measured as transfer of Ca^{2+} to the mitochondria. n = 10 for Mock, n = 11 for FLAG-TMX1, n = 14 for FLAG-TMX1-SXXS, n = 6 for FLAG-TMX1-CCAA. Mock *vs* FLAG-TMX1: p = 0.03. *Experiments in panels A, B and C were performed by Arun Raturi.*

3.2.6 TMX1 increases ER-mitochondria contacts

In addition to alterations in Ca^{2+} signalling, changes in Ca^{2+} transfer to the mitochondria can be explained by changes in ER-mitochondria contact formation. TMX1 promotes the transfer of Ca^{2+} to mitochondria from the ER, suggesting that it also increases ER-mitochondria contact formation. To test the effect of TMX1, ER-mitochondria contacts were observed using electron microscopy, and the distance and extent of ER-mitochondria contacts was measured **(Figure 3.8A)**. Cells that lack TMX1 have the same ER-mitochondria distance than cells that have TMX1 **(Figure 3.8B)**. Nevertheless, the length of the contacts was significantly shorter in TMX1 knockout cells, suggesting that TMX1 promotes interaction between ER and mitochondria **(Figure 3.8C)**. Accordingly, there is a significant reduction in the coefficient *contact length / distance* in cells that lack TMX1 **(Figure 3.8D)**. These results suggest that TMX1 participates in the formation of ER-mitochondria contacts, but it controls the extent of the contacts and not the distance between the two organelles. Consistently, the frequency of different ER-mitochondria distances, classified as Super tight (0 to 12 nm), Tight (12 to 24 nm), and Loose (24 to 50 nm), was unchanged between TMX1 wild type and knockout cells **(Figure 3.8E)**. Taken together, TMX1 increases ER-mitochondria contact formation, suggesting that the increased Ca^{2+} transfer to mitochondria is due to the increased organelle proximity. The increased release of Ca^{2+} from the ER through the IP_3Rs could also play a role in the improved Ca^{2+} transfer to the mitochondria promoted by TMX1. However, when the release of Ca^{2+} to the cytosol through IP_3R was equalized by removing extracellular Ca^{2+} **(Figure 3.4)**, TMX1 wild type cells still had better transfer of Ca^{2+} to the mitochondria **(Figure 3.5A and B)**. This suggests that the ER-mitochondria contacts maintained by TMX1 are required to keep a normal Ca^{2+} flux to mitochondria.

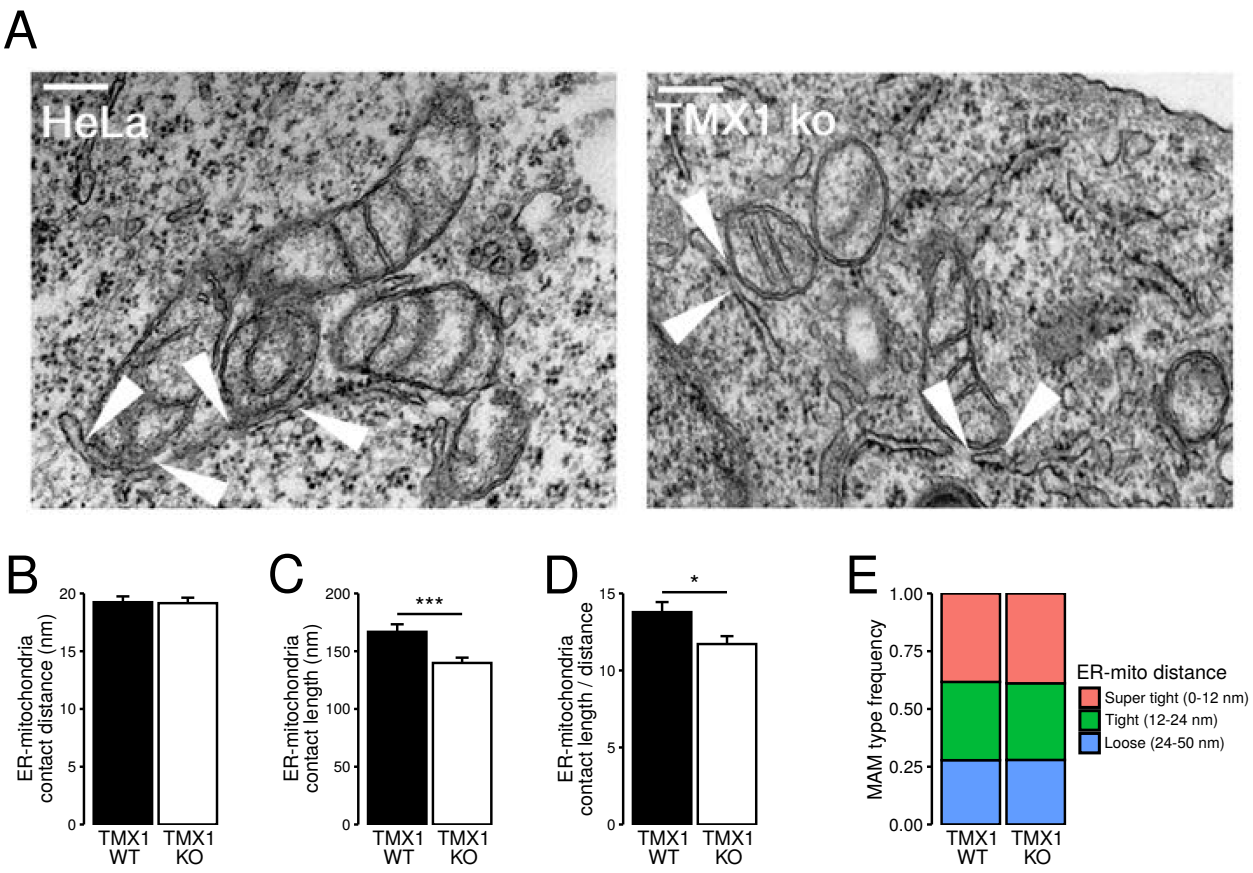

Figure 3.8 – TMX1 increases ER-mitochondria contact formation. A: Electron microscopy images of TMX1 wild type and knockout HeLa cells. Regions of ER-mitochondria contacts are indicated with white arrowheads. Scale bar = 150 nm. **B:** ER-mitochondria distance. n = 593 for HeLa TMX1 WT, n = 648 for HeLa TMX1 KO; p = 0.9. **C:** ER-mitochondria contact length. n = 593 for HeLa TMX1 WT, n = 648 for HeLa TMX1 KO; p = 0.00064. **D:** *Contact length / distance* ratio. n = 593 for HeLa TMX1 WT, n = 648 for HeLa TMX1 KO; p = 0.012. **E:** Frequency of ER-mitochondria contacts classified by distance into Super tight (0 to 12 nm), Tight (12 to 24 nm), and Loose (24 to 50 nm). n = 593 for HeLa TMX1 WT, n = 648 for HeLa TMX1 KO. *The images were analyzed with the help of Carolina Ortiz-Sandoval.*

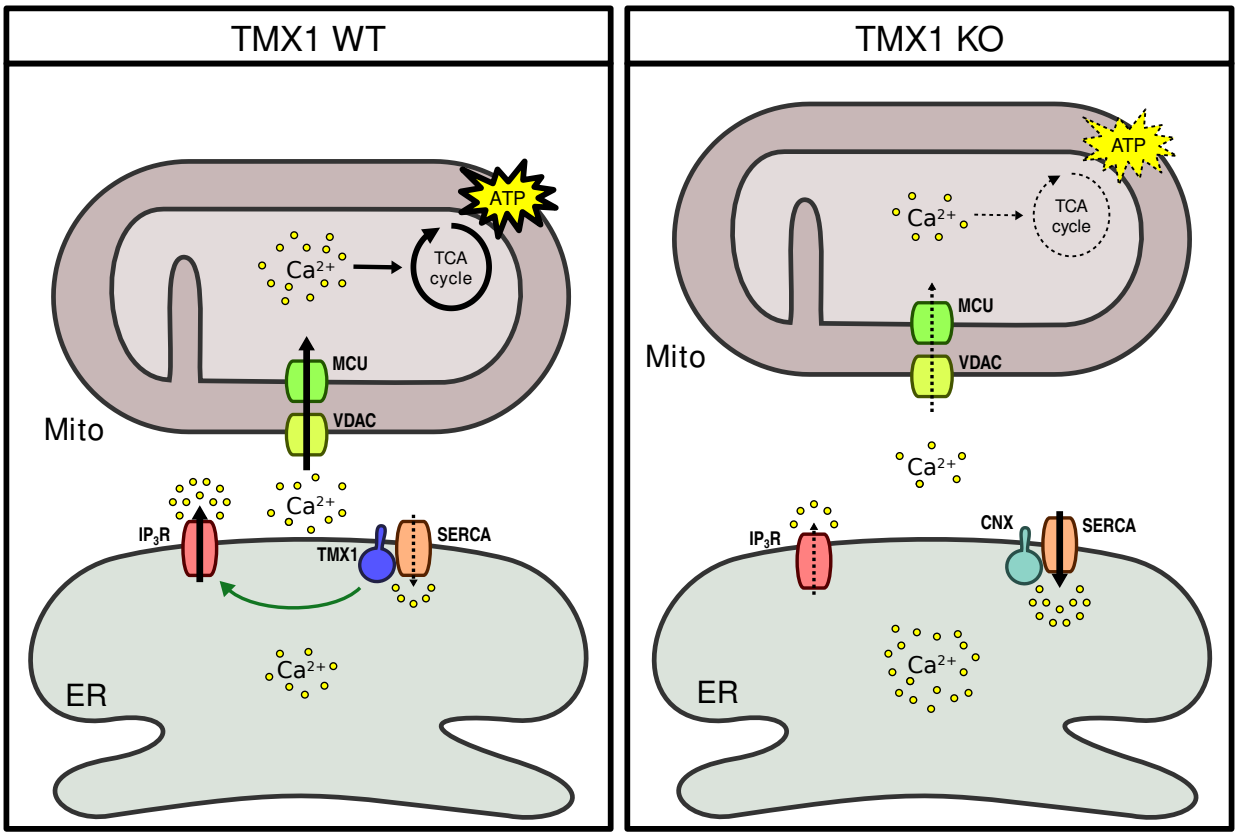

Figure 3.9 – Schematic representation of the proposed effect of TMX1 in the MAM. TMX1 binds and inhibits SERCA, resulting in the depletion of ER Ca^{2+} stores. It also promotes the release of Ca^{2+} from the ER through IP_3R and the formation of ER-mitochondria contacts. As a result, TMX1 increases mitochondrial Ca^{2+} flux and mitochondrial respiration and energy production. In the absence of TMX1, SERCA is more active and the ER Ca^{2+} stores are augmented. There is also a reduction in ER-mitochondria length (depicted as a change in distance) and Ca^{2+} release from the ER through IP_3R. This results in impaired Ca^{2+} flux to mitochondria and reduced mitochondrial metabolism. Solid black arrows represent normal activity; dashed black arrows represent reduced activity.

3.3 Discussion

3.3.1 TMX1 regulates SERCA activity and ER Ca^{2+} content from the MAM

TMX1 controls ER Ca^{2+} content as a result of an inhibition of SERCA activity, as summarized in **Figure 3.9**. Indeed, the results show that TMX1 interacts with SERCA2b **(Figure 3.1A)**, reducing ER Ca^{2+} levels to half of cells that lack TMX1 **(Figure 3.2)**. In addition, the MAM localization of TMX1 is also important for its Ca^{2+} signalling regulation. The TMX1 mutant TMX1-CCAA that lacks the palmitoylation site, the critical switch for MAM targeting [146], is unable to interact with SERCA, and cannot regulate ER Ca^{2+} content; this suggests that palmitoylation and/or MAM location are critical for the Ca^{2+} regulatory functions of TMX1 **(Figure 3.7)**. Nevertheless, unlike TMX1, SERCA is not MAM targeted. It can be found in the MAM, but it is also abundant in the bulk ER. This means that TMX1 MAM targeting is not enough to explain its regulatory effect on SERCA. Some mechanism must be in place that prevents non-MAM TMX1 to inhibit SERCA.

One alternative that could explain why TMX1 inhibits SERCA only at the MAM is if TMX1 has an unidentified binding partner exclusively found at the MAM that is required for TMX1-SERCA interaction and inhibition. There are other oxidoreductases that have binding partners that give specificity to their redox targets. For instance, is well known that the oxidoreductase ERp57 binds the lectin chaperones CNX and CRT and targets preferentially glycosylated proteins for disulfide bond formation [132]. Similarly, the oxidoreductase P5 binds to the chaperone BiP, and targets BiP client proteins [199]. TMX1 also forms a functional complex with CNX for disulfide bond formation, similar to ERp57 [135]. Since both TMX1 and CNX are MAM-targeted proteins, it is possible that they are interacting at the MAM. Accordingly, the result shows that both TMX1 and CNX interact with SERCA2b **(Figure 3.1A)**, suggesting a possible functional complex between TMX1 and CNX with SERCA as a target. Nevertheless, TMX1 and CNX compete for SERCA interaction, and the absence of one of them increases SERCA interaction for the other **(Figure 3.1B and C)**. These results suggest that SERCA is not a target of a functional TMX1-CNX complex, but forms independent complexes with either TMX1 or CNX. Whether the presence of SERCA interferes with TMX1-CNX interac-

tion is not known, and would have to be explored in future experiments. Regardless, this interplay between TMX1, CNX and SERCA discards CNX as a third member of a MAM-exclusive TMX1-SERCA complex. So far, the existence of a binding partner for TMX1 and SERCA at the MAM cannot be discarded. But the identification of this protein would require future experiments.

Another option for the MAM-specific SERCA inhibition by TMX1 is the presence of other binding partners exclusively found outside the MAM that compete with SERCA for TMX1 interaction. In this scenario, CNX would be an excellent candidate, because it competes with TMX1 for SERCA binding (**Figure 3.1**). Nevertheless, both TMX1 and CNX are located in the MAM, making this interference unlikely in the bulk ER. But there is a fraction of CNX, approximately 10%, that localizes in the bulk ER, and is found in the light membranes under normal conditions after cellular fractionation [114]. This non-MAM CNX could be able to prevent the interaction and inhibition of SERCA by TMX1 by competing with TMX1 for SERCA interaction. But even the overexpression of the non-palmitoylable TMX1-CCAA mutant was unable to rescue the normal Ca^{2+} flux to mitochondria. Whether 10% of CNX is enough to completely block the effect of TMX1-CCAA overexpression remains to be tested, but it seems unlikely.

Finally, it is possible that palmitoylation itself is the signal required for SERCA interaction. Thus, non-palmitoylated TMX1 and TMX1-CCAA would be unable to interact with SERCA, regardless of their location. This suggests that TMX1 palmitoylation has two separate functions. One is two target TMX1 to the MAM, and the other is to regulate its interacting partners. With the results presented here, it is not possible to discard that palmitoylation is required for the inhibitory effect of TMX1. However, demonstrating that palmitoylation has an effect on TMX1 activity independent of MAM targeting would be quite complicated from an experimental point of view. It would require a non-palmitoylable MAM-targeted and/or a palmitoylated non-MAM-targeted TMX1. Both options seem unlikely with our current understanding of TMX1 MAM targeting. Regardless, palmitoylation is a modification that can change protein-protein interactions by steric hindrance and/or changes in protein conformation, in addition to changes in protein localization [200]. For instance, CNX palmitoylation

also regulates its protein interactions. CNX depalmitoylation by ER stress increases its interaction with ERp57 and decreases the interaction with SERCA, despite the increased co-fractionation of CNX and SERCA in the rough ER [114]. In the future, it would be interesting to explore protein interactions of palmitoylated and non-palmitoylated TMX1. The interplay between TMX1 and other SERCA regulators like CNX and ERp57 would clarify the mechanism by which TMX1 regulates Ca^{2+} signalling and whether other proteins are involved.

3.3.2 TMX1 regulates SERCA activity probably through redox modifications

The results show that TMX1 knockout cells have increased ER Ca^{2+} levels compared to TMX1 wild type cells, suggesting that TMX1 has an inhibitory effect on SERCA **(Figure 3.2)**. Since TMX1 interacts with SERCA, as found by co-immunoprecipitation, the inhibitory effect on SERCA is probably through their proximity or interaction **(Figure 3.1A)**. While re-expression of TMX1 is able to rescue the defects observed in TMX1 knockout cells, the thioredoxin mutant TMX1-SXXS is unable to rescue Ca^{2+} transfer to mitochondria, and only partially able to rescue ER Ca^{2+} content **(Figure 3.7)**. These results suggest that TMX1 regulates SERCA in part through its oxidoreductase activity, even through SERCA activity was not directly measured. The first step to further understand the regulation of Ca^{2+} signalling by TMX1 would be to measure SERCA activity. This measurement can be done in future experiments using the SERCA ATPase measurement, described in section 2.6, in TMX1 wild type and knockout cells.

Assuming that TMX1 regulates SERCA activity, the mechanism of SERCA inhibition by TMX1 is not clear. More experiments are needed to understand this mechanism, but the results show that the oxidoreductase activity of TMX1 is partially required. SERCA2b contains two cysteines in positions 875 and 887 in the L4 lumenal loop that form an inhibitory disulfide bond [154]. Since TMX1 and SERCA interact, the most likely scenario is that TMX1 acts on SERCA2b lumenal disulfide bonds to regulate its activity. In addition, TMX1 preferentially targets membrane proteins [135], making SERCA2b a likely target for its oxidoreductase activity. There are two experiments that can clarify the effect of TMX1 in SERCA2b disulfide bond formation. One is to directly measure SERCA

redox state. This can be done using the BIAM labelling of reduced cysteines, as described in section 2.15. This would indicate, for example, if SERCA is more reduced in TMX1 knockout cells. But this method is not specific for disulfide bonds or other forms of oxidative modification. In order to test if SERCA is a specific target for TMX1 oxidoreductase activity, it is possible to use a TMX1 trapping mutant. During disulfide bond oxidation or reduction, the cysteines at the thioredoxin domain catalytic site (CXXC) form a transient mixed disulfide with the target protein. By mutating the C-terminal cysteine of the active site, it is possible to trap the mixed disulfide effectively linking the oxidoreductase with its target. A TMX1 trapping mutant, $TMX1_{C/A}$, was used in a previous publication to find folding targets of TMX1 (SERCA was not mentioned as a TMX1 target, but the list provided is not exhaustive) [135]. By using this TMX1 mutant it would be possible to test if TMX1 specifically targets SERCA2b lumenal disulfide bond. If this is the case, there are two possible mechanisms for SERCA2b inhibition by TMX1. One possible mechanism is that TMX1 has the same activity as ERp57, an oxidoreductase that catalyzes the formation of SERCA2b disulfide bond [154]. So when TMX1 and SERCA2b interact, TMX1 oxidizes SERCA2b forming the disulfide bond that results in SERCA2b inhibition. But if TMX1 is inactive or if it cannot interact with SERCA2b, then the inhibitory disulfide bond gets reduced and SERCA2b activity is increased. The problem with this mechanism is that it requires TMX1 to act as an oxidase, while the literature indicates that TMX1 acts as a reductase, breaking disulfide bonds rather than forming them [136–138,197]. The second possible mechanism is that TMX1 acts as a reductase, targeting the same inhibitory disulfide bond on SERCA2b but instead of reducing it completely, it forms a mixed disulfide with SERCA2b; rather than reducing both cysteines in the disulfide bond, it forms a bond between one of the cysteines in SERCA2b and one of the cysteines on its thioredoxin active site. This mixed disulfide is a intermediary step between complete oxidation and reduction of disulfide bonds **(Figure 1.2)**, but some oxidoreductases form stable interactions with their targets through a mixed disulfide. For example, ERdj5 is an ER oxidoreductase with reducing activity, similar to TMX1; it can reduce the inhibitory disulfide bond in SERCA2b forming a stable mixed disulfide that can be detected as a high molecular weight protein complex using Western blot in non-denaturing conditions

[155]. TMX1 could act in a similar way, forming a stable complex with SERCA2b that results in SERCA2b inhibition. This fits with TMX1 acting as a reductase and having an inhibitory effect on SERCA2b, but the formation of a stable mixed disulfide between these two proteins would have to be demonstrated using non-denaturing Western blot. To test if TMX1 is targeting cysteines 875 and 887, SERCA2b mutants with these cysteines modified can be used; for example, a cysteine to serine mutation (SERCA-CCSS). This SERCA mutant should be permanently active and immune to ERp57 inhibition. If TMX1 and ERp57 have the same target, it should be immune to TMX1 regulation too. This can be tested by expressing SERCA-CCSS in TMX1 knockout cells, and then co-express TMX1 to see if there is an increase in SERCA activity.

Interestingly, the thioredoxin mutant TMX1-SXXS loses MAM targeting, in addition to SERCA interaction **(Figure 3.7)**. This raises the question whether oxidoreductase activity is involved in TMX1 MAM targeting. Unfortunately, the palmitoylation state of TMX1-SXXS was not evaluated, so it is unknown if losing oxidoreductase activity is enough to lose MAM targeting, or if oxidoreductase activity is required for the palmitoylation. It is possible that the thioredoxin domain itself is required for TMX1 MAM targeting. There is one other protein whose MAM-targeting depends on its redox activity: Ero1α. Under normal conditions, Ero1α localization depends on the formation of a mixed disulfide bond with the oxidoreductase ERp44; this interaction retains Ero1α in the ER [201]. However, the formation of this mixed disulfide bond requires an oxidizing environment in the ER; under reducing conditions the Ero1α–ERp44 disulfide bond is lost, and Ero1α leaves the MAM [163]. It is possible that a similar mechanism operates for TMX1 retention at the ER, with ERp44 acting as an anchor for Ero1α and TMX1. Since TMX1-SXXS is unable to form disulfide bonds, it cannot be retained by ERp44 and relocates to the bulk ER. If TMX1 forms a mixed disulfide with SERCA2b, then this bond could also work as an anchor for TMX1 in the MAM, as long as this specific mixed disulfide is formed only at the MAM. However, future experiments would be needed to determine if TMX1 forms mixed disulfide bonds with ERp44 or SERCA2b in order to retain its MAM localization, or if the oxidation state of TMX1 is actually regulating its palmitoylation.

3.3.3 TMX1 is a regulator of Ca^{2+} flux and mitochondrial metabolism

A previous report from our lab showed that TMX1 is localized at the MAM, suggesting that it could have an additional function in addition to protein folding [146]. The present work shows that MAM located TMX1 is a regulator of Ca^{2+} signalling. TMX1 increases Ca^{2+} flux from ER to mitochondria **(Figure 3.5** and **Figure 3.6)**, which then activates mitochondrial respiration **(Figure 3.6D)**. TMX1 exerts its regulatory effect on Ca^{2+} signalling through the interaction with SERCA2b **(Figure 3.1** and **Figure 3.7)**. Cells that lack TMX1 have improved Ca^{2+} clearance from the cytosol **(Figure 3.4)**, and accumulate more Ca^{2+} in the ER **(Figure 3.2)**. These results are consistent with TMX1 acting as a SERCA inhibitor. Thus, when Ca^{2+} is released from the ER, the inhibitory effect of TMX1 on SERCA2b prevents the clearance of the released Ca^{2+}, resulting in an improved Ca^{2+} transfer to mitochondria. TMX1 acts like a switch that changes the balance of Ca^{2+} in the cell from ER to mitochondria.

TMX1 has an additional layer of control of Ca^{2+} flux to mitochondria, the regulation of ER-mitochondria contacts, which have a reduced length in cells that lack TMX1 **(Figure 3.8)**. Thus, TMX1 promotes Ca^{2+} flux to mitochondria by two parallel mechanisms, by promoting ER-mitochondria contact formation, and by inhibiting SERCA and preventing Ca^{2+} uptake at the ER-mitochondria interface. But the mechanism that TMX1 uses to promote contact formation was not explored in this work. Since TMX1 has a transmembrane and cytosolic domain, it is possible that it acts as a tether, establishing a physical link between ER and mitochondria, even though no potential partner on the mitochondrial side has been described. It is more likely that TMX1 modulates the function of other MAM proteins similar to its effect on SERCA. It is interesting that the length of the ER-mitochondria was altered but not the distance between organelles **(Figure 3.8)**. This suggests that TMX1 acts by recruiting or stabilizing existing tethers at the MAM. The loss of TMX1 prevents the formation of these tethers, reducing the extent of MAM. However, the overall structure of the contacts must remains the same, since the distance is unchanged. As mentioned before, the regulatory effect of TMX1 on SERCA depends on its thioredoxin domain, probably by reducing

SERCA disulfide bonds **(Figure 3.7)**. Finding new TMX1 binding partners using the $TMX1_{C/A}$ trapping mutant would be helpful to discover new MAM proteins regulated by TMX1. In addition, it would be interesting to know what is the effect of TMX1-CCAA and TMX1-SXXS mutants on ER-mitochondria contacts using electron microscopy. These mutants were unable to rescue Ca^{2+} flux to mitochondria and are not targeted to the MAM **(Figure 3.7)**. With this experiment it would be possible to determine if the effect of TMX1 on Ca^{2+} signalling and ER-mitochondria contacts share a similar mechanism.

3.3.4 TMX1 is a tumor suppressor that regulates cancer cell metabolism

Mitochondrial Ca^{2+} can have positive or negative effects on cancer progression. The accumulation of mitochondrial Ca^{2+} can increase mitochondrial ROS production, promoting cell migration, metastasis and cancer progression [195,202,203]. Yet, many cancer types present an anomalous metabolism that consists of relying primarily on glycolysis for energy production, and reducing the requirement of mitochondrial respiration [180]. Since mitochondrial Ca^{2+} is required to maintain a basal level of mitochondrial respiration [80], this phenotype is consistent with cancer cells having reduced ER-mitochondria Ca^{2+} flux. In addition, preventing mitochondrial Ca^{2+} accumulation also has the advantage of preventing cell death through mitochondrial Ca^{2+} overload [67,69], another hallmark of cancer [180]. Similar to TMX1, the tumor suppressor p53 is targeted to the MAM and increases Ca^{2+} flux to mitochondria [61]. Interestingly, p53 has the opposite effect than TMX1 on SERCA activity and Ca^{2+} loading. p53 activates SERCA and increases ER Ca^{2+} stores, increasing Ca^{2+} availability for apoptotic Ca^{2+} signalling towards mitochondria [61]. TMX1 decreases the amount of ER Ca^{2+} through its inhibitory effect on SERCA **(Figure 3.2)**, but it also increases the extent of ER-mitochondria contacts **(Figure 3.8)**, thus promoting the flux of Ca^{2+} **(Figure 3.5** and **Figure 3.6)**. These results suggest that TMX1 could act as a tumor suppressor, increasing Ca^{2+} flux and preventing cancer progression. Indeed, results from our lab show that TMX1 slows down tumor growth *in vivo*, suggesting that the critical factor in tumor suppressor MAM proteins is the induction of ER-mitochondria contacts and Ca^{2+} flux, rather than the available Ca^{2+} in the ER [204]. TMX1 has the

opposite effect of FATE1, an oncoprotein that reduces Ca^{2+} flux to mitochondria by decreasing the number of ER-mitochondria contacts [205]. Again, a better understanding of TMX1 interactome is essential to find the critical mediators of TMX1 MAM regulation. This will help us understand the MAM changes during tumorigenesis and, potentially, design better treatments. Interestingly, a recent work confirmed our findings on the role of TMX1 in MAM formation, showing that loss of TMX1 results in reduced ER-mitochondria contacts in a melanoma cancer model [206]. Nevertheless, loss of TMX1 also resulted in increased plasma membrane-mitochondria contacts. As a consequence, reduced expression of TMX1 still results in mitochondrial Ca^{2+} accumulation and elevated ROS levels, despite their reduced MAM formation [206]. However, in this model the elevated ROS production was not tumorigenic. On the contrary, ROS inhibited the phosphatase Calcineurin and the transcription factor NFAT1, reducing proliferation and migration in melanoma cells [206]. This highlights the interconnected signalling pathways and regulatory mechanisms that take place at the MAM in cancer.

Chapter 4

Calnexin regulates ER-mitochondria contact formation and Ca^{2+} flux

4.1 Introduction

4.1.1 Calnexin is an ER chaperone that binds glycoproteins during protein folding

Calnexin (CNX) is transmembrane ER protein that participates in quality control of *N*-glycosylated protein folding in the ER. It binds to newly synthesized glycosylated proteins after they enter the ER through the translocon [207]. The binding of CNX results in retention of folding intermediates in the ER, slowing down the folding process; but at the same time, the maturation process is more efficient and there is less misfolded protein aggregation [124,125].

CNX binds to glycoproteins through a carbohydrate-binding lectin domain in its N-terminal region. Next is the P domain, a flexible arm that extends from the lectin domain. The P domain is followed by a transmembrane region and a short cytoplasmic domain [208]. The P domain functions as an adapter for other protein folding assistants. So far, three assistants have been identified: the disulfide isomerases ERp57 and ERp29, and the prolyl *cis-trans* isomerase Cyclophilin B [209–211]. Thus,

CNX guides these accessory folding assistants to target preferentially glycoproteins. The best characterized of the CNX folding assistants is ERp57. CNX association with ERp57 results in a greater interaction of ERp57 with newly synthesized glycoproteins [212,213]. This CNX guiding mechanism is required for an efficient disulfide bond formation and isomerization by ERp57, increasing the correct folding of CNX targeted proteins and preventing protein aggregation [132,214,215]. CNX interaction with ERp57 increases during ER stress, boosting CNX folding capacity [146]. Thus, CNX is a versatile and dynamic chaperone, able to adapt to different requirements depending on its protein-protein interactions.

4.1.2 Calnexin beyond protein folding: Mitochondria-Associated Membranes and the regulation of Ca^{2+} signalling

CNX interacting partners are not limited to chaperones and folding assistants. It also interacts with proteins at the MAM, extending the repertoire of regulatory functions from protein folding to Ca^{2+} signalling and apoptosis. Indeed, an important portion of CNX can be found in the MAM [146,216–218]. The key for CNX enrichment in the MAM is the palmitoylation of two cysteines close to the transmembrane region, cysteines 502 and 503, by the palmitoyl transferase DHHC6 [147]. The inhibition of CNX palmitoylation moves it away from the MAM, and distributes CNX in the bulk ER [146]. This suggests that CNX is normally found in its palmitoylated form. Palmitoylation also regulates CNX interaction with other proteins. Palmitoylated CNX forms part of the translocon, the protein complex responsible for the co-translational translocation of newly synthesized proteins into the ER [147]. This interaction stabilizes the translocon, improving the folding of glycoproteins [147]. Palmitoylated CNX also interacts with the ER Ca^{2+} pump SERCA isoform 2b (SERCA2b). It is not clear whether CNX regulates SERCA2b activity directly, but loss of CNX or loss of CNX palmitoylation results in a reduction in ER Ca^{2+} content [114]. This suggest that CNX activates SERCA2b pumping function, promoting the loading of Ca^{2+} in the ER. An additional function of CNX at the MAM is the regulation of Ca^{2+} flux to the mitochondria. CNX prevents the transfer of Ca^{2+} from ER to mitochondria, but only when it is palmitoylated. Non-palmitoylated CNX or the

loss of CNX makes Ca^{2+} transfer to mitochondria more efficient [114]. How CNX regulates Ca^{2+} transfer to mitochondria, and the consequences for mitochondrial function, is currently unknown.

4.1.3 Calnexin beyond protein folding: regulation of reactive oxygen species

An additional function of CNX is the regulation of reactive oxygen species (ROS) production at the ER, specifically through the regulation of NADPH oxidase 4 (NOX4). CNX interacts and stabilizes NOX4, increasing NOX4 H_2O_2 production [219]. Unlike other NOX proteins, NOX4 is constitutively active [220]; this property allows NOX4 to act as a O_2 sensor, increasing H_2O_2 production at high O_2 levels [221]. NOX4 protein expression and activity also increase during ER stress, promoting the expression of apoptotic transcription factors like CHOP and inducing apoptosis [222,223]. Thus, NOX4 behaves similarly to Ero1α, since the latter is also upregulated during ER stress and induce apoptosis via ROS production [72]; although NOX4 activity has not been linked to oxidative protein folding. On the other hand, unlike Ero1α, NOX4 overexpression is not always associated with cell death. NOX4 is abundantly expressed in some forms of cancer, where it enhances proliferation and survival [224]. The protective and growth promoting effects of NOX4 in cancer are associated to an accelerated glutamine metabolism and increased production of glutathione, which provides resistance to H_2O_2-induced oxidative damage [225]. At the same time, NOX4 activates the Akt/HIF1α signalling pathway, which increases survival, proliferation and invasion in cancer cells, and also shifts the metabolism towards glycolysis [226,227]. Finally, NOX4 also regulates ER Ca^{2+} channels. It oxidizes and activates ryanodine receptors (RyR) channels, increasing Ca^{2+} release from the ER and the contractile function of muscle cells [228]. NOX4 can also oxidize and regulate the ER Ca^{2+} pump SERCA, but the effect on SERCA activity depends on other pathophysiological conditions, and possibly the cell type. The key difference is the type of oxidative modification in cysteine 674; sulfonylation inhibits SERCA, while glutathionylation increases SERCA activity, but it also requires the presence of nitric oxide [162,229,230]. Under stressful and damaging conditions like obesity or high glucose, upregulation of NOX4 is responsible for the sulfonylation and inactivation of SERCA in rat smooth muscle cells [231,232]. On the other hand, NOX4 is also activated by VEGF in endothelial

cells under normal physiological conditions, resulting in an increased SERCA glutathionylation and activity, promoting cell migration and angiogenesis [233]. Even though CNX stabilizes and increases NOX4 H_2O_2 production [219], it is not known if NOX4 activity is involved in CNX regulation of SERCA, or if CNX regulates the apoptotic or metabolic effects of NOX4.

4.1.4 Aims

In this chapter, the role of CNX in the regulation of SERCA, and its consequences for ER-mitochondria Ca^{2+} communication will be investigated. In order to do this, the following aims are proposed: (*i*) measure the effect of CNX on SERCA ATPase activity and ER Ca^{2+} content; (*ii*) evaluate the consequences of SERCA regulation by CNX on Ca^{2+} signalling; (*iii*) evaluate the role of CNX on ER-mitochondria contact formation, Ca^{2+} flux and mitochondrial function; and (*iv*) investigate whether CNX regulates SERCA activity by redox modifications, and the possible participation of Ero1α and NOX4 as ER ROS sources responsible for SERCA oxidation. These aims were evaluated in a CNX knockout Mouse Embryonic Fibroblast (MEF) cell line, in addition to other molecular tools to knockdown or overexpress CNX.

The results show that CNX increases ER Ca^{2+} content by activating SERCA. Mechanistically, SERCA activation is a result of oxidative modifications mediated by Ero1α and NOX4 ROS production. In addition, CNX reduces ER-mitochondria contacts, increasing the distance between the two organelles. Notably, CNX is also required to maintain mitochondrial Ca^{2+} content and respiration, suggesting that CNX promotes Ca^{2+} flux to mitochondria, in spite of the increased ER-mitochondria distance. Together, the results show that CNX is a critical regulator of SERCA activity, ER-mitochondria contacts, and mitochondrial metabolism.

4.2 Results

4.2.1 Calnexin regulates SERCA activity by redox modifications

In a previous work our lab found that CNX promotes the accumulation of Ca^{2+} in the ER and also interacts with SERCA, suggesting that CNX activates SERCA [114]. Since oxidative modification is an important mechanism to regulate SERCA activity, the role of CNX on oxidative modifications in SERCA was evaluated. The BIAM assay was used to determine if cysteines were in their oxidized or reduced state. The oxidative agent Diamide and the reducing agent dithiothreitol (DTT) were used as controls to see the minimum and maximum reduced states of SERCA cysteines. The result shows that SERCA is partially oxidized in cells that have CNX; in the absence of CNX, SERCA cysteines are in their reduced state **(Figure 4.1A)**. The effect of CNX on SERCA oxidation was also tested in cells with a transient CNX knockdown **(Figure 4.1B)**. Similar to CNX knockout, CNX knockdown cells also show more SERCA cysteines in their reduced state compared to control cells **(Figure 4.1C)**. These results indicate that CNX is necessary to maintain SERCA oxidation, and suggest that CNX maintains SERCA activity by promoting an activating oxidative modification in some cysteines.

4.2.2 Calnexin activates SERCA and regulates ER and cytosolic Ca^{2+}

To understand the regulation of SERCA by CNX, SERCA ATPase activity was measured in CNX wild type and knockout cells. The result shows that cells that lack CNX have significantly reduced SERCA ATPase activity **(Figure 4.2A)**. To confirm the role of CNX in the regulation of SERCA, CNX expression was rescued in knockout cells by a stable transfection using a plasmid that express CNX (CNX-WT-FLAG stable) **(Figure 4.2B)**. The rescue experiment shows that the reintroduction of CNX in the knockout cells increases SERCA ATPase activity, even though the increase is not statistically significant **(Figure 4.2C)**. SERCA ATPase activity was also tested in HeLa cells with a transient CNX knockdown using siRNA. The result shows that CNX knockdown reduces SERCA ATPase activity, but to a lesser extent that CNX knockout **(Figure 4.2D)**.

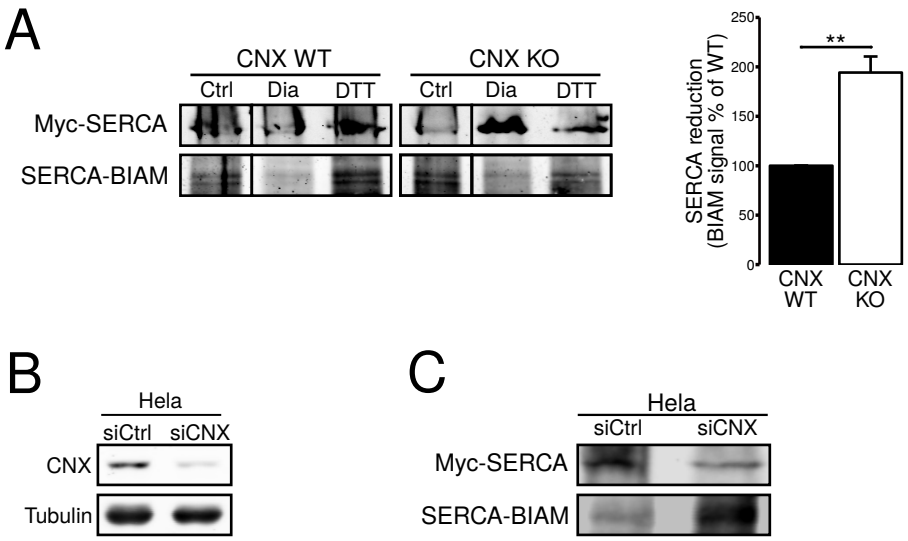

Figure 4.1 – CNX increases oxidation in SERCA2b cysteines. A: CNX wild type and knockout MEFs were transfected with myc-SERCA2b and treated with the oxidative agent Diamide and the reducing agent DTT. Cells were lysed and reduced cysteines were labelled using a biotinylated iodoacetamide (BIAM) assay. The specific SERCA2b BIAM labeling was detected by immunoprecipitating myc-SERCA2b and detecting the BIAM labeling probing the proteins with Streptavidin. n = 4; p = 0.0011. **B:** HeLa cells transfected with siCNX and immunoblotted for CNX and Tubulin as a loading control. n = 2. **C:** BIAM assay of SERCA2b in HeLa cells transfected with siCNX and analyzed by Western blot for the myc-SERCA2b and BIAM signals. n = 2. *BIAM assays were performed by Megan Yap.*

SERCA activity was also indirectly evaluated by measuring the speed at which Ca^{2+} is cleared from the cytosol after triggering a release of Ca^{2+} from the ER. Since the function of SERCA is to clear Ca^{2+} from the cytosol, it is expected that the speed at which Ca^{2+} is removed is proportional to SERCA activity. The fluorescent Ca^{2+} probe Fura-2 was used to measure cytosolic Ca^{2+}, and Ca^{2+} release from the ER through IP_3R was triggered by adding 600 μM ATP to the cells. The result shows that the cytosolic Ca^{2+} clearance was faster in cells that have CNX compared to knockout cells **(Figure 4.2E)**. This suggests that cells that lack CNX have reduced SERCA activity. In contrast, CNX had no effect on the amplitude of the Ca^{2+} signal in the cytoplasm **(Figure 4.2F)**. Taken together, these results indicate that CNX activates SERCA.

The activation of SERCA by CNX was also evaluated by measuring the accumulation of Ca^{2+} in the ER in CNX wild type and knockout cells. ER Ca^{2+} content was measured with the ER-targeted fluorescent Ca^{2+} probe ER-LAR-GECO1 and fluorescent microscopy. The amount of Ca^{2+} in the ER was estimated by depleting ER Ca^{2+} stores with a combination of the SERCA inhibitor TBHQ, and the removal of extracellular Ca^{2+}. The result shows that cells that lack CNX have less Ca^{2+} in their ER **(Figure 4.3A)**. This indicates that the increased SERCA activity induced by CNX correlates with more accumulation of Ca^{2+} in the ER.

In addition to an increase in SERCA activity, the increased ER Ca^{2+} stores can also be explained by a decrease in passive Ca^{2+} release from the ER. If Ca^{2+} escapes faster from the ER, the ER Ca^{2+} stores would also be reduced. The rate of passive Ca^{2+} release from the ER was evaluated by measuring the slope of the decrease in Ca^{2+} levels during ER Ca^{2+} depletion. The result shows a decrease in the rate of passive Ca^{2+} release in cells that lack CNX **(Figure 4.3B)**. This suggests that CNX knockout cells not only have less Ca^{2+} in the ER, they also retain ER Ca^{2+} better. There are different ways of passive Ca^{2+} release, or leak, from the ER. One of the main sources of ER Ca^{2+} leak is the translocon [234]. Ca^{2+} leak through the translocon was evaluated by using the translocon leak inhibitor Anisomycin, and measuring the rate of passive Ca^{2+} release. The result shows that Anisomycin abolished the difference in leak between normal cells and CNX knockout cells **(Figure 4.3C)**. This suggests that

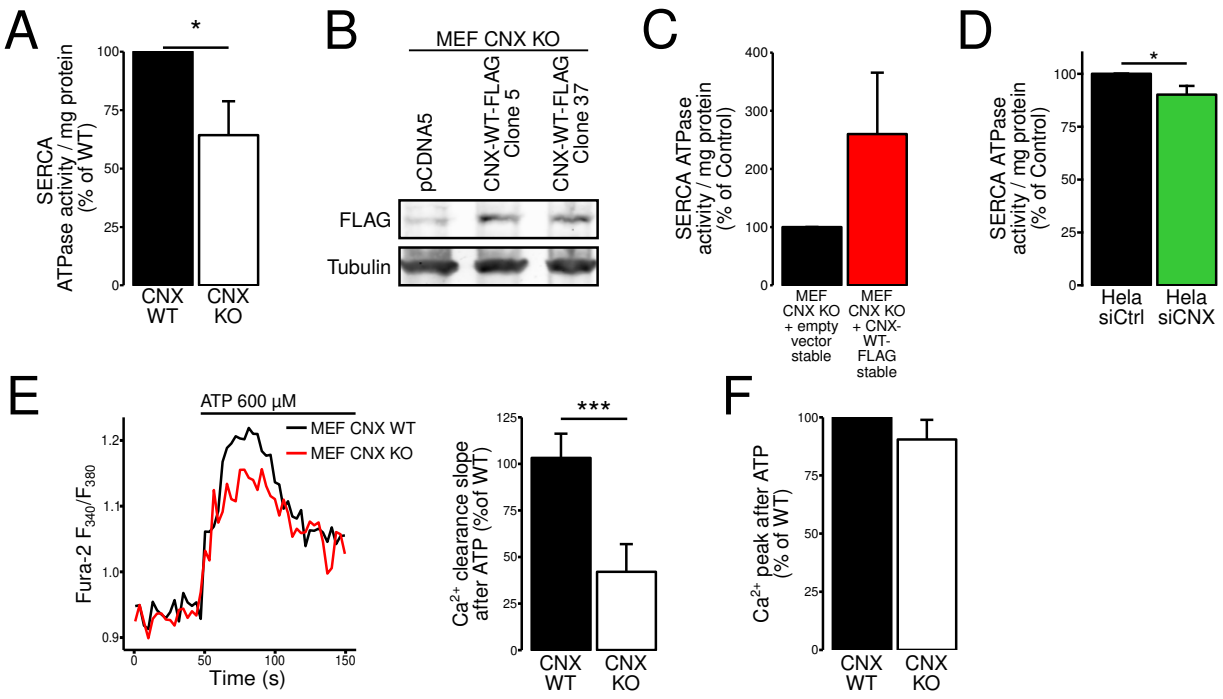

Figure 4.2 – CNX activates SERCA. A: SERCA ATPase was measured in light membranes of CNX wild type and knockout MEF cells and normalized to protein concentration. n = 7; p = 0.03. **B:** CNX knockout MEF cells were stably transfected with a pcDNA5 plasmid expressing FLAG tagged CNX (CNX-WT-FLAG). Two clones were analyzed by Western blot for CNX and Tubulin as a loading control. **C:** SERCA ATPase was measured in light membranes of CNX knockout MEF cells stably transfected with empty pcDNA5 or CNX-WT-FLAG (clone #5) and normalized to protein concentration. n = 5; p = 0.17. **D:** SERCA ATPase was measured in light membranes of HeLa cells transfected with siCNX and normalized to protein concentration. n = 5; p = 0.044. **E:** Cytoplasmic Ca^{2+} was quantified using the Fura-2 fluorescent Ca^{2+} probe in CNX wild type and knockout MEF cells. ATP 600 µM was added to trigger a Ca^{2+} release through the IP_3Rs. Cytoplasmic Ca^{2+} clearance was determined by the decay slope after the peak. n = 6; p = 0.00023. **F:** Cytoplasmic Ca^{2+} was quantified using the Fura-2 fluorescent Ca^{2+} probe in CNX wild type and knockout MEF cells. ATP 600 µM was added to trigger a Ca^{2+} release through the IP_3Rs. Cytoplasmic Ca^{2+} peak was determined. n = 6; p = 0.29.

CNX promotes Ca^{2+} leak through the translocon.

The reduction in ER Ca^{2+} could also be a consequence of reduced Store-Operated Ca^{2+} Entry (SOCE), responsible for filling the ER Ca^{2+} stores from the extracellular medium [236]. SOCE was measured by removing Ca^{2+} from the cells while inhibiting SERCA, and then adding Ca^{2+} back to the medium. Under these conditions there is an influx of Ca^{2+} from the extracellular medium proportional to SOCE activity. The result shows that the influx of Ca^{2+} was bigger in cells that lack CNX **(Figure 4.3D)**. This suggests that CNX might be a SOCE inhibitor, and rules out the possibility that CNX increases ER Ca^{2+} content by the activation of SOCE.

The effect of CNX on ER Ca^{2+} content was also evaluated in CNX knockout cells rescued with the stable transfection of a plasmid expressing CNX (CNX-WT-FLAG stable). The result shows that the CNX rescued cells have more Ca^{2+} in their ER **(Figure 4.3E)**. Nevertheless, HeLa cells with a transient CNX knockdown show no difference in ER Ca^{2+} content compared to the controls **(Figure 4.3F)**. This suggests that small amounts of CNX are sufficient to maintain normal ER Ca^{2+} levels, or that cells can compensate for a mild reduction in SERCA activity.

Taken together, these results indicate that CNX activation of SERCA helps to maintain normal levels of ER Ca^{2+} content. If CNX is absent, ER Ca^{2+} stores decline. In addition, CNX decreases Ca^{2+} influx from the extracellular medium through SOCE, and increases ER Ca^{2+} leak through the translocon. Thus, SOCE and ER Ca^{2+} leak alterations cannot explain the reduction in ER Ca^{2+} levels, suggesting that CNX controls ER Ca^{2+} mainly by its regulation of SERCA activity. CNX activation of SERCA also results in a reduction of Ca^{2+} availability in the cytoplasm by increasing Ca^{2+} uptake.

4.2.3 Calnexin inhibits ER-mitochondria contact formation

The positioning of mitochondria in the cell depends on cytosolic Ca^{2+}. When cytosolic Ca^{2+} levels are high, mitochondrial movement is stopped by the inhibition of Ca^{2+}-sensitive regulators of mitochondrial movement through the microtubules [117]. This results in accumulation of mitochondria in areas where cytosolic Ca^{2+} levels are elevated, like Ca^{2+} release channels in the ER [118]. Since

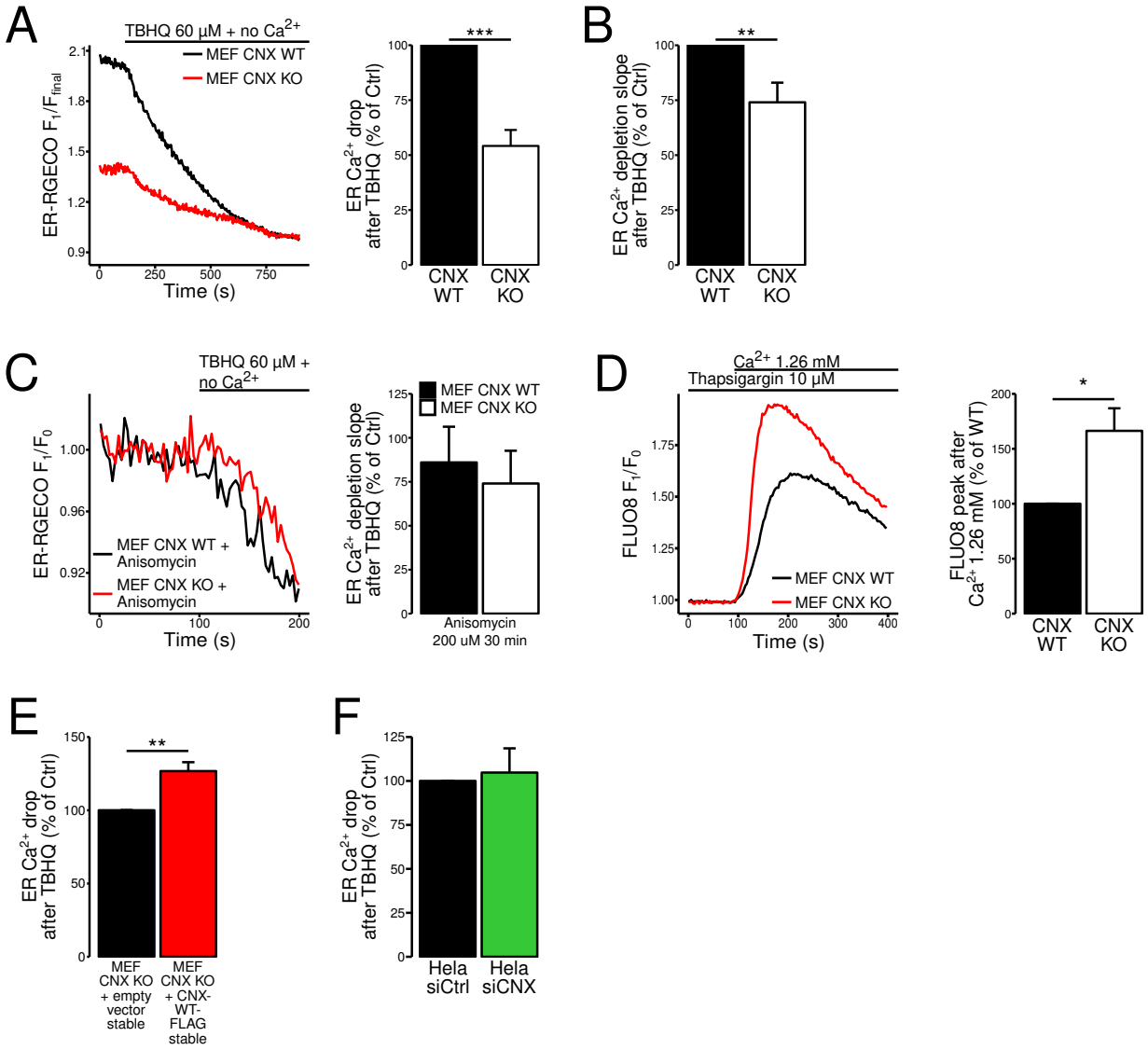

Figure 4.3 – CNX increases ER Ca^{2+} content. A: ER Ca^{2+} content was measured by depleting ER Ca^{2+} stores with 60 µM TBHQ and no Ca^{2+} medium. The drop in ER Ca^{2+} upon depletion was measured in CNX wild type and knockout MEF cells. n = 12; p = 2.4×10^{-6}. **B:** ER Ca^{2+} leak was also measured by quantifying the depletion slopes. n = 13; p = 0.0078. **C:** ER Ca^{2+} leak was measured by quantifying the depletion slopes after 60 µM TBHQ and no Ca^{2+} medium. ER Ca^{2+} leak through the translocon was evaluated by treating the cells with 200 µM Anisomycin for 30 min. n = 4; p = 0.68. **D:** SOCE was measured by inhibiting SERCA and adding Ca^{2+} back to cells previously starved of Ca^{2+}. Cytoplasmic Ca^{2+} was quantified using the Fluo-8 fluorescent Ca^{2+} probe in CNX wild type and knockout MEF cells. n = 3; p = 0.032. **E** ER Ca^{2+} content and the drop in ER Ca^{2+} upon depletion was measured in CNX knockout MEF cells stably transfected with empty pcDNA5 or FLAG-CNX. n = 4; p = 0.0056. **F:** ER Ca^{2+} content and the drop in ER Ca^{2+} upon depletion was measured in HeLa cells transfected with siCNX. n = 7; p = 0.74.

CNX knockout cells have slower cytosolic Ca^{2+} clearance, it is possible that these cells have increased Ca^{2+} levels in the proximity of the ER. Thus, the effect of CNX on ER-mitochondria proximity was evaluated. The distance between ER and mitochondria was measured using electron microscopy **(Figure 4.4A)**. The result shows a decrease in ER-mitochondria distance and an increase in the length ER-mitochondria contacts, which leads to a increase in the coefficient *contact length / distance* in cells that lack CNX **(Figure 4.4B)**. The frequency of different distances was calculated and classified as Super tight (0 to 12 nm), Tight (12 to 24 nm), and Loose (24 to 50 nm). The result shows that CNX knockout cells have increased frequency of Super tight contacts, with a decrease in the Tight and Loose categories **(Figure 4.4C)**. These results indicate that CNX prevents the formation of ER-mitochondria contacts.

The effect of CNX on ER-mitochondria contacts was also measured using the split-GFP-based contact site sensor SPLICS [177]. SPLICS is a probe designed to fluoresce only when ER and mitochondria are in close proximity. There are two versions of SPLICS, designed to measure contacts of different distances. SPLICS-short measures ER-mitochondria contacts between 8 and 10 nm wide, and SPLICS-long measures distances between 40 and 50 nm. In addition, to test if SERCA oxidation by CNX is involved in ER-mitochondria contacts, CNX wild type and knockout cells were incubated with the antioxidant *N*-acetylcysteine (NAC). The presence of NAC should prevent CNX control over SERCA and reduce the difference in ER-mitochondria contacts between CNX wild type and knockout cells. The result shows that the number of SPLICS-short contacts per cell were the same between CNX wild type and knockout MEF cells. While the NAC treatment reduced the number of contacts in both cell lines **(Figure 4.5A)**. On the other hand, cells that lack CNX have significantly more SPLICS-long contacts, and the difference between CNX wild type and knockout MEF cells disappears with the NAC treatment **(Figure 4.5B)**. These results suggest that CNX prevents the formation of ER-mitochondria contacts of 40 to 50 nm width, while the antioxidant NAC prevents CNX control over ER-mitochondria contacts and reduces the differences between CNX wild type and knockout cells.

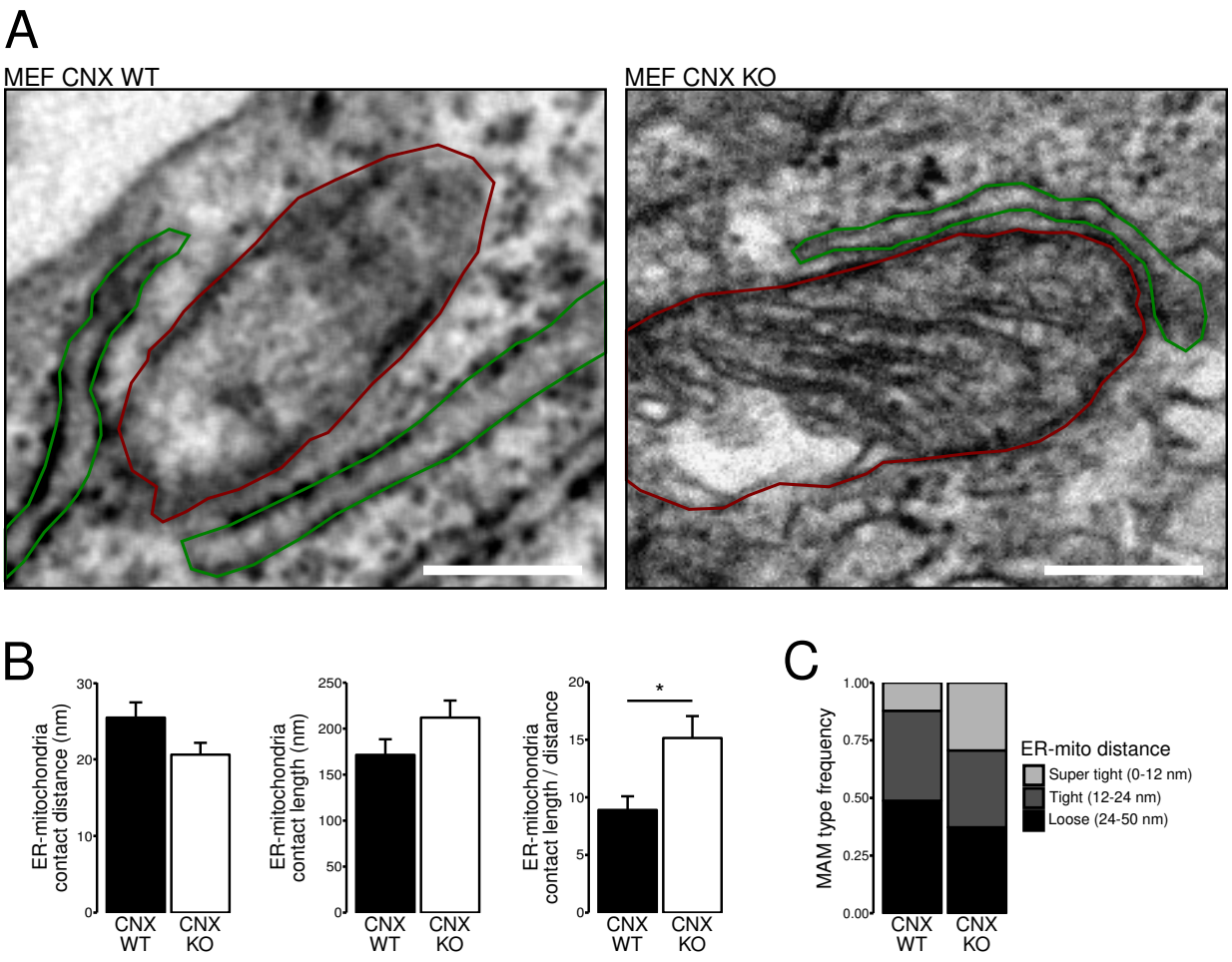

Figure 4.4 – CNX prevents the formation of ER-mitochondria contacts. A: Electron microscopy images of CNX wild type and knockout MEF cells. Mitochondria are labeled in red and the ER in green. Scale bar = 200 nm. **B:** Average ER-mitochondria distance (n = 41 for MEF CNX WT, n = 51 for MEF CNX KO; p = 0.054), contact length (n = 41 for MEF CNX WT, n = 51 for MEF CNX KO; p = 0.12), and *contact length / distance* ratio (n = 41 for MEF CNX WT, n = 51 for MEF CNX KO; p = 0.01). **C:** Frequency of ER-mitochondria contacts classified by distance into Super tight (0 to 12 nm), Tight (12 to 24 nm), and Loose (24 to 50 nm). n = 41 for MEF CNX WT, n = 51 for MEF CNX KO.

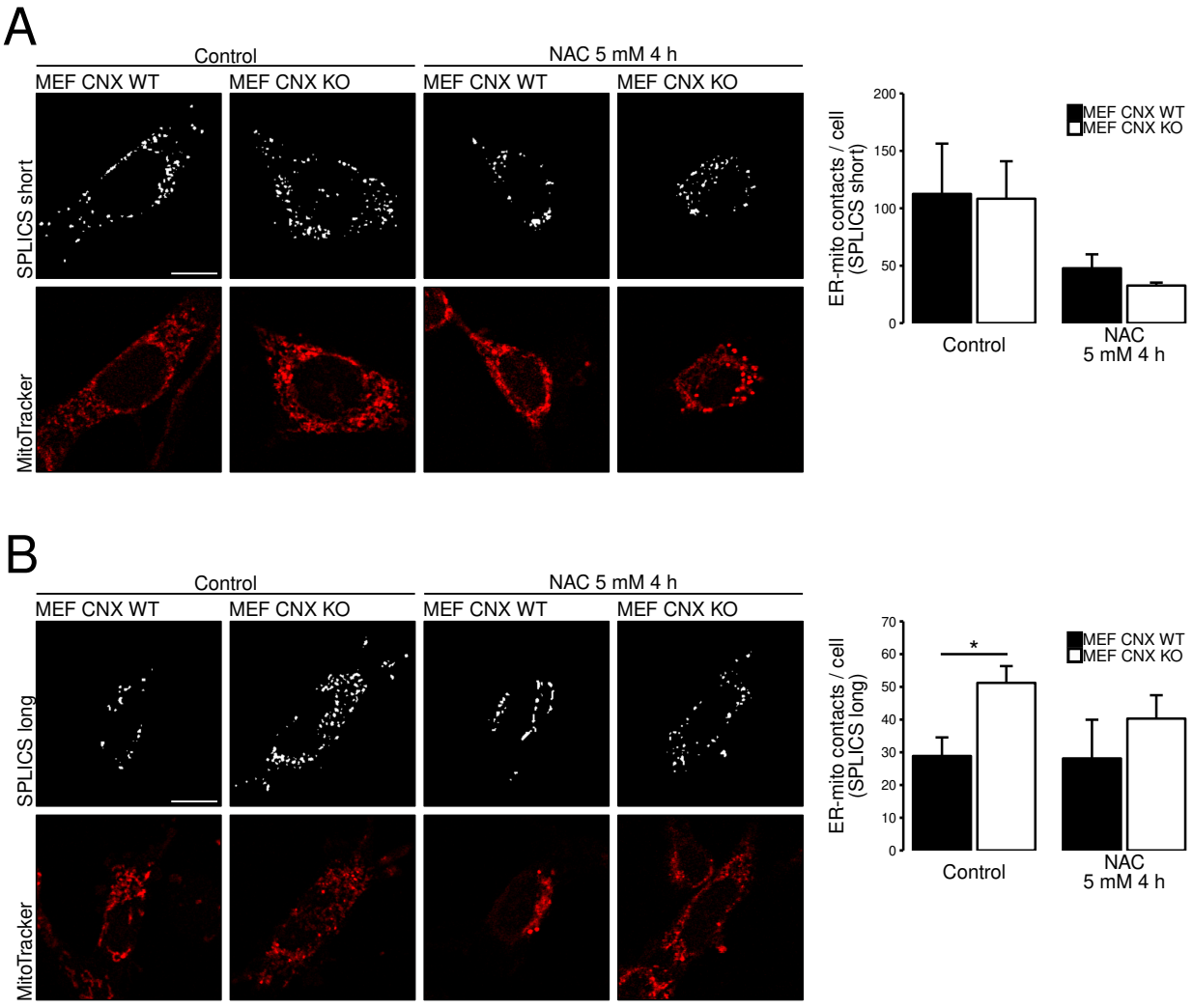

Figure 4.5 – ROS is required for the regulatory effect of CNX in ER-mitochondria contacts. A: SPLICS-short (8 to 10 nm) and MitoTracker Red signals in CNX wild type and knockout MEF cells treated with 5 mM of the antioxidant *N*-acetylcysteine (NAC) for 4 hours. The number of SPLICS-short puncta per cell was quantified. Control: n = 11 for MEF CNX WT, n = 23 for MEF CNX KO; p = 0.94. NAC: n = 9 for MEF CNX WT, n = 19 for MEF CNX KO; p = 0.11. Scale bar = 20 µm. **B:** SPLICS-long (40 to 50 nm) and MitoTracker Red signals in CNX wild type and knockout MEF cells treated with 5 mM of the antioxidant *N*-acetylcysteine (NAC) for 4 hours. The number of SPLICS-long puncta per cell was quantified. Control: n = 8 for MEF CNX WT, n = 9 for MEF CNX KO; p = 0.01. NAC: n = 8 for MEF CNX WT, n = 10 for MEF CNX KO; p = 0.37. Scale bar = 20 µm.

Taken together, these results indicate that CNX inhibits the formation of ER-mitochondria contacts. CNX activates SERCA through oxidative modifications, resulting in an increased cytosolic Ca^{2+} clearance. Potentially, the accelerated clearance results in reduced Ca^{2+} levels in the proximity of the ER, preventing the docking of mitochondria. If the oxidative modification of SERCA is prevented, CNX cannot control SERCA, and the regulatory effect of CNX on ER-mitochondria distance is lost.

4.2.4 CNX increases mitochondrial Ca^{2+} content

The previous results show that CNX inhibits the formation of ER-mitochondria contacts and also increases ER Ca^{2+} content, two major factors in Ca^{2+} flux between the two organelles. To test the effect of CNX on Ca^{2+} flux, the mitochondrial Ca^{2+} content was measured in CNX wild type and knockout cells using the mitochondria targeted fluorescent Ca^{2+} probe mito-LAR-GECO1.2. The total mitochondrial Ca^{2+} content was determined by measuring the amount of Ca^{2+} released from the mitochondria after dissipating the mitochondrial potential with the protonophore FCCP. Mitochondria require the mitochondrial potential to retain Ca^{2+} in their matrix; when the mitochondrial potential is dissipated, mitochondria are depleted of Ca^{2+}. The amount of Ca^{2+} released is proportional to the mitochondrial Ca^{2+} content. The result shows that cells that have CNX have more mitochondrial Ca^{2+} than cells that lack CNX **(Figure 4.6A)**, suggesting that CNX is required to maintain normal mitochondrial Ca^{2+} content. Then, the mitochondrial Ca^{2+} measurement was repeated but instead of adding FCCP, the Ca^{2+} in the extracellular medium was removed. The removal of Ca^{2+} from the extracellular medium reduces ER Ca^{2+} store content, because it cannot be replenished by extracellular Ca^{2+}. Since CNX wild type cells have more Ca^{2+} in their ER and more ER Ca^{2+} leak, it is possible that these cells maintain high levels of mitochondrial Ca^{2+} through a stronger flux of Ca^{2+} to mitochondria that requires the presence of extracellular Ca^{2+} to be maintained. Indeed, the reduction in mitochondrial Ca^{2+} after the removal of extracellular Ca^{2+} was greater in cells that have CNX than in CNX knockout cells **(Figure 4.6B)**. This suggests that CNX maintains the flow of Ca^{2+} from ER to mitochondria, but this flow of Ca^{2+} is disrupted if Ca^{2+} stores are reduced by the removal of extracellular Ca^{2+}. On the other hand, the removal of extracellular Ca^{2+} does not have a big effect on

CNX knockout cells because they already have less ER and mitochondrial Ca^{2+}, so the flux of Ca^{2+} to mitochondria is already disrupted. This suggests that CNX is not only important to retain Ca^{2+} in the ER, but it is also required to maintain normal mitochondrial Ca^{2+} flux and mitochondrial Ca^{2+} levels. Next, we evaluated the effect of CNX in Ca^{2+} transfer to mitochondria after a release of Ca^{2+} from the ER through IP_3R. To test this, CNX wild type and knockout cells were treated with ATP to trigger a release of Ca^{2+} through the IP_3R while measuring mitochondrial Ca^{2+} with a mitochondrial Ca^{2+} probe. The result shows no difference in the transfer of Ca^{2+} to mitochondria between CNX wild type and knockout cells (**Figure 4.6C**). This result suggests that IP_3R is not involved in CNX regulation of mitochondrial Ca^{2+}.

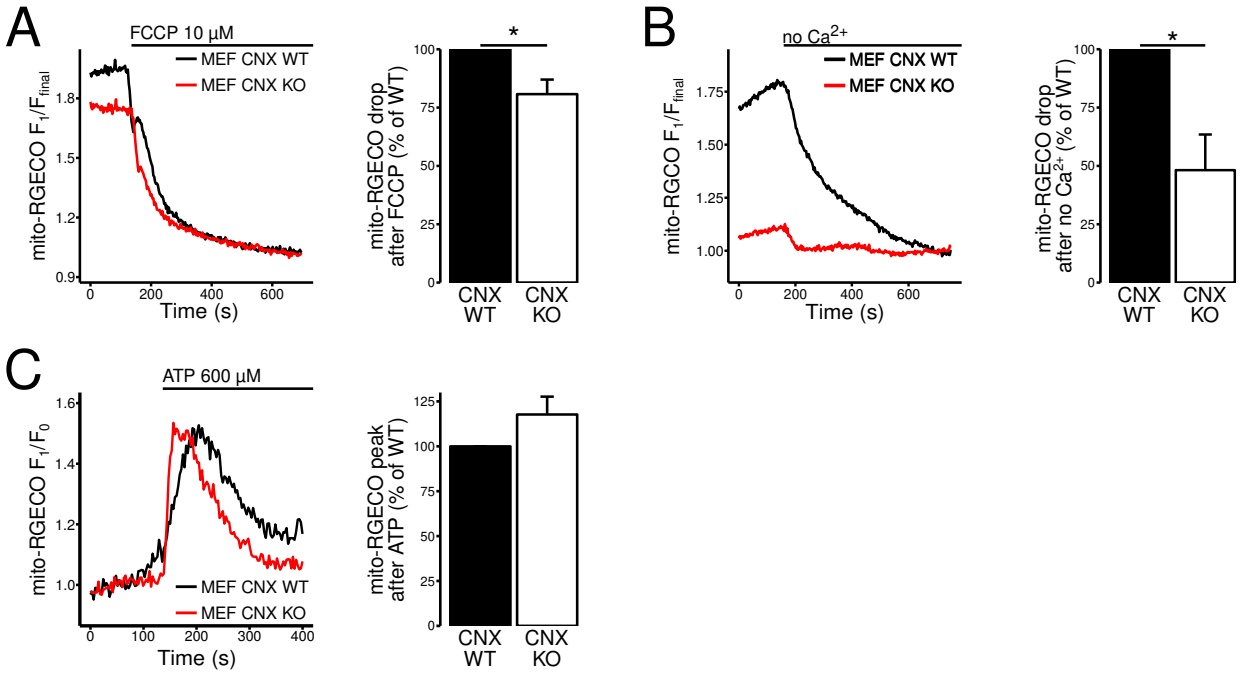

Figure 4.6 – CNX increases mitochondrial Ca^{2+} content. A: Mitochondrial Ca^{2+} content was measured by depleting mitochondrial Ca^{2+} with 10 µM FCCP. The drop in mitochondrial Ca^{2+} upon depletion was measured in CNX wild type and knockout MEF cells. n = 4; p = 0.022. **B:** Mitochondrial Ca^{2+} was measured upon removal of extracellular Ca^{2+} in CNX wild type and knockout MEF cells. n = 3; p = 0.028. **C:** Mitochondrial Ca^{2+} was measured after a release of Ca^{2+} through the IP_3Rs triggered by 600 µM ATP. n = 3; p = 0.15.

The role of CNX on mitochondrial function was further investigated by measuring the mitochondrial potential using the fluorescent mitochondrial potential probe TMRM. The result shows no differences in the mitochondrial potential between CNX wild type and knockout cells (**Figure 4.7A**). Neverthe-

less, when a large release of Ca^{2+} from the ER was triggered using the SERCA inhibitor thapsigargin, the drop in mitochondrial potential was bigger in CNX knockout cells **(Figure 4.7B)**. This result suggests that CNX reduces Ca^{2+} transfer to mitochondria after a large release of Ca^{2+} from the ER, probably because of the increased ER-mitochondria distance induced by CNX.

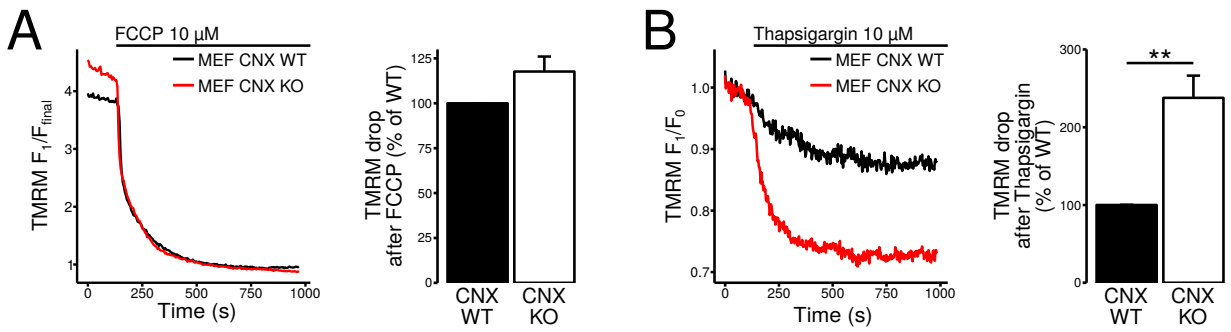

Figure 4.7 – Mitochondria are more responsive to Ca^{2+} delivered from the ER in CNX knockout cells. A: Mitochondrial potential was measured upon dissipation of mitochondrial potential using 10 µM FCCP in CNX wild type and knockout MEF cells. n = 3; p = 0.1. **B:** Mitochondrial potential was measured upon release of Ca^{2+} from the ER with 10 µM thapsigargin in CNX wild type and knockout MEF cells. n = 3; p = 0.0085.

Taken together, these results show that CNX promotes mitochondrial Ca^{2+} accumulation, suggesting that normal ER Ca^{2+} stores are required to maintain mitochondrial Ca^{2+}. Ca^{2+} transfer to the mitochondria through IP_3R is not regulated by CNX. But cells that lack CNX have a better response to the delivery of ER Ca^{2+} after SERCA inhibition. This suggests that the closer proximity between ER and mitochondria facilitates the transfer of Ca^{2+} in cells that lack CNX. But this improved transfer can only be observed when large amounts of Ca^{2+} are released, like when SERCA is inhibited and the entire ER Ca^{2+} stores are poured into the cytoplasm. In normal conditions, there is not enough Ca^{2+} available in the ER to maintain mitochondrial Ca^{2+} flux. Thus, in cells that lack CNX, both ER and mitochondria are depleted of Ca^{2+}. The increased ER-mitochondria contacts found in CNX knockout cells is not enough to sustain a normal Ca^{2+} flux.

4.2.5 CNX increases mitochondrial metabolism

So far, the results show that CNX is necessary to maintain mitochondrial Ca^{2+} levels, suggesting that it increases mitochondrial metabolism. On the other hand, CNX increases ER-mitochondria distance, potentially resulting in a reduction of mitochondrial function. Thus, the role of CNX in mitochondrial function was evaluated.

To determine the effect of CNX on metabolism, total cellular ATP levels were measured. The result shows that the presence of CNX makes no difference in cellular ATP levels **(Figure 4.8A)**. But cellular ATP can be produced by different sources, like mitochondria or glycolysis. To discriminate the source of ATP, mitochondrial ATP production was blocked by treating the cells with the mitochondrial ATP synthase inhibitor oligomycin. The result shows that the reduction in ATP levels was greater in normal cells compared to CNX knockout cells **(Figure 4.8B)**. This suggests that CNX wild type cells have a greater reliance on mitochondrial for their ATP production than CNX knockout cells. Cells were also treated with the non-metabolizable glucose analog 2-Deoxy-D-glucose (2-DG), a glycolysis inhibitor that also prevents further glucose oxidation in the mitochondria. The result shows that 2-DG reduced ATP levels in both CNX wild type and knockout cells **(Figure 4.8B)**. This indicates that both CNX wild type and knockout cells rely on glucose to a similar extent for their energy needs. The difference is that cells that lack CNX rely more on glycolysis to produce ATP, whereas CNX wild type cells oxidize glucose in their mitochondria. Thus, the protein levels of glycolysis enzymes and glucose transporters were measured. The result shows a statistically significant increase in the glycolytic enzyme Hexokinase 1 in CNX knockout cells. However, overall, glycolytic enzymes and glucose transporters remained unchanged **(Figure 4.8C)**. These results suggest that CNX promotes mitochondrial metabolism, and that cells that lack CNX use more glycolysis to produce ATP. They can produce ATP in their mitochondria, but less than CNX wild type cells.

Next, the effect of CNX on mitochondrial biogenesis was evaluated. The level of mitochondrial proteins was measured and no differences were found between CNX wild type and knockout cells **(Figure 4.9A)**. This suggests that the increased mitochondrial ATP production promoted by CNX

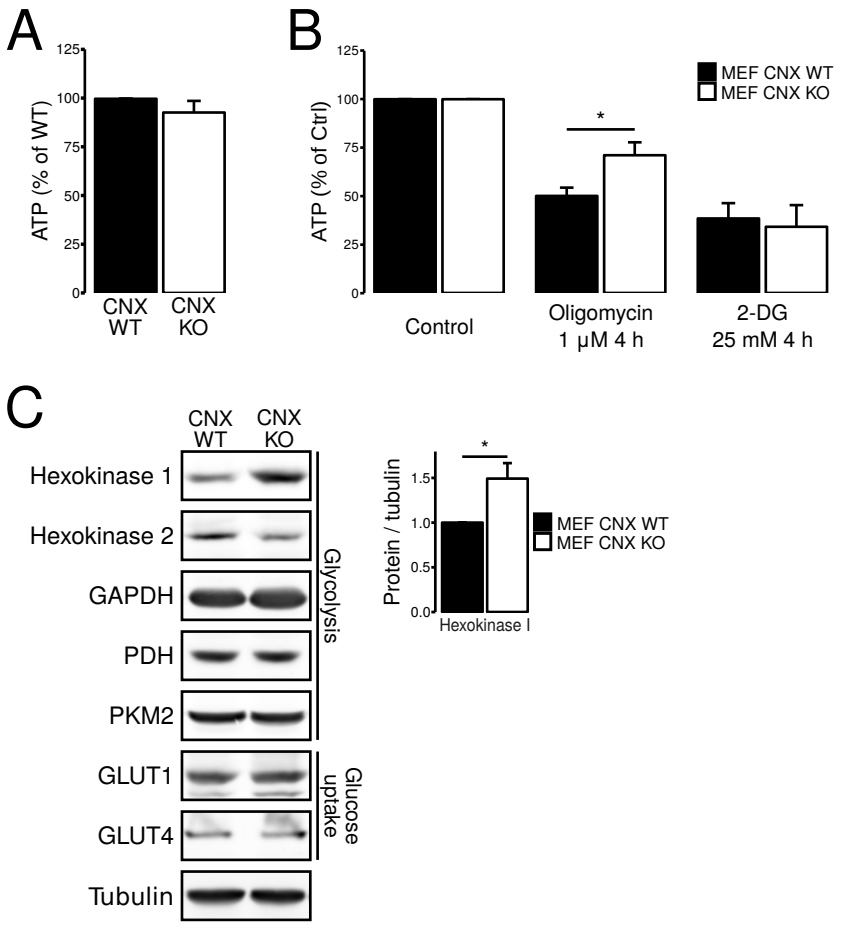

Figure 4.8 – CNX increases mitochondrial ATP production. A: Total cellular ATP was measured in CNX wild type and knockout MEF cells. n = 35; p = 0.11. **B:** Total cellular ATP was measured in CNX wild type and knockout MEF cells in the presence of 1 µM oligomycin for 4 hours or 25 mM 2-Deoxy-D-glucose (2-DG) for 4 hours. Oligomycin: n = 6; p = 0.024. 2-DG: n = 4; p = 0.76. **C:** Western blot of the indicated glycolytic enzymes and glucose transporters in CNX wild type and knockout MEF cells. Hexokinase 1: n = 5; p = 0.022.

is not associated with changes in mitochondrial mass. Then, mitochondrial number and size were measured in CNX wild type and knockout cells to confirm that CNX has no effect on cellular mitochondrial content. This was measured by labelling mitochondria with the mitochondrial targeted fluorescent probe MitoTracker Green, and observing the mitochondria under the microscope. The result shows that CNX has no effect on mitochondrial number or size **(Figure 4.9B)**. This indicates that CNX is not involved in the regulation of mitochondrial mass, suggesting that it exerts a direct control on mitochondrial activity.

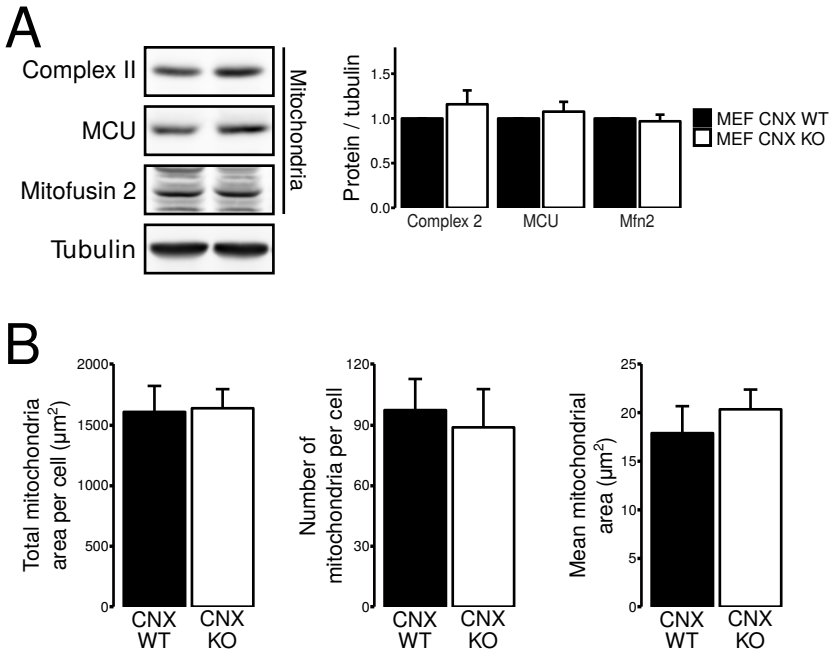

Figure 4.9 – CNX does not regulate mitochondrial mass, number or size. A: Western blot of the indicated mitochondrial proteins in CNX wild type and knockout MEF cells. Complex 2: n = 3; p = 0.37. Mitochondrial Ca^{2+} uniporter (MCU): n = 8; p = 0.5. Mitofusin 2 (Mfn2): n = 3; p = 0.69. **B:** Mitochondria were labelled with 1 μM MitoTracker for 30 minutes and the number and size of mitochondria was quantified. n = 5 for CNX wild type and n = 6 for CNX knockout; p = 0.91 for total mitochondria area; p = 0.74 for number of mitochondria per cell; p = 0.48 for mean mitochondria area.

To test the effect of CNX in the regulation of mitochondrial function, the mitochondrial oxygen consumption rate was measured. This is a more direct measurement of mitochondrial respiration. The result shows that under basal conditions, cells that lack CNX have less oxygen consumption than wild type cells. Similarly, the ATP turnover (respiration linked to ATP production) and the maximum Electron Transport Chain (ETC) capacity were also reduced in CNX knockout cells **(Figure 4.10A)**.

To confirm this result, the oxygen consumption rate was also measured in HeLa cells transfected with siCNX. Again, CNX knockdown significantly reduced mitochondrial respiration **(Figure 4.10B)**. This indicates that CNX is required to maintain a normal mitochondrial respiration. Taken together, these results suggest that CNX is required to maintain ER and mitochondrial Ca^{2+} content by activating SERCA. The absence of CNX results in a depletion of ER Ca^{2+}, resulting in a reduction of mitochondrial Ca^{2+} and mitochondrial respiration.

To evaluate the consequences of CNX metabolic regulation, the activation of the metabolic sensor AMPK by phosphorylation was also measured. AMPK is usually activated and phosphorylated when the cellular ATP levels are low, and activates glucose and fatty acids uptake and oxidation [92]. Consistent with their mitochondrial dysfunction, CNX knockout cells have increased AMPK phosphorylation **(Figure 4.10C)**, suggesting that the cell adapts its metabolism to compensate for the loss of CNX in order to maintain normal ATP levels. Next, the reliance of CNX wild type and knockout cells on mitochondrial metabolism for survival was evaluated. To test the importance of mitochondrial metabolism, cells were treated with the mitochondrial ATP synthase inhibitor oligomycin, and with the respiratory Complex I inhibitor rotenone. Equal numbers of cells were treated, and the number of viable cells was counted after 24 hours. The result shows that cells that lack CNX are more resistant to oligomycin and rotenone than cells that have CNX **(Figure 4.10D)**. This indicates that CNX wild type cells rely more on mitochondrial energy production for their survival than knockout cells, and is consistent with the reduced use of mitochondria as an energy source in CNX knockout cells.

In summary, the role of CNX on metabolic regulation consists of an activation of mitochondrial respiration by maintaining mitochondrial Ca^{2+} content. When CNX is not present, cells compensate by increasing glycolysis to maintain normal ATP levels.

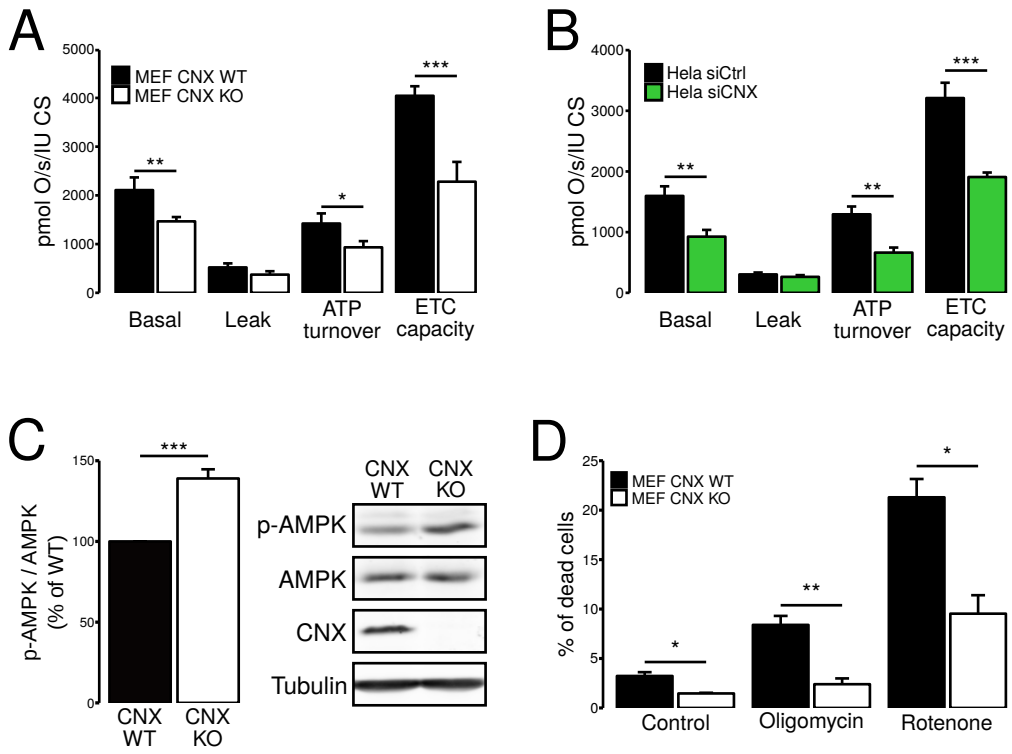

Figure 4.10 – CNX increases mitochondrial respiration. A: Mitochondrial respiration was measured in CNX wild type and knockout MEF cells. n = 10; p = 0.0072 for Basal; p = 0.06 for Leak; p = 0.017 for ATP turnover; $p = 9.9 \times 10^{-5}$ for ETC capacity. **B:** Mitochondrial respiration was measured in HeLa cells transfected with siCNX. n = 6; p = 0.006 for Basal; p = 0.36 for Leak; p = 0.0021 for ATP turnover; p = 0.00058 for ETC capacity. **C:** Western blot of AMPK and phosphorylated AMPK (p-AMPK) in CNX wild type and knockout MEF cells. n = 4; p = 0.00047. **D:** Cell viability was measured in CNX wild type and knockout MEF cells treated with 1 µM oligomycin or 1 µM rotenone for 24 hours. n = 3. Control: p = 0.01. Oligomycin: p = 0.0051. Rotenone: p = 0.011.

4.2.6 CNX increases mitochondrial respiration by maintaining Ca^{2+} flux

So far, the results show that CNX regulates Ca^{2+} signalling and flux to the mitochondria, ER-mitochondria contacts, and mitochondrial metabolism. These are all functions intimately related to Mitochondria-Associated Membranes (MAM). Next, the effect of CNX on MAM protein composition was evaluated using Western blotting. The protein levels of the ER and mitochondrial Ca^{2+} channels VDAC1 and IP_3R isoforms 1 were significantly increased in CNX knockout cells, while no changes were found for IP_3R isoform 3 **(Figure 4.11A)**. This suggests that despite the depletion in ER Ca^{2+} stores, CNX knockout cells retain or have an improved ability to transfer Ca^{2+} to the mitochondria. The protein levels and phosphorylation state of the ER stress signalling kinase PERK were also evaluated. PERK is an ER stress sensor that is phosphorylated when active, but it can also function as a tether and promote the formation of ER-mitochondria contacts [237]. The result shows that there is no difference in PERK or p-PERK protein levels, suggesting that there is no ER stress activated in CNX knockout cells, and that PERK does not participate in the increased ER-mitochondria contacts in these cells **(Figure 4.11A)**.

The levels of the ER oxidoreductase ERp57 and the ER Ca^{2+} pump SERCA2b were also measured. ERp57 can activate Store Operated Ca^{2+} Entry (SOCE) [238] and also inhibit SERCA [154]. But no differences were found in ERp57 protein levels between CNX wild type and knockout cells, suggesting that is not involved in SOCE or SERCA regulation by CNX. SERCA2b was also unchanged in CNX knockout cells, indicating that the reduced ER Ca^{2+} content in these cells is not due to reduced SERCA levels **(Figure 4.11A)**. Surprisingly, the levels of NADPH oxidase 4 (NOX4) was unchanged, despite previous reports indicating that CNX is required for NOX4 stability [219]. Similarly, the levels of the autophagy marker p62 were unchanged in cells that lack CNX **(Figure 4.11A)**. On the other hand, the protein levels of the ER oxidoreductase TMX1 were increased in CNX knockout cells **(Figure 4.11A)**. TMX1 can reduce ER Ca^{2+} content, so the increased TMX1 protein levels could be involved in the reduced ER Ca^{2+} in CNX knockout cells.

To confirm these findings, the levels of some of these proteins were also measured in HeLa cells

transfected with siCNX. Unlike CNX knockout cells, CNX knockdown cells have reduced levels of TMX1 and SERCA2b **(Figure 4.11B)**. Interestingly, since MEF CNX knockout and HeLa CNX knockdown have similar Ca^{2+} signalling and metabolic phenotypes, but opposite changes in TMX1 levels, it is unlikely that TMX1 plays a major role in the CNX knockout cells phenotype. Similarly, NOX4 levels were also reduced in CNX knockdown HeLa cells, consistent with previous reports [219] **(Figure 4.11B)**.

To have a closer look at the MAM proteome, cells were fractionated and the isolated Microsomes, Pure Mitochondria, and MAM fractions were analyzed using Western blot. A small enrichment of IP_3R3 was found in the MAM fraction of CNX knockout cells compared to their wild type counterparts **(Figure 4.11C)**. But no major changes were found in MAM protein composition, suggesting that CNX does not regulate MAM protein composition.

The reduced ER and mitochondrial Ca^{2+} suggest that CNX knockout cells have reduced mitochondrial respiration because they have an impaired mitochondrial Ca^{2+} flux. To test this, oxygen consumption rate was measured in the presence of the intracellular Ca^{2+} chelator BAPTA-AM. Ca^{2+} is necessary to maintain mitochondrial metabolism under normal conditions [80], so BAPTA-AM should reduce mitochondrial respiration in normal cells. If Ca^{2+} flux is impaired in cells that lack CNX, the effect of BAPTA-AM should be smaller than in normal cells. The result shows that BAPTA-AM has a greater impact in oxygen consumption in CNX wild type cells than in knockout cells, eliminating the difference between the two cells lines **(Figure 4.12)**. This suggests that the reduced mitochondrial respiration observed in cells that lack CNX is a consequence of an impaired Ca^{2+} flux due to depleted ER Ca^{2+} stores.

4.2.7 Oxidizing conditions are necessary for the metabolic roles of CNX

So far, the results show a reduction in SERCA activity in cells that lack CNX. As a consequence, these cells have reduced ER Ca^{2+} content and mitochondrial Ca^{2+} flux, and impaired mitochondrial respiration. At the same time, CNX knockout cells have reduced SERCA oxidation while SERCA

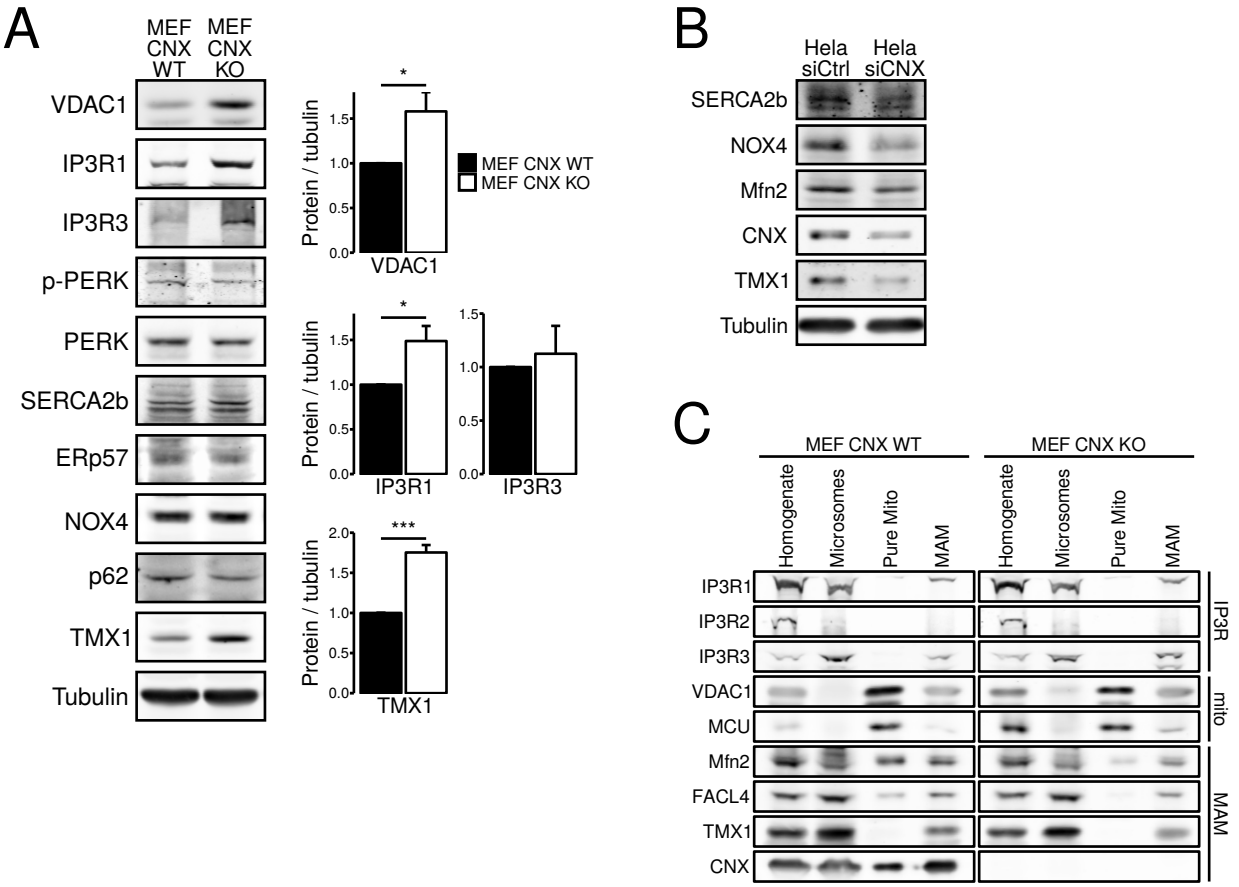

Figure 4.11 – **CNX effect on ER and MAM protein levels. A:** Western blot of the indicated proteins in CNX wild type and knockout MEF cells. VDAC1: n = 6; p = 0.022. IP_3R1: n = 8; p = 0.012. IP_3R3: n = 6; p = 0.64. TMX1: n = 4; p = 0.00019. **B:** Western blot of the indicated proteins in HeLa cells transfected with siCNX. n = 2. **C:** Western blot of Microsomes, Mitochondria, and MAM subcellular fractions from CNX wild type and knockout MEF cells. n = 2.

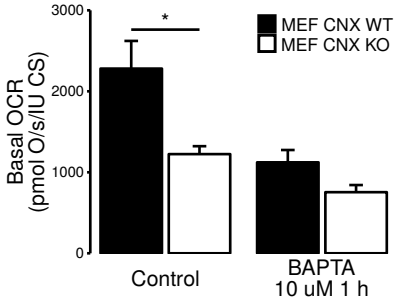

Figure 4.12 – **CNX increases mitochondrial respiration by maintaining Ca^{2+} flux.** Mitochondrial basal oxygen consumption rate (OCR) was measured in CNX wild type and knockout MEF cells treated with 10 µM BAPTA-AM for 1 hour. n = 5. Control: p = 0.018. BAPTA: p = 0.07.

protein levels remain unchanged. It is possible that the SERCA oxidation observed in cells that have CNX is a consequence of a higher ROS production in these cells compared to CNX knockout cells. To test if CNX oxidizes SERCA by increasing ROS levels, SERCA oxidation was evaluated in cells treated with the antioxidant NAC. As expected, the result shows that NAC treatment resulted in the reduction of SERCA cysteines **(Figure 4.13A)**. In addition, NAC reduced ER Ca^{2+} content in CNX wild type cells resulting in ER Ca^{2+} levels similar to CNX knockout cells **(Figure 4.13B)**. Similarly, the ER Ca^{2+} leak was also reduced in CNX wild type cells **(Figure 4.13C)**. This result suggests that CNX activates SERCA by promoting SERCA oxidation through ROS production, and this activation can be prevented by reverting SERCA oxidation. Consistently, NAC treatment also resulted in reduced mitochondrial respiration specifically in CNX wild type cells, eliminating the difference with CNX knockout cells **(Figure 4.13D)**. To confirm this observation, the effect of NAC on mitochondrial respiration was also measured in HeLa cells transfected with siCNX. Again, NAC reduced basal mitochondrial respiration only in cells with normal levels of CNX. However, the difference between HeLa siCtrl and HeLa siCNX was statistically significant even with the NAC treatment **(Figure 4.13E)**. Together, these results suggest that CNX controls ER and mitochondrial respiration by increasing SERCA oxidation.

The next aim was to identify the source of the ROS responsible for SERCA modification. The mitochondria-targeted fluorescent ROS probe mitoSOX was used to measure mitochondrial ROS levels, but no differences were found between CNX wild type and knockout cells **(Figure 4.14A)**. On the other hand, the cellular ROS fluorescent probe cellROX indicated that cellular ROS levels were significantly lower in CNX knockout cells compared to the wild type **(Figure 4.14B)**. These results suggest that CNX induces ROS production from an extra-mitochondrial source. In consequence, SERCA oxidation by the two main ROS-producing ER proteins was tested, NOX4, and the Ero1 enzymes Ero1α and Ero1β. Ero1α and Ero1β oxidize other ER oxidoreductases that catalyze disulfide bond formation, resulting in the reduction of the Ero1 enzymes. Then, Ero1α and Ero1β are oxidized by O_2, generating H_2O_2 as a result **(Figure 1.2)** [239]. NOX4 is an ER residing protein that locally produces H_2O_2 [220]. The role of Ero1α and Ero1β was tested with the inhibitor EN460,

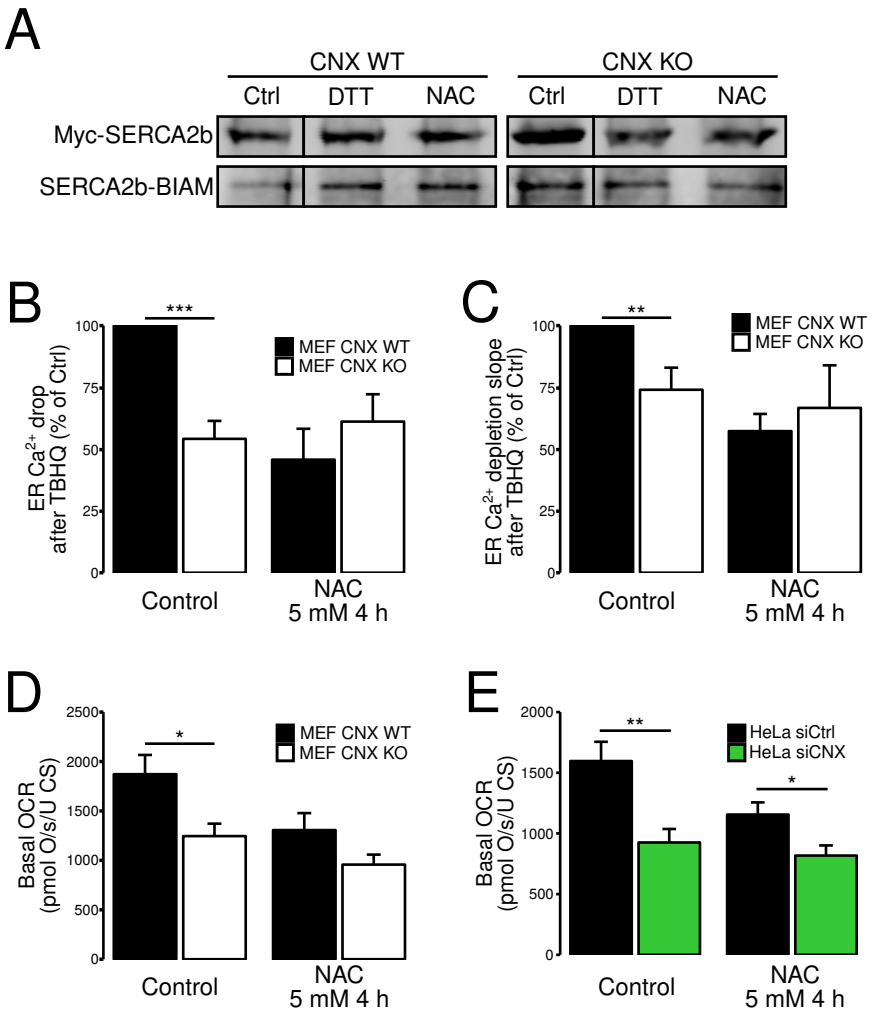

Figure 4.13 – CNX activation of mitochondrial respiration depends on SERCA oxidation. A: CNX wild type and knockout MEFs were transfected with myc-SERCA2b and treated with the reducing agent DTT or 5 mM NAC for 4 hours. Cells were lysed and reduced cysteines were labeled using a biotinylated iodoacetamide (BIAM) assay. The specific SERCA2b BIAM labeling was detected by immunoprecipitating myc-SERCA2b and detecting the BIAM labeling probing the proteins with Streptavidin. n = 2. **B:** ER Ca^{2+} content was measured by depleting ER Ca^{2+} stores with 60 µM TBHQ and no Ca^{2+} medium. The drop in ER Ca^{2+} upon depletion was measured in CNX wild type and knockout MEF cells treated with 5 mM NAC for 4 hours. Control: n = 12; p = 2.4×10^{-6}. NAC: n = 6; p = 0.38. **C:** ER Ca^{2+} leak was measured by quantifying the depletion slopes after 60 µM TBHQ and no Ca^{2+} medium. The slope in ER Ca^{2+} upon depletion was measured in CNX wild type and knockout MEF cells treated with 5 mM NAC for 4 hours. Control: n = 13; p = 0.0078. NAC: n = 6; p = 0.62. **D:** Mitochondrial basal oxygen consumption rate (OCR) was measured in CNX wild type and knockout MEF cells treated with 5 mM NAC for 4 hours. Control: n = 10; p = 0.015. NAC: n = 5; p = 0.118. **E:** Mitochondrial basal oxygen consumption rate (OCR) was measured in HeLa cells transfected with siCNX treated with 5 mM NAC for 4 hours. Control: n = 6; p = 0.0061. NAC: n = 6; p = 0.027. *Experiment in panel A was performed by Megan Yap.*

and the role of NOX4 with the inhibitor GKT [240]. The BIAM oxidation assay showed that EN460 had a small effect on SERCA oxidation while GKT had a stronger effect **(Figure 4.14C)**. However, both drugs had a similar effect on SERCA ATPase, reducing SERCA activity in CNX wild type cells cells **(Figure 4.14D)**. Similarly, both drugs removed the difference in ER Ca^{2+} content between CNX wild type and knockout cells **(Figure 4.14E)**. These results suggest that a combined effect of ER ROS sources might be responsible for SERCA oxidation and activity.

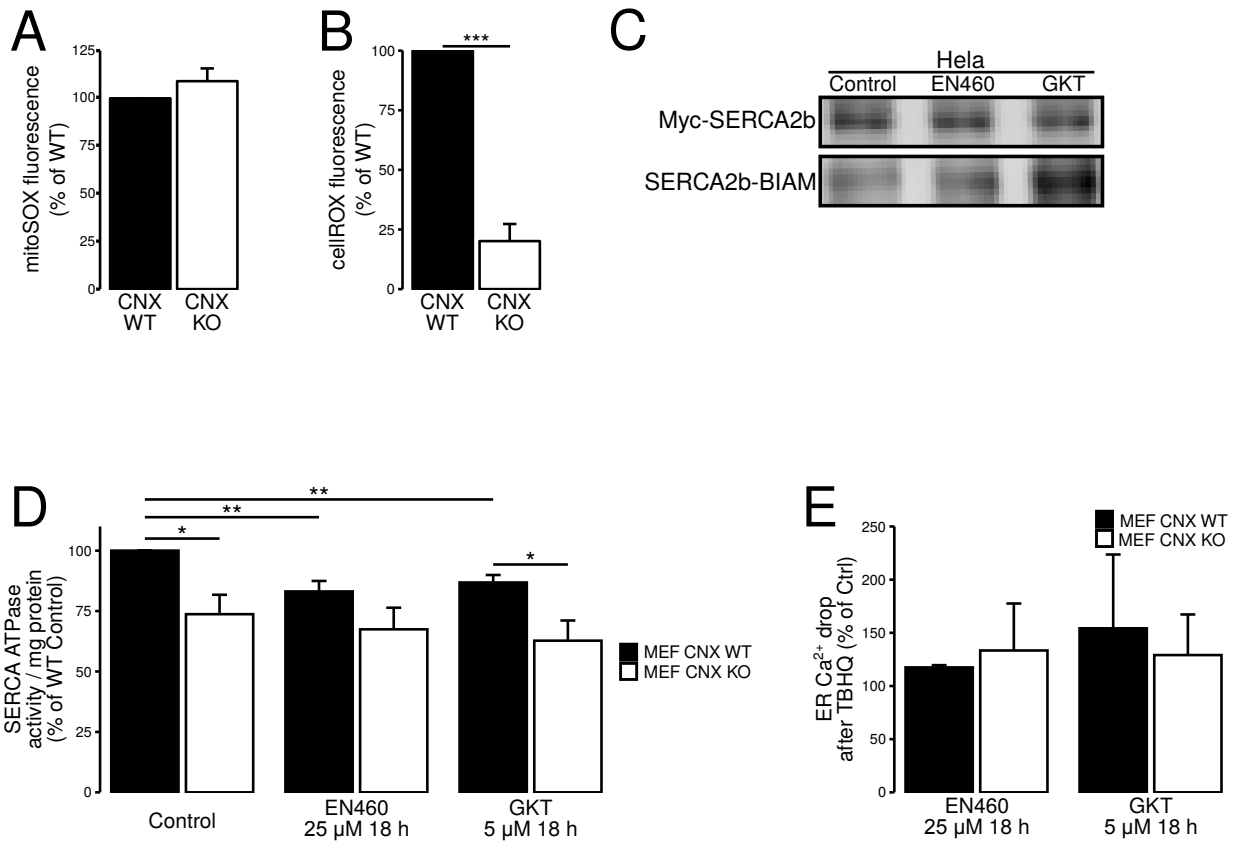

Figure 4.14 – CNX oxidizes and activates SERCA through Ero1 and NOX4. A: Mitochondrial ROS was measured using the fluorescent probe mitoSOX in CNX wild type and knockout MEF cells. n = 7; p = 0.2. **B:** Cellular ROS was measured using the fluorescent probe cellROX in CNX wild type and knockout MEF cells. n = 3; p = 0.0004. **C:** HeLa cells were transfected with myc-SERCA2b and treated with 25 µM EN460 (Ero1α and Ero1β inhibitor) for 18 hours or 5 µM GKT (NOX4 inhibitor) for 18 hours. Cells were lysed and reduced cysteines were labelled using a biotinylated iodoacetamide (BIAM) assay. The specific SERCA2b BIAM labelling was detected by immunoprecipitating myc-SERCA2b and detecting the BIAM labelling probing the proteins with Streptavidin. n = 2. **D:** SERCA ATPase was measured in light membranes of CNX wild type and knockout MEF cells treated with 25 µM EN460 (Ero1α and Ero1β inhibitor) for 18 hours or 5 µM GKT (NOX4 inhibitor) for 18 hours and normalized to protein concentration. n = 4. Control: p = 0.017. EN460: p = 0.166. GKT: p = 0.035. CNX WT Control *vs* CNX WT EN460: p = 0.0081. CNX WT Control *vs* CNX WT GKT: p = 0.0054. **E:** ER Ca^{2+} content was measured by depleting ER Ca^{2+} stores with 60 µM TBHQ and no Ca^{2+} medium. The drop in ER Ca^{2+} upon depletion was measured in CNX wild type and knockout MEF cells treated with 25 µM EN460 (Ero1α and Ero1β inhibitor) for 18 hours or 5 µM GKT (NOX4 inhibitor) for 18 hours. EN460: n = 3; p = 0.74. GKT: n = 3; p = 0.77.

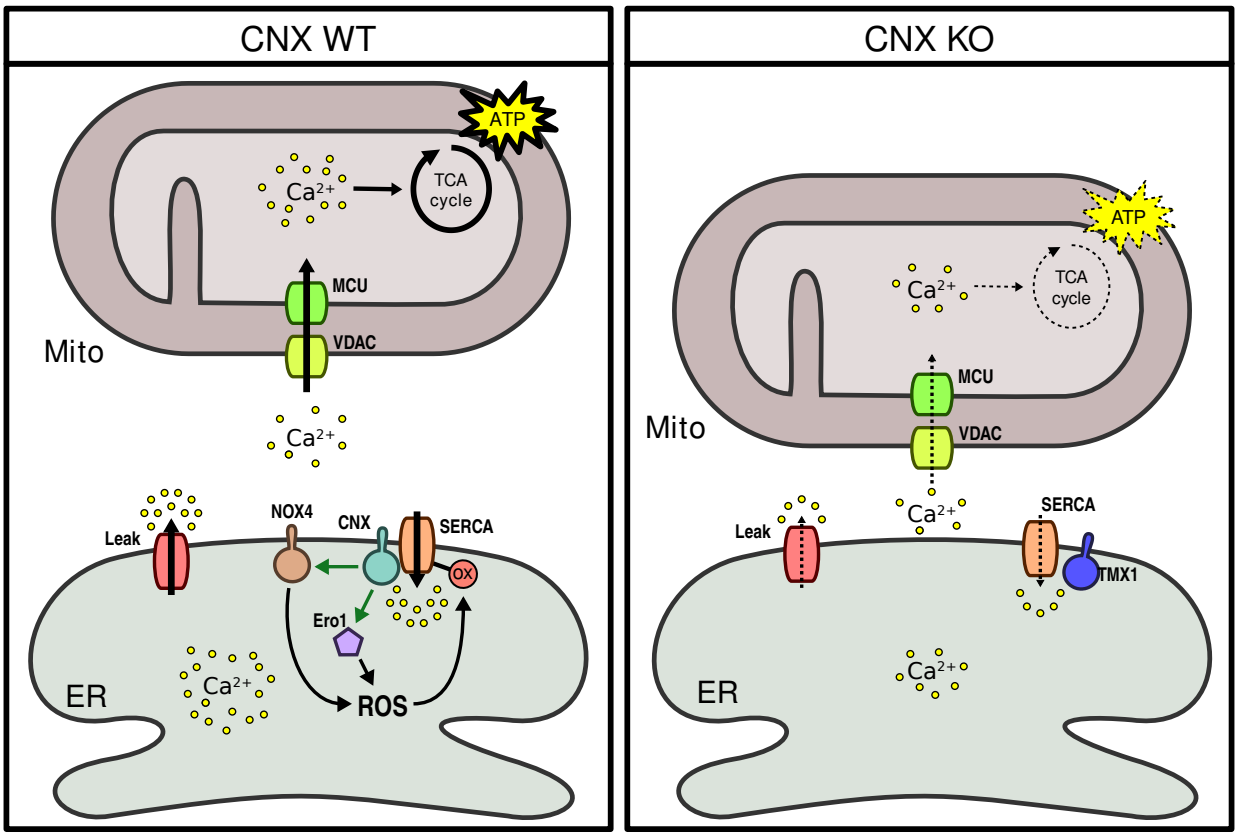

Figure 4.15 – Schematic representation of the proposed effect of CNX in the MAM. CNX increases SERCA oxidation by activating NOX4 and Ero1. SERCA oxidation activates its Ca^{2+} pumping activity increasing ER Ca^{2+} content. As a result, Ca^{2+} flux and mitochondrial Ca^{2+} content are increased, which promotes mitochondrial metabolism and energy production. In the absence of CNX, SERCA activity and oxidation are reduced, resulting in the depletion of ER Ca^{2+} stores. With less Ca^{2+} available in the ER, Ca^{2+} flux is disrupted and mitochondrial energy output decreases. The loss of CNX also increases ER-mitochondria contacts, but this is not enough to compensate for the reduction in Ca^{2+} flux.

4.3 Discussion

4.3.1 Calnexin is necessary to maintain SERCA oxidation and activity

In a previous work our lab found that CNX promotes the accumulation of Ca^{2+} in the ER, probably through the regulation of SERCA activity [114]. The present work confirms the activatory effect of CNX on SERCA activity using direct SERCA ATPase measurements **(Figure 4.2A)**, in addition to ER Ca^{2+} content **(Figure 4.3A)** and speed of Ca^{2+} clearance from the cytosol **(Figure 4.2E)**. Additionally, this work shows that CNX activation correlates with oxidation of SERCA cysteines **(Figure 4.1A)**. These results, summarized in **Figure 4.15**, suggest that CNX activates SERCA by an oxidative post-translational cysteine modification. Unfortunately, the method used to detect cysteine oxidation, the BIAM labelling, does not detect the site, type or number of modifications. SERCA2b, the most ubiquitous SERCA isoform, contains 29 cysteines that could potentially be modified. The antioxidant NAC reduced SERCA oxidation, ER Ca^{2+} levels and mitochondrial respiration to levels similar to the ones found in CNX knockout cells **(Figure 4.13)**, indicating that ROS production mediated by CNX **(Figure 4.14B)** is involved in SERCA regulation and the subsequent metabolic changes.

Since CNX is not able to produce ROS by itself, this prompted us to find other ROS producing enzymes that could be working together with CNX. Cells that lack CNX did not show a difference in ROS levels in their mitochondria **(Figure 4.14A)**, but they did show a significant decrease in ROS in the whole cell **(Figure 4.14B)**, suggesting an extra-mitochondrial ROS source. Hence, the participation of NOX4 was tested, a constitutive active NADPH oxidase that produces H_2O_2 locally at the ER that is able to oxidize other ER proteins [242]. Unlike other ER NOX proteins, NOX4 interacts with CNX, forming protein complexes at the ER and suggesting that NOX4 also localizes in the MAM. As a result, CNX stabilizes NOX4 and increases NOX4 protein levels and H_2O_2 production [219]. This makes NOX4 a prime target for CNX oxidative regulation. Accordingly, a reduction of NOX4 protein level was found in CNX knockdown HeLa cells **(Figure 4.11B)**, and less SERCA2b oxidation in HeLa cells treated with the NOX4 inhibitor GKT **(Figure 4.14C)**. Nevertheless, no

reduction in NOX4 protein level was found in CNX knockdown cells **(Figure 4.11A)**. NOX4 inhibition significantly reduced SERCA ATPase activity in CNX wild type cells, but not in CNX knockout cells **(Figure 4.14D)**, levelling the difference in ER Ca^{2+} content **(Figure 4.14E)**. Thus, NOX4 is probably involved in the oxidative activation of SERCA2b by CNX.

A similar result was found with the Ero1 enzymes Ero1α and Ero1β. The inhibition of the Ero1 enzymes resulted in a minor reduction in SERCA2b oxidation compared to NOX4 inhibition **(Figure 4.14C)**. However, it was still able to reduce SERCA ATPase activity and ER Ca^{2+} content in CNX wild type cells to levels similar to CNX knockout cells **(Figure 4.14D y E)**. The partial effect of NOX4 and Ero1α/β inhibition on SERCA suggest that CNX modulates a combination of ROS sources for the normal regulation of SERCA2b oxidation and activity. Since the regulation of SERCA by oxidative modifications is quite complex, and depends on the site and type of modification, the participation of other ROS producing ER enzymes cannot be discarded. More experiments with a combination of inhibitors, like testing EN460 and GSK at the same time, or a simultaneous NOX4 and Ero1α/β knockout or knockdown, would be necessary to evaluate whether there are more ROS sources regulating SERCA. These molecular approaches would also help to confirm the participation of these proteins.

Interestingly, previous reports have explored the effect of NOX4 and Ero1 in SERCA activity. NOX4 has a inhibitory effect on SERCA during obesity in vascular smooth muscle cells; this inhibitory effect is associated with the sulfonylation of cysteine 674 in SERCA [232]. On the other hand, NOX4 also has an activatory effect on SERCA during VEGF signalling in endothelial cells; in this case, associated with the glutathionylation of the same cysteine 674 in SERCA [233]. Thus, the effect of NOX4 on SERCA activity depends on the type of oxidative modification, although SERCA glutathionylation also requires the presence of nitric oxide (NO) and glutathione [162]. Similarly, Ero1 activity is also associated with the sulfonylation of SERCA cysteines, but on a lumenal loop of SERCA2b. This modification reduces SERCA activity and ER Ca^{2+} content [243]. So far, among the different oxidative modifications, the only one that increases SERCA activity is the glutathionylation in cysteine

674 [160,161]. Thus, it is critical that future experiments evaluate if CNX increases NO levels and promotes glutathionylation of SERCA cysteine 674. This question could be addressed by using an intracellular fluorescent NO indicator like DAF-FM to evaluate NO levels in CNX wild type and knockout cells; using specific antibodies for SERCA cysteine 674 sulfonylation (like the one used in [232]); and testing the effect of a redox-inactive SERCA mutant (with cysteine 674 changed to serine) in CNX wild type and knockout cells. These experiments would clarify if CNX is inducing the activating glutathionylation on cysteine 674. If this is not the case, it would be a novel SERCA activatory oxidative modification.

4.3.2 Calnexin activates mitochondrial metabolism by activating SERCA and maintaining ER Ca^{2+} levels

CNX is a lectin chaperone that folds glycosylated proteins in the ER [124,125], and it can interact with the translocon complex to fold newly synthesized proteins [147]. At the same time, it can be found in the MAM interacting with SERCA2b and regulating Ca^{2+} signalling [114]. The present work further characterized the mechanisms of CNX as a regulator of Ca^{2+} signalling, and analyzed its role as a regulator of Ca^{2+} flux to the mitochondria. In addition to increase ER Ca^{2+} loading **(Figure 4.3A)** and SERCA activity **(Figure 4.2A)**, CNX also promotes the accumulation of Ca^{2+} in mitochondria **(Figure 4.6A)**. Indeed, the loss of CNX results in a reduction in mitochondrial respiration **(Figure 4.10A)** and activation of AMPK, probably as an adaptation for an energetically compromised state **(Figure 4.10C)**. ER Ca^{2+} loading is an important determinant of Ca^{2+} signalling and transfer to mitochondria. For instance, p53 also activates SERCA increasing Ca^{2+} loading and Ca^{2+} flux to mitochondria [61]. Similarly, the reload of ER Ca^{2+} stores through the coordinated action of SOCE and SERCA is also a determinant for effective IP_3R Ca^{2+} release [244]. Previous reports suggest that ER Ca^{2+} leak through the translocon can also result in mitochondrial Ca^{2+} overload and apoptosis during ER stress [245]. This suggests that the increased Ca^{2+} leak induced by CNX **(Figure 4.3B and C)** could also play a role in the increased mitochondrial Ca^{2+} content and mitochondrial metabolism. Unfortunately, the participation of CNX-regulated translocon leak in mitochondrial

Ca^{2+} flux will need to be evaluated in future experiments. Thus, the results suggest that CNX promotes mitochondrial Ca^{2+} flux and mitochondrial metabolism through maintaining full ER Ca^{2+} stores by activating SERCA.

In addition to ER Ca^{2+} loading, CNX also regulates ER-mitochondria distance, another determinant for mitochondrial Ca^{2+} flux [46]. Electron microscopy analysis shows that CNX increases the distance between ER and mitochondria, while also reducing the length of the contacts **(Figure 4.4A)**. As a result, cells that lack CNX have more *contact length / distance* than wild type cells **(Figure 4.4B)**. CNX seems to change the preferred distance for ER-mitochondria contacts, reducing the frequency of Super Tight contacts (0-12 nm), and favouring the formation of Tight and Loose contacts (12-24 and 24-50 respectively) **(Figure 4.4C)**. A slightly different effect is observed when the number of contacts per cell are counted with the SPLICS fluorescent probes. No change was observed in the number of SPLICS short puncta per cells between CNX wild type and knockout cells, suggesting that CNX does not change the frequency of contacts between 8-10 nm **(Figure 4.5A)**. On the other hand, the SPLICS long puncta number per cell was reduced by CNX, suggesting that CNX prevented the formation of 40-50 nm contacts **(Figure 4.5B)**. Thus, similar to the electron microscopy results, the SPLICS experiments also show that CNX decreases ER-mitochondria contacts, but only the long range ones. One limitation of SPLICS is that there is no intermediate probe between 10 and 40 nm, the most relevant distance for efficient Ca^{2+} transfer [98]. Since 40 to 50 nm is too long for efficient Ca^{2+} transfer, it is uncertain if these changes in ER-mitochondria contacts would have any effect on Ca^{2+} transfer to mitochondria. Taken together, and considering that electron microscopy is the gold standard for ER-mitochondria contact measurement, our results indicate that CNX prevents ER-mitochondria contact formation. This potentially puts CNX in the selected group of MAM spacers, proteins with anti-tether properties that reduce ER-mitochondria contacts [1].

The mechanism that CNX uses to control ER-mitochondria distance is unknown, but the SPLICS experiment shows that it is associated with redox signalling. When CNX knockout cells are treated with the antioxidant NAC, the number of SPLICS long punta is partially reduced, shortening the

difference between wild type and knockout cells **(Figure 4.5B)**. This suggests that CNX control of ER-mitochondria distance is linked to its redox regulation, similar to its effect on Ca^{2+} signalling. It is possible that Ca^{2+} itself acts as a link between the two organelles. Since CNX activates SERCA, this would cause a relative reduction in Ca^{2+} concentration in the proximity of the ER, because Ca^{2+} is cleared faster from the cytoplasm. Elevated cytoplasmic Ca^{2+} stops mitochondrial movement through the microtubule network [117], so mitochondria stop close to Ca^{2+} release sites, like ER Ca^{2+} channels [118]. This Ca^{2+}-based tethering mechanism has been described before for S1T, a truncated variant of SERCA isoform 1 that cannot pump Ca^{2+} but leaks Ca^{2+} from the ER. As a result, mitochondria stopped moving in the proximity of the ER, increasing ER-mitochondria contacts and Ca^{2+} flux [119]. In CNX knockout cells, mitochondria could be moving closer to the ER as a consequence of the reduced SERCA activity that could potentially result in higher Ca^{2+} levels in the ER proximity, because of the reduced cytosolic Ca^{2+} clearance. This idea can be tested by measuring ER-mitochondria contacts with electron microscopy in CNX wild type and knockout cells, and treating the cells with the intracellular Ca^{2+} chelator BAPTA-AM. If the increased contacts in cells that lack CNX depend on Ca^{2+}, BAPTA-AM will detach the two organelles, removing the difference between wild type and knockout cells. Similarly, repeating the measurements using NAC, EN460 and GKT would address whether the regulation of ER-mitochondria contacts is associated with CNX redox regulation. In addition, the speed of mitochondrial movement over time can be measured to test if CNX controls mitochondrial and ER proximity through reducing mitochondrial motility. These experiments would indicate if CNX is a Ca^{2+}-based regulator of ER-mitochondria contacts.

Interestingly, the decreased ER-mitochondria contacts observed in cells that have CNX seems to oppose the positive effect of CNX in mitochondrial Ca^{2+} loading. Normally, a decrease in ER-mitochondrial contacts should result in a reduction in mitochondrial Ca^{2+} flux, and a depletion of mitochondrial Ca^{2+}. Nevertheless, the opposite effect is observed, with CNX promoting both ER-mitochondria separation **(Figure 4.4A)** and Ca^{2+} flux **(Figure 4.6A and B)**. Thus, CNX regulation of Ca^{2+} flux is not mediated by the change in ER-mitochondria distance. The most likely explanation is that the critical regulator of Ca^{2+} flux is ER Ca^{2+} loading. Since CNX activates SERCA and maintains

a normal ER Ca^{2+} content, it also maintains enough Ca^{2+} available for an efficient flux of Ca^{2+} from ER to mitochondria. Cells that lack CNX do not have enough Ca^{2+} available in their ER stores to maintain a normal Ca^{2+} flux; as a result, their mitochondrial Ca^{2+} content is also reduced. The increased ER-mitochondria contacts observed in cells that lack CNX might partially compensate for the loss of available Ca^{2+}, but it is not enough. As a result, cells that lack CNX have reduced mitochondrial Ca^{2+} and metabolism, even though they have more ER-mitochondria contacts. The idea that CNX knockout cells have increased ER-mitochondria contacts as a compensatory mechanism, but it is not enough to sustain a normal Ca^{2+} flux to mitochondria, could be tested in future experiments. To do this, the ER Ca^{2+} content of cells with and without CNX would have to be equalized, and then mitochondrial Ca^{2+} content would be measured. In order to equalize ER Ca^{2+} content between cells, they can be incubated with different concentrations of extracellular Ca^{2+}. For example, CNX knockout cells would have to be incubated in medium with more Ca^{2+} than CNX wild type cells, since they have less Ca^{2+} in their ER. Different extracellular Ca^{2+} concentrations would have to be tested, and ER Ca^{2+} content would have to be closely monitored, in order to find the appropriate conditions. Once ER Ca^{2+} concentrations are equalized, mitochondrial Ca^{2+} concentration would be measured. If this hypothesis is correct, and mitochondrial Ca^{2+} is a reflection of ER Ca^{2+}, then the differences between CNX wild type and knockout cells would be reversed. Only the effect of ER-mitochondria distance on mitochondrial Ca^{2+} flux would remain. In this scenario, CNX knockout cells would have an increased mitochondrial Ca^{2+} flux and mitochondrial Ca^{2+} content than CNX wild type cells, since they have closer ER-mitochondria contacts. As a result, the CNX knockout phenotype would be reverted. This shows that ER-mitochondria distance is not enough to predict Ca^{2+} flux; an understanding of other factors, like Ca^{2+} available at the source, is also required.

Chapter 5

ER stress compensates for the loss of Mitofusin-2 ER-mitochondria tethers

5.1 Introduction

5.1.1 Mitofusin structure and mitochondrial fusion

Mitochondria are double membrane bound organelles composed of an outer mitochondrial membrane (OMM) and an inner mitochondrial membrane (IMM), separated by the intermembrane space. In addition, they form a dynamic and interconnected network in the cytosol, driven by fusion and fission events that continuously reshape mitochondrial morphology. Fusion and fission events require a specific set of proteins responsible for the OMM and IMM remodelling. Mitofusin-1 (Mfn1) and Mitofusin-2 (Mfn2) are OMM proteins and critical mediators of mitochondrial fusion [99]. Mfn2 structure consists of a cytosolic GTPase domain in its N-terminal, followed by an heptad-repeat domain (HR1), a proline-rich region, two transmembrane domains, and a second HR domain (HR2) at the C-terminal also facing the cytosol [246]; although this conformation has been recently challenged with a topology that contains only one transmembrane domain, leaving the N-terminal the cytosol and the C-terminal in the mitochondrial intermembrane space [247]. Even though the precise molecular

events have not been completely elucidated, Mfn1 and Mfn2 fuse the OMM of adjacent mitochondria by a combination of inter-organellar dimerization through their GTPase and/or HR domains [248–250], followed by a GTP hydrolysis-driven conformational change that brings the OMM to closer [251]. Mfn2 can also oligomerize in *cis* through the formation of disulfide bonds, greatly increasing mitochondrial fusion during oxidative stress [252]. Like other tail-anchored protein, the targeting of Mfn2 to the OMM depends on the presence of basic amino acids in the region downstream of the transmembrane domain [246]; the composition of this region determines whether the tail-anchored protein is inserted into the OMM or the ER [253]. Mfn1 and Mfn2 share approximately 80% of their sequence, and they are partially able to rescue the phenotype of the other [99]. Nevertheless, Mfn1 has a higher GTPase activity, and is more efficient at fusing membranes [254]; and only Mfn2 is targeted to the ER, and able to regulate ER-mitochondria contacts [100].

5.1.2 Mitofusin-2 is an ER-mitochondria tether with controversial functions in ER-mitochondria contact formation

In addition to its effects on mitochondria morphology, Mfn2 was the first MAM protein described to form a physical link between ER and mitochondria, by forming dimers between the opposing organelles [100]. Based on its function as a promoter of OMM tether and fusion, it makes sense that Mfn2 has a positive effect in the formation of ER-mitochondria contacts. Indeed, several observations suggested that Mfn2 acts as a ER-mitochondria tether, promoting ER-mitochondria contacts. *In vitro* experiments using Mfn2 knockout mouse embryonic fibroblasts (MEF) cells and confocal fluorescence microscopy showed that fluorescent-labelled ER and mitochondria interaction was reduced [100]. Similarly, the extent of the ER-mitochondria contacts, measured using electron microscopy, was decreased [255]. A similar reduction in ER-mitochondria apposition was observed in cardiomyocytes [256] and neurons [257]. This evidence suggests that Mfn2 is a tether that promotes ER-mitochondria contact formation. Accordingly, measurements of MAM function like Ca^{2+} flux and phospholipid transfer were also decreased in Mfn2 knockout cells [100,255,258]. Yet, some reports show that the effect of Mfn2 is the opposite of the original findings. Studies in the same

Mfn2 knockout MEF model found that the lack of Mfn2 actually increased the contacts between ER and mitochondria [259–261]. This discrepancy was, in part, attributed to the inability of fluorescence microscopy to correctly measure ER-mitochondria apposition. Specifically, the alterations in mitochondrial morphology induced by the loss of Mfn2 was mistakenly detected as loss of colocalization when measured by fluorescence colocalization analysis [260]. In addition, it was found that Mfn2 knockout MEF cells had reduced expression of the mitochondrial Ca^{2+} uniporter (MCU), the Ca^{2+} channel responsible for the entry of Ca^{2+} into the mitochondrial matrix. This explained the reduced Ca^{2+} flux observed in Mfn2 knockout cells; on the other hand, transient Mfn2 knockdown did increase Ca^{2+} flux to mitochondria, since these cells did not have a downregulation in MCU protein levels [260,262]. Due to these confounding factors, it was proposed that the most reliable technique to measure ER-mitochondria contacts is electron microscopy, which showed an increased ER-mitochondria proximity in both Mfn2 knockout and knockdown cells [259–261]. Overall, it was clear that the use of co-localization using fluorescence microscopy was not the best tool to measure ER-mitochondria interaction, at least when any of the two organelles undergoes important morphological changes, as is the case with Mfn2 knockout cells. Nevertheless, different groups have found opposite results in terms of ER-mitochondria distance using electron microscopy, making the two positions hard to reconcile [255,260].

There are some additional factors that can help to understand why opposite results are found in similar cellular systems. First, the culture conditions of the cell lines can play an important role in the formation of ER-mitochondria contacts. For instance, ER stress and nutrient availability can modulate the interaction between ER and mitochondria [96,263]. Similarly, cells cultured at higher densities have slightly more contacts, and reduced MCU expression [255]. These findings suggest that differences in culture conditions between labs can be responsible for some of the differences observed. Second, rather than changes in contacts as a whole, Mfn2 could be regulating a specific type of contact. As mentioned before, the novel split-GFP-based contact site sensor SPLICS can measure ER-mitochondria proximity at two different distances: 8 to 10 nm (SPLICS-short), and 40 to 50 nm (SPLICS-long). Analysis of the effect of Mfn2 on contact formation using the SPLICS

probes showed that Mfn2 knockdown induces an increase in close contacts and a reduction in the long ones [177]. This is similar to our findings shown in the previous chapter, where CNX reduced the formation of long distance contacts, although it did not affect short distance ones **(Figure 4.5A)**. Similarly, knocking down Mfn2 in fibrosarcoma cells that express high Mfn2 resulted in an increase in ER-mitochondria contacts, specifically between mitochondria and the rough ER [97]. Overall, these reports show that Mfn2 might be regulating the formation of specific types of MAM, rather that a global increase or decrease of contact formation. Thus, the lack of distinction between different MAM types could be an additional confounding factor that can explain the diverse results found in the literature. This asks for a higher level of granularity in the quantification of ER-mitochondria contacts in order to clearly identify the role of Mfn2; ideally, classifying the contacts according to the ER-mitochondria distance, and the presence or absence of ribosomes. Third, it is possible that the loss of Mfn2 changes the activity of other MAM tethers. The clearest example of this is the regulation of PKR-like Endoplasmic Reticulum Kinase (PERK) by Mfn2. PERK is better known for its participation in ER stress, where it inhibits protein translation [264]. In addition to this canonical function, PERK localizes to the MAM and regulates ER-mitochondria communication. PERK knockout cells show less ER-mitochondria contacts than normal cells. In addition, cells subjected to oxidative stress showed more ER-mitochondria contacts, but this increase was blocked in cells that lack PERK. The impaired contact formation during oxidative stress protected PERK knockout cells from cell death [237]. Interestingly, Mfn2 not only interacts with PERK, it is also an upstream inhibitor of PERK activity. Accordingly, loss of Mfn2 cause ER stress and ROS production [265,266], and a sustained activation of PERK, resulting in mitochondrial Ca^{2+} overload and cell death [267,268]. Thus, the activation of compensatory MAM tethers like PERK could also explain the different experimental outcomes observed after the loss of Mfn2.

5.1.3 Aims

In this chapter, I want to investigate the effect of Mfn2 in the formation of ER-mitochondria contacts and regulation of mitochondrial function, with a focus on ER stress as a compensatory mechanism

that increases ER-mitochondria contacts. In order to do this, I proposed the following aims: (*i*) measure the effects of Mfn2 on mitochondrial function and metabolism; (*ii*) evaluate if Mfn2 regulates ER stress activation, specifically PERK and Ero1; (*iii*) measure the effect of PERK and Ero1 in the metabolic regulation by Mfn2; and (*iv*) measure the role of Mfn2 in the ER-mitochondria contacts regulation by PERK and Ero1. These aims were evaluated in a Mfn2 knockout Mouse Embryonic Fibroblast (MEF) cell line. To evaluate the role of PERK and Ero1, their specific inhibitors GSK [269] and EN460 [240] were used.

The results show that Mfn2 knockout MEF cells have increased mitochondrial ATP production and respiration, and more ER-mitochondria contacts, suggesting that Mfn2 acts as a MAM spacer, separating the two organelles. In addition, these cells have active ER stress and increased ROS levels. Interestingly, the activation of two ER stress proteins, PERK and Ero1, was required for the alterations observed in Mfn2 knockout cells. Together, these suggest that Mfn2 is a MAM spacer that prevents the formation of ER-mitochondria contacts by blocking the tethering effect of PERK and Ero1.

5.2 Results

5.2.1 Mitofusin-2 reduces mitochondrial metabolism

ER-mitochondria contacts and Ca^{2+} transfer to the mitochondria critically regulate mitochondrial functions such as ATP production and apoptosis. Since Mfn2 has been reported to regulate both ER-mitochondria contact formation and Ca^{2+} flux to the mitochondria [100], the effect of Mfn2 on mitochondrial metabolism was evaluated as in indirect measurement of ER-mitochondria coupling.

First, cellular ATP levels were measured as an indicator of energy production in the cell. MEF cells that lack Mfn2 showed increased ATP levels compared to normal MEF cells **(Figure 5.1A)**. But ATP can be produced from different sources, like glycolysis or mitochondrial respiration. To determine the mitochondrial contribution to ATP production, cells were treated with the mitochondrial ATP

synthase inhibitor oligomycin. Oligomycin treatment reduced the ATP levels in Mfn2 knockout cells to a greater extent than in Mfn2 wild type cells, and eliminated the difference between both cell lines **(Figure 5.1A)**. This result suggests that the extra ATP found in cells that lack Mfn2 comes from increased mitochondrial ATP production. Since mitochondrial Ca^{2+} activates mitochondrial metabolism, the requirement of Ca^{2+} flux to mitochondria was also evaluated. To test if Ca^{2+} flux to mitochondria is involved in the increased mitochondrial ATP production in Mfn2 knockout cells, cells were treated with the intracellular Ca^{2+} chelator BAPTA-AM. Upon blockade of Ca^{2+} flux, the increased ATP observed in Mfn2 knockout MEF cells returned to levels similar to wild type cells **(Figure 5.1A)**. Together, these results suggest that cells that lack Mfn2 have increased Ca^{2+} flux and, as a consequence, increased mitochondrial metabolism and ATP production compared to cells that have normal Mfn2 levels.

Next, mitochondrial oxygen consumption rate (OCR) was measured to evaluate if Mfn2 regulates mitochondria function. This is a more direct measurement of mitochondrial respiration. Under basal conditions, cells that lack Mfn2 have significantly more oxygen consumption than wild type cells. Similarly, other indicators of mitochondria respiration were also altered in Mfn2 knockout cells. Proton leak (mitochondrial respiration not linked to ATP synthesis), ATP turnover (respiration linked to ATP production) and the maximum Electron Transport Chain (ETC) capacity were all increased in Mfn2 knockout cells **(Figure 5.1B)**. These results suggest that Mfn2 inhibits mitochondrial metabolism and respiration.

Then, the reliance on mitochondrial ATP production for cell survival was evaluated. This was tested by blocking mitochondrial ATP production with the mitochondrial ATP synthase inhibitor oligomycin, and measuring cell death. Since Mfn2 knockout MEF cells have increased mitochondrial energy production compared to wild type cells, they could be more sensitive to oligomycin-induced cell death. Consistent with the previous result, cells that lack Mfn2 are more sensitive to oligomycin induced cell death, suggesting that these cells depend more on mitochondria energy production to survive **(Figure 5.1C)**. Together, these results suggest that Mfn2 prevent mitochondrial respiration

and energy production. Since Ca^{2+} is required for the increased mitochondrial energy production in Mfn2 knockout, it is possible that Mfn2 has an inhibitory effect on mitochondrial Ca^{2+} flux at the MAM.

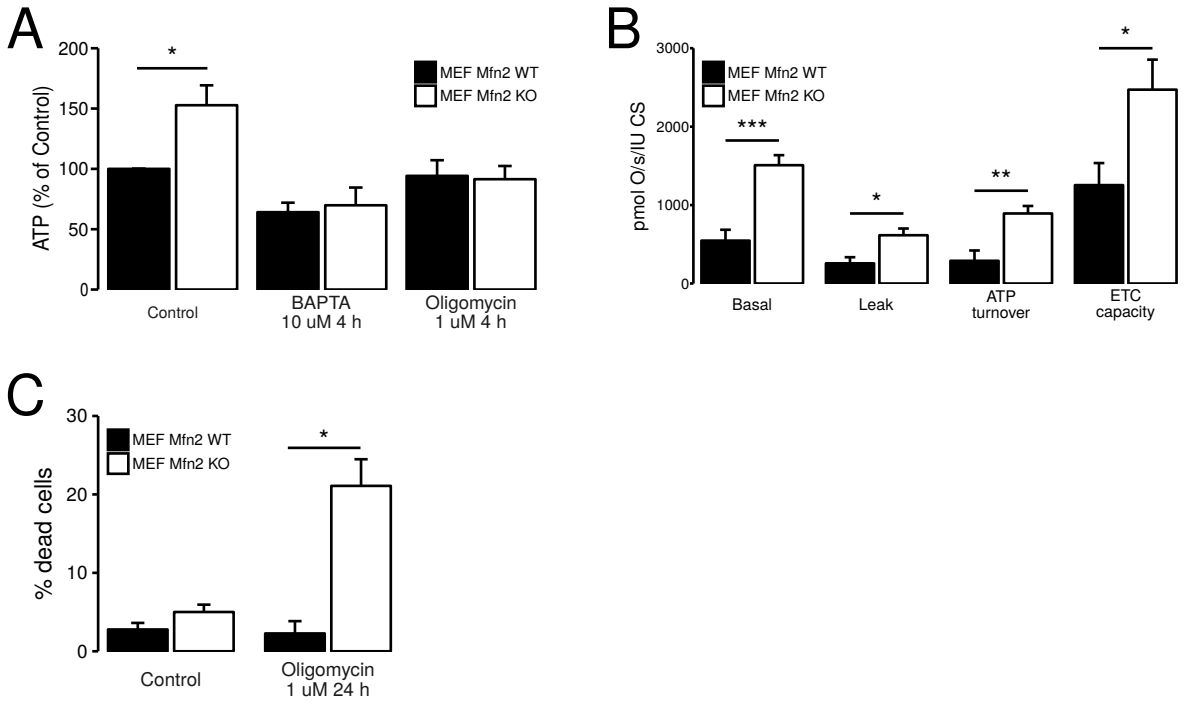

Figure 5.1 – Cells that lack Mfn2 have increased mitochondrial metabolism. A: Total cellular ATP was measured in Mfn2 wild type and knockout MEF cells treated with 10 μM BAPTA-AM for 4 hours or 1 μM oligomycin 4 hours. Control: n = 27; p = 0.0037. BAPTA: n = 5; p = 0.74. Oligomycin: n = 2; p = 0.89. **B:** Mitochondrial respiration was measured in Mfn2 wild type and knockout MEF cells. n = 5; p = 0.00093 for Basal; p = 0.015 for Leak; p = 0.006 for ATP turnover; p = 0.033 for ETC capacity. **C:** Cell viability was measured in Mfn2 wild type and knockout MEF cells treated with 1 μM oligomycin for 24 hours. Control: n = 5; p = 0.11. Oligomycin: n = 3; p = 0.0073.

5.2.2 Mitofusin-2 inhibits ROS production and ER stress signalling

Mfn2 knockout cells have increased mitochondrial metabolism, suggesting that Mfn2 prevents the flow of Ca^{2+} to mitochondria and reduces mitochondrial function. Alternatively, Mfn2 could be acting as an inhibitor for other MAM tethers, which are more active in the absence of Mfn2 promoting Ca^{2+} flux and mitochondrial metabolism. Previous reports show that the loss of Mfn2 activates ER stress and ROS production [265,266]; and both ER and oxidative stress can increase Ca^{2+} flux to mitochondria [71,72,112,163,164,171]. Thus, the participation of ER stress and ROS in the Mfn2

knockout phenotype was explored. Western blotting analysis shows an increase in the ER stress markers XBP1 and CHOP, as well as in the phosphorylated form of PERK, and the ER chaperones BiP and CNX **(Figure 5.2A)**. This suggests that ER stress is indeed more active in Mfn2 knockout MEF cells. Similarly, Mfn2 knockout MEF cells have increased cellular ROS levels **(Figure 5.2B)**. Therefore, consistent with the literature, Mfn2 knockout cells have increased ER stress and ROS levels.

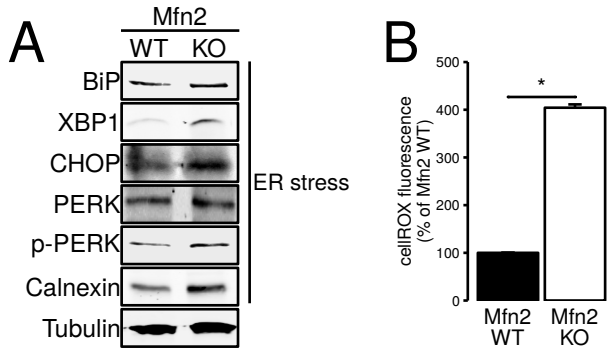

Figure 5.2 – Cells that lack Mfn2 have activated ER stress and ROS production. A: Western blot of ER stress markers in Mfn2 wild type and knockout MEF cells. **B:** Cellular ROS was measured using the fluorescent probe cellROX in CNX wild type and knockout MEF cells. n = 2; p = 0.015.

5.2.3 PERK and Ero1α/β increase mitochondrial metabolism in cells that lack Mfn2

To evaluate if the increased ROS levels observed in cells that lack Mfn2 are involved in the changes in metabolism, total ATP levels were measured in cells treated with the antioxidant *N*-acetylcysteine (NAC). The result shows that the increased ATP levels in Mfn2 knockout cells were reduced to levels similar to Mfn2 wild type cells with NAC treatment **(Figure 5.3A)**. This suggests that ROS plays an important role in the metabolic changes induced by the loss of Mfn2. One of the main sources of ROS production during ER stress is Ero1α, one of the two Ero1 enzymes which generates ROS and promotes Ca^{2+} transfer from ER to mitochondria during ER stress by activating IP_3R-mediated Ca^{2+} release [72,164,165]. To test if the ROS producing Ero1 enzymes are participating in the metabolic changes in Mfn2 knockout, cells were treated with EN460, an inhibitor of both Ero1α and Ero1β [240]. The inhibition of Ero1α/β reduced the increased ATP levels observed in cells that lack Mfn2 **(Figure 5.3A)**, suggesting that Ero1α/β participates in the metabolic changes in

Mfn2 knockout cells. To test if the ER-mitochondria tether and ER stress signalling protein PERK is involved in the metabolic changes in Mfn2 knockout, cells were treated with the PERK inhibitor GSK [269]. Similarly, PERK inhibition resulted in a reduction in ATP levels particularly in cells that lack Mfn2 **(Figure 5.3A)**. This suggests that ER stress induction and activation of PERK promotes mitochondrial ATP production in cells that lack Mfn2.

Ca^{2+} flux to mitochondria is an activator of mitochondrial metabolism [80]. This flux is more efficient when ER-mitochondria contacts are increased. Thus, if Mfn2 knockout cells have more contacts, Ca^{2+} flux should be improved. To evaluate Ca^{2+} transfer from ER to mitochondria, mitochondrial Ca^{2+} was measured after inducing a release of Ca^{2+} from the ER through the IP_3Rs using histamine. The result shows that there are no differences in the mitochondrial Ca^{2+} peak between Mfn2 wild type and knockout MEF cells **(Figure 5.3B left)**. However, when cells were treated with the PERK inhibitor GSK, the transfer of Ca^{2+} was more efficient in wild type cells compared to Mfn2 knockout **(Figure 5.3B right)**. This indicates that Ca^{2+} flux is equal between Mfn2 wild type and knockout under normal conditions. But, unlike wild type cells, Mfn2 knockout cells require PERK activity to maintain a normal Ca^{2+} transfer to the mitochondria, suggesting that the absence of Mfn2 activates PERK.

The increased mitochondrial metabolism and ATP production in cells that lack Mfn2 suggests that there is a change in the metabolic preference of these cells. Since Mfn2 knockout cells have increased energy production in their mitochondria, these cells might have a change in the balance between glycolysis and mitochondrial respiration. During glycolysis, glucose is metabolized into pyruvate. This pyruvate can be either converted to lactate and secreted, or to acetyl-coenzyme A and enter the Krebs cycle in the mitochondria. The use of glucose as a metabolic substrate was evaluated by measuring the amount of lactate produced per glucose consumed, also known as glycolytic flux. Lactate is produced from pyruvate and it is not further metabolized, but secreted from the cell. If glycolytic flux is high, it means that a large proportion of glucose is converted into lactate and not further metabolized. If glycolytic flux is low, a greater proportion of glucose is further metabolized after glycolysis and

probably oxidized in the mitochondria. In general, high glycolytic flux suggests that the cell prefers to use only glycolysis for energy production, whereas a low glycolytic flux suggests that cells also oxidize glucose and use more mitochondrial respiration. The results show that cells that lack Mfn2 have less glycolytic flux than normal cells, even though the difference is not statistically significant **(Figure 5.3C)**. This suggests that Mfn2 knockout cells preferentially oxidize pyruvate in their mitochondria rather than secreting it as lactate, compared to wild type cells. In addition, treating the cells with either EN460 or GSK increased the glycolytic flux of Mfn2 knockout cells to levels similar to Mfn2 wild type cells **(Figure 5.3C)**. This suggests that Ero1 and PERK mediate the increase in mitochondrial respiration observed in Mfn2 knockout cells. In addition, the composition of glycolytic and mitochondrial enzymes was also evaluated. Consistent with their preference of mitochondrial respiration for energy production, Mfn2 knockout cells have reduced levels of the glycolytic enzyme Hexokinase I, and increased levels of the mitochondrial respiratory complex Complex II, relative to normal cells **(Figure 5.3D)**. When cells were treated with the PERK inhibitor GSK, Mfn2 knockout cells reverted to a protein composition similar to the WT cells **(Figure 5.3D)**, suggesting that the change in protein levels depends on the activation of PERK.

Taken together, these results suggest that Mfn2 reduces mitochondrial respiration and promotes a glycolytic metabolism. Cells that lack Mfn2 shift their metabolism towards mitochondrial respiration instead of glycolysis. This change depends on the activation of PERK and Ero1, suggesting that Mfn2 inhibits these proteins under normal conditions. Since PERK promotes ER-mitochondria proximity, and the distance between ER and mitochondria determines mitochondrial activity, these data suggest that cells that lack Mfn2 have increased ER-mitochondria contacts.

5.2.4 Mfn2 prevents normal ER-mitochondria contact formation

The synthesis of Phosphatidylethanolamine (PE) from Phosphatidylserine (PS) is an essential MAM function that requires close ER-mitochondria contacts [2]. If Mfn2 modulates ER-mitochondria proximity, this should be reflected in changes in PE synthesis from PS. Nevertheless, the results show no significant differences in PE synthesis between Mfn2 wild type and knockout cells at any time point,

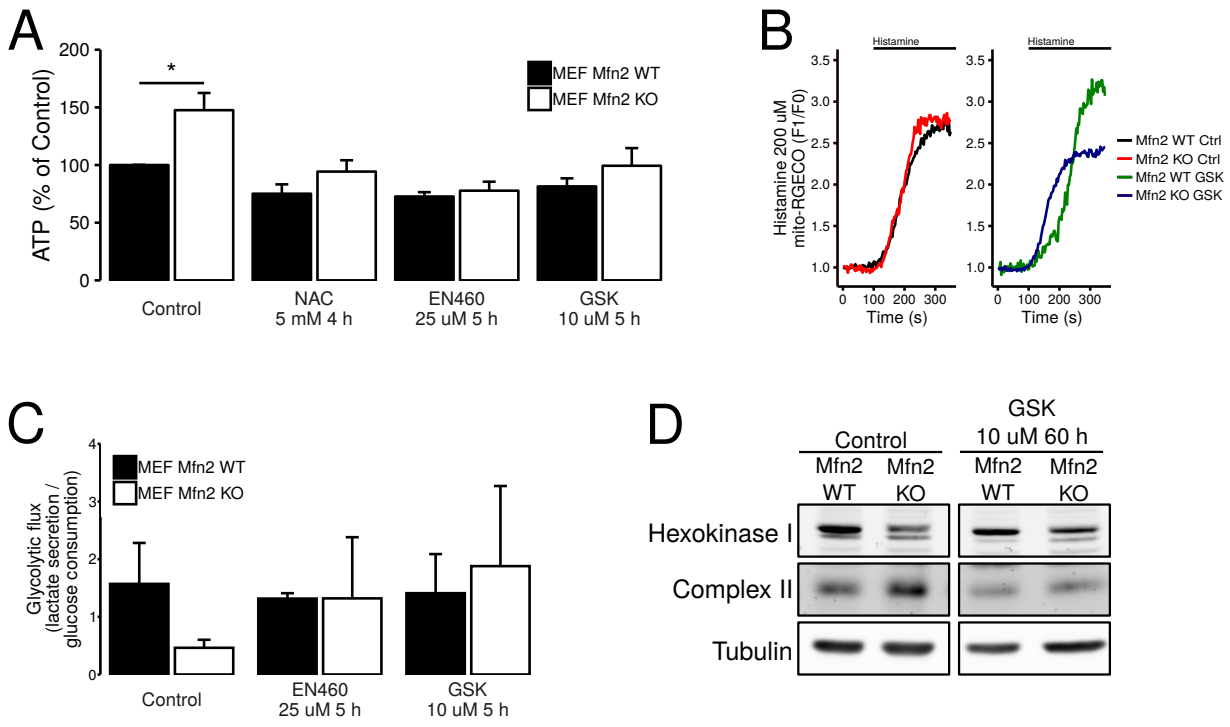

Figure 5.3 – Cells that lack Mfn2 have activated ER stress and ROS production. A: Total cellular ATP was measured in Mfn2 wild type and knockout MEF cells in the presence of 5 mM NAC for 4 hours, 25 μM EN460 for 5 hours or 10 μM GSK for 5 hours. Control: n = 27; p = 0.037. NAC: n = 3; p = 0.209. EN460: n = 3; p = 0.601. GSK: n = 9; p = 0.31. **B:** Mitochondrial Ca^{2+} was measured after a release of Ca^{2+} through the IP_3Rs triggered by 200 μM histamine in Mfn2 wild type and knockout MEF cells in the presence of 10 μM GSK for 5 hours. **C:** Glycolytic flux was measured in Mfn2 wild type and knockout MEF cells in the presence of 25 μM EN460 for 24 hours or 10 μM GSK for 24 hours. Control: n = 3; p = 0.2. EN460 and GSK: n = 2. **D:** Western blot of Hexokinase I and Complex II with Tubulin used as loading control in Mfn2 wild type and knockout MEF cells in the presence of 10 μM GSK for 60 hours. n = 2.

suggesting that Mfn2 does not interfere with lipid transfer between ER and mitochondria or ER-mitochondria contacts **(Figure 5.4)**.

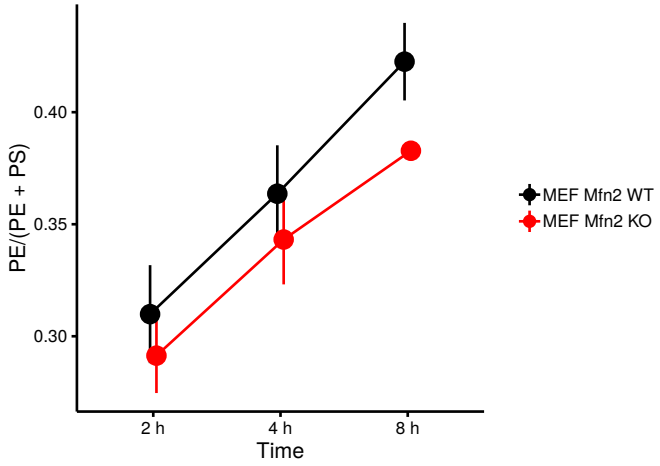

Figure 5.4 – Mfn2 does not regulate lipid transfer between ER and mitochondria. Lipid transfer between ER and mitochondria was measured as PE synthesis from PS in Mfn2 wild type and knockout MEF cells. PE and PS were measured at the indicated time points after labeling with ^{3}H-serine. n = 4; p = 0.53 for 2 hours; p = 0.51 for 4 hours; p = 0.14 for 8 hours.

Therefore, to clarify the effect of Mfn2 in ER-mitochondria contact formation, we directly measured the distance between ER and mitochondria using electron microscopy **(Figure 5.5)**. Cells that lack Mfn2 have closer and longer contacts, indicating an increase in ER-mitochondria apposition **(Figure 5.6A and B)**. These two measurements were combined in a single factor that represents the amount of ER-mitochondria contacts by calculating *contact length / distance*, which was also increased in cells that lack Mfn2 **(Figure 5.6C)**. Accordingly, the number of Tight (12 to 24 nm) contacts was increased in Mfn2 knockout cells, while the number of Loose (24 to 50 nm) contacts was reduced **(Figure 5.6D)**. Consistent with previous results, the PERK inhibitor GSK reverted the increased contacts found in Mfn2 knockout cells. This suggests that PERK is active in Mfn2 knockout cells, and promotes the formation of ER-mitochondria contacts. But when PERK is inhibited, the increased contacts in Mfn2 knockout cells return to levels similar to wild type cells. Next, I evaluated if these changes in ER-mitochondria contacts are associated with a change in MAM protein composition.

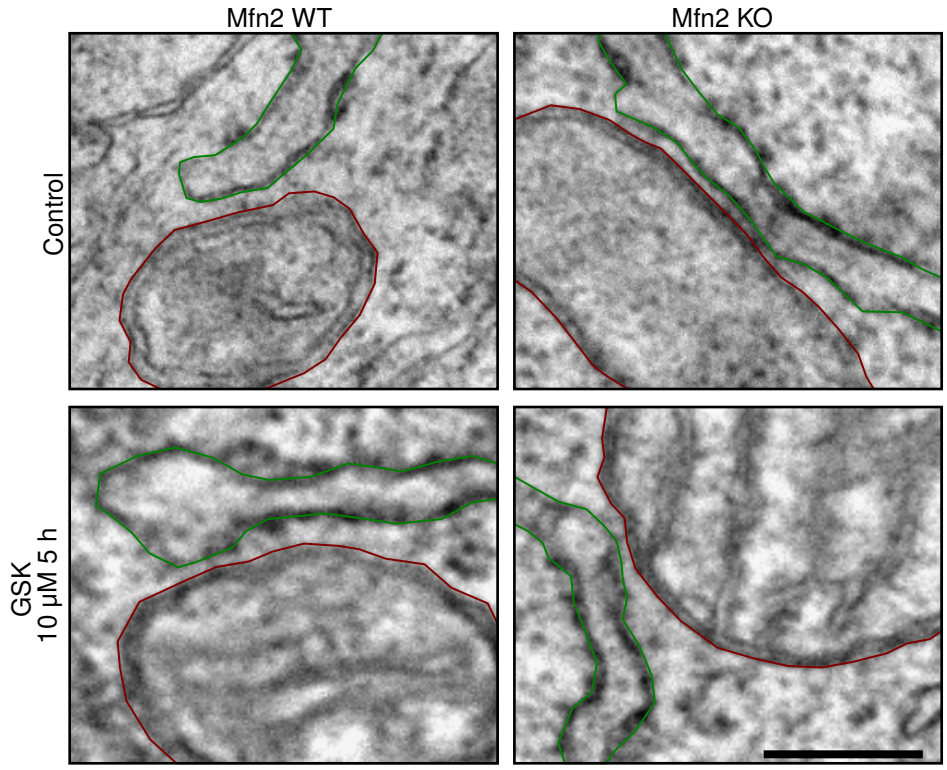

Figure 5.5 – Electron microscopy images of ER-mitochondria contacts in Mfn2 knockout cells. Electron microscopy images of Mfn2 wild type and knockout MEF cells treated with 10 µM of the PERK inhibitor GSK for 5 hours. Mitochondria are labeled in red and the ER in green. Scale bar = 200 nm.

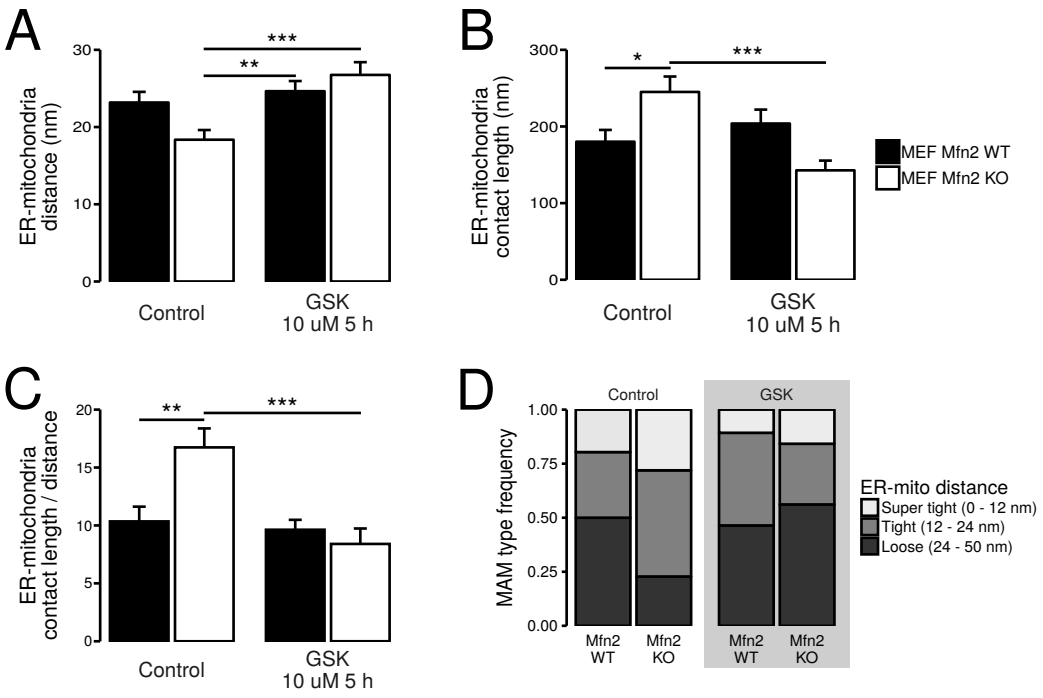

Figure 5.6 – PERK increases ER-mitochondria contacts in Mfn2 knockout cells. A: Average ER-mitochondria distance. n = 50. Mfn2 KO Control *vs* Mfn2 WT GSK: p = 0.0087. Mfn2 KO Control *vs* Mfn2 KO GSK: p = 0.00025. **B:** Average ER-mitochondria contact length. n = 50. Mfn2 WT Control *vs* Mfn2 KO Control: p = 0.022. Mfn2 KO Control *vs* Mfn2 KO GSK: p = 0.0005. **C:** Average ER-mitochondria `contact length / distance` ratio. n = 50. Mfn2 WT Control *vs* Mfn2 KO Control: p = 0.0052. Mfn2 KO Control *vs* Mfn2 KO GSK: p = 0.00085. **D:** Frequency of ER-mitochondria contacts classified by distance into Super tight (0 to 12 nm), Tight (12 to 24 nm), and Loose (24 to 50 nm). n = 50.

5.2.5 PERK and Ero1α localize to the Mitochondria-Associated Membranes during ER stress

So far, the results show that Mfn2 knockout cells have increased mitochondrial respiration, ATP production and ER-mitochondria contacts. In addition, PERK and Ero1α/β are required for some of these changes induced by the loss of Mfn2. This suggests that they might be regulating mitochondrial function by increasing ER-mitochondria contacts. Thus, the presence of PERK and Ero1α in the Mitochondria-Associated Membranes (MAM) was evaluated. The proteins localized in the MAM were identified by cellular fractionation, and the bulk of the ER (Microsomes) was separated from the MAM using Percoll fractionation. Western blotting analysis of these fractions show that IP_3R isoform 1, Ero1α and PERK can be found in the MAM of wild type cells, but their MAM presence was increased in cells that lack Mfn2 **(Figure 5.7A)**. This suggests that the presence of Mfn2 prevents the movement of these proteins to the MAM fraction under normal conditions. Interestingly, when Mfn2 knockout cells were treated with GSK, the enrichment of PERK in the MAM was lost, suggesting that PERK activation is required for its MAM enrichment **(Figure 5.7A)**. Similar results were found by differential centrifugation fractionation. In Mfn2 knockout cells, Ero1α and PERK were enriched in the Heavy membranes (10,000 rcf pellet) compared to the Light membranes (100,000 rcf) **(Figure 5.7B)**, again suggesting that these proteins move from the bulk ER to the MAM. In addition, when Mfn2 wild type cells were treated with the ER stress inducer Tunicamycin for 1 hour, Ero1α and PERK were also enriched in the Heavy membranes fraction **(Figure 5.7B)**. This shows that Ero1α and PERK move to the MAM during early stages of ER stress, and suggests that ER stress could be involved in altered MAM protein composition in Mfn2 knockout cells.

Since Ero1α/β and PERK participate in the phenotype of Mfn2 knockout cells, and Ero1α and PERK move to the MAM at the same time, it is possible that they interact at the MAM during their activation. Therefore, Ero1α and PERK interaction was evaluated by transfecting the cells with a plasmid expressing FLAG-tagged PERK and co-immunoprecipitating Ero1α. Western blotting analysis shows that Ero1α co-immunoprecipitated with PERK. In addition, the interaction was increased in

cells treated with Tunicamycin to induce ER stress, and was reduced in cells treated with GSK (**Figure 5.7C**). This suggests that Ero1α and PERK interact during ER stress, and that PERK activity is needed for this interaction. Since Ero1α and PERK are enriched in the MAM fraction during ER stress and in Mfn2 knockout cells, it is possible that the Ero1α-PERK interaction is taking place at the MAM.

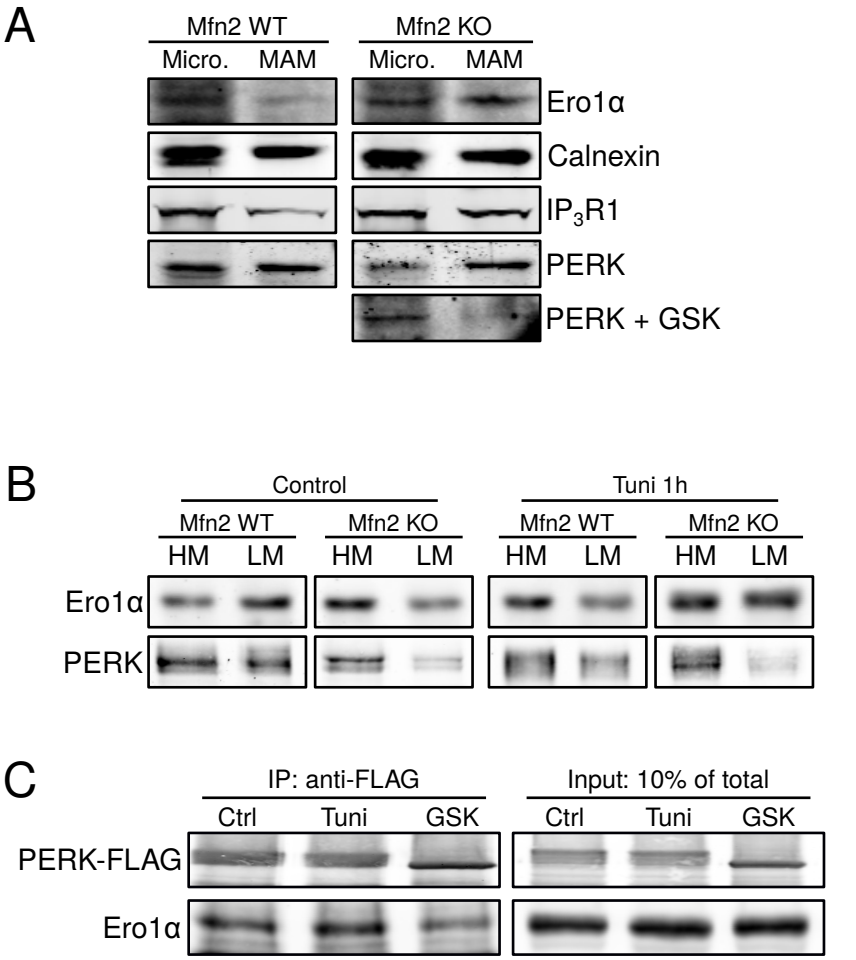

Figure 5.7 – PERK and Ero1α form a complex that is targeted to the MAM in cells that lack Mfn2. **A:** Western blot of a Percoll fractionation showing Microsomes and MAM subcellular fractions from Mfn2 wild type and knockout MEF cells treated with 10 μM of the PERK inhibitor GSK for 5 hours. n = 1. **B:** Western blot of a Simple fractionation showing Heavy membranes (mitochondria + MAM, HM) and Light membranes (ER, LM) fractions from Mfn2 wild type and knockout MEF cells treated with 1 μg/mL of the ER stress inducer Tunicamycin for 1 hour . n = 1. **C:** Co-immunoprecipitation of Ero1α with PERK-FLAG from protein extracts of Hela cells transfected with a PERK-FLAG plasmid and treated with 1 μg/mL Tunicamycin for 1 hour or 10 μM of GSK for 5 hours. n = 1. *Experiment in panel C was performed by Megan Yap.*

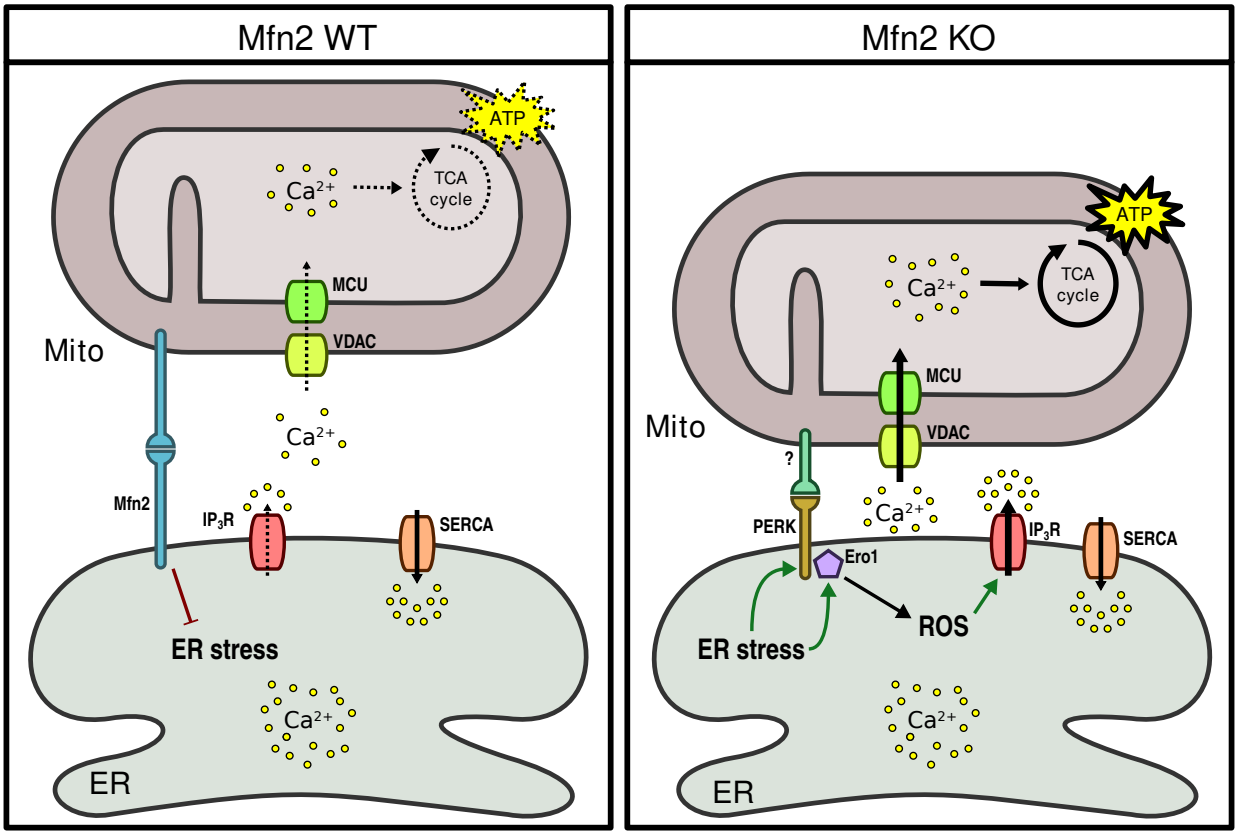

Figure 5.8 – Schematic representation of the proposed effect of Mfn2 in the MAM. Mfn2 inhibits the activation of ER stress signalling at the ER. In the absence of Mfn2, ER stress is activated. The activation of ER stress recruits PERK and Ero1 to the MAM. PERK promotes the formation of ER-mitochondria contacts, while ROS production by Ero1 activates IP_3R, as reported in the literature. As a result, Ca^{2+} flux to mitochondria and mitochondrial metabolism are increased.

5.3 Discussion

5.3.1 Mitofusin-2. A tether or a spacer?

Among ER-mitochondria tethers, Mfn2 is probably the most controversial. It was the first protein suggested to directly bridge ER and mitochondria [100]. This conclusion was largely based on two observations. First, a loss of co-localization between ER and mitochondria labelled with fluorescent probes using confocal microscopy in Mfn2 knockout cells. Second, after an equal release of Ca^{2+} from the ER to the cytosol, Mfn2 knockout cells had a smaller increase in mitochondrial Ca^{2+} than wild type cells, suggesting that Ca^{2+} flux was impaired after the loss of Mfn2. Following this report, other groups also found that Mfn2 participated in Ca^{2+} flux to mitochondria [255,270,271], ER-mitochondria distance [255–257] and apoptosis induction [272]. However, other works found that Mfn2 acts as a spacer, inhibiting ER-mitochondria contacts. In particular, electron microscopy images showed increased ER-mitochondria contacts in Mfn2 knockout cells, contradicting fluorescent confocal microscopy co-localization analysis in the same samples [259]. These paradoxical results were proposed to be a consequence of mitochondrial morphology alterations induced by the reduced levels of Mfn2, creating artefacts that were detected as a loss of co-localization in fluorescent microscopy analyzes [260]. In addition, other studies also found that loss of Mfn2 reduced the extent and number of ER-mitochondria contacts, and the flux of Ca^{2+} to mitochondria [261,262]. The effect of Mfn2 on ER-mitochondria distance was also evaluated using the SPLICS probes, showing that Mfn2 knockout cells have an increased number of SPLICS short puncta (8-10 nm) and a decrease in the number of SPLICS long (40-50 nm), suggesting that Mfn2 prevents the formation of close contacts while preserving long range contacts [177].

Overall, whether Mfn2 is a tether or a spacer is quite a debated subject, and these contradictory data are hard to reconcile. In addition, ER-mitochondria contacts adapt to environmental conditions like ER stress and nutrient availability [71,96,112]; and cells with low Mfn2 grow faster that wild type cells (our observations and [273]). Considering this, it has been proposed that special care has to be taken during cell culture to prevent stressful conditions like high cell density, which would alter

accurate ER-mitochondria measurements [255].

The aim of the present work was to clarify the role of Mfn2 in contact formation, and the main findings are summarized in **Figure 5.8**. The evaluation of MAM function showed that Mfn2 has an inhibitory effect on mitochondrial respiration **(Figure 5.1B)** which correlated with a reduction in cellular ATP levels **(Figure 5.1A)**, suggesting that Mfn2 reduces mitochondrial function potentially through a reduction in ER-mitochondria coupling. However, the measurement of phospholipid transfer between ER and mitochondria showed that Mfn2 had no effect **(Figure 5.4)**, suggesting that Mfn2 does not control close ER-mitochondria contacts. Evaluation of Ca^{2+} flux upon release of Ca^{2+} through IP_3R using histamine showed no differences between Mfn2 wild type and knockout cells, suggesting that Mfn2 does not regulate Ca^{2+} flux to mitochondria **(Figure 5.3B)**. Nevertheless, triggered Ca^{2+} flux does not necessarily reflect mitochondrial Ca^{2+} content in a steady state. Thus, it is essential to measure mitochondrial Ca^{2+} content in Mfn2 wild type and knockout cells in future experiments. Direct measurements of ER-mitochondria contact formation using electron microscopy show that, indeed, Mfn2 increased the distance and reduced the length of ER-mitochondria contacts **(Figure 5.6A and B)**. As a result, Mfn2 reduces the *contact length / distance* ratio, indicating an inhibition of contact formation **(Figure 5.6C)**. In addition, Mfn2 specifically decreased the frequency of Tight contacts (12 to 24 nm), while favouring Loose contacts (24 to 50 nm) **(Figure 5.6D)**. The inhibition of Tight contacts by Mfn2 fits with a reduced Ca^{2+} flux, since contacts between 12 and 24 nm are the preferred for Ca^{2+} transfer [47]. Similarly, the fact that Super Tight contacts (0 to 12 nm) remain relatively unchanged by Mfn2 fits with the observation that lipid transfer also remains unchanged **(Figure 5.6D** and **Figure 5.4)**. Taken together, our results fit better with Mfn2 acting as a spacer, not a tether. In particular, Mfn2 inhibits Tight (12 to 24 nm) contacts involved in Ca^{2+} flux to mitochondria, thus regulating mitochondrial activity.

5.3.2 Possible spacing mechanisms of Mfn2

The idea that Mfn2 works as a tether is based on its ability to form dimers connecting two opposing membranes, mirroring its activity during mitochondrial fusion [99]. But this mechanism is not com-

patible with Mfn2 acting as a spacer. The present work explores the idea, also previously proposed by others [274,275], that Mfn2 prevents contact formation by sequestering other tethers.

In line with other MAM proteins, Mfn2 has multiple functions, and it has a particularly tight relation with ER stress. Interestingly, ER stress is a condition that increases ER-mitochondria contact formation in order to boost Ca^{2+} flux to mitochondria and mitochondrial respiration [112]. The loss of Mfn2 causes activation of ER stress, in addition to an increase in ROS cellular levels, indicating that Mfn2 prevents ER stress [266]. Additionally, Mfn2 levels are increased during ER stress, and the deletion of Mfn2 increases the susceptibility to cell death induced by the activation of ER stress, suggesting that Mfn2 has a protective role [265]. The key mediator of the increased ER-mitochondria contacts during ER stress is PERK. Upon ER stress induction, PERK promotes ER-mitochondria contacts through the expression of a truncated form of SERCA1, S1T, that cannot pump Ca^{2+} but acts as a ER Ca^{2+} leak source [276]. S1T is targeted to the MAM and leaks Ca^{2+} resulting in increased ER-mitochondria proximity, and more efficient Ca^{2+} transfer to mitochondria [119]. In addition to inducing the expression of S1T, PERK itself is targeted to the MAM, and tethers ER and mitochondria independent of its ER stress signalling activity, even though no interacting partner on the mitochondrial side has been identified [237]. Interestingly, Mfn2 deficiency activates PERK, resulting in increased ROS production and mitochondrial Ca^{2+} overload [267]. Taken together, PERK is a prime candidate for a tethering factor that could be more active after the loss of Mfn2. Thus, the role of PERK in the increased ER-mitochondria contacts and mitochondrial metabolism activation observed upon loss of Mfn2 was tested. Indeed, Mfn2 knockout cells have increased ER stress markers **(Figure 5.2A)** and ROS levels **(Figure 5.2B)**, in agreement with previous reports [266,267]. In terms of the participation of PERK in the Mfn2 knockout metabolic phenotype, PERK inhibition with GSK resulted in a reduction of the extra ATP levels found in cells that lack Mfn2 **(Figure 5.3A)**. This suggest that PERK activation is required for the increased mitochondrial metabolism in Mfn2 knockout cells. The flux of Ca^{2+} to mitochondria was unchanged by Mfn2 depletion, but inhibition of PERK with GSK did show a reduced transfer of Ca^{2+} only in the knockout cells **(Figure 5.3B)**, again suggesting that PERK is active and promotes ER-mitochondria coupling only in Mfn2 knock-

out cells. Direct measurement of ER-mitochondria contacts using electron microscopy also shows that PERK activation is required to maintain the increased contacts observed in cells that lack Mfn2 **(Figure 5.5)**. Accordingly, upon PERK inhibition, the increased contacts in Mfn2 knockout cells return to levels similar to wild type cells **(Figure 5.6)**. Together, these results show that PERK is a tethering factor that increases ER-mitochondria contacts in cells that lack Mfn2. In agreement with the hypothesis that Mfn2 is a spacer that inhibits other tether, PERK inhibition reverts the changes in ER-mitochondria contacts in Mfn2 deficient cells.

In addition to PERK, the effect of increased ROS levels, in particular the participation of the ROS producing oxidoreductases Ero1α and Ero1β, was also evaluated. Ero1α and Ero1β participate in disulfide bond formation during protein folding by reoxidizing other oxidoreductases in a reaction that produces H_2O_2 **(Figure 1.2)** [139]. ROS produced by Ero1α can oxidize IP_3R at the MAM increasing Ca^{2+} flux to mitochondria [164]. During ER stress, Ero1α expression is increased, resulting in elevated ROS levels and apoptotic Ca^{2+} signalling to mitochondria [72,165]. Thus, the participation of Ero1α in the increased mitochondrial metabolism observed in Mfn2 deficient cells was tested. Similar to PERK, the increased ATP levels observed in Mfn2 knockout cells returned to normal levels after treating the cells with the antioxidant NAC or the Ero1α/β inhibitor EN460 **(Figure 5.3A)**. This result suggests that Ero1α/β are activated in Mfn2 depleted cells, and promotes mitochondrial ATP production through ROS production. But this result is just the starting point for a complete characterization of the role of the Ero1 enzymes in the Mfn2 knockout phenotype. The role of Ero1β could be explored since it has the same function as Ero1α and its expression is also increased during ER stress [277], but it has not been associated with the regulation of Ca^{2+} channels and it is unknown if it localizes in the MAM. Future experiments need to evaluate Ca^{2+} flux and ER mitochondria Ca^{2+} content measurements to determine if Ero1α/β activate Ca^{2+} signalling. It would be also required to determine whether Ero1α/β ROS production generate some form of redox modifications in SERCA and IP_3R, since this is a mechanism for Ero1α regulation of Ca^{2+} flux [164]. Finally, it is essential to measure ER-mitochondria contacts using electron microscopy in Mfn2 knockout cells treated with NAC and EN460 to determine if Mfn2 prevents contact formation by sequestering Ero1α/β.

5.3.3 PERK and Ero1α might form a novel complex that promotes ER-mitochondria contacts

A novel but quite preliminary result of this work is the formation of a complex composed by PERK and Ero1α at the MAM. The formation of this complex is suggested by three main findings: First, we found that Ero1α and PERK are enriched and co-fractionate in the MAM of Mfn2 knockout cells, suggesting that they coordinately regulate mitochondrial function from the MAM **(Figure 5.7A)**. Second, Ero1α and PERK moved to the Heavy membranes fraction (10,000 rcf pellet, mitochondria + MAM) and co-fractionated after ER stress induction, suggesting that Mfn2 deficiency and ER stress have similar MAM remodelling effects **(Figure 5.7B)**. Third, Ero1α and PERK co-immunoprecipitate, suggesting protein-protein interaction. This interaction was increased during ER stress, and reduced by PERK inhibition with GSK **(Figure 5.7C)**. Taken together, these results suggest that in Mfn2 knockout cells or upon ER stress induction, Ero1α and PERK move from the bulk ER to the MAM, where they interact and form a complex that promotes ER-mitochondria contacts. Considering that both proteins are required for the metabolic changes observed in Mfn2 knockout cells, it is possible that this Ero1α-PERK complex is responsible for the metabolic phenotype of Mfn2 deficient cells. Future experiments could test this idea by repeating the ER-mitochondria contact measurement, the co-fractionation and the co-immunoprecipitation with PERK and Ero1 inhibitors, and in PERK and Ero1α knockout cells. With this, it would be possible to determine if PERK and Ero1α work independently but in parallel, or if the interaction between the two is required for their effect on ER-mitochondria contact formation and MAM localization.

It is interesting that ER stress and Mfn2 depletion have the same effect on Ero1α and PERK MAM enrichment. Indeed, loss of Mfn2 and ER stress induction share some similarities, including increased ROS levels [266,278], and more ER-mitochondria contacts [112,260]. In addition, as previously mentioned, ER stress is activated in cells that lack Mfn2 [265]. Thus, ER stress seems to be responsible for the enrichment of Ero1α and PERK in the MAM; Mfn2 is simply preventing ER stress activation. The present work proposes that ER stress induces the formation of the Ero1α-PERK

complex at the MAM to increase ER-mitochondria contacts; while Mfn2 would have an inhibitory effect on ER stress, preventing the formation of this complex under normal conditions. However, the results shown here are preliminary, and more experiments would be required to confirm this idea.

Chapter 6

Discussion

6.1 Redox regulation of SERCA

Both TMX1 and CNX have a regulatory effect on SERCA, but their effects are opposite. On the one hand, CNX activates SERCA2b, resulting in increased ER Ca^{2+} levels. On the other hand, TMX1 inhibits SERCA2b, resulting in reduced ER Ca^{2+} content. Interestingly, both proteins interact with SERCA in a competitive way. SERCA interaction with CNX increases in TMX1 knockout cells, and vice versa **(Figure 3.1)**. This suggests that these two proteins might exert their control over SERCA through the same mechanism, but with opposing effects. So far, the mechanisms that CNX uses to control SERCA are relatively clear; an oxidative modification that increases SERCA ATPase activity **(Figure 4.13)**. The only known activatory oxidative modification in SERCA is glutathionylation on cysteine 674 [160,161]. Our results suggest that this is the mechanism that CNX uses to activate SERCA, even though the specific type of modification was not evaluated. The mechanism for TMX1 inhibition, however, is not as clear. Since TMX1 is an oxidoreductase, and its thioredoxin domain is required for the regulation of Ca^{2+} content and signalling **(Figure 3.7)**, it is likely that the regulatory effect of TMX1 is associated with an oxidative modification catalyzed by its oxidoreductase activity. As discussed previously in section 3.3.2 in the chapter about TMX1, there are two possi-

ble mechanisms for TMX1 regulation of SERCA. One option is that it catalyzes the formation of a disulfide bond in one of the lumenal loops on SERCA2b, similar to the oxidoreductase ERp57 [154], but this is unlikely because TMX1 has reductase activity, not oxidase activity. The second option is that TMX1 acts as a reductase and targets the inhibitory disulfide bond on SERCA2b, but forming an inhibitory mixed disulfide rather than reducing it completely, similar to the oxidoreductase ERdj5 [155]. This second option fits better with the reductase activity of TMX1, but the existence of a stable mixed disulfide between TMX1 and SERCA2b has not been demonstrated. Regardless of TMX1 inhibitory mechanism, it is likely that TMX1 and CNX have different and independent control over SERCA2b, which could even be operating at the same time. Nevertheless, they do seem to bind to SERCA on the same site, as suggested by their competitive interaction. One possible mechanism of interaction is that CNX binds to TMX1 and, together, they bind to SERCA. This would be similar to the way CNX directs TMX1 for disulfide bond formation of transmembrane protein during protein folding [135]. In this scenario CNX would act as a scaffold between SERCA and TMX1. However, this form of interaction is highly unlikely, because it does not fit with the competitive nature of the TMX1-SERCA and CNX-SERCA binding. A more feasible model is that TMX1 and CNX bind to the same site on SERCA. A previous publication shows that CNX can interact with the lumenal C-terminal domain of SERCA2b. This interaction requires the presence of a glycosylation site in the C-terminal domain of SERCA2b, even though no glycosylation was found [150]. It is possible that TMX1 also interacts with SERCA2b C-terminal domain, and that TMX1 and CNX compete for the same binding site. In addition, a previous work from our lab also shows that the association of CNX with SERCA requires a functional CNX palmitoylation site [114]. Similarly, TMX1 also requires to be palmitoylated to interact with SERCA **(Figure 3.7)**. It is well documented that palmitoylation regulates the protein targeting to the MAM and that non-MAM targeted CNX and TMX1 are unable to interact with SERCA outside the MAM. This confirms that palmitoylation is the key switch that allows the interaction with SERCA. Overall, this suggests that palmitoylated CNX and TMX1 interact competitively with the C-terminal domain of SERCA2b.

The effect of Mfn2 on SERCA was not tested in this work. Yet, there are some indications that point

towards a regulation of ER Ca^{2+} content by Mfn2. Previous reports indicate that ER Ca^{2+} content is increased in cells that lack Mfn2 [255], which was not a consequence of a more active SOCE [100]. This suggests that Mfn2 could be acting as a SERCA inhibitor. In addition, the loss of Mfn2 triggers the activation of ER stress, as observed here **(Figure 5.2)** and in previous publications [266,267]. In general, ER stress results in the depletion of ER Ca^{2+} stores. This is a consequence of increased ER Ca^{2+} leak [119,279], and the depalmitoylation of CNX and subsequent inhibition of SERCA [114]. It is plausible that in Mfn2 knockout cells, CNX loses its MAM targeting due to depalmitoylation, as expected during ER stress, resulting in a similar phenotype as CNX knockout cells. Yet, knocking out CNX or Mfn2 have opposite effects on ER Ca^{2+} content, the former has less and the latter has more Ca^{2+} in their ER. There are two possible explanations for these results. Either loss of Mfn2 induces some form of incomplete ER stress where CNX is not depalmitoylated, so it maintains its activatory effect on SERCA; or a parallel mechanism activates SERCA, bypassing the inhibitory effect of CNX depalmitoylation. Interestingly, Ero1 activity is required for the oxidation and activation of SERCA by CNX (**Figure 4.14**), and also mediates the metabolic phenotype in Mfn2 knockout cells **(Figure 5.3)**. In addition, increased levels of Ero1α have been observed in cells during late stages of ER stress [72]. The activation of Ero1α in Mfn2 knockout cells could possibly trigger the activating oxidation of SERCA, independent of CNX. This would place Ero1α as an activator of SERCA that can integrate diverse upstream events. Future experiments evaluating SERCA oxidation and activity in the absence of Mfn2, and the participation of Ero1α are required to confirm this idea.

6.2 ER-mitochondria contact regulation

This work shows that Mfn2 and CNX work as negative regulators of MAM formation, or spacers. But their mechanism of contact formation and final effects on MAM function are quite different. The mechanism that Mfn2 uses to prevent ER-mitochondria contacts is not completely clear, but the preliminary data shown here suggests that Mfn2 inhibits the formation of a tether comprised of PERK, which probably are inactive in cells without ER stress **(Figure 5.5)**. On the other hand, it is

not clear whether CNX physically interacts with other tethers or if it inhibits other tethering factors. One possible mechanism is the inhibition of SERCA in the absence of CNX. The reduced SERCA Ca^{2+} uptake from the cytosol could increase Ca^{2+} levels in the ER proximity, which could result in mitochondria being stuck close to the ER by inhibiting mitochondrial movement [117,118]. Nevertheless, it is unlikely that the increased ER-mitochondria contacts observed in CNX knockout cells are a result of PERK activation, as is the case with Mfn2, because PERK phosphorylation was not increased in CNX knockout cells compared to wild type cells **(Figure 4.11A)**. Thus, the increased ER-mitochondria contacts in CNX and Mfn2 knockout must be parallel events with independent mechanisms. The TMX1 tethering mechanism is even more obscure, and there is not enough evidence to determine if other tethers are also participating. Considering the mechanisms discussed so far, SERCA inhibition could be a possible explanation for the increased ER-mitochondria contacts induced by TMX1, since more contacts fit with reduced SERCA activity. However, there is no evidence to suggest that PERK could be engaged in TMX1-induced contact formation. A more thorough analysis of TMX1 interactions and MAM protein composition in TMX1 knockout compared to wild type cells would be required to evaluate the TMX1 tethering mechanism.

One of the MAM functions explored in this work was Ca^{2+} flux to mitochondria. This is a complex Ca^{2+} signal that integrates many factors, including ER Ca^{2+} content, ER Ca^{2+} release, and ER-mitochondria distance. In this work, the use of BAPTA in combination with the measurement of mitochondrial respiration **(Figure 4.12)** and cellular ATP levels **(Figure 5.1A)** were also used to determine if Ca^{2+} flux was involved in the control of mitochondrial function. For TMX1 and Mfn2, the changes in ER-mitochondria contacts correlates with the changes in Ca^{2+} flux and mitochondrial function, but this was not the case for CNX. Mfn2 reduces ER Ca^{2+} content [255], ER-mitochondria contacts **(Figure 5.5)** and mitochondrial respiration **(Figure 5.1B)**. CNX also reduces ER-mitochondria contacts **(Figure 4.4)**, which would suggest a reduction in Ca^{2+} flux to mitochondria. But unlike Mfn2, CNX also activates SERCA, increasing ER Ca^{2+} content. As a result, there is more Ca^{2+} available for transfer, so Ca^{2+} flux to mitochondria and mitochondrial metabolism are increased, in spite of the reduced ER-mitochondria contacts. Thus, the regulation of the contacts is potentially a

compensatory mechanism that may prevent mitochondrial Ca^{2+} overload in the presence of CNX. The predominant effect of CNX must be the regulation of SERCA and ER Ca^{2+} content, which in the end determines the flux of Ca^{2+} to mitochondria. This illustrates the complex regulation of mitochondrial function at the MAM; just measuring the distance between ER and mitochondria is not enough to determine the effect of a tether in ER-mitochondria communication. On the other hand, TMX1 has the opposite effect to Mfn2, since it increases ER-mitochondria contacts, Ca^{2+} flux, and mitochondrial respiration. Nevertheless, both TMX1 and Mfn2 reduce ER Ca^{2+} content. According to the findings in CNX knockout cells, ER Ca^{2+} content is a key variable for Ca^{2+} flux, and it can be even more important than ER-mitochondria distance. Yet, TMX1 reduces ER Ca^{2+} content, and at the same time increases Ca^{2+} transfer to mitochondria. In addition, TMX1 not only improves Ca^{2+} flux to mitochondria, it also increases Ca^{2+} release to the cytoplasm. So the increase in Ca^{2+} flux is not explained exclusively through the increased ER-mitochondria contacts; the release of Ca^{2+} from the ER is increased globally, not only in the ER-mitochondria interface. Together, this suggests that TMX1 could activate ER Ca^{2+} release channels, possibly IP_3R, in addition to the inhibition of SERCA. One option is that TMX1 activates Ero1α, which oxidizes IP_3R increasing the release of Ca^{2+} [72,164]. Future experiments will be required to explore if and how TMX1 activates IP_3R.

6.3 Keeping the balance between calcium flux, contact formation, and metabolism in a dynamic ER-mitochondria interaction

There is a close relation between ER chaperones and oxidoreductases, and the MAM function. This relation is notably shown during ER stress, where the coordinated regulation and reorganization of chaperones and oxidoreductases modulate protein folding, Ca^{2+} signalling and mitochondrial function. As a result, folding capacity is augmented, and Ca^{2+} flux to mitochondria and mitochondrial metabolism are increased, which provides energy to cope with the stress [263]. The present work provides new insights about the role of ER proteins in the control of MAM function. How does this new knowledge fit with the regulation of MAM function during ER stress? During ER stress, CNX

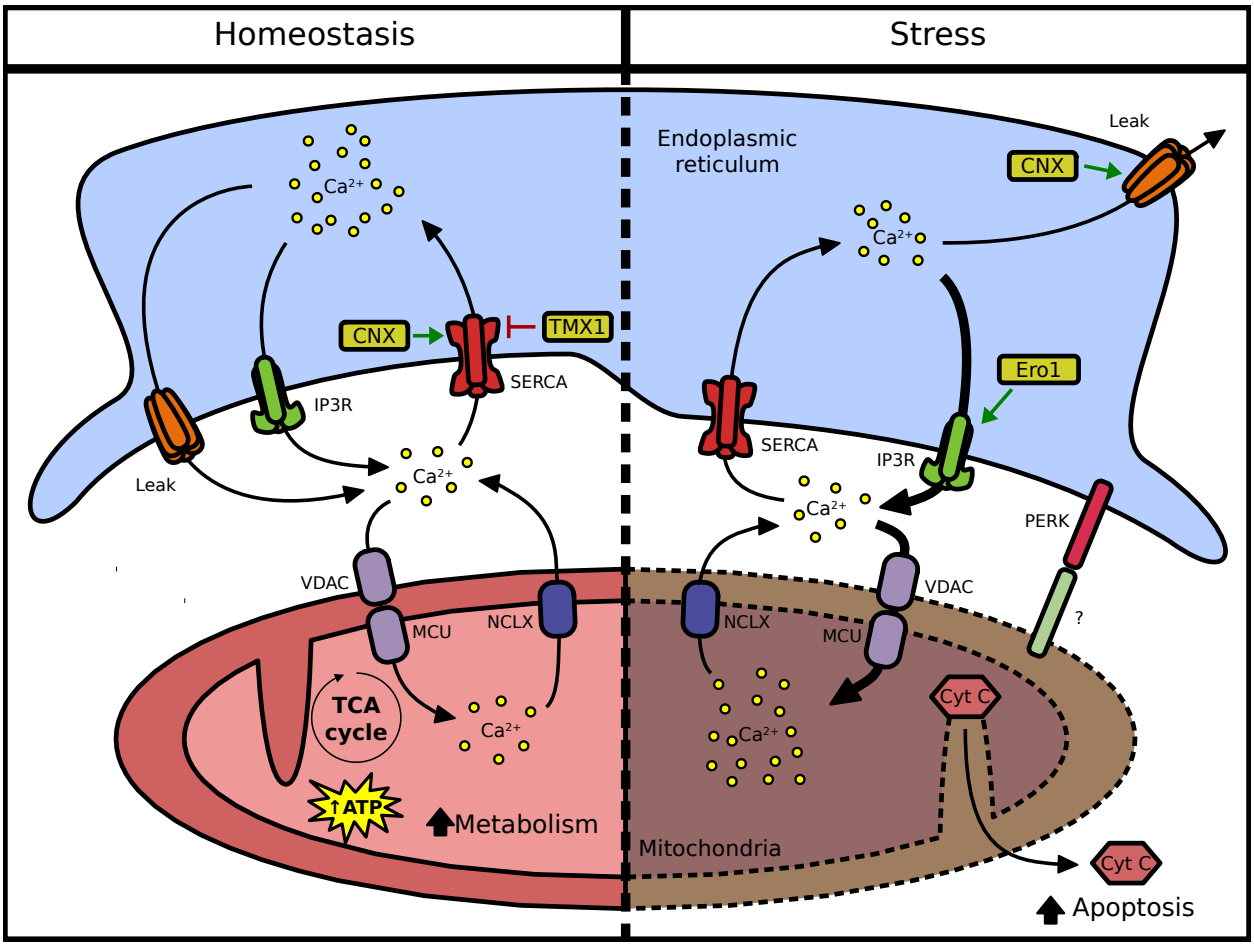

Figure 6.1 – Proposed model of MAM changes during ER stress. During ER stress, CNX and TMX1 leave the MAM and stop regulating SERCA. Ca^{2+} leak at the ER depletes ER Ca^{2+} stores. PERK and Ero1 move to the MAM and increase ER-mitochondria contacts and Ca^{2+} release respectively. As a result, Ca^{2+} flux to mitochondria is increased. This can increase mitochondrial metabolism and energy production, but sustained mitochondrial Ca^{2+} overload can result in permeabilization of mitochondrial membranes and induction of cell death.

is depalmitoylated, moves away from the MAM, and engages in protein folding [114]. In terms of Ca^{2+} signalling regulation, the result is a phenotype similar to CNX knockout cells: the activatory effect on SERCA is released, resulting in a reduction of ER Ca^{2+}. In addition, the loss of CNX also results in more ER-mitochondria contacts, probably by increasing Ca^{2+} levels in the proximity of the ER. Thus, during ER stress, CNX movement away from the MAM could be one of the main drivers of ER-mitochondria proximity. Nevertheless, CNX knockout cells also have reduced mitochondrial Ca^{2+} and respiration, the opposite of what is observed in ER stressed cells. The discrepancy between increased ER-mitochondria contacts and reduced Ca^{2+} flux is most likely a consequence of the ER Ca^{2+} depletion, resulting from the loss of SERCA activity when CNX leaves the MAM. CNX might be important for the maintenance of mitochondrial function during non-stressed conditions, but it cannot explain the improved mitochondrial metabolism observed in stressed cells by itself. Similar to CNX, TMX1 MAM targeting also requires palmitoylation. But it is not known if TMX1 palmitoylation is also removed during ER stress. Thus, any change in TMX1 function during ER stress attributed to its MAM localization is just speculation. However, it has been shown that the interaction between CNX and TMX1 is increased during ER stress, and both increase their folding activity [136]. So it is possible that during ER stress both CNX and TMX1 move away from the MAM and stop exerting their regulatory effect on SERCA. Assuming that TMX1 is also depalmitoylated during ER stress and behaves similar to TMX1 knockout, the main result would be the release of its inhibitory effect on SERCA. This fits with previous reports indicating that SERCA is more active during ER stress [280]. In the context of ER stress activation, this would balance the ER Ca^{2+} depletion resulting from the depalmitoylation of CNX, and could help maintain the ER Ca^{2+} stores required for Ca^{2+} flux to mitochondria. Otherwise, TMX1 depalmitoylation does not completely fit with the phenotype observed during ER stress. Unsurprisingly, loss of Mfn2 is the condition that fits the ER stress phenotype better, since Mfn2 knockout cells actually have ER stress. Accordingly, it provides insight into two key pieces for MAM regulation during ER stress: PERK and Ero1. Both are required for some of the metabolic changes observed in Mfn2 knockout cells. In addition, PERK activity is also required for their increased ER-mitochondria contacts. PERK activation and tethering

has been described previously during ER stress [237], as well as Ero1α expression, ROS production and IP_3R activation [72,165]. This suggests that PERK and Ero1α engagement in metabolic and MAM regulation could be a general ER stress function, and not a specific regulation by Mfn2.

Taken together, our results suggest that MAM regulation during ER stress would proceed as follows: CNX and TMX1 are depalmitoylated and move away from the MAM, and they stop regulating SERCA and switch to protein folding duties. PERK, usually inactive and distributed throughout the ER, is activated and moves to the MAM. This would result in ER-mitochondria tethering by PERK, increasing ER-mitochondria contacts and Ca^{2+} flux. Preliminary data also suggest that Ero1α interacts with PERK and moves towards the MAM, where it could potentially activate IP_3R in the ER-mitochondria interface further increasing Ca^{2+} flux **(Figure 6.1)**. Nevertheless, there are some points that need to be clarified. The interaction between PERK and Ero1α and movement to the MAM during ER stress could be demonstrated with a combination of co-immunoprecipitation and cellular fractionation in ER stressed cells. The interaction and movement of Ero1β during ER stress should also be explored in a similar way. Ero1β expression is increased during ER stress and could play an important role in the adaptive response to ER stress [277]. The participation of Ero1α and PERK in the increased ER-mitochondria contacts and mitochondrial metabolism observed during ER stress is also unclear. This can be explored using the characterization described in this thesis: cellular ATP levels, mitochondrial respiration, mitochondrial potential, mitochondrial ATP, glycolytic flux and ER-mitochondria distance using electron microscopy in ER stressed cells; the participation of Ero1α and PERK can be demonstrated with the use of specific drug inhibitors, in addition to molecular tools like knock down and knockout cells. Finally, the effect of CNX and TMX1 on SERCA activity in an ER stress context is not completely clear. What is the net effect on SERCA activity if both CNX and TMX1 stop exerting their regulatory action during ER stress? Previous reports show that ER stress results in the depletion of ER Ca^{2+} stores, in part attributed to increased ER Ca^{2+} leak [119], while SERCA activity is increased [280]. This suggests that the combination of effects results in SERCA activation. The novel findings about SERCA regulation by TMX1, CNX, and redox modifications gained in this thesis could help clarify the molecular events that regulate SERCA during ER

stress. SERCA activity could be measured in cells under ER stress, and the effect of TMX1, CNX, NOX4 and Ero1 could be evaluated with a combination of molecular tools and chemical inhibitors. Changes in SERCA oxidation should also be measured during ER stress, using similar strategies to evaluate the role of TMX1, CNX, NOX4 and Ero1; and the effects of redox modifications on specific SERCA cysteines can be evaluated using different SERCA mutants with changes on critical cysteines. This would advance the understanding of the adaptations on metabolism, Ca^{2+} signalling and ER-mitochondria contacts during ER stress, and how ER chaperones and oxidoreductases participate in the process.

6.4 Conclusion

Our understanding of Mitochondria-Associated Membranes and ER-mitochondria contacts has expanded greatly since the first electron microscopy observations in the 50s. A series of important findings over the years have uncovered the function of these contacts in the cell: Ca^{2+} regulation of mitochondrial respiration and apoptosis, lipid and Ca^{2+} transfer from ER to mitochondria, and the identification of MAM tethers, spacers and regulatory proteins. This thesis focused on ER chaperones and oxidoreductases, a diverse group of proteins responsible for the folding of newly synthesized proteins in the ER. They also have an important presence in the MAM, and play a critical role in the regulation of MAM function. Our findings highlight several properties of MAM regulation by these ER proteins: they integrate oxidative modifications, Ca^{2+} signalling, and ER-mitochondria distance to finely tune mitochondrial function; they can dynamically move in or out of the MAM to adapt its function to environmental conditions; and they can regulate more that one signalling mechanism at the same time. In addition, these ER chaperones and oxidoreductases interact and trigger feedback loops, showing how the regulation of MAM is the result of the combination of several Ca^{2+} channels, tethers, spacers and regulators. Together, they sense cellular energy requirements, stress, growth, and other cues in a complex MAM regulatory network. MAM deregulation has been implicated in many human conditions and diseases, like aging [281], cancer [282], neurodegeneration [283], dia-

betes [284] and immune responses [285]. Understanding how MAM is regulated and the intricacies of ER-mitochondria communication can help to explain the origin of these diseases, and potentially design better treatments.

References

1. Scorrano L, De Matteis MA, Emr S, Giordano F, Hajnóczky G, Kornmann B, Lackner LL, Levine TP, Pellegrini L, Reinisch K, et al. (2019) Coming together to define membrane contact sites. *Nature Communications* **10**: 1287.

2. Vance JE (1990) Phospholipid synthesis in a membrane fraction associated with mitochondria. *Journal of Biological Chemistry* **265**: 7248–7256.

3. Rizzuto R, Pinton P, Carrington W, Fay FS, Fogarty KE, Lifshitz LM, Tuft RA, Pozzan T (1998) Close contacts with the endoplasmic reticulum as determinants of mitochondrial Ca^{2+} responses. *Science* **280**: 1763–1766.

4. Hay ED (1958) The fine structure of blastema cells and differentiating cartilage cells in regenerating limbs of amblystoma larvae. *The Journal of Biophysical and Biochemical Cytology* **4**: 583–592.

5. Copeland DE, Dalton AJ (1959) An association between mitochondria and the endoplasmic reticulum in cells of the pseudobranch gland of a teleost. *The Journal of Biophysical and Biochemical Cytology* **5**: 393–396.

6. Vance JE (2018) Historical perspective: Phosphatidylserine and phosphatidylethanolamine from the 1800s to the present. *Journal of Lipid Research* **59**: 923–944.

7. Vance JE (1991) Newly made phosphatidylserine and phosphatidylethanolamine are preferentially translocated between rat liver mitochondria and endoplasmic reticulum. *Journal of Biological Chemistry* **266**: 89–97.

8. Shiao Y, Lupo G, Vance J (1995) Evidence that phosphatidylserine is imported into mitochondria via a mitochondria-associated membrane and that the majority of mitochondrial phosphatidylethanolamine is derived from decarboxylation of phosphatidylserine. *Journal of Biological Chemistry* **270**: 11190–11198.

9. Zborowski J, Dygas A, Wojtczak L (1983) Phosphatidylserine decarboxylase is located on the external side of the inner mitochondrial membrane. *FEBS Letters* **157**: 179–182.

10. Steenbergen R, Nanowski TS, Beigneux A, Kulinski A, Young SG, Vance JE (2005) Disruption of the phosphatidylserine decarboxylase gene in mice causes embryonic lethality and mitochondrial defects. *Journal of Biological Chemistry* **280**: 40032–40040.

11. Stone SJ, Vance JE (2000) Phosphatidylserine synthase-1 and -2 are localized to mitochondria-associated membranes. *Journal of Biological Chemistry* **275**: 34534–34540.

12. Rusiñol AE, Cui Z, Chen MH, Vance JE (1994) A unique mitochondria-associated membrane fraction from rat liver has a high capacity for lipid synthesis and contains pre-Golgi secretory proteins including nascent lipoproteins. *Journal of Biological Chemistry* **269**: 27494–27502.

13. Stone SJ, Levin MC, Zhou P, Han J, Walther TC, Farese RV (2008) The endoplasmic reticulum enzyme DGAT2 is found in mitochondria-associated membranes and has a mitochondrial targeting signal that promotes its association with mitochondria. *Journal of Biological Chemistry* **284**: 5352–5361.

14. Voelker DR (1989) Phosphatidylserine translocation to the mitochondrion is an ATP-dependent process in permeabilized animal cells. *Proceedings of the National Academy of Sciences* **86**: 9921–9925.

15. Voelker DR (1990) Characterization of phosphatidylserine synthesis and translocation in permeabilized animal cells. *Journal of Biological Chemistry* **265**: 14340–14346.

16. Voelker DR (1993) The atp-dependent translocation of phosphatidylserine to the mitochondria is a process that is restricted to the autologous organelle. *The Journal of biological chemistry* **268**:

7069–7074.

17. Shiao Y-j, Balcerzak B, Vance JE (1998) A mitochondrial membrane protein is required for translocation of phosphatidylserine from mitochondria-associated membranes to mitochondria. *Biochemical Journal* **331**: 217–223.

18. Kornmann B, Currie E, Collins SR, Schuldiner M, Nunnari J, Weissman JS, Walter P (2009) An ER-mitochondria tethering complex revealed by a synthetic biology screen. *Science* **325**: 477–481.

19. Kojima R, Endo T, Tamura Y (2016) A phospholipid transfer function of ER-mitochondria encounter structure revealed in vitro. *Scientific Reports* **6**: 30777.

20. Schauder CM, Wu X, Saheki Y, Narayanaswamy P, Torta F, Wenk MR, Camilli PD, Reinisch KM (2014) Structure of a lipid-bound extended synaptotagmin indicates a role in lipid transfer. *Nature* **510**: 552–555.

21. AhYoung AP, Jiang J, Zhang J, Dang XK, Loo JA, Zhou ZH, Egea PF (2015) Conserved SMP domains of the ERMES complex bind phospholipids and mediate tether assembly. *Proceedings of the National Academy of Sciences* **112**: E3179–E3188.

22. Jeong H, Park J, Lee C (2016) Crystal structure of mdm12 reveals the architecture and dynamic organization of the ERMES complex. *EMBO reports* **17**: 1857–1871.

23. Hirabayashi Y, Kwon S-K, Paek H, Pernice WM, Paul MA, Lee J, Erfani P, Raczkowski A, Petrey DS, Pon LA, et al. (2017) ER-mitochondria tethering by PDZD8 regulates Ca^{2+} dynamics in mammalian neurons. *Science* **358**: 623–630.

24. Kentala H, Weber-Boyvat M, Olkkonen VM (2016) OSBP-related protein family: Mediators of lipid transport and signaling at membrane contact sites. In, *International review of cell and molecular biology* pp 299–340. Elsevier.

25. Chung J, Torta F, Masai K, Lucast L, Czapla H, Tanner LB, Narayanaswamy P, Wenk MR, Nakatsu F, Camilli PD (2015) PI4P/phosphatidylserine countertransport at ORP5- and

ORP8-mediated ER-plasma membrane contacts. *Science* **349**: 428–432.

26. Galmes R, Houcine A, Vliet AR, Agostinis P, Jackson CL, Giordano F (2016) ORP5/ORP8 localize to endoplasmic reticulummitochondria contacts and are involved in mitochondrial function. *EMBO reports* **17**: 800–810.

27. Berridge MJ, Bootman MD, Roderick HL (2003) Calcium signalling: Dynamics, homeostasis and remodelling. *Nature Reviews Molecular Cell Biology* **4**: 517–529.

28. Meldolesi J, Pozzan T (1998) The heterogeneity of ER Ca^{2+} stores has a key role in nonmuscle cell signaling and function. *Journal of Cell Biology* **142**: 1395–1398.

29. Gunteski-Hamblin AM, Greeb J, Shull GE (1988) A novel Ca^{2+} pump expressed in brain, kidney, and stomach is encoded by an alternative transcript of the slow-twitch muscle sarcoplasmic reticulum Ca-ATPase gene. Identification of cDNAs encoding Ca^{2+} and other cation-transporting ATPases using an oligonucleotide probe derived from the ATP-binding site. *The Journal of biological chemistry* **263**: 15032–15040.

30. Vandecaetsbeek I, Vangheluwe P, Raeymaekers L, Wuytack F, Vanoevelen J (2011) The Ca^{2+} pumps of the endoplasmic reticulum and Golgi apparatus. *Cold Spring Harbor perspectives in biology* **3**: a004184.

31. Zhang SL, Yu Y, Roos J, Kozak JA, Deerinck TJ, Ellisman MH, Stauderman KA, Cahalan MD (2005) STIM1 is a Ca^{2+} sensor that activates CRAC channels and migrates from the Ca^{2+} store to the plasma membrane. *Nature* **437**: 902–905.

32. Roos J, DiGregorio PJ, Yeromin AV, Ohlsen K, Lioudyno M, Zhang S, Safrina O, Kozak JA, Wagner SL, Cahalan MD, et al. (2005) STIM1, an essential and conserved component of store-operated Ca^{2+} channel function. *Journal of Cell Biology* **169**: 435–445.

33. Liou J, Kim ML, Heo WD, Jones JT, Myers JW, Ferrell JE, Meyer T (2005) STIM is a Ca^{2+} sensor essential for Ca^{2+}-store-depletion-triggered Ca^{2+} influx. *Current Biology* **15**: 1235–1241.

34. Zhang SL, Yeromin AV, Zhang XH-F, Yu Y, Safrina O, Penna A, Roos J, Stauderman KA, Cahalan MD (2006) Genome-wide RNAi screen of Ca^{2+} influx identifies genes that regulate Ca^{2+} release-activated Ca^{2+} channel activity. *Proceedings of the National Academy of Sciences* **103**: 9357–9362.

35. Vig M (2006) CRACM1 is a plasma membrane protein essential for store-operated Ca^{2+} entry. *Science* **312**: 1220–1223.

36. Feske S, Gwack Y, Prakriya M, Srikanth S, Puppel S-H, Tanasa B, Hogan PG, Lewis RS, Daly M, Rao A (2006) A mutation in Orai1 causes immune deficiency by abrogating CRAC channel function. *Nature* **441**: 179–185.

37. Wu MM, Buchanan J, Luik RM, Lewis RS (2006) Ca^{2+} store depletion causes STIM1 to accumulate in ER regions closely associated with the plasma membrane. *Journal of Cell Biology* **174**: 803–813.

38. Park CY, Hoover PJ, Mullins FM, Bachhawat P, Covington ED, Raunser S, Walz T, Garcia KC, Dolmetsch RE, Lewis RS (2009) STIM1 clusters and activates CRAC channels via direct binding of a cytosolic domain to Orai1. *Cell* **136**: 876–890.

39. Kühn B, Schmid A, Harteneck C, Gudermann T, Schultz G (1996) G proteins of the Gq family couple the H2 histamine receptor to phospholipase C. *Molecular Endocrinology* **10**: 1697–1707.

40. Barnard EA, Burnstock G, Webb TE (1994) G protein-coupled receptors for ATP and other nucleotides: A new receptor family. *Trends in Pharmacological Sciences* **15**: 67–70.

41. Meissner G (1986) Ryanodine activation and inhibition of the Ca^{2+} release channel of sarcoplasmic reticulum. *The Journal of biological chemistry* **261**: 6300–6306.

42. Flourakis M, Van Coppenolle F, Lehen'kyi V, Beck B, Skryma R, Prevarskaya N (2006) Passive calcium leak via translocon is a first step for iPLA2-pathway regulated store operated channels activation. *The FASEB journal* **20**: 1215–1217.

43. Slater EC, Cleland KW (1953) The effect of calcium on the respiratory and phosphorylative activities of heart-muscle sarcosomes. *Biochemical Journal* **55**: 566–580.

44. Rizzuto R, Brini M, Murgia M, Pozzan T (1993) Microdomains with high Ca^{2+} close to IP_3-sensitive channels that are sensed by neighboring mitochondria. *Science* **262**: 744–747.

45. Csordás G, Thomas AP, Hajnóczky G (1999) Quasi-synaptic calcium signal transmission between endoplasmic reticulum and mitochondria. *The EMBO Journal* **18**: 96–108.

46. Csordás G, Várnai P, Golenár T, Roy S, Purkins G, Schneider TG, Balla T, Hajnóczky G (2010) Imaging interorganelle contacts and local calcium dynamics at the ER-mitochondrial interface. *Molecular Cell* **39**: 121–132.

47. Giacomello M, Drago I, Bortolozzi M, Scorzeto M, Gianelle A, Pizzo P, Pozzan T (2010) Ca^{2+} hot spots on the mitochondrial surface are generated by Ca^{2+} mobilization from stores, but not by activation of store-operated Ca^{2+} channels. *Molecular Cell* **38**: 280–290.

48. Shoshan-Barmatz V, Krelin Y, Shteinfer-Kuzmine A (2017) VDAC1 functions in Ca^{2+} homeostasis and cell life and death in health and disease. *Cell Calcium* **69**: 81–100.

49. Tan W, Colombini M (2007) VDAC closure increases calcium ion flux. *Biochimica et Biophysica Acta (BBA) - Biomembranes* **1768**: 2510–2515.

50. DeLuca HF, Engstrom GW (1961) CALCIUM UPTAKE BY RAT KIDNEY MITOCHONDRIA. *Proceedings of the National Academy of Sciences* **47**: 1744–1750.

51. Vasington JV F. D. And Murphy (1962) Ca^{2+} ion uptake by rat kidney mitochondria and its dependence on respiration and phosphorylation. *The Journal of biological chemistry* **237**: 2670–2677.

52. Kirichok Y, Krapivinsky G, Clapham DE (2004) The mitochondrial calcium uniporter is a highly selective ion channel. *Nature* **427**: 360–364.

53. De Stefani D, Raffaello A, Teardo E, Szabò I, Rizzuto R (2011) A forty-kilodalton protein of the

inner membrane is the mitochondrial calcium uniporter. *Nature* **476**: 336–340.

54. Baughman JM, Perocchi F, Girgis HS, Plovanich M, Belcher-Timme CA, Sancak Y, Bao XR, Strittmatter L, Goldberger O, Bogorad RL, et al. (2011) Integrative genomics identifies MCU as an essential component of the mitochondrial calcium uniporter. *Nature* **476**: 341–345.

55. Csordás G, Golenár T, Seifert EL, Kamer KJ, Sancak Y, Perocchi F, Moffat C, Weaver D, Fuente Perez S de la, Bogorad R, et al. (2013) MICU1 controls both the threshold and cooperative activation of the mitochondrial Ca^{2+} uniporter. *Cell metabolism* **17**: 976–987.

56. Mallilankaraman K, Doonan P, Cárdenas C, Chandramoorthy HC, Müller M, Miller R, Hoffman NE, Gandhirajan RK, Molgó J, Birnbaum MJ, et al. (2012) MICU1 is an essential gatekeeper for MCU-mediated mitochondrial Ca^{2+} uptake that regulates cell survival. *Cell* **151**: 630–644.

57. Palty R, Silverman WF, Hershfinkel M, Caporale T, Sensi SL, Parnis J, Nolte C, Fishman D, Shoshan-Barmatz V, Herrmann S, et al. (2009) NCLX is an essential component of mitochondrial Na^{+}/Ca^{2+} exchange. *Proceedings of the National Academy of Sciences* **107**: 436–441.

58. Gunter KK, Zuscik MJ, Gunter TE (1991) The Na^{+}-independent Ca^{2+} efflux mechanism of liver mitochondria is not a passive Ca^{2+}/$2H^{+}$ exchanger. *The Journal of biological chemistry* **266**: 21640–21648.

59. Szalai G, Krishnamurthy R, Hajnóczky G (1999) Apoptosis driven by IP3-linked mitochondrial calcium signals. *The EMBO Journal* **18**: 6349–6361.

60. Pinton P, Ferrari D, Rapizzi E, Di Virgilio F, Pozzan T, Rizzuto R (2001) The Ca^{2+} concentration of the endoplasmic reticulum is a key determinant of ceramide-induced apoptosis: Significance for the molecular mechanism of Bcl-2 action. *The EMBO Journal* **20**: 2690–2701.

61. Giorgi C, Bonora M, Sorrentino G, Missiroli S, Poletti F, Suski JM, Ramirez FG, Rizzuto R, Virgilio FD, Zito E, et al. (2015) p53 at the endoplasmic reticulum regulates apoptosis in a Ca^{2+}-dependent manner. *Proceedings of the National Academy of Sciences* **112**: 1779–1784.

62. Giorgi C, Bonora M, Missiroli S, Poletti F, Ramirez FG, Morciano G, Morganti C, Pandolfi PP, Mammano F, Pinton P (2014) Intravital imaging reveals p53-dependent cancer cell death induced by phototherapy via calcium signaling. *Oncotarget* **6**: 1435–1445.

63. Zheng Y, Shen X (2005) H_2O_2 directly activates inositol 1,4,5-trisphosphate receptors in endothelial cells. *Redox Report* **10**: 29–36.

64. Stefani DD, Bononi A, Romagnoli A, Messina A, Pinto VD, Pinton P, Rizzuto R (2011) VDAC1 selectively transfers apoptotic Ca^{2+} signals to mitochondria. *Cell Death & Differentiation* **19**: 267–273.

65. Galluzzi L, Vitale I, Aaronson SA, Abrams JM, Adam D, Agostinis P, Alnemri ES, Altucci L, Amelio I, Andrews DW, et al. (2018) Molecular mechanisms of cell death: Recommendations of the nomenclature committee on cell death 2018. *Cell Death & Differentiation* **25**: 486–541.

66. Baines CP, Kaiser RA, Purcell NH, Blair NS, Osinska H, Hambleton MA, Brunskill EW, Sayen MR, Gottlieb RA, Dorn GW, et al. (2005) Loss of cyclophilin d reveals a critical role for mitochondrial permeability transition in cell death. *Nature* **434**: 658–662.

67. Bonora M, Morganti C, Morciano G, Pedriali G, Lebiedzinska-Arciszewska M, Aquila G, Giorgi C, Rizzo P, Campo G, Ferrari R, et al. (2017) Mitochondrial permeability transition involves dissociation of F_1F_0 ATP synthase dimers and C-ring conformation. *EMBO reports* **18**: 1077–1089.

68. Ichas F, Mazat J-P (1998) From calcium signaling to cell death: Two conformations for the mitochondrial permeability transition pore. Switching from low- to high-conductance state. *Biochimica et Biophysica Acta (BBA) - Bioenergetics* **1366**: 33–50.

69. Baumgartner HK, Gerasimenko JV, Thorne C, Ferdek P, Pozzan T, Tepikin AV, Petersen OH, Sutton R, Watson AJM, Gerasimenko OV (2009) Calcium elevation in mitochondria is the main Ca^{2+} requirement for mitochondrial permeability transition pore (mPTP) opening. *Journal of Biological Chemistry* **284**: 20796–20803.

70. Boehning D, Patterson RL, Sedaghat L, Glebova NO, Kurosaki T, Snyder SH (2003) Cytochrome

C binds to inositol (1,4,5) trisphosphate receptors, amplifying calcium-dependent apoptosis. *Nature Cell Biology* **5**: 1051–1061.

71. Csordás G, Renken C, Várnai P, Walter L, Weaver D, Buttle KF, Balla T, Mannella CA, Hajnóczky G (2006) Structural and functional features and significance of the physical linkage between ER and mitochondria. *The Journal of cell biology* **174**: 915–921.

72. Li G, Mongillo M, Chin K-T, Harding H, Ron D, Marks AR, Tabas I (2009) Role of ERO1-α mediated stimulation of inositol 1,4,5-triphosphate receptor activity in endoplasmic reticulum stress-induced apoptosis. *The Journal of Cell Biology* **186**: 783–792.

73. Qiao X, Jia S, Ye J, Fang X, Zhang C, Cao Y, Xu C, Zhao L, Zhu Y, Wang L, et al. (2017) PTPIP51 regulates mouse cardiac ischemia/reperfusion through mediating the mitochondria-SR junction. *Scientific Reports* **7**: 45379.

74. Giorgi C, Ito K, Lin H-K, Santangelo C, Wieckowski MR, Lebiedzinska M, Bononi A, Bonora M, Duszynski J, Bernardi R, et al. (2010) PML regulates apoptosis at endoplasmic reticulum by modulating calcium release. *Science* **330**: 1247–1251.

75. Hedgepeth SC, Garcia MI, Wagner LE, Rodriguez AM, Chintapalli SV, Snyder RR, Hankins GDV, Henderson BR, Brodie KM, Yule DI, et al. (2015) The BRCA1 tumor suppressor binds to inositol 1,4,5-trisphosphate receptors to stimulate apoptotic calcium release. *Journal of Biological Chemistry* **290**: 7304–7313.

76. Bononi A, Giorgi C, Patergnani S, Larson D, Verbruggen K, Tanji M, Pellegrini L, Signorato V, Olivetto F, Pastorino S, et al. (2017) BAP1 regulates IP_3R3-mediated Ca^{2+} flux to mitochondria suppressing cell transformation. *Nature* **546**: 549–553.

77. Bononi A, Bonora M, Marchi S, Missiroli S, Poletti F, Giorgi C, Pandolfi PP, Pinton P (2013) Identification of PTEN at the ER and MAMs and its regulation of Ca^{2+} signaling and apoptosis in a protein phosphatase-dependent manner. *Cell Death & Differentiation* **20**: 1631–1643.

78. White C, Li C, Yang J, Petrenko NB, Madesh M, Thompson CB, Foskett JK (2005) The endo-

plasmic reticulum gateway to apoptosis by bcl-XL modulation of the InsP3R. *Nature Cell Biology* **7**: 1021–1028.

79. Betz C, Stracka D, Prescianotto-Baschong C, Frieden M, Demaurex N, Hall MN (2013) mTOR complex 2-Akt signaling at mitochondria-associated endoplasmic reticulum membranes (MAM) regulates mitochondrial physiology. *Proceedings of the National Academy of Sciences* **110**: 12526–12534.

80. Cárdenas C, Miller RA, Smith I, Bui T, Molgó J, Müller M, Vais H, Cheung K-H, Yang J, Parker I, et al. (2010) Essential regulation of cell bioenergetics by constitutive IP_3 receptor Ca^{2+} transfer to mitochondria. *Cell* **142**: 270–283.

81. Territo PR, Mootha VK, French SA, Balaban RS (2000) Ca^{2+} activation of heart mitochondrial oxidative phosphorylation: Role of the F(0)/F(1)-ATPase. *American Journal of Physiology Cell Physiology* **278**: C423–435.

82. Hansford RG, Chappell JB (1967) The effect of Ca^{2+} on the oxidation of glycerol phosphate by blowfly flight-muscle mitochondria. *Biochemical and Biophysical Research Communications* **27**: 686–692.

83. Denton RM, Randle PJ, Martin BR (1972) Stimulation by calcium ions of pyruvate dehydrogenase phosphate phosphatase. *Biochemical Journal* **128**: 161–163.

84. Denton RM, Richards DA, Chin JG (1978) Calcium ions and the regulation of NAD^+-linked isocitrate dehydrogenase from the mitochondria of rat heart and other tissues. *Biochemical Journal* **176**: 899–906.

85. McCormack JG, Denton RM (1979) The effects of calcium ions and adenine nucleotides on the activity of pig heart 2-oxoglutarate dehydrogenase complex. *Biochemical Journal* **180**: 533–544.

86. Hajnóczky G, Robb-Gaspers LD, Seitz MB, Thomas AP (1995) Decoding of cytosolic calcium oscillations in the mitochondria. *Cell* **82**: 415–424.

87. Wakai T, Fissore RA (2019) Constitutive IP_3R1-mediated Ca^{2+} release reduces Ca^{2+} store content and stimulates mitochondrial metabolism in mouse GV oocytes. *Journal of Cell Science* **132**: jcs.225441.

88. Harris DA, Das AM (1991) Control of mitochondrial ATP synthesis in the heart. *Biochemical Journal* **280**: 561–573.

89. Neely JR, Denton RM, England PJ, Randle PJ (1972) The effects of increased heart work on the tricarboxylate cycle and its interactions with glycolysis in the perfused rat heart. *Biochemical Journal* **128**: 147–159.

90. Bell CJ, Bright NA, Rutter GA, Griffiths EJ (2006) ATP regulation in adult rat cardiomyocytes. *Journal of Biological Chemistry* **281**: 28058–28067.

91. Robert V (2001) Beat-to-beat oscillations of mitochondrial [Ca^{2+}] in cardiac cells. *The EMBO Journal* **20**: 4998–5007.

92. Carling D, Mayer FV, Sanders MJ, Gamblin SJ (2011) AMP-activated protein kinase: Natures energy sensor. *Nature Chemical Biology* **7**: 512–518.

93. Gross AS, Graef M (2020) Mechanisms of autophagy in metabolic stress response. *Journal of Molecular Biology* **432**: 28–52.

94. Mallilankaraman K, Cárdenas C, Doonan PJ, Chandramoorthy HC, Irrinki KM, Golenár T, Csordás G, Madireddi P, Yang J, Müller M, et al. (2012) MCUR1 is an essential component of mitochondrial Ca^{2+} uptake that regulates cellular metabolism. *Nature cell biology* **14**: 1336–1343.

95. Gherardi G, Nogara L, Ciciliot S, Fadini GP, Blaauw B, Braghetta P, Bonaldo P, Stefani DD, Rizzuto R, Mammucari C (2018) Loss of mitochondrial calcium uniporter rewires skeletal muscle metabolism and substrate preference. *Cell Death & Differentiation* **26**: 362–381.

96. Sood A, Jeyaraju DV, Prudent J, Caron A, Lemieux P, McBride HM, Laplante M, Tóth K, Pellegrini L (2014) A Mitofusin-2–dependent inactivating cleavage of Opa1 links changes in mitochondria

cristae and ER contacts in the postprandial liver. *Proceedings of the National Academy of Sciences* **111**: 16017–16022.

97. Wang PT, Garcin PO, Fu M, Masoudi M, St-Pierre P, Panté N, Nabi IR (2015) Distinct mechanisms controlling rough and smooth endoplasmic reticulum contacts with mitochondria. *J Cell Sci* **128**: 2759–2765.

98. Giacomello M, Pellegrini L (2016) The coming of age of the mitochondria-ER contact: A matter of thickness. *Cell Death & Differentiation* **23**: 1417–1427.

99. Chen H, Detmer SA, Ewald AJ, Griffin EE, Fraser SE, Chan DC (2003) Mitofusins Mfn1 and Mfn2 coordinately regulate mitochondrial fusion and are essential for embryonic development. *The Journal of Cell Biology* **160**: 189–200.

100. Brito OM de, Scorrano L (2008) Mitofusin 2 tethers endoplasmic reticulum to mitochondria. *Nature* **456**: 605–610.

101. De Vos KJ, Mórotz GM, Stoica R, Tudor EL, Lau K-F, Ackerley S, Warley A, Shaw CE, Miller CC (2011) VAPB interacts with the mitochondrial protein PTPIP51 to regulate calcium homeostasis. *Human molecular genetics* **21**: 1299–1311.

102. Szabadkai G, Bianchi K, Várnai P, Stefani DD, Wieckowski MR, Cavagna D, Nagy AI, Balla T, Rizzuto R (2006) Chaperone-mediated coupling of endoplasmic reticulum and mitochondrial Ca^{2+} channels. *The Journal of Cell Biology* **175**: 901–911.

103. Zahedi RP, Sickmann A, Boehm AM, Winkler C, Zufall N, Schönfisch B, Guiard B, Pfanner N, Meisinger C (2006) Proteomic analysis of the yeast mitochondrial outer membrane reveals accumulation of a subclass of preproteins. *Molecular Biology of the Cell* **17**: 1436–1450.

104. Thoudam T, Ha C-M, Leem J, Chanda D, Park J-S, Kim H-J, Jeon J-H, Choi Y-K, Liangpunsakul S, Huh YH, et al. (2018) PDK4 augments ER–mitochondria contact to dampen skeletal muscle insulin signaling during obesity. *Diabetes* **68**: 571–586.

105. Liu Y, Ma X, Fujioka H, Liu J, Chen S, Zhu X (2019) DJ-1 regulates the integrity and function of ER-mitochondria association through interaction with IP3R3-Grp75-VDAC1. *Proceedings of the National Academy of Sciences* **116**: 25322–25328.

106. Tambini MD, Pera M, Kanter E, Yang H, Guardia-Laguarta C, Holtzman D, Sulzer D, Area-Gomez E, Schon EA (2015) ApoE4 upregulates the activity of mitochondria-associated ER membranes. *EMBO reports* **17**: 27–36.

107. Castanier C, Garcin D, Vazquez A, Arnoult D (2009) Mitochondrial dynamics regulate the RIG-i-like receptor antiviral pathway. *EMBO reports* **11**: 133–138.

108. Horner SM, Liu HM, Park HS, Briley J, Gale M (2011) Mitochondrial-associated endoplasmic reticulum membranes (MAM) form innate immune synapses and are targeted by hepatitis C virus. *Proceedings of the National Academy of Sciences* **108**: 14590–14595.

109. Sutendra G, Dromparis P, Wright P, Bonnet S, Haromy A, Hao Z, McMurtry MS, Michalak M, Vance JE, Sessa WC, et al. (2011) The role of nogo and the mitochondria-endoplasmic reticulum unit in pulmonary hypertension. *Science Translational Medicine* **3**: 88ra55–88ra55.

110. Simmen T, Aslan JE, Blagoveshchenskaya AD, Thomas L, Wan L, Xiang Y, Feliciangeli SF, Hung C-H, Crump CM, Thomas G (2005) PACS-2 controls endoplasmic reticulum-mitochondria communication and Bid-mediated apoptosis. *The EMBO journal* **24**: 717–729.

111. Matsuzaki H, Fujimoto T, Tanaka M, Shirasawa S (2013) Tespa1 is a novel component of mitochondria-associated endoplasmic reticulum membranes and affects mitochondrial calcium flux. *Biochemical and Biophysical Research Communications* **433**: 322–326.

112. Bravo R, Vicencio JM, Parra V, Troncoso R, Munoz JP, Bui M, Quiroga C, Rodriguez AE, Verdejo HE, Ferreira J, et al. (2011) Increased ER-mitochondrial coupling promotes mitochondrial respiration and bioenergetics during early phases of ER stress. *Journal of Cell Science* **124**: 2143–2152.

113. Hetz C (2012) The unfolded protein response: Controlling cell fate decisions under ER stress

and beyond. *Nature Reviews Molecular Cell Biology* **13**: 89–102.

114. Lynes EM, Raturi A, Shenkman M, Sandoval CO, Yap MC, Wu J, Janowicz A, Myhill N, Benson MD, Campbell RE, et al. (2013) Palmitoylation is the switch that assigns Calnexin to quality control or ER Ca^{2+} signaling. *Journal of Cell Science* **126**: 3893–3903.

115. Bravo-Sagua R, Parra V, Ortiz-Sandoval C, Navarro-Marquez M, Rodríguez AE, Diaz-Valdivia N, Sanhueza C, Lopez-Crisosto C, Tahbaz N, Rothermel BA, et al. (2018) Caveolin-1 impairs PKA-DRP1-mediated remodelling of ERmitochondria communication during the early phase of ER stress. *Cell Death & Differentiation* **26**: 1195–1212.

116. Bravo-Sagua R, López-Crisosto C, Parra V, Rodriguez-Peña M, Rothermel BA, Quest AFG, Lavandero S (2016) mTORC1 inhibitor rapamycin and ER stressor tunicamycin induce differential patterns of ER-mitochondria coupling. *Scientific Reports* **6**: 36394.

117. Saotome M, Safiulina D, Szabadkai G, Das S, Fransson A, Aspenstrom P, Rizzuto R, Hajnoczky G (2008) Bidirectional Ca^{2+}-dependent control of mitochondrial dynamics by the miro GTPase. *Proceedings of the National Academy of Sciences* **105**: 20728–20733.

118. Yi M, Weaver D, Hajnóczky G (2004) Control of mitochondrial motility and distribution by the calcium signal. *The Journal of Cell Biology* **167**: 661–672.

119. Chami M, Oulès B, Szabadkai G, Tacine R, Rizzuto R, Paterlini-Bréchot P (2008) Role of SERCA1 truncated isoform in the proapoptotic calcium transfer from ER to mitochondria during ER stress. *Molecular Cell* **32**: 641–651.

120. Ellgaard L, McCaul N, Chatsisvili A, Braakman I (2016) Co- and post-translational protein folding in the ER. *Traffic* **17**: 615–638.

121. Pobre KFR, Poet GJ, Hendershot LM (2018) The endoplasmic reticulum (ER) chaperone BiP is a master regulator of ER functions: Getting by with a little help from ERdj friends. *Journal of Biological Chemistry* **294**: 2098–2108.

122. Shrimal S, Cherepanova NA, Gilmore R (2015) Cotranslational and posttranslocational *N*-glycosylation of proteins in the endoplasmic reticulum. *Seminars in Cell & Developmental Biology* **41**: 71–78.

123. Vassilakos A, Michalak M, Lehrman MA, Williams DB (1998) Oligosaccharide binding characteristics of the molecular chaperones calnexin and calreticulin. *Biochemistry* **37**: 3480–3490.

124. Hebert DN, Foellmer B, Helenius A (1996) Calnexin and calreticulin promote folding, delay oligomerization and suppress degradation of influenza hemagglutinin in microsomes. *The EMBO Journal* **15**: 2961–2968.

125. Vassilakos A, Cohen-Doyle MF, Peterson PA, Jackson MR, Williams DB (1996) The molecular chaperone calnexin facilitates folding and assembly of class I histocompatibility molecules. *The EMBO Journal* **15**: 1495–1506.

126. Lucocq JM, Brada D, Roth J (1986) Immunolocalization of the oligosaccharide trimming enzyme glucosidase II. *The Journal of Cell Biology* **102**: 2137–2146.

127. Tannous A, Patel N, Tamura T, Hebert DN (2015) Reglucosylation by UDP-glucose:Glycoprotein glucosyltransferase 1 delays glycoprotein secretion but not degradation. *Molecular Biology of the Cell* **26**: 390–405.

128. Fagioli C, Sitia R (2001) Glycoprotein quality control in the endoplasmic reticulum. *Journal of Biological Chemistry* **276**: 12885–12892.

129. Appenzeller-Herzog C, Ellgaard L (2008) The human PDI family: Versatility packed into a single fold. *Biochimica et Biophysica Acta (BBA) - Molecular Cell Research* **1783**: 535–548.

130. Schwaller M, Wilkinson B, Gilbert HF (2002) Reduction-reoxidation cycles contribute to catalysis of disulfide isomerization by protein-disulfide isomerase. *Journal of Biological Chemistry* **278**: 7154–7159.

131. Braakman I, Helenius J, Helenius A (1992) Manipulating disulfide bond formation and protein

folding in the endoplasmic reticulum. *The EMBO Journal* **11**: 1717–1722.

132. Jessop CE, Tavender TJ, Watkins RH, Chambers JE, Bulleid NJ (2008) Substrate specificity of the oxidoreductase ERp57 is determined primarily by its interaction with calnexin and calreticulin. *Journal of Biological Chemistry* **284**: 2194–2202.

133. Galligan JJ, Petersen DR (2012) The human protein disulfide isomerase gene family. *Human Genomics* **6**: 6.

134. Matsuo Y, Nishinaka Y, Suzuki S, Kojima M, Kizaka-Kondoh S, Kondo N, Son A, Sakakura-Nishiyama J, Yamaguchi Y, Masutani H, et al. (2004) TMX, a human transmembrane oxidoreductase of the thioredoxin family: The possible role in disulfide-linked protein folding in the endoplasmic reticulum. *Archives of Biochemistry and Biophysics* **423**: 81–87.

135. Pisoni GB, Ruddock LW, Bulleid N, Molinari M (2015) Division of labor among oxidoreductases: TMX1 preferentially acts on transmembrane polypeptides. *Molecular Biology of the Cell* **26**: 3390–3400.

136. Matsuo Y, Masutani H, Son A, Kizaka-Kondoh S, Yodoi J (2009) Physical and Functional Interaction of Transmembrane Thioredoxin-related Protein with Major Histocompatibility Complex Class I Heavy Chain: Redox-based Protein Quality Control and Its Potential Relevance to Immune Responses. *Molecular Biology of the Cell* **20**: 4552–4562.

137. Matsuo Y, Hirota K (2017) Transmembrane thioredoxin-related protein TMX1 is reversibly oxidized in response to protein accumulation in the endoplasmic reticulum. *FEBS Open Bio* **7**: 1768–1777.

138. Guerra C, Pisoni GB, Soldà T, Molinari M (2018) The reductase TMX1 contributes to ERAD by preferentially acting on membrane-associated folding-defective polypeptides. *Biochemical and Biophysical Research Communications* **503**: 938–943.

139. Cabibbo A, Pagani M, Fabbri M, Rocchi M, Farmery MR, Bulleid NJ, Sitia R (2000) ERO1-l, a human protein that favors disulfide bond formation in the endoplasmic reticulum. *Journal of*

Biological Chemistry **275**: 4827–4833.

140. Tu BP, Weissman JS (2002) The FAD- and O_2-dependent reaction cycle of Ero1-mediated oxidative protein folding in the endoplasmic reticulum. *Molecular Cell* **10**: 983–994.

141. Dias-Gunasekara S, Gubbens J, Lith M van, Dunne C, Williams JAG, Kataky R, Scoones D, Lapthorn A, Bulleid NJ, Benham AM (2005) Tissue-specific expression and dimerization of the endoplasmic reticulum oxidoreductase Ero1β. *Journal of Biological Chemistry* **280**: 33066–33075.

142. Zito E, Chin K-T, Blais J, Harding HP, Ron D (2010) ERO1-β, a pancreas-specific disulfide oxidase, promotes insulin biogenesis and glucose homeostasis. *The Journal of Cell Biology* **188**: 821–832.

143. Zito E, Melo EP, Yang Y, Wahlander, Neubert TA, Ron D (2010) Oxidative protein folding by an endoplasmic reticulum-localized peroxiredoxin. *Molecular Cell* **40**: 787–797.

144. Konno T, Melo EP, Lopes C, Mehmeti I, Lenzen S, Ron D, Avezov E (2015) ERO1-independent production of H_2O_2 within the endoplasmic reticulum fuels Prdx4-mediated oxidative protein folding. *Journal of Cell Biology* **211**: 253–259.

145. Gutiérrez T, Simmen T (2018) Endoplasmic reticulum chaperones tweak the mitochondrial calcium rheostat to control metabolism and cell death. *Cell Calcium* **70**: 64–75.

146. Lynes EM, Bui M, Yap MC, Benson MD, Schneider B, Ellgaard L, Berthiaume LG, Simmen T (2011) Palmitoylated TMX and calnexin target to the mitochondria-associated membrane. *The EMBO Journal* **31**: 457–470.

147. Lakkaraju AKK, Abrami L, Lemmin T, Blaskovic S, Kunz B, Kihara A, Dal Peraro M, Van Der Goot FG (2012) Palmitoylated calnexin is a key component of the ribosome–translocon complex. *The EMBO journal* **31**: 1823–1835.

148. Wong HN, Ward MA, Bell AW, Chevet E, Bains S, Blackstock WP, Solari R, Thomas DY, Bergeron JJM (1998) Conserved in vivo phosphorylation of Calnexin at Casein Kinase II sites as well

as a Protein Kinase C/Proline-directed Kinase site. *Journal of Biological Chemistry* **273**: 17227–17235.

149. Chevet E (1999) Phosphorylation by CK2 and MAPK enhances calnexin association with ribosomes. *The EMBO Journal* **18**: 3655–3666.

150. Roderick HL, Lechleiter JD, Camacho P (2000) Cytosolic phosphorylation of Calnexin controls intracellular Ca^{2+} oscillations via an interaction with SERCA2b. *The Journal of Cell Biology* **149**: 1235–1248.

151. Myhill N, Lynes EM, Nanji JA, Blagoveshchenskaya AD, Fei H, Simmen KC, Cooper TJ, Thomas G, Simmen T (2008) The subcellular distribution of calnexin is mediated by PACS-2. *Molecular biology of the cell* **19**: 2777–2788.

152. Bousette N, Abbasi C, Chis R, Gramolini AO (2014) Calnexin silencing in mouse neonatal cardiomyocytes induces Ca^{2+} cycling defects, ER stress, and apoptosis. *Journal of cellular physiology* **229**: 374–383.

153. Camacho P, Lechleiter JD (1995) Calreticulin inhibits repetitive intracellular Ca^{2+} waves. *Cell* **82**: 765–771.

154. Li Y, Camacho P (2003) Ca^{2+}-dependent redox modulation of SERCA2b by ERp57. *The Journal of Cell Biology* **164**: 35–46.

155. Ushioda R, Miyamoto A, Inoue M, Watanabe S, Okumura M, Maegawa K-i, Uegaki K, Fujii S, Fukuda Y, Umitsu M, et al. (2016) Redox-assisted regulation of Ca^{2+} homeostasis in the endoplasmic reticulum by disulfide reductase ERdj5. *Proceedings of the National Academy of Sciences* **113**: E6055–E6063.

156. Sayers LG, Brown GR, Michell RH, Michelangeli F (1993) The effects of thimerosal on calcium uptake and inositol 1,4,5-trisphosphate-induced calcium release in cerebellar microsomes. *Biochemical Journal* **289**: 883–887.

157. Xu KY, Zweier JL, Becker LC (1997) Hydroxyl radical inhibits sarcoplasmic reticulum Ca^{2+}-ATPase function by direct attack on the ATP binding site. *Circulation Research* **80**: 76–81.

158. Kaplan P (2003) Free radical-induced protein modification and inhibition of Ca^{2+}-ATPase of cardiac sarcoplasmic reticulum. *Molecular and Cellular Biochemistry* **248**: 41–47.

159. Cohen RA, Weisbrod RM, Gericke M, Yaghoubi M, Bierl C, Bolotina VM (1999) Mechanism of nitric oxideInduced vasodilatation. *Circulation Research* **84**: 210–219.

160. Thompson MD, Mei Y, Weisbrod RM, Silver M, Shukla PC, Bolotina VM, Cohen RA, Tong X (2014) Glutathione adducts on sarcoplasmic/endoplasmic reticulum Ca^{2+} ATPase Cys-674 regulate endothelial cell calcium stores and angiogenic function as well as promote ischemic blood flow recovery. *Journal of Biological Chemistry* **289**: 19907–19916.

161. Herrmann A-K, Wüllner V, Moos S, Graf J, Chen J, Kieseier B, Kurschus FC, Albrecht P, Vangheluwe P, Methner A (2019) Dimethyl fumarate alters intracellular Ca^{2+} handling in immune cells by redox-mediated pleiotropic effects. *Free Radical Biology and Medicine* **141**: 338–347.

162. Adachi T, Weisbrod RM, Pimentel DR, Ying J, Sharov VS, Schöneich C, Cohen RA (2004) *S*-glutathiolation by peroxynitrite activates SERCA during arterial relaxation by nitric oxide. *Nature Medicine* **10**: 1200–1207.

163. Gilady SY, Bui M, Lynes EM, Benson MD, Watts R, Vance JE, Simmen T (2010) Ero1α requires oxidizing and normoxic conditions to localize to the mitochondria-associated membrane (MAM). *Cell Stress and Chaperones* **15**: 619–629.

164. Anelli T, Bergamelli L, Margittai E, Rimessi A, Fagioli C, Malgaroli A, Pinton P, Ripamonti M, Rizzuto R, Sitia R (2012) Ero1α regulates Ca^{2+} fluxes at the endoplasmic reticulum–mitochondria interface (MAM). *Antioxidants & redox signaling* **16**: 1077–1087.

165. Marciniak SJ (2004) CHOP induces death by promoting protein synthesis and oxidation in the stressed endoplasmic reticulum. *Genes & Development* **18**: 3066–3077.

166. Higo T, Hattori M, Nakamura T, Natsume T, Michikawa T, Mikoshiba K (2005) Subtype-specific and ER lumenal environment-dependent regulation of inositol 1, 4, 5-trisphosphate receptor type 1 by ERp44. *Cell* **120**: 85–98.

167. Chin K-T, Kang G, Qu J, Gardner LB, Coetzee WA, Zito E, Fishman GI, Ron D (2011) The sarcoplasmic reticulum luminal thiol oxidase ERO1 regulates cardiomyocyte excitation-coupled calcium release and response to hemodynamic load. *The FASEB Journal* **25**: 2583–2591.

168. Bootman MD, Taylor CW, Berridge MJ (1992) The thiol reagent, thimerosal, evokes Ca^{2+} spikes in HeLa cells by sensitizing the inositol 1,4,5-trisphosphate receptor. *The Journal of biological chemistry* **267**: 25113–25119.

169. Missiaen L, Taylor CW, Berridge MJ (1991) Spontaneous calcium release from inositol trisphosphate-sensitive calcium stores. *Nature* **352**: 241–244.

170. Bánsághi S, Golenár T, Madesh M, Csordás G, RamachandraRao S, Sharma K, Yule DI, Joseph SK, Hajnóczky G (2014) Isoform- and species-specific control of inositol 1,4,5-trisphosphate (IP3) receptors by reactive oxygen species. *Journal of Biological Chemistry* **289**: 8170–8181.

171. Booth DM, Enyedi B, Geiszt M, Várnai P, Hajnóczky G (2016) Redox nanodomains are induced by and control calcium signaling at the ER-mitochondrial interface. *Molecular Cell* **63**: 240–248.

172. Wu J, Prole DL, Shen Y, Lin Z, Gnanasekaran A, Liu Y, Chen L, Zhou H, Chen SRW, Usachev YM, et al. (2014) Red fluorescent genetically encoded Ca^{2+} indicators for use in mitochondria and endoplasmic reticulum. *Biochemical Journal* **464**: 13–22.

173. Schindelin J, Arganda-Carreras I, Frise E, Kaynig V, Longair M, Pietzsch T, Preibisch S, Rueden C, Saalfeld S, Schmid B, et al. (2012) Fiji: An open-source platform for biological-image analysis. *Nature Methods* **9**: 676–682.

174. Rueden CT, Schindelin J, Hiner MC, DeZonia BE, Walter AE, Arena ET, Eliceiri KW (2017) ImageJ2: ImageJ for the next generation of scientific image data. *BMC Bioinformatics* **18**: 529.

175. Linkert M, Rueden CT, Allan C, Burel J-M, Moore W, Patterson A, Loranger B, Moore J, Neves C, MacDonald D, et al. (2010) Metadata matters: Access to image data in the real world. *The Journal of Cell Biology* **189**: 777–782.

176. Wolmarans A, Lee B, Spyracopoulos L, LaPointe P (2016) The mechanism of hsp90 ATPase stimulation by aha1. *Scientific Reports* **6**: 33179.

177. Cieri D, Vicario M, Giacomello M, Vallese F, Filadi R, Wagner T, Pozzan T, Pizzo P, Scorrano L, Brini M, et al. (2017) SPLICS: A split green fluorescent protein-based contact site sensor for narrow and wide heterotypic organelle juxtaposition. *Cell Death & Differentiation* **25**: 1131–1145.

178. R Core Team (2018) *R: A language and environment for statistical computing*. R Foundation for Statistical Computing, Vienna, Austria.

179. Wickham H, Averick M, Bryan J, Chang W, McGowan L, François R, Grolemund G, Hayes A, Henry L, Hester J, et al. (2019) Welcome to the tidyverse. *Journal of Open Source Software* **4**: 1686.

180. Hanahan D, Weinberg RA (2011) Hallmarks of cancer: The next generation. *Cell* **144**: 646–674.

181. Pinton P, Ferrari D, Magalhães P, Schulze-Osthoff K, Virgilio FD, Pozzan T, Rizzuto R (2000) Reduced Loading of Intracellular Ca^{2+} Stores and Downregulation of Capacitative Ca^{2+} Influx in Bcl-2–Overexpressing Cells. *The Journal of Cell Biology* **148**: 857–862.

182. Foyouzi-Youssefi R, Arnaudeau S, Borner C, Kelley WL, Tschopp J, Lew DP, Demaurex N, Krause K-H (2000) Bcl-2 decreases the free Ca^{2+} concentration within the endoplasmic reticulum. *Proceedings of the National Academy of Sciences* **97**: 5723–5728.

183. Oakes SA, Scorrano L, Opferman JT, Bassik MC, Nishino M, Pozzan T, Korsmeyer SJ (2004) Proapoptotic BAX and BAK regulate the type 1 inositol trisphosphate receptor and calcium leak from the endoplasmic reticulum. *Proceedings of the National Academy of Sciences* **102**: 105–110.

184. Eckenrode EF, Yang J, Velmurugan GV, Foskett JK, White C (2010) Apoptosis Protection

by Mcl-1 and Bcl-2 Modulation of Inositol 1,4,5-Trisphosphate Receptor-dependent Ca^{2+} Signaling. *Journal of Biological Chemistry* **285**: 13678–13684.

185. Dremina ES, Sharov VS, Kumar K, Zaidi A, Michaelis EK, Schöneich C (2004) Anti-apoptotic protein Bcl-2 interacts with and destabilizes the sarcoplasmic/endoplasmic reticulum Ca^{2+}-ATPase (SERCA). *Biochemical Journal* **383**: 361–370.

186. Warburg O (1956) On the origin of cancer cells. *Science* **123**: 309–314.

187. Altenberg B, Greulich KO (2004) Genes of glycolysis are ubiquitously overexpressed in 24 cancer classes. *Genomics* **84**: 1014–1020.

188. Racker E, Resnick RJ, Feldman R (1985) Glycolysis and methylaminoisobutyrate uptake in rat-1 cells transfected with *ras* or *myc* oncogenes. *Proceedings of the National Academy of Sciences* **82**: 3535–3538.

189. Biaglow JE, Cerniglia G, Tuttle S, Bakanauskas V, Stevens C, McKenna G (1997) Effect of oncogene transformation of rat embryo cells on cellular oxygen consumption and glycolysis. *Biochemical and Biophysical Research Communications* **235**: 739–742.

190. Shim H, Dolde C, Lewis BC, Wu C-S, Dang G, Jungmann RA, Dalla-Favera R, Dang CV (1997) c-Myc transactivation of *LDH-A*: Implications for tumor metabolism and growth. *Proceedings of the National Academy of Sciences* **94**: 6658–6663.

191. Ying H, Kimmelman AC, Lyssiotis CA, Hua S, Chu GC, Fletcher-Sananikone E, Locasale JW, Son J, Zhang H, Coloff JL, et al. (2012) Oncogenic Kras Maintains Pancreatic Tumors through Regulation of Anabolic Glucose Metabolism. *Cell* **149**: 656–670.

192. Ward PS, Thompson CB (2012) Metabolic Reprogramming: A Cancer Hallmark Even Warburg Did Not Anticipate. *Cancer Cell* **21**: 297–308.

193. Cárdenas C, Müller M, McNeal A, Lovy A, Jaňa F, Bustos G, Urra F, Smith N, Molgó J, Diehl JA, et al. (2016) Selective vulnerability of cancer cells by inhibition of Ca^{2+} transfer from

endoplasmic reticulum to mitochondria. *Cell Reports* **14**: 2313–2324.

194. Marchi S, Vitto VAM, Patergnani S, Pinton P (2019) High mitochondrial Ca^{2+} content increases cancer cell proliferation upon inhibition of mitochondrial permeability transition pore (mPTP). *Cell Cycle*.

195. Ishikawa K, Takenaga K, Akimoto M, Koshikawa N, Yamaguchi A, Imanishi H, Nakada K, Honma Y, Hayashi J-I (2008) ROS-generating mitochondrial DNA mutations can regulate tumor cell metastasis. *Science* **320**: 661–664.

196. Huang H, Shah K, Bradbury NA, Li C, White C (2014) Mcl-1 promotes lung cancer cell migration by directly interacting with VDAC to increase mitochondrial Ca^{2+} uptake and reactive oxygen species generation. *Cell Death & Disease* **5**: e1482–e1482.

197. Matsuo Y, Akiyama N, Nakamura H, Yodoi J, Noda M, Kizaka-Kondoh S (2001) Identification of a novel thioredoxin-related transmembrane protein. *Journal of Biological Chemistry* **276**: 10032–10038.

198. Higo T, Hamada K, Hisatsune C, Nukina N, Hashikawa T, Hattori M, Nakamura T, Mikoshiba K (2010) Mechanism of ER stress-induced brain damage by IP_3 receptor. *Neuron* **68**: 865–878.

199. Jessop CE, Watkins RH, Simmons JJ, Tasab M, Bulleid NJ (2009) Protein disulphide isomerase family members show distinct substrate specificity: P5 is targeted to BiP client proteins. *Journal of Cell Science* **122**: 4287–4295.

200. Charollais J, Goot FGVD (2009) Palmitoylation of membrane proteins (review). *Molecular Membrane Biology* **26**: 55–66.

201. Anelli T (2003) Thiol-mediated protein retention in the endoplasmic reticulum: The role of ERp44. *The EMBO Journal* **22**: 5015–5022.

202. Tosatto A, Sommaggio R, Kummerow C, Bentham RB, Blacker TS, Berecz T, Duchen MR, Rosato A, Bogeski I, Szabadkai G, et al. (2016) The mitochondrial calcium uniporter regulates breast

cancer progression via HIF -1α. *EMBO Molecular Medicine* **8**: 569–585.

203. Ren T, Zhang H, Wang J, Zhu J, Jin M, Wu Y, Guo X, Ji L, Huang Q, Zhang H, et al. (2017) MCU-dependent mitochondrial Ca^{2+} inhibits NAD^{+}/SIRT3/SOD2 pathway to promote ROS production and metastasis of HCC cells. *Oncogene* **36**: 5897–5909.

204. Raturi A, Gutiérrez T, Ortiz-Sandoval C, Ruangkittisakul A, Herrera-Cruz MS, Rockley JP, Gesson K, Ourdev D, Lou P-H, Lucchinetti E, et al. (2016) TMX1 determines cancer cell metabolism as a thiol-based modulator of ER-mitochondria Ca^{2+} flux. *The Journal of Cell Biology* **214**: 433–444.

205. Doghman-Bouguerra M, Granatiero V, Sbiera S, Sbiera I, Lacas-Gervais S, Brau F, Fassnacht M, Rizzuto R, Lalli E (2016) FATE1 antagonizes calcium-and drug-induced apoptosis by uncoupling ER and mitochondria. *EMBO reports* **17**: 1264–1280.

206. Zhang X, Gibhardt CS, Will T, Stanisz H, Körbel C, Mitkovski M, Stejerean I, Cappello S, Pacheu-Grau D, Dudek J, et al. (2019) Redox signals at the ER mitochondria interface control melanoma progression. *The EMBO Journal* **38**: e100871.

207. Chen W, Helenius J, Braakman I, Helenius A (1995) Cotranslational folding and calnexin binding during glycoprotein synthesis. *Proceedings of the National Academy of Sciences* **92**: 6229–6233.

208. Schrag JD, Bergeron JJM, Li Y, Borisova S, Hahn M, Thomas DY, Cygler M (2001) The structure of calnexin, an ER chaperone involved in quality control of protein folding. *Molecular Cell* **8**: 633–644.

209. Frickel E-M, Riek R, Jelesarov I, Helenius A, Wuthrich K, Ellgaard L (2002) TROSY-NMR reveals interaction between ERp57 and the tip of the calreticulin p-domain. *Proceedings of the National Academy of Sciences* **99**: 1954–1959.

210. Kozlov G, Bastos-Aristizabal S, Määttänen P, Rosenauer A, Zheng F, Killikelly A, Trempe J-F, Thomas DY, Gehring K (2010) Structural basis of cyclophilin B binding by the calnexin/calreticulin P-domain. *Journal of Biological Chemistry* **285**: 35551–35557.

211. Kozlov G, Muñoz-Escobar J, Castro K, Gehring K (2017) Mapping the ER interactome: The P domains of calnexin and calreticulin as plurivalent adapters for foldases and chaperones. *Structure* **25**: 1415–1422.

212. Oliver JD (1997) Interaction of the thiol-dependent reductase ERp57 with nascent glycoproteins. *Science* **275**: 86–88.

213. Molinari M, Helenius A (1999) Glycoproteins form mixed disulphides with oxidoreductases during folding in living cells. *Nature* **402**: 90–93.

214. Zapun A, Darby NJ, Tessier DC, Michalak M, Bergeron JJM, Thomas DY (1998) Enhanced catalysis of ribonuclease b folding by the interaction of calnexin or calreticulin with ERp57. *Journal of Biological Chemistry* **273**: 6009–6012.

215. Soldà T, Garbi N, Hämmerling GJ, Molinari M (2006) Consequences of ERp57 deletion on oxidative folding of obligate and facultative clients of the calnexin cycle. *Journal of Biological Chemistry* **281**: 6219–6226.

216. Hayashi T, Su T-P (2003) Intracellular dynamics of σ-1 receptors (σ1 binding sites) in NG108-15 cells. *Journal of Pharmacology and Experimental Therapeutics* **306**: 726–733.

217. Poston CN, Krishnan SC, Bazemore-Walker CR (2013) In-depth proteomic analysis of mammalian mitochondria-associated membranes (MAM). *Journal of proteomics* **79**: 219–230.

218. Wang X, Wen Y, Dong J, Cao C, Yuan S (2018) Systematic in-depth proteomic analysis of mitochondria-associated endoplasmic reticulum membranes in mouse and human testes. *PROTEOMICS* **18**: 1700478.

219. Prior K-K, Wittig I, Leisegang MS, Groenendyk J, Weissmann N, Michalak M, Jansen-Dürr P, Shah AM, Brandes RP (2016) The endoplasmic reticulum chaperone calnexin is a NADPH oxidase NOX4 interacting protein. *Journal of Biological Chemistry* **291**: 7045–7059.

220. Martyn KD, Frederick LM, Loehneysen K von, Dinauer MC, Knaus UG (2006) Functional

analysis of Nox4 reveals unique characteristics compared to other NADPH oxidases. *Cellular Signalling* **18**: 69–82.

221. Nisimoto Y, Diebold BA, Cosentino-Gomes D, Lambeth JD (2014) Nox4: A hydrogen peroxide-generating oxygen sensor. *Biochemistry* **53**: 5111–5120.

222. Pedruzzi E, Guichard C, Ollivier V, Driss F, Fay M, Prunet C, Marie J-C, Pouzet C, Samadi M, Elbim C, et al. (2004) NAD(P)H oxidase Nox-4 mediates 7-ketocholesterol-induced endoplasmic reticulum stress and apoptosis in human aortic smooth muscle cells. *Molecular and Cellular Biology* **24**: 10703–10717.

223. Santos CXC, Tanaka LY, Wosniak J, Laurindo FRM (2009) Mechanisms and implications of reactive oxygen species generation during the unfolded protein response: Roles of endoplasmic reticulum oxidoreductases, mitochondrial electron transport, and NADPH oxidase. *Antioxidants & Redox Signaling* **11**: 2409–2427.

224. Shono T, Yokoyama N, Uesaka T, Kuroda J, Takeya R, Yamasaki T, Amano T, Mizoguchi M, Suzuki SO, Niiro H, et al. (2008) Enhanced expression of NADPH oxidase nox4 in human gliomas and its roles in cell proliferation and survival. *International Journal of Cancer* **123**: 787–792.

225. Zeng C, Wu Q, Wang J, Yao B, Ma L, Yang Z, Li J, Liu B (2016) NOX4 supports glycolysis and promotes glutamine metabolism in non-small cell lung cancer cells. *Free Radical Biology and Medicine* **101**: 236–248.

226. Gupta P, Jagavelu K, Mishra DP (2015) Inhibition of NADPH oxidase-4 potentiates 2-deoxy-d-glucose-induced suppression of glycolysis, migration, and invasion in glioblastoma cells: Role of the Akt/HIF1α/HK-2 signaling axis. *Antioxidants & Redox Signaling* **23**: 665–681.

227. Tang P, Dang H, Huang J, Xu T, Yuan P, Hu J, Sheng J-f (2018) NADPH oxidase NOX4 is a glycolytic regulator through mROS-HIF1α axis in thyroid carcinomas. *Scientific Reports* **8**: 15897.

228. Sun Q-A, Hess DT, Nogueira L, Yong S, Bowles DE, Eu J, Laurita KR, Meissner G, Stamler JS (2011) Oxygen-coupled redox regulation of the skeletal muscle ryanodine receptor-Ca^{2+} release

channel by NADPH oxidase 4. *Proceedings of the National Academy of Sciences* **108**: 16098–16103.

229. Ying J, Tong X, Pimentel DR, Weisbrod RM, Trucillo MP, Adachi T, Cohen RA (2007) Cysteine-674 of the sarco/endoplasmic reticulum calcium ATPase is required for the inhibition of cell migration by nitric oxide. *Arteriosclerosis, Thrombosis, and Vascular Biology* **27**: 783–790.

230. Evangelista AM, Thompson MD, Weisbrod RM, Pimental DR, Tong X, Bolotina VM, Cohen RA (2012) Redox regulation of SERCA2 is required for vascular endothelial growth factor-induced signaling and endothelial cell migration. *Antioxidants & Redox Signaling* **17**: 1099–1108.

231. Tong X, Schröder K (2009) NADPH oxidases are responsible for the failure of nitric oxide to inhibit migration of smooth muscle cells exposed to high glucose. *Free Radical Biology and Medicine* **47**: 1578–1583.

232. Tong X, Hou X, Jourd'heuil D, Weisbrod RM, Cohen RA (2010) Upregulation of Nox4 by TGFβ1 oxidizes SERCA and inhibits NO in arterial smooth muscle of the prediabetic Zucker rat. *Circulation Research* **107**: 975–983.

233. Evangelista AM, Thompson MD, Bolotina VM, Tong X, Cohen RA (2012) Nox4- and Nox2-dependent oxidant production is required for VEGF-induced SERCA cysteine-674 *S*-glutathiolation and endothelial cell migration. *Free Radical Biology and Medicine* **53**: 2327–2334.

234. Van Coppenolle F, Abeele FV, Slomianny C, Flourakis M, Hesketh J, Dewailly E, Prevarskaya N (2004) Ribosome-translocon complex mediates calcium leakage from endoplasmic reticulum stores. *Journal of Cell Science* **117**: 4135–4142.

235. Schäuble N, Lang S, Jung M, Cappel S, Schorr S, Ulucan Ö, Linxweiler J, Dudek J, Blum R, Helms V, et al. (2012) BiP-mediated closing of the Sec61 channel limits Ca^{2+} leakage from the ER. *The EMBO journal* **31**: 3282–3296.

236. Hogan PG, Rao A (2015) Store-operated calcium entry: Mechanisms and modulation. *Biochemical and Biophysical Research Communications* **460**: 40–49.

237. Verfaillie T, Rubio N, Garg AD, Bultynck G, Rizzuto R, Decuypere J-P, Piette J, Linehan C, Gupta S, Samali A, et al. (2012) PERK is required at the ER-mitochondrial contact sites to convey apoptosis after ROS-based ER stress. *Cell Death & Differentiation* **19**: 1880–1891.

238. Prins D, Groenendyk J, Touret N, Michalak M (2011) Modulation of STIM1 and capacitative Ca^{2+} entry by the endoplasmic reticulum luminal oxidoreductase ERp57. *EMBO reports* **12**: 1182–1188.

239. Enyedi B, Várnai P, Geiszt M (2010) Redox State of the Endoplasmic Reticulum Is Controlled by *Ero*1L-alpha and Intraluminal Calcium. *Antioxidants & Redox Signaling* **13**: 721–729.

240. Blais JD, Chin K-T, Zito E, Zhang Y, Heldman N, Harding HP, Fass D, Thorpe C, Ron D (2010) A small molecule inhibitor of endoplasmic reticulum oxidation 1 (ERO1) with selectively reversible thiol reactivity. *Journal of Biological Chemistry* **285**: 20993–21003.

241. Somanna NK, Valente AJ, Krenz M, Fay WP, Delafontaine P, Chandrasekar B (2015) The Nox1/4 dual inhibitor GKT137831 or Nox4 knockdown inhibits angiotensin-II-induced adult mouse cardiac fibroblast proliferation and migration. AT1 physically associates with Nox4. *Journal of Cellular Physiology* **231**: 1130–1141.

242. Chen K, Kirber MT, Xiao H, Yang Y, Keaney JF (2008) Regulation of ROS signal transduction by NADPH oxidase 4 localization. *The Journal of Cell Biology* **181**: 1129–1139.

243. Marino M, Stoilova T, Giorgi C, Bachi A, Cattaneo A, Auricchio A, Pinton P, Zito E (2014) SEPN1, an endoplasmic reticulum-localized selenoprotein linked to skeletal muscle pathology, counteracts hyperoxidation by means of redox-regulating SERCA2 pump activity. *Human Molecular Genetics* **24**: 1843–1855.

244. Courjaret R, Machaca K (2014) Mid-range Ca^{2+} signalling mediated by functional coupling between store-operated Ca^{2+} entry and IP3-dependent Ca^{2+} release. *Nature Communications* **5**: 3916.

245. Hammadi M, Oulidi A, Gackière F, Katsogiannou M, Slomianny C, Roudbaraki M, Dewailly E,

Delcourt P, Lepage G, Lotteau S, et al. (2013) Modulation of ER stress and apoptosis by endoplasmic reticulum calcium leak *via* translocon during unfolded protein response: Involvement of GRP78. *The FASEB Journal* **27**: 1600–1609.

246. Rojo M, Legros F, Chateau D, Lombès A (2002) Membrane topology and mitochondrial targeting of mitofusins, ubiquitous mammalian homologs of the transmembrane GTPase Fzo. *Journal of cell science* **115**: 1663–1674.

247. Mattie S, Riemer J, Wideman JG, McBride HM (2017) A new mitofusin topology places the redox-regulated C terminus in the mitochondrial intermembrane space. *The Journal of Cell Biology* **217**: 507–515.

248. Cao Y-L, Meng S, Chen Y, Feng J-X, Gu D-D, Yu B, Li Y-J, Yang J-Y, Liao S, Chan DC, et al. (2017) MFN1 structures reveal nucleotide-triggered dimerization critical for mitochondrial fusion. *Nature* **542**: 372–376.

249. Qi Y, Yan L, Yu C, Guo X, Zhou X, Hu X, Huang X, Rao Z, Lou Z, Hu J (2016) Structures of human mitofusin 1 provide insight into mitochondrial tethering. *Journal of Cell Biology* **215**: 621–629.

250. Koshiba T (2004) Structural basis of mitochondrial tethering by mitofusin complexes. *Science* **305**: 858–862.

251. Yan L, Qi Y, Huang X, Yu C, Lan L, Guo X, Rao Z, Hu J, Lou Z (2018) Structural basis for GTP hydrolysis and conformational change of MFN1 in mediating membrane fusion. *Nature Structural & Molecular Biology* **25**: 233–243.

252. Shutt T, Geoffrion M, Milne R, McBride HM (2012) The intracellular redox state is a core determinant of mitochondrial fusion. *EMBO reports* **13**: 909–915.

253. Borgese N, Gazzoni I, Barberi M, Colombo S, Pedrazzini E (2001) Targeting of a tail-anchored protein to endoplasmic reticulum and mitochondrial outer membrane by independent but competing pathways. *Molecular Biology of the Cell* **12**: 2482–2496.

254. Ishihara N (2004) Mitofusin 1 and 2 play distinct roles in mitochondrial fusion reactions via GTPase activity. *Journal of Cell Science* **117**: 6535–6546.

255. Naon D, Zaninello M, Giacomello M, Varanita T, Grespi F, Lakshminaranayan S, Serafini A, Semenzato M, Herkenne S, Hernández-Alvarez MI, et al. (2016) Critical reappraisal confirms that mitofusin 2 is an endoplasmic reticulummitochondria tether. *Proceedings of the National Academy of Sciences* **113**: 11249–11254.

256. Chen Y, Csordás G, Jowdy C, Schneider TG, Csordás N, Wang W, Liu Y, Kohlhaas M, Meiser M, Bergem S, et al. (2012) Mitofusin 2-Containing Mitochondrial-Reticular Microdomains Direct Rapid Cardiomyocyte Bioenergetic Responses Via Interorganelle Ca^{2+} Crosstalk. *Circulation Research* **111**: 863–875.

257. Schneeberger M, Dietrich MO, Sebastián D, Imbernón M, Castaño C, Garcia A, Esteban Y, Gonzalez-Franquesa A, Rodríguez IC, Bortolozzi A, et al. (2013) Mitofusin 2 in POMC neurons connects ER stress with leptin resistance and energy imbalance. *Cell* **155**: 172–187.

258. Hernández-Alvarez MI, Sebastián D, Vives S, Ivanova S, Bartoccioni P, Kakimoto P, Plana N, Veiga SR, Hernández V, Vasconcelos N, et al. (2019) Deficient endoplasmic reticulum-mitochondrial phosphatidylserine transfer causes liver disease. *Cell* **177**: 881–895.

259. Cosson P, Marchetti A, Ravazzola M, Orci L (2012) Mitofusin-2 independent juxtaposition of endoplasmic reticulum and mitochondria: An ultrastructural study. *PLoS ONE* **7**: e46293.

260. Filadi R, Greotti E, Turacchio G, Luini A, Pozzan T, Pizzo P (2015) Mitofusin 2 ablation increases endoplasmic reticulum–mitochondria coupling. *Proceedings of the National Academy of Sciences* **112**: E2174–E2181.

261. Filadi R, Greotti E, Turacchio G, Luini A, Pozzan T, Pizzo P (2016) Presenilin 2 Modulates Endoplasmic Reticulum-Mitochondria Coupling by Tuning the Antagonistic Effect of Mitofusin 2. *Cell Reports* **15**: 2226–2238.

262. Leal NS, Schreiner B, Pinho CM, Filadi R, Wiehager B, Karlström H, Pizzo P, Ankarcrona M

(2016) Mitofusin-2 knockdown increases ER-mitochondria contact and decreases amyloid β-peptide production. *Journal of Cellular and Molecular Medicine* **20**: 1686–1695.

263. Bravo R, Gutierrez T, Paredes F, Gatica D, Rodriguez AE, Pedrozo Z, Chiong M, Parra V, Quest AF, Rothermel BA, et al. (2012) Endoplasmic reticulum: ER stress regulates mitochondrial bioenergetics. *The international journal of biochemistry & cell biology* **44**: 16–20.

264. Harding HP, Zhang Y, Ron D (1999) Protein translation and folding are coupled by an endoplasmic-reticulum-resident kinase. *Nature* **397**: 271–274.

265. Ngoh GA, Papanicolaou KN, Walsh K (2012) Loss of mitofusin 2 promotes endoplasmic reticulum stress. *Journal of Biological Chemistry* **287**: 20321–20332.

266. Sebastian D, Hernandez-Alvarez MI, Segales J, Sorianello E, Munoz JP, Sala D, Waget A, Liesa M, Paz JC, Gopalacharyulu P, et al. (2012) Mitofusin 2 (Mfn2) links mitochondrial and endoplasmic reticulum function with insulin signaling and is essential for normal glucose homeostasis. *Proceedings of the National Academy of Sciences* **109**: 5523–5528.

267. Muñoz JP, Ivanova S, Sánchez-Wandelmer J, Martínez-Cristóbal P, Noguera E, Sancho A, Díaz-Ramos A, Hernández-Alvarez MI, Sebastián D, Mauvezin C, et al. (2013) Mfn2 modulates the UPR and mitochondrial function via repression of PERK. *The EMBO journal* **32**: 2348–2361.

268. Xin Y, Wu W, Qu J, Wang X, Lei S, Yuan L, Liu X (2019) Inhibition of mitofusin-2 promotes cardiac fibroblast activation via the PERK/ATF4 pathway and reactive oxygen species. *Oxidative Medicine and Cellular Longevity* **2019**: 1–16.

269. Axten JM, Medina JR, Feng Y, Shu A, Romeril SP, Grant SW, Li WHH, Heerding DA, Minthorn E, Mencken T, et al. (2012) Discovery of 7-methyl-5-(1-{[3-(trifluoromethyl)phenyl]acetyl}-2,3-dihydro-1*H*-indol-5-yl)-7*H*-pyrrolo[2,3-*d*]pyrimidin-4-amine (GSK2606414), a potent and selective first-in-class inhibitor of Protein Kinase R (PKR)-like Endoplasmic Reticulum Kinase (PERK). *Journal of Medicinal Chemistry* **55**: 7193–7207.

270. Sugiura A, Nagashima S, Tokuyama T, Amo T, Matsuki Y, Ishido S, Kudo Y, McBride HM,

Fukuda T, Matsushita N, et al. (2013) MITOL Regulates Endoplasmic Reticulum-Mitochondria Contacts via Mitofusin2. *Molecular Cell* **51**: 20–34.

271. Kuo IY, Brill AL, Lemos FO, Jiang JY, Falcone JL, Kimmerling EP, Cai Y, Dong K, Kaplan DL, Wallace DP, et al. (2019) Polycystin 2 regulates mitochondrial Ca^{2+} signaling, bioenergetics, and dynamics through mitofusin 2. *Science Signaling* **12**: eaat7397.

272. Wang W, Xie Q, Zhou X, Yao J, Zhu X, Huang P, Zhang L, Wei J, Xie H, Zhou L, et al. (2015) Mitofusin-2 triggers mitochondria Ca^{2+} influx from the endoplasmic reticulum to induce apoptosis in hepatocellular carcinoma cells. *Cancer Letters* **358**: 47–58.

273. Bucha S, Mukhopadhyay D, Bhattacharyya NP (2015) Regulation of mitochondrial morphology and cell cycle by microRNA-214 targeting mitofusin2. *Biochemical and Biophysical Research Communications* **465**: 797–802.

274. Filadi R, Greotti E, Pizzo P (2018) Highlighting the endoplasmic reticulum-mitochondria connection: Focus on mitofusin 2. *Pharmacological Research* **128**: 42–51.

275. Filadi R, Pendin D, Pizzo P (2018) Mitofusin 2: From functions to disease. *Cell Death & Disease* **9**: 330.

276. Chami M, Gozuacik D, Lagorce D, Brini M, Falson P, Peaucellier G, Pinton P, Lecoeur H, Gougeon M-L, Maire M le, et al. (2001) SERCA1 Truncated Proteins Unable to Pump Calcium Reduce the Endoplasmic Reticulum Calcium Concentration and Induce Apoptosis. *The Journal of Cell Biology* **153**: 1301–1314.

277. Pagani M, Fabbri M, Benedetti C, Fassio A, Pilati S, Bulleid NJ, Cabibbo A, Sitia R (2000) Endoplasmic reticulum oxidoreductin 1-lβ (ERO1-lβ), a human gene induced in the course of the unfolded protein response. *Journal of Biological Chemistry* **275**: 23685–23692.

278. Harding HP, Zhang Y, Zeng H, Novoa I, Lu PD, Calfon M, Sadri N, Yun C, Popko B, Paules R, et al. (2003) An integrated stress response regulates amino acid metabolism and resistance to oxidative stress. *Molecular Cell* **11**: 619–633.

279. Yamamoto WR, Bone RN, Sohn P, Syed F, Reissaus CA, Mosley AL, Wijeratne AB, True JD, Tong X, Kono T, et al. (2018) Endoplasmic reticulum stress alters ryanodine receptor function in the murine pancreatic β cell. *Journal of Biological Chemistry* **294**: 168–181.

280. Larsen AH, Frandsen A, Treiman M (2001) Upregulation of the SERCA-type Ca^{2+} pump activity in response to endoplasmic reticulum stress in PC12 cells. *BMC Biochemistry* **2**: 4.

281. Picca A, Calvani R, Coelho-Junior HJ, Landi F, Bernabei R, Marzetti E (2020) Inter-organelle membrane contact sites and mitochondrial quality control during aging: A geroscience view. *Cells* **9**: 598.

282. Herrera-Cruz MS, Simmen T (2017) Cancer: Untethering mitochondria from the endoplasmic reticulum? *Frontiers in Oncology* **7**: 105.

283. Vallese F, Barazzuol L, Maso L, Brini M, Calì T (2019) ER-mitochondria calcium transfer, organelle contacts and neurodegenerative diseases. In, *Advances in experimental medicine and biology* pp 719–746. Springer International Publishing.

284. Tubbs E, Rieusset J (2017) Metabolic signaling functions of ER–mitochondria contact sites: Role in metabolic diseases. *Journal of Molecular Endocrinology* **58**: R87–R106.

285. Martinvalet D (2018) The role of the mitochondria and the endoplasmic reticulum contact sites in the development of the immune responses. *Cell Death & Disease* **9**: 336.